Nov
2020

ICON Tutorial

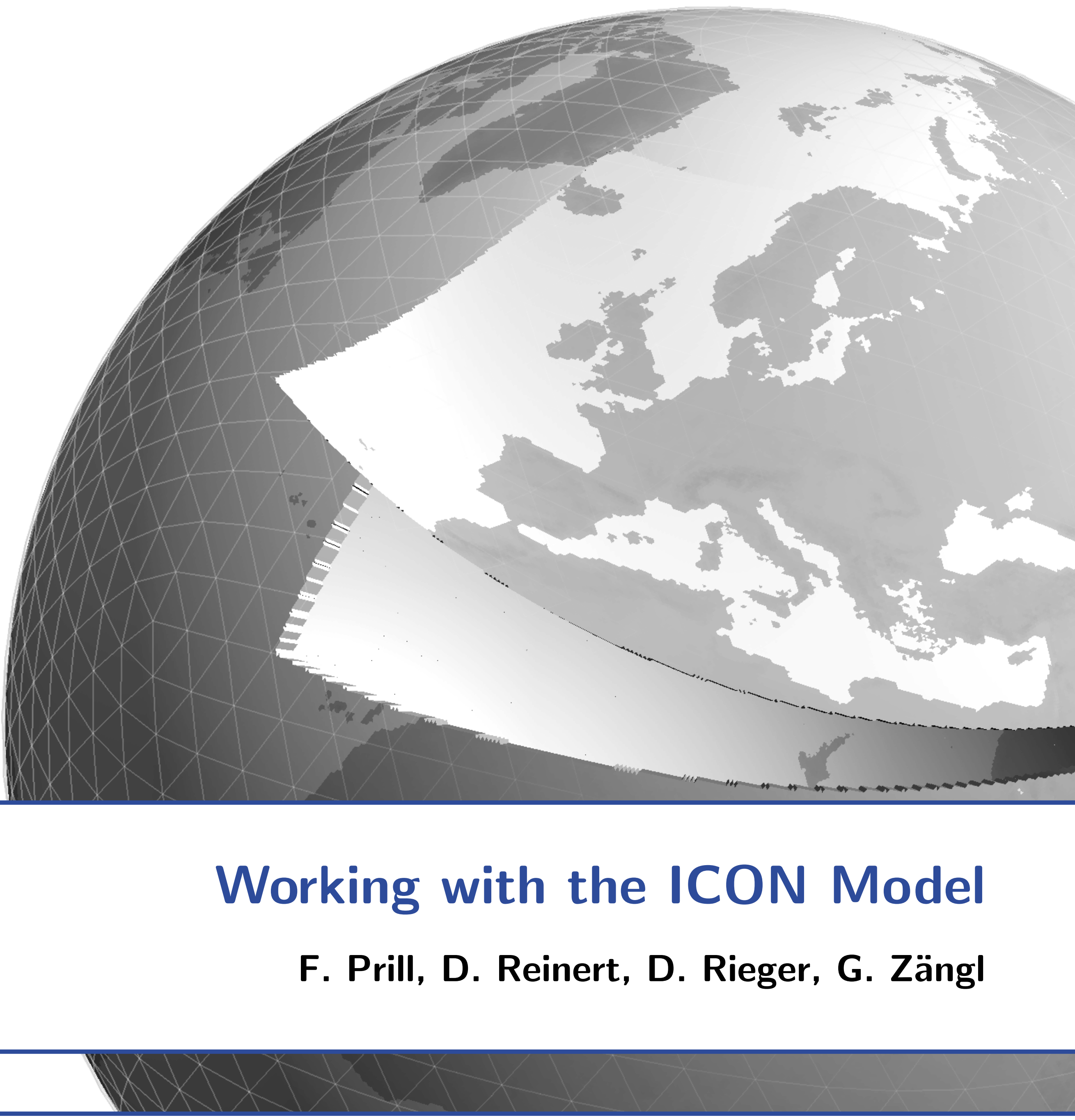

Working with the ICON Model

F. Prill, D. Reinert, D. Rieger, G. Zängl

Deutscher Wetterdienst
Wetter und Klima aus einer Hand

Karlsruhe Institute of Technology

Max-Planck-Institut
für Meteorologie

Acknowledgments

Many people contributed to this manuscript.
The section on ICON physics was partly provided by J. Helmert (land-soil model TERRA, Section 3.8.11), D. Klocke (convection parameterization, Section 3.8.4), M. Köhler (cloud-cover parameterization and turbulence, Sections 3.8.5, 3.8.6), D. Mironov (summary of sea-ice and lake model, Sections 3.8.9, 3.8.10), M. Raschendorfer (turbulence, Section 3.8.6), and A. Seifert (grid-scale microphysics parameterization, Section 3.8.3), DWD Physical Processes Division.
Section 6.2 (ICON-LAM nudging) includes contributions by S. Borchert, DWD. Section 6.5 was created mostly based on experiences by U. Blahak, DWD, for tuning the COSMO model for tropical setups.
S. Rast (MPI-M) provided useful specifics on the grid construction, internal representation of fields and other details, see Rast (2017), in particular in Ch. 8.
Section 9.3.3 (Visualization with R) has been contributed by J. Förstner, DWD Physical Processes Division.
Chapter 10 was in its original form provided by R. Potthast and A. Fernandez del Rio, DWD Data Assimilation Division.
The Appendix A on the basic usage of DWD's HPC platform is based on T. Steinert's and U. Schättler's (DWD) documentation of the NEC SX-Aurora.

DOI: 10.5676/DWD_pub/nwv/icon_tutorial2020

;

Publisher
Deutscher Wetterdienst
Business Area "Research and Development"
Frankfurter Straße 135
63067 Offenbach
www.dwd.de

Editors
Daniel Reinert, DWD,
daniel.reinert@dwd.de
Daniel Rieger, DWD,
daniel.rieger@dwd.de
Florian Prill, DWD,
florian.prill@dwd.de

Contents

0. Preface

The ICON (ICOsahedral Nonhydrostatic) modeling framework (Zängl et al., 2015) is a joint project between the Deutscher Wetterdienst (DWD) and the Max-Planck-Institute for Meteorology (MPI-M) for developing a unified next-generation global numerical weather prediction (NWP) and climate modeling system.

The main goals formulated in the initial phase of the collaboration are

- better conservation properties than in the existing global models, with the obligatory requirement of exact local mass conservation and mass-consistent transport,
- better scalability on future massively parallel high-performance computing architectures,
- the availability of some means of static mesh refinement. ICON is capable of mixing one-way nested and two-way nested grids within one model application, combined with an option for vertical nesting. This allows the global grid to extend into the mesosphere (which facilitates the assimilation of satellite data) whereas the nested domains extend only into the lower stratosphere in order to save computing time.
- applicability on a wide range of scales down to $\mathcal{O}(1\,\text{km})$ and beyond (which of course requires a nonhydrostatic dynamical core).

The ICON modeling framework became operational in DWD's forecast system in January 2015. During the first six months only global simulations were executed with a horizontal grid spacing of 13 km and 90 vertical levels. Starting from July 21st, 2015, model simulations have been complemented by a nesting region over Europe.

In January 2018, the global 40 member ICON-EPS (Ensemble Prediction System) was released for the operational service at DWD. Since November 2019, the convection-permitting model setup ICON-D2 (i.e. using the limited-area mode of ICON) runs in pre-operational mode at DWD. It will become operational in Q4/2020 and replaces the COSMO model (Baldauf et al. (2011)).

The model source code has been made available for scientific use under an institutional license since 2015.

0.1. How This Document Is Organized

Not all topics in this manuscript are covered during the workshop. Therefore, the manuscript can be used as a textbook, similar to a user manual for the ICON model. Readers are assumed to have a basic knowledge of the design and usage of numerical weather prediction models.

Even though the chapters in this textbook are largely independent, they should preferably not be treated in an arbitrary order.

- For getting started with the ICON model: read Chapters 1 – 5.
- New users who are interested in the *regional* model should read Chapter 6 in addition.
- More advanced topics are covered by Chapters 7 – 10.

Paragraphs describing common pitfalls and containing details for advanced users are marked by the symbol 🚀.

At the end of the document a number of exercises is provided (see page 235). These exercises revisit the topics of the individual chapters and range from easy tests to the setup of complex forecast simulations.

To some extent this document can also be used as a reference manual. We refer to the index on page 275 for a quick look-up of namelist parameters.

0.2. How to Obtain a Copy of the ICON Model Code

To institutions, the ICON model is distributed under an **institutional license** issued by DWD. To obtain a grant of license that must be signed and returned to the DWD, please contact `icon@dwd.de` or follow the information on the public ICON web site

`https://code.mpimet.mpg.de/projects/iconpublic`

To individuals, the ICON model is distributed under a **personal non-commercial research license** distributed by MPI-M, see also the instructions on the public ICON web site. Access to the source code management system *git* is limited to the development partners of the ICON project.

Additionally, we have established the mailing list `icon-community@mpimet.mpg.de` to stay in touch with the ICON community. Please visit `https://listserv.gwdg.de/mailman/listinfo/icon-community` and subscribe to this list in order to receive announcements about new releases and features.

Data Services

On the ICON web page under the mentioned URL you will also find the access to the **grid generator web service** (see Section 2.1.6), and the web links to ICON's official grid download site and GRIB2 definitions.

DWD has made a number of **model forecast data sets** publicly available, mostly free of charge (with a retention of 48 h). This service has started in July 2017 and can be reached under `https://opendata.dwd.de/weather/nwp/icon`. See the content description under `https://www.dwd.de/EN/ourservices/opendata/opendata.html` for a list of spatial data sets.

For further **data requests** with respect to DWD operational data products please contact `klima.vertrieb@dwd.de`.

0.3. Further Documentation

The ICON model is accompanied by various other manuals and documentation. An extensive list is available and constantly kept up-to-date in the documentation section of the public ICON web site `https://code.mpimet.mpg.de/projects/iconpublic`.

We restrict ourselves to a small subset in the following.

Scientific Documentation

Up to now there is no comprehensive scientific documentation available. In this respect, we refer to the publication Zängl et al. (2015) and the references cited therein.

Recent information on ICON's hydrostatic dynamical core and the LES model can be found in Wan et al. (2013), Dipankar et al. (2015), Heinze et al. (2017).

Detailed information and evaluation of the atmospheric component of ICON using the climate physics package is given by Giorgetta et al. (2018), Crueger et al. (2018).

The *Reports on ICON* are a new series of non-peer-reviewed articles dedicated to ICON:

`https://www.dwd.de/EN/ourservices/reports_on_icon/reports_on_icon.html`

These are not attributed to DWD or MPI-M alone and allow for a fast and straightforward publication of technical and scientific contributions. All ICON developers are invited to contribute.

The extended modules for Aerosols and Reactive Trace gases (ART) are described in Rieger et al. (2015), Schröter et al. (2018). Not covered by this tutorial, a description of the ocean component ICON-O within the ICON modeling system can be found in Korn (2017), Korn and Danilov (2017).

Technical Documentation

For model users who intend to process data products of DWD's operational runs, the DWD database documentation may be a valuable resource, see Reinert et al. (2020). It can be found (in English language) on the DWD web site

`www.dwd.de/SharedDocs/downloads/DE/`
`modelldokumentationen/nwv/icon/icon_dbbeschr_aktuell.pdf`.

A complete list of namelist switches can be found in the namelist documentation

`icon/doc/Namelist_overview.pdf`

which is deployed together with the code.

The pre- and post-processing tools of the DWD ICON Tools collection are described in more detail in the DWD ICON Tools manual, see Prill (2020).

Finally, please note the FAQ section on the ICON web site which covers a variety of common pitfalls.

1. Installation of the ICON Model Package

The purpose of this tutorial is to give you some practical experience in installing and running the ICON model package. Exercises are carried out on the supercomputers at DWD but the principal steps of the installation can directly be transferred to other systems.

1.1. The ICON Model Package

The source code for the ICON model package consists of the following three components:

- **The ICOsahedral Nonhydrostatic model (ICON)**
  For this tutorial the release v2.6.2.2 of the ICON code is used (state *October 2020*). It is close to DWD's currently operational *icon-nwp* version (see below for explanation). The code also contains the ocean model developed at MPI-M which is, however, not covered by this tutorial.

- **ICON-ART for aerosols and reactive trace gases**
  The ART module, where ART stands for Aerosols and Reactive Trace gases, is an extension of the ICON model to enable the simulation of gases, aerosol particles and related feedback processes in the atmosphere. The module is provided by the Karlsruhe Institute of Technology (KIT) and requires a separate license.

- **DWD ICON Tools**
  The ICON Tools are a set of command-line tools for remapping, extracting and querying ICON data files. They are based on a common library and written in Fortran 90/95 and Fortran 2003.

ICON-NWP code version: The versioning of ICON is a bit complex and reflects the parallel development in several "flavors" like "atmosphere", "ocean", and several more. There are four important branches tagging versions that reached certain milestones: *icon-aes* (atmosphere in the Earth system, mainly Echam physics in the atmosphere), *icon-nwp* (numerical weather prediction, mainly dynamics and physics of the LEM and NWP configurations of the atmospheric model), *icon-oes* (ocean in the Earth system), *icon-les* (land in the Earth system). The common release version integrates the stable components of all branches.

Each tag contains all model components, but the latest tag of *icon-aes* may not contain the most recent developments of the ocean physics although these are already included into the latest *icon-oes* tag.

1.1.1. Directory Layout

Figure 1.1 shows a brief description of the directory structure of the ICON model and of the directories containing the test case data under the root tree.

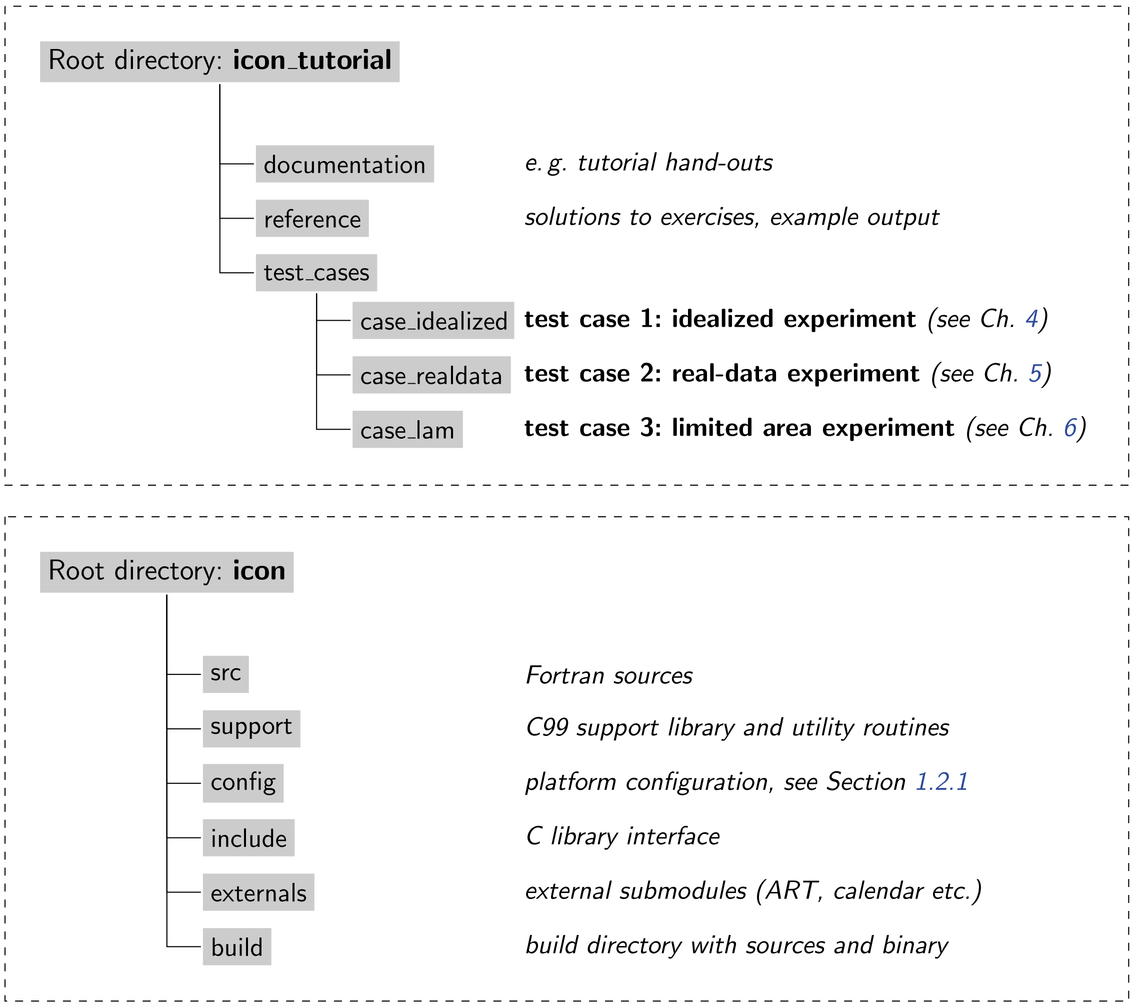
Root directory: **icon_tutorial**
documentation — *e. g. tutorial hand-outs*
reference — *solutions to exercises, example output*
test_cases
case_idealized — **test case 1: idealized experiment** *(see Ch. 4)*
case_realdata — **test case 2: real-data experiment** *(see Ch. 5)*
case_lam — **test case 3: limited area experiment** *(see Ch. 6)*
Root directory: **icon**
src — *Fortran sources*
support — *C99 support library and utility routines*
config — *platform configuration, see Section 1.2.1*
include — *C library interface*
externals — *external submodules (ART, calendar etc.)*
build — *build directory with sources and binary*

Figure 1.1.: Directory structure of the ICON model and of the directories containing the test case data under the root tree. Note that the ICON-ART source code modules are distributed in a separate tarball.

The ICON model code is located in the directory `icon`. The most important subdirectories are described in the following:

Subdirectory `build`

Within the `build` directory, a subdirectory with the name of your computer architecture is created during compilation. When you open this newly created folder you find a `bin` subdirectory containing the ICON binary `icon` and several other subdirectories containing the compiled module files.

Subdirectory `config`

Inside the `config` directory, different machine-dependent configurations are stored in configuration script files (see Section 1.2.1).

Subdirectory `src`

Within the `src` directory we have the source code of ICON including the main program and ICON modules. The modules are organized in several subdirectories:

The main program `icon.f90` can be found inside the subdirectory `src/drivers`. Additionally, this directory contains the modules for a hydrostatic and a nonhydrostatic setup.

The configuration of ICON run-time settings is implemented within the modules inside `src/configure_model` and `src/namelists`. Modules regarding the configuration of idealized test cases can be found inside `src/testcases`.

The dynamics of ICON are implemented inside `src/atm_dyn_iconam` and the physical parameterizations inside `src/atm_phy_nwp`. Surface parameterizations can be found inside `src/lnd_phy_nwp`.

Shared infrastructure modules for 3D and 4D variables are located within `src/shared`. Routines that are primarily related to horizontal grids and 2D fields (e.g. external parameters) are stored within `src/shr_horizontal`.

Modules handling the parallelization can be found in `src/parallel_infrastructure`.

Input and output modules are stored in `src/io`.

The ICON code comes with its own LAPACK and BLAS sources. For performance reasons, these libraries may be replaced by machine-dependent optimizations. However, please note that LAPACK and BLAS routines are *not* actively used by the *nonhydrostatic* model.

1.1.2. Libraries Needed for Data Input and Output

The ICON model package lets you integrate a whole variety of external libraries. See the corresponding table in the document `README.md` in the root directory of the ICON source code for a detailed list of required and optional libraries for ICON.

The libraries play a particularly important role in the execution of I/O tasks. Two data formats are implemented in the package to read and write data from or to disk: GRIB and NetCDF.

- GRIB *(GRIdded Binary)* is a standard defined by the World Meteorological Organization (WMO) for the exchange of processed data in the form of grid point values expressed in binary form. GRIB coded data consists of a continuous bit-stream made of a sequence of octets (1 octet = 8 bits). Please note that the ICON model does support only the GRIB2 version of the standard.
- NetCDF (Network Common Data Form) is a set of software libraries and machine-independent data formats that support the creation, access, and sharing of array-oriented scientific data. NetCDF files contain the complete information about the

dependent variables, the history, and the fields themselves. The NetCDF file format is also used for the definition of the computational mesh (grid topology).
For more information on NetCDF see http://www.unidata.ucar.edu.

To work with the formats described above the following libraries are utilized by the ICON model package. For this training course, the paths to access these libraries on the used computer system are already specified in the `Makefile`.

The Climate Data Interfaces (CDI) – `externals/cdi`

This library has been developed and implemented by the Max-Planck-Institute for Meteorology in Hamburg. It provides a C and Fortran interface to access climate and NWP model data. Among others, supported data formats are GRIB1/2 and NetCDF.

For more information see https://code.mpimet.mpg.de/projects/cdi.

A copy of the CDI is distributed together with the ICON model package. However, users can download and install this library before configuring ICON and use it instead. Note that the CDI are also used by the DWD ICON Tools.

The NetCDF library – `libnetcdf.a`

A special library, the NetCDF library, is necessary to write and read data using the NetCDF format. This library also contains tools for manipulating and visualizing the data (`ncdump` utility, see Section 9.1.1).

If the library is not yet installed on your system, you can get the source code and documentation from

http://www.unidata.ucar.edu/software/netcdf/index.html

This includes a description how to install the library on different platforms. Please make sure that the F90 package is also installed, since the model reads and writes grid data through the F90 NetCDF functions.

Note that there exists a restriction regarding the file size. While the classic NetCDF format could not deal with files larger than 2 GiB the new NetCDF-4/HDF5 format permits storing files as large as the underlying file system supports. However, NetCDF-4/HDF5 files are unreadable to the NetCDF library before version 4.0.

The ECMWF ecCodes package[1] – `libeccodes.a, libeccodes_f90.a`

The European Centre for Medium-Range Weather Forecasts (ECMWF) has developed an application programmers interface (API) to pack and unpack GRIB1 as well as GRIB2

[1] *ecCodes* is an evolution of the former GRIB-API software package. To facilitate the alternative use of both libraries, ICON implements only backward-compatible API function names. The GRIB-API libraries, however, would be `libgrib_api.a, libgrib_api_f90.a`.

formatted data. For reading and setting meta-data, the *ecCodes* package uses the so-called key/value approach, which means that all the information contained in the GRIB message is retrieved through alphanumeric names. Indirect use of this ecCodes library in the ICON model is implemented through the CDI.

In addition to the GRIB library, there are some command-line tools to provide an easy way to check and manipulate GRIB data from the shell. Amongst them, the most important ones are `grib_ls` and `grib_dump` for listing the contents of a GRIB file, and `grib_set` for (re)-setting specific key/value pairs.

For more information on ecCodes we refer to the ECMWF web page:

https://confluence.ecmwf.int/display/ECC

Installation: The source code for the ecCodes package can be downloaded from the ECMWF web page.

Please refer to the `README` for installing the ecCodes libraries, which is done with a `configure` script. Check the following settings:

- The ecCodes package can make use of optional JPEG packing of the GRIB records, but this requires the installation of additional libraries. Since the ICON model does not apply this packing algorithm, the support for JPEG can be disabled during the configure step with the option `--disable-jpeg`.
- To use statically linked libraries and binaries you should set the configure option `--enable-shared=no`.

```
./configure --prefix=/your/install/dir   \
            --disable-jpeg --enable-shared=no
```

After the configuration has finished, the ecCodes library can be built with `make` and then `make install`.

GRIB Definition Files

An installation of the ecCodes package always consists of two parts: First, there is the binary compiled library itself with its functions for accessing GRIB files. But, second, there is the *definitions directory* which contains plain-text descriptions of meta data.

GRIB definition files are external text files which constitute a kind of parameter database. They describe the decoding rules and the keys which are used to identify the meteorological fields. For example, these definition files contain information about the variable short name and the corresponding GRIB code triplet.

Example. In contrast to the GRIB triplet, the short name, e.g., “`OMEGA`” for vertical velocity (pressure), is not stored in data files. The definition file therefore constitutes an essential link: If the definition files in two institutes are different from each other it is possible that the same data file shows the record "`OMEGA`" on one site (our DWD system), while the same GRIB record bears the short name "`w`" on the other site (both have the same GRIB triplet `discipline=0,parameterCategory=2,parameterNumber=8`).

DWD-specific definition files. The ICON model accesses its input data by their name ("shortName" key). Therefore the DWD-specific definition files ("EDZW"=DWD Offenbach) are essential for the read-in process. In theory, the above situation could be solved by changing all field names in the ICON name list setup, where possible. However, it is likely that further related errors may follow in the ICON model when this searches for a specific variable name. In this case you might need to change the definition files after all.

The DWD definition files for the ecCodes package can be obtained via

https://opendata.dwd.de/weather/lib/grib/

The new directory needs to be communicated to the ecCodes package at run-time by setting the `ECCODES_DEFINITION_PATH` environment variable[2]:

```
export \
ECCODES_DEFINITION_PATH=/yourpath/definitions.edzw:/yourpath/definitions
```

Here, the `definitions` directory provided by ECMWF is extended by DWD's own installation (`definitions.edzw`). Note that both paths have to be specified in this environment variable, and that `definitions.edzw` has to be the first! The current setting of the definition files path can be displayed with the command-line tool `codes_info`.

Note that for *writing* GRIB2 files, the ICON model does not use DWD-specific shortNames. Therefore, the model output can be written in GRIB2 format without the proper definition files at hand.

1.1.3. Namelist Input for the ICON Model

In general, the ICON model is controlled by a so-called parameter file which uses Fortran NAMELIST syntax. Default values are set for all parameters, so that you only have to specify values that differ from the default.

Assuming that ICON has been compiled successfully, the next step is to adapt these ICON namelists. The run scripts in this tutorial create a file `NAMELIST_NWP` which contains all user-defined namelist parameters, together with some substituted shell script variables. Discussing all available namelist switches is definitely beyond the scope of this tutorial. We will merely focus on the particular subset of namelist switches that is necessary to setup an idealized model run as well as real case runs using the NWP physics package. A complete list of namelist switches can be found in the namelist documentation

```
icon/doc/Namelist_overview.pdf
```

[2]Setting the `GRIB_DEFINITION_PATH` environment variable is still accepted as a fallback by the ecCodes package for backward compatibility reasons.

1.2. Configuring and Compiling the Model Code

This section explains the configuration process of the ICON model. It is assumed that the libraries and programs discussed in Section 1.1.2 are present on your computer system. For convenience, the compiler version and the ecCodes version are documented in the log output of each model run.

1.2.1. Computer Platforms

For a small number of HPC platforms settings are provided with the code, for example

NEC SX-Aurora cluster (Research Cluster Ludwigshafen "rcl.dwd.de")
containing
1856 NEC SX-Autora Tsubasa vector engine CPUs

- 1.584 GHz, double precision peak performance ca. 2.15 TFLOPS,
- 48 GiB HBM2 3D-stacked memory

232 x86 Vector Hosts with 8 Vector Engines attached to each host
AMD EPYC "Rome" (24 cores, 2.8GHz, 256 GiB memory)

MPI:	`NEC MPI 2.6.0`
NetCDF:	Version 4.7.3
Compiler:	NEC Fortran 3.0.8 / gcc v9.1.0

HLRE-3 cluster "Mistral" (DKRZ Hamburg)
1550 compute nodes Intel Haswell (2 CPUs/node, 12 cores/CPU)
1750 compute nodes Intel Broadwell (2 CPUs/node, 18 cores/CPU)

MPI:	`OpenMPI 2.0.2p1-hpcx`
NetCDF:	Version 4.4.3
Compiler:	Intel Fortran compiler `ifort 18.0.5`

Due to the usage of modern Fortran 2003/2008 features, ICON places high demands on the compilers. Please make also sure that a compatible compiler for the C99 routines in the package is available. Both components, the Fortran parts and the C parts use a source pre-processor. Table 1.1 provides a list of compilers which are known to successfully build the recent ICON code. There's a good chance that more recent compiler versions might work as well. However, be aware that this is not necessarily the case. E.g. many of the newer versions of the Cray compiler (`ftn v8.4.1` < *`version`* < `ftn 8.6.0`) might have issues.

Intel `ifort` compiler: When compiling with ifort before version 17.0.1, the default behavior is for the compiler not to use the Fortran rules for automatic allocation on intrinsic assignment. You will need to use an option like `-assume realloc-lhs`.

Fortran Compiler	Working Version
GNU	`gcc` v6.4.0
Cray	`ftn` v8.7.11
Intel	`ifort` v18.0.5
NAG	`nagfor` v6.0.1064
NEC	`nfort` v3.0.8

Table 1.1.: Compiler versions which are known to successfully build the ICON code (state *September 2020*).

MPI and OpenMP. The ICON model supports different modes of parallel execution, see Section 7.4 for details:

- In the first place, ICON has been implemented for distributed memory parallel computers using the *Message Passing Interface* (MPI). MPI is a library specification, proposed as a standard by a broadly based committee of vendors, implementors, and users, see `http://www.mcs.anl.gov/research/projects/mpi`.
- Moreover, on multi-core platforms, the ICON model can run in parallel using *shared-memory parallelism with OpenMP*. The OpenMP API is a portable, scalable technique that gives shared-memory parallel programmers a simple and flexible interface for developing parallel applications on platforms ranging from embedded systems and accelerator devices to multi-core systems and shared-memory systems, see `http://openmp.org`.

Finally, note that although ICON has been implemented for distributed memory parallel computers using the *Message Passing Interface* (MPI), the model can also be installed on sequential computers, where MPI and/or OpenMP are not available. Of course, this execution mode limits the model to rather small problem sizes.

1.2.2. Configuring and Compiling

The process of building ICON consists of two parts: *configuring* the options and compiler flags, and *building* the source code with those options and flags.

The configuration step is normally done by running the `configure` script (which is part of the GNU Autotools) with command-line arguments, which, among other things, tell the script where to locate libraries and tools required for building. Again we refer to the document `README.md` in the root directory of the ICON source code which contains a very detailed description of the configuration process.

The `configure` command scans the build environment and generates an appropriate `Makefile`. The list of arguments enabling a successful configuration might be quite long and difficult to compose, therefore, instead of running the generic `configure` script directly, users are recommended to execute a corresponding platform- or machine-specific configuration wrapper that sets the required compiler and linker flags as well as the recommended set of configure options.

The wrapper scripts can be found in the respective subdirectories of the directory `icon/config`. If your platform is not among the list of presets, or if you need to add a specific compiler or change your compiler flags, you have to set up the appropriate call of the `configure` yourself. Numerous platform-dependent options are allowed. Some more details on configure options can be found in the help of the configure command:

```
./configure --help
```

Be warned that you need some knowledge about Unix / Linux, compilers and Makefiles to make the necessary adjustments w.r.t. the computing environment. If the configuration process fails, take a look at the text file `config.log` that is created during the configuration process. This technical log file may contain hints on which particular library has been found missing.

The building stage is done with GNU `make` upon successful completion of the configuration stage. On most machines you can also compile the routines in parallel by using the GNU-make with the command `gmake -j` *np*, where *np* gives the number of processors to use (*np* typically about 8).

If you wish to re-configure ICON it is advisable first to clean the old setup by giving:

```
make distclean
```

Example: Configuration and build process for the NEC SX-Aurora. The NEC platform represents a special case in the sense that two separate ICON binaries are created, which will be simultaneously executed on the x86 hosts nodes and the vector engines.

It is advisable to create a `build` subdirectory which will contain the binaries for your computer architecture. The building system of ICON supports so-called *out-of-source builds*. This means that you can build ICON in a directory other than the source root directory. The main advantage of this is that you can easily switch between several different configurations and compilers later (each in its own build directory), while working on the same source code. For the case of the NEC SX-Aurora, we will have different builds for the x86 hosts nodes and the vector engines.

In order to start the compilation process, please log into the NEC SX-Aurora cross-compilation node `rcl` and change into the subdirectory `icon`. Please type:

```
mkdir -p build/VE,VH

cd build/VE
../../config/dwd/rcl.VE.nfort-3.0.8
make -j4

cd ../../build/VH
../../config/dwd/rcl.VH.gcc-9.1.0
make -j4
```

Pre-compiled Binaries: Users of the NEC SX-Aurora system may find recent pre-compiled binaries in the following subdirectory `$NWP_BIN`. Note that the `nwp` module needs to be pre-loaded.

Users of the ECMWF system may find recent pre-compiled binaries in the following subdirectory:

```
/sc1/home/zde/routfox/abs
```

1.3. The DWD ICON Tools

1.3.1. General Overview

The DWD ICON Tools provide a number of utilities for the pre- and post-processing of ICON model runs. All of these tools can run in parallel on multi-core systems (OpenMP) and some offer an MPI-parallel execution mode in addition. The DWD ICON utilities use the ecCodes package for reading data in GRIB2 format. The ecCodes package is indirectly accessed by the Climate Data Interface (CDI).

The directory structure of the DWD ICON tools is shown in Fig. 1.2. We give a short overview over several tools in the following and refer to the documentation Prill (2020) for details.

ICONGRIDGEN – Used in Section 2.1.5

The `icongridgen` tool is a simple grid generator. It creates icosahedral grids from scratch, which can be fed into the ICON model. Alternatively, an existing global or local grid file is taken as input and parts of this input grid (or the whole grid) are refined via bisection. No storage of global grids is necessary and the tool also provides an HTML plot of the grid. The grid generator provides the basis for the DWD grid generator web tool under `https://webservice.dwd.de/cgi-bin/spp1167/webservice.cgi`.

ICONREMAP – Used in Sections 2.2.3, 2.3

The `iconremap` utility is especially important for pre-processing the initial data for the basic test setups in this manuscript. `iconremap` (*ICO*sahedral *N*onhydrostatic model *REMAP*ping) is a utility program for horizontally interpolating ICON data onto regular grids and vice versa. Besides, it offers the possibility to interpolate between triangular grids of different grid spacing.

The `iconremap` tool reads and writes data files in GRIB2 or NetCDF file format. For triangular grids an additional grid file in NetCDF format must be provided.

Several interpolation algorithms are available: Nearest-neighbor remapping, radial basis function (RBF) approximation of scalar fields, area-weighted formula for scalar fields, RBF

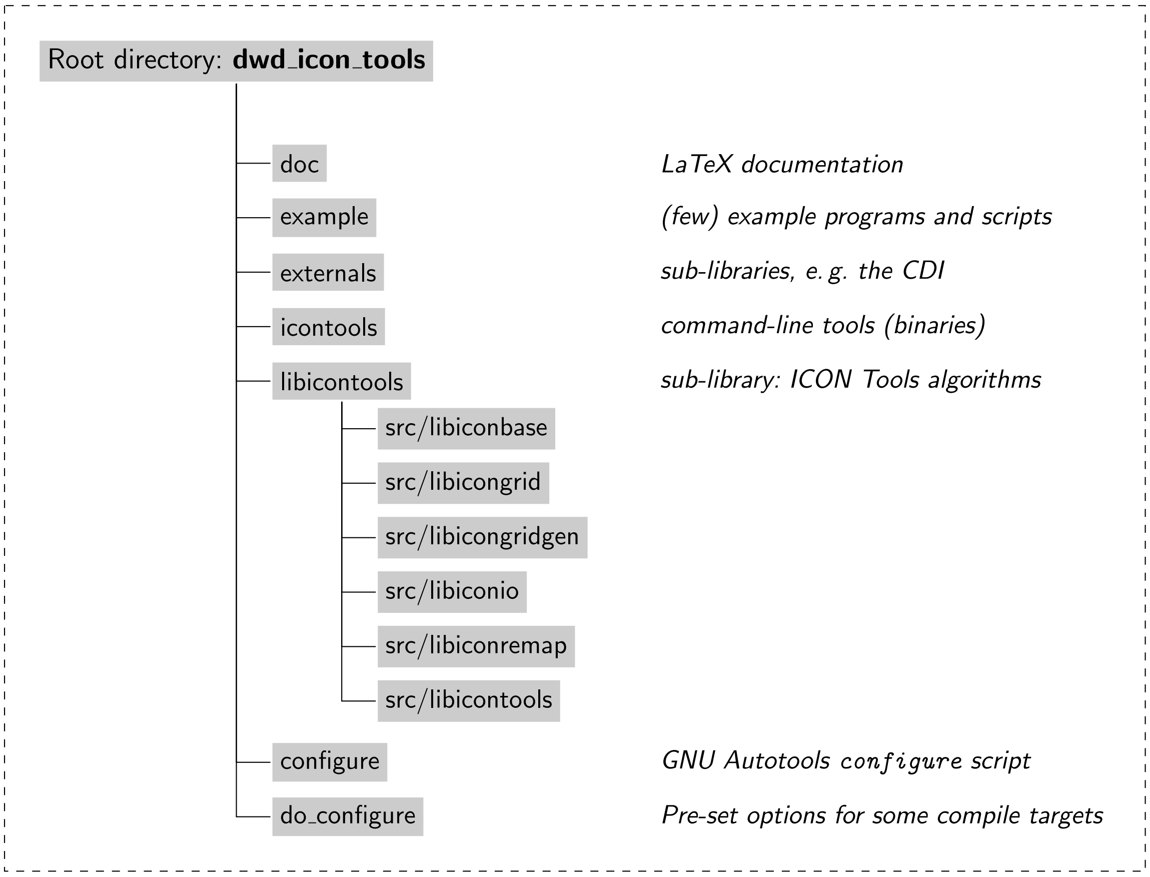
Root directory: dwd_icon_tools
doc
LaTeX documentation
example
(few) example programs and scripts
externals
sub-libraries, e. g. the CDI
icontools
command-line tools (binaries)
libicontools
sub-library: ICON Tools algorithms
src/libiconbase
src/libicongrid
src/libicongridgen
src/libiconio
src/libiconremap
src/libicontools
configure
GNU Autotools configure script
do_configure
Pre-set options for some compile targets

Figure 1.2.: Directory structure of the DWD ICON tools, which are distributed in the separate tarball `icontools-2.4.12.tar.gz`. Only the most relevant important directories are shown.

interpolation for wind fields from cell-centered zonal, meridional wind components `u`, `v` to normal and tangential wind components at edge midpoints of ICON triangular grids (and reverse), and barycentric interpolation. For more remarks on the available interpolation methods, see Section 7.1.2.

> Note that `iconremap` only performs a *horizontal* remapping, while the vertical interpolation onto the model levels of ICON is handled by the model itself.

ICONSUB – Used in Section 2.3

The `iconsub` tool (*ICO*sahedral *N*onhydrostatic model *SUB*grid extraction) allows "cutting" sub-areas out of ICON data sets.

After reading a data set on an unstructured ICON grid in GRIB2 or NetCDF file format, the tool comprises the following functionality: It may 'cut out" a subset, specified by two corners and a rotation pole (similar to the COSMO model). Alternatively, a boundary region of a local ICON grid, specified by parent-child relations, may be extracted. This execution mode is especially important for the setup of the limited area model ICON-LAM.

Multiple sub-areas can be extracted in a single run of `iconsub`. Finally, the extracted data is stored in GRIB2- or NetCDF file format.

ICONGPI

The `icongpi` tool (*ICO*sahedral *N*onhydrostatic model *G*rid *P*oint *I*nformation) is a utility program for searching / accessing individual grid points of an ICON grid. It can be used to determine cells in a triangular grid corresponding to a given geographical position and to determine the geographical position for a given cell index.

ICONDELAUNAY – see Section 7.1.2

The `icondelaunay` tool processes existing ICON grid files. It appends a Delaunay triangulation of the cell circumcenters to the grid file. This auxiliary triangulation can then be used for interpolation purposes.

1.3.2. Configuring and Compiling the DWD ICON Tools

To compile the DWD ICON Tools binaries, log into the Linux cluster node `rclh`[3] for NEC SX-Aurora cross-compilation and change into the base directory:

```
cd dwd_icon_tools
```

This directory contains a GNU Autotools `configure` script which, when run, scans the build environment and generates a `Makefile` appropriate for that build environment.

The `configure` expects numerous platform-dependent options which can be listed by the command `configure --help`.

After the configuration has finished, the binary can be created by typing

```
make
```

List of pre-configured platforms: Pre-set options for a short list of available compile targets are contained in the `do_configure.sh` auxiliary script.

[3]Note that `rclh` serves as an alias for one of the Linux cluster nodes `rcnl*`.

Hostname	Target description
`oflws*`	Generic Linux platform without MPI support; compiled with the `gcc` compiler.
`lc*`	Cray Linux Cluster (DWD) with MPI support; compiled with the Intel compiler.
`xc*`	Cray XC40 (DWD) with MPI support; compiled with the Cray compiler.
`rcnl*`	Current DWD Linux cluster.
`rcnl*`	cross compilation for DWD NEC SX-Aurora vector host with MPI support.
`mlogin*`	DKRZ "mistral" Linux cluster (Intel compiler with MPI support).
`cca-*`	ECMWF CCA cluster.
`daint*`	compilation for CSCS Daint cluster.

The `oflw*` target in the `do_configure.sh` helper script is related to a more or less generic Linux workstation but probably requires adaptation.

In the following, we list the invocation of the `do_configure.sh` helper script in detail:

DWD, `rcnl`: Cross compilation for NEC vector hosts

```
module purge && \
module load sx/default apps gcc/9.1.0 mpi/2.3.1 \
            netcdf4/4.7.3-VH-gnu hdf5/1.10.5-VH-gnu \
            eccodes/2.14.1-VH-gnu aec/1.0.3-VH-gnu \
            szip/2.1.1-VH-gnu
./do_configure.sh
```

DWD, `rcnl`: Compilation for Linux cluster with GNU compiler (without MPI)

```
module purge && \
module load x86/default apps gcc/9.1.0 \
            netcdf4/4.7.3-x86-gnu hdf5/1.10.5-x86-gnu \
            eccodes/2.14.1-x86-gnu aec/1.0.3-x86-gnu \
            szip/2.1.1-x86-gnu
target=rcl ./do_configure.sh
```

DKRZ, `mlogin`: Compilation for "mistral"

```
module purge && \
module load gcc/6.4.0 openmpi/2.0.2p2_hpcx-gcc64
./do_configure.sh
```

2. Necessary Input Data

Before anything else, preparation is the key to success.

Alexander Graham Bell

Besides the source code of the ICON package and the technical libraries, several data files are needed to perform runs of the ICON model. There are four categories of necessary data: Horizontal grid files, external parameters, and data describing the initial state (DWD analysis or ECMWF IFS data). Finally, running ICON in limited-area mode in addition requires accurate boundary conditions sampled at regular time intervals.

2.1. Horizontal Grids

In order to run ICON, it is necessary to load the horizontal grid information as an input parameter. This information is stored within so-called grid files. For an ICON run, at least one global grid is required. For model runs with nested domains, additional grids are necessary. Optionally, a reduced radiation grid for the global domain may be used (see Section 3.10).

The following nomenclature has been established: In general, by RnBk we denote a grid that originates from an icosahedron whose edges have been initially divided into n parts, followed by k subsequent edge bisections. See Figure 2.1 for an illustration of the grid creation process. The total number of cells in a global ICON grid RnBk is given by $n_{\text{cells}} := 20\, n^2\, 4^k$. The cell circumcenters serve as data sites for most ICON variables. As an exception, the orthogonal normal wind is given at the midpoints of the triangle edges and is measured orthogonal to the edges.

The effective mesh size can be estimated as

$$\overline{\Delta x} \approx 5050/(n\, 2^k)\ [\text{km}]\,. \tag{2.1}$$

This formula is motivated as follows:

The average triangle area is calculated from the surface of the Earth divided by the number of triangles of the grid. Then, we imagine a square with the same area and define its edge length as the effective mesh size of the triangular grid. This results in

$$\overline{\Delta x} = \sqrt{S_{\text{earth}}/n_{\text{cells}}} = \sqrt{\frac{4\, R_{\text{earth}}^2\, \pi}{n_{\text{cells}}}} = \frac{R_{\text{earth}}}{n\, 2^k}\sqrt{\frac{\pi}{5}} \approx 5050/(n\, 2^k)\ [\text{km}]\,,$$

where S_{earth} and R_{earth} define the Earth's surface and radius, respectively.

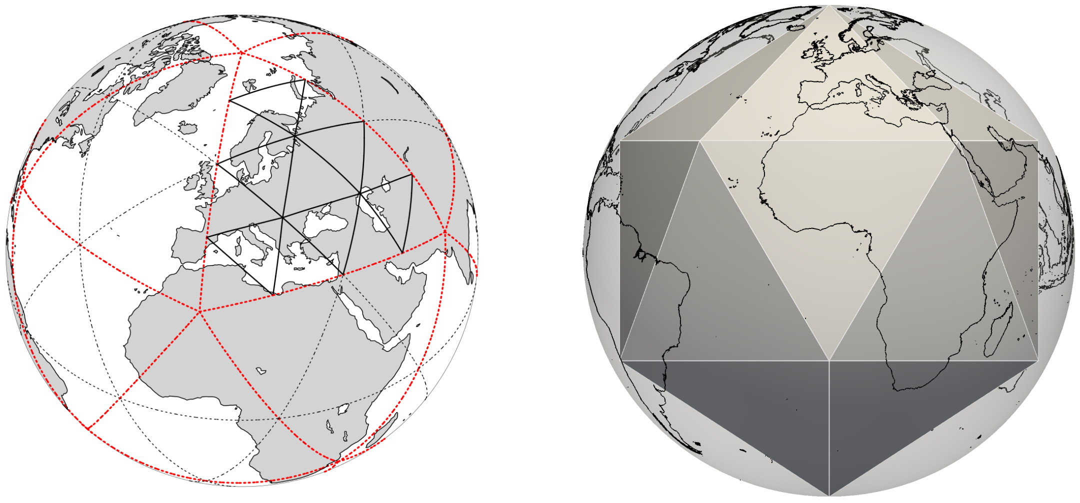

Figure 2.1.: *Left:* Illustration of the grid construction procedure. The original spherical icosahedron is shown in red, denoted as R*1*B*00* following the nomenclature described in the text. In this example, the initial division (n=2; black dotted), followed by one edge bisection (k=1) yields an R*2*B*01* grid (solid lines). *Right:* Graphical representation of the 12 pentagon points. Here, the base icosahedron is rotated exactly like the DWD operational grids.

Pentagon Points

Note that by construction, each vertex of a global grid is adjacent to exactly 6 triangular cells, with the exception of the original vertices of the icosahedron, the *pentagon points*, which are adjacent to only 5 cells.

The grids used in production at DWD have their pentagon points located at the following longitude/latitude positions (in degrees):

$$(-180, \pm 90), (0, -m), (-180, m), (\pm 36, m), (\pm 72, -m), (\pm 108, m), (\pm 144, -m)$$

where the constant m is derived from the golden ratio $\phi := \frac{1+\sqrt{5}}{2}$ as

$$m := 90 - \frac{180}{\pi} \operatorname{atan}\left(\frac{\sqrt{1+\phi^2+\phi^4}}{\phi}\right) \approx 26.565\,[\text{degrees}].$$

See Fig. 2.1 for a graphical representation of the pentagon points.

Cell Neighborhoods

Apart from areas with pentagon cells, the number of cells in an area covered by a central cell and N_r rings of cells around the central cell is

$$N_c(N_r) = 1 + 12 \sum\nolimits_{r=1}^{N_r} r = 6\, N_r(N_r+1) + 1\,.$$

Then $N_c(1) = 13$, $N_c(2) = 37$, $N_c(3) = 73$, …

Proof by mathematical induction. For the inductive step it is convenient to visualize all cells organized in horizontal rows. If the statement holds for N_r then we need to count the number of additional steps for $N_r + 1$: We have $2\,N_r + 1$ horizontal cell rows in the area covered by N_r. Therefore we get $4\,(2\,N_r + 1)$ new cells in these horizontal cell rows. Furthermore, we have two additional horizontal cell rows, containing $2(N_r + 1) + 1$ cells and $2(N_r + 2) + 1$ cells. In total we get the following number of new cells:

$$4\,(2\,N_r + 1) + 2\,(N_r + 1) + 1 + 2\,(N_r + 2) + 1 = 12\,(N_r + 1)\,.$$

This is $N_c(N_r + 1) - N_c(N_r)$ from the formula above. □

Dual Hexagonal Grid

The centers of the equilateral triangles contained in each triangle of the original icosahedron after triangulation are defined by the intersection of the angle bisectors (which are at the same time also altitudes) of the triangle. The centers of the triangles form a hexagonal grid that is called to be dual to the grid of triangle vertices. On the ICON grid, the centers of the slightly distorted triangles form a dual grid of slightly distorted hexagons.

Spring Dynamics Optimization

This grid on the sphere is optimized in a next step by so-called *spring dynamics*. We give the idea of the optimization only and refer to Tomita et al. (2002) for an in-depth description of the algorithm.

Imagine that we have a collection of springs all of them of the same strength and length. First, we attach a mass to each triangle vertex and fix it with glue on the circumscribed sphere. We replace each edge by one of the springs. Depending on the actual length of the edge, we have to tension some springs a bit more for the larger triangles, less for smaller ones. Now, the glue is melted away and the vertices move until an equilibrium is reached provided that there is some friction of the mass points on the sphere.

By this procedure, we will obtain a slightly different grid of triangles which are still slightly distorted and of unequal size, however, the vertices reached positions that reflect some "energy minimum". These triangles are the basis of the ICON horizontal grid. Such a grid has particularly advantageous numeric properties. The North and South Pole of the Earth are chosen to be located at two vertices of the icosahedron that are opposite to each other.

2.1.1. ICON Grid Files

The unstructured triangular ICON grid resulting from the grid generation process is represented in NetCDF format. This file stores coordinates and topological index relations between cells, edges and vertices.

The most important data entries of the main grid file are

- `cell` (INTEGER dimension)
  number of (triangular) cells

- `vertex` (INTEGER dimension)
  number of triangle vertices
- `edge` (INTEGER dimension)
  number of triangle edges
- `clon`, `clat` (double array, dimension: #triangles, given in radians)
  longitude/latitude of the midpoints of triangle circumcenters
- `vlon`, `vlat` (double array, dimension: #triangle vertices, given in radians)
  longitude/latitude of the triangle vertices
- `elon`, `elat` (double array, dimension: #triangle edges, given in radians)
  longitude/latitude of the edge midpoints
- `cell_area` (double array, dimension: #triangles)
  triangle areas
- `vertex_of_cell` (INTEGER array, dimensions: [3, #triangles])
  The indices `vertex_of_cell(:,i)` denote the vertices that belong to the triangle `i`. The `vertex_of_cell` index array is ordered counter-clockwise for each cell.
- `edge_of_cell` (INTEGER array, dimensions: [3, #triangles])
  The indices `edge_of_cell(:,i)` denote the edges that belong to the triangle `i`.
- `clon/clat_vertices` (double array, dimensions: [#triangles, 3], given in radians)
  `clon/clat_vertices(i,:)` contains the longitudes/latitudes of the vertices that belong to the triangle `i`.
- `neighbor_cell_index` (INTEGER array, dimensions: [3, #triangles])
  The indices `neighbor_cell_index(:,i)` denote the cells that are adjacent to the triangle `i`.
- `zonal/meridional_normal_primal_edge`: (INTEGER array, #triangle edges)
  components of the normal vector at the triangle edge midpoints. Note that the edge's primal normal must not be mixed up with a primal cell's outer normal.
- `adjacent_cell_of_edge`: (INTEGER array, [2, #triangle edges])
  For cells i_1, i_2 adjacent to a given edge i, moving from i_1 to i_2 follows the direction of the edge's primal normal.
- `zonal/meridional_normal_dual_edge`: (INTEGER array, #triangle edges)
  These arrays contain the components of the normal vector at the facets of the dual control volume.
  Note that each facet corresponds to a triangle edge and that the dual normal matches the direction of the primal tangent vector but signs can be different.
- `uuidOfHGrid` (global attribute)
  Grid fingerprint (see Section 2.1.8).

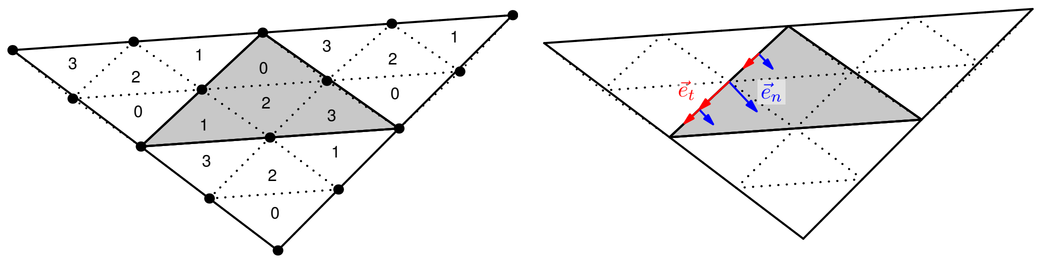

Figure 2.2.: Illustration of the parent-child relationship in refined grids. *Left:* Triangle subdivision and local cell indices. *Right:* The grids fulfill the ICON requirement of a right-handed coordinate system $[\vec{e}_t, \vec{e}_n, \vec{e}_w]$. Note: the primal tangent and the dual cell normal are aligned but do not necessarily coincide!

2.1.2. ICON "Nests"

ICON has the capability for running

- global simulations on a single grid,
- limited area simulations (see Chapter 6), and
- global or limited-area simulations with refined nests (so called patches or domains).

For the subtle difference between nested and limited-area setups the reader is referred to Section 6.1. Section 3.9.1 explains the exchange of information between the domains.

Additional topological information is required for ICON's refined nests: Each "parent" triangle is split into four "child" cells, and each parent edge is split into two child edges. In the grid file only child-to-parent relations are stored while the parent-to-child relations are computed in the model setup. The local numbering of the four child cells (see Fig. 2.2) is also computed in the model setup.

The refinement information is stored in the following data entries of the grid file:

- `uuidOfParHGrid` (global attribute)
  Fingerprint of the parent grid (see Section 2.1.8). If your grid does not contain the `uuidOfParHGrid` global attribute, then you'll need the namelist parameter `dynamics_parent_grid_id`, see below.
- `parent_cell_index` (INTEGER array, dimension: #triangles)
  Global index of coarser parent triangle in the parent grid.
- `parent_edge_index` (INTEGER array, dimension: #triangle edges)
  Global index of parent edge (with double length) in the parent grid.
- `parent_vertex_index` (INTEGER array, dimension: #triangle vertices)
  Global index of parent vertex in the parent grid.

Since the grids of the different refinement levels are stored in separate files, the usual way to establish a parent-child relationship between these grids is to read the header information from the list of provided grid files, see Section 4.1.2. Then, the parent-child relationships can be inferred from the NetCDF attributes `uuidOfHGrid` and `uuidOfParHGrid`.

However, there are still older grid files in circulation which do not contain these descriptive attributes. In this case there is no other possibility than defining the parent-child relationship by a namelist parameter.

`dynamics_parent_grid_id` (namelist `grid_nml`, list of INTEGER values)

This parameter array is closely related to the namelist parameter `dynamics_grid_filename`. The `i`th entry of `dynamics_parent_grid_id` contains the index of the parent grid of domain `i`. Indices start at 1, an index of 0 indicates *no parent*.

For older grid files that are still in circulation, the refinement information may be provided in a separate file (suffix `-grfinfo.nc`), which happens to be the case especially for legacy data sets. This optional *grid connectivity* file acts as a fallback at model startup if the expected information is not found in the main grid file.

Finally, note that the data points on the triangular grid are the cell circumcenters. Therefore the global grid data points are located closely to nest data points, but they *do not coincide* exactly.

2.1.3. Mapping of Geodesic Coordinates to the Sphere

Usually, geographic coordinate data is given with respect to an ellipsoidal reference system. The WGS84 ellipsoid, for example, is given by the following semi-major and minor axes:

$$a := 6.378137 \cdot 10^6 \text{ m} , \qquad b := 6.356752314245 \cdot 10^6 \text{ m}$$

Input data usually refers to the *geographic (geodetic) latitude* of this ellipsoid, which is the angle that a line perpendicular to the surface of the ellipsoid at the given point makes with the plane of the Equator, see the blue line in Fig. 2.3. It must not be confused with the geocentric latitude (red in Fig. 2.3), which is the angle made by a line to the center of the ellipsoid with the equatorial plane, see Snyder (1987). A post-processing tool that misinterprets geocentric and geographic latitudes will notice a shift of up to 22 km.

The ICON model, however, uses a *spherical* approximation with an earth radius of

$$r_e = 6.371229 \cdot 10^6 \text{ m}.$$

Generally speaking, a mapping rule needs to be defined between the ellipsoid and the sphere. For the ICON model this mapping is prescribed by the ExtPar tool which pre-processes numerous invariant parameter fields, e. g. the topography, the land-sea mask, the soil type and atmospheric aerosols. The ExtPar data set will be in detail described in Section 2.4.

Here, the important fact is that the ExtPar tool re-interprets coordinates with a trivial mapping rule, i. e. WGS84 latitudes are directly applied without transformation to the sphere.

This definition must be kept consistent for all pre-processing parts of the model (grids, namelists, etc.): For example, when the user specifies meteogram locations, he usually

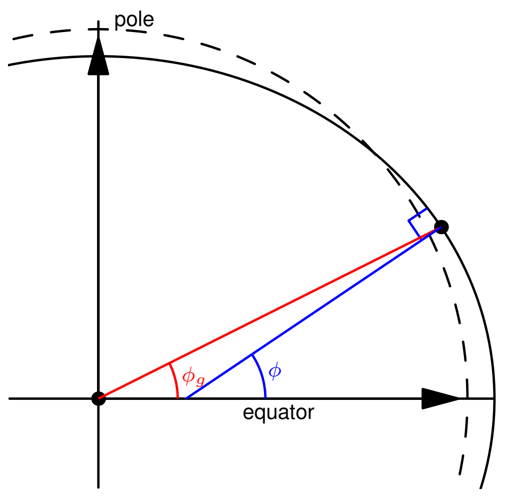

Figure 2.3.: Illustration of an ellipsoid with geodetic (geographic) latitude ϕ and geocentric latitude ϕ_g. The dashed line shows a spherical surface for comparison.

applies a mapping from ellipsoidal to spherical coordinates, often without realizing this transformation. For ICON, however, the user must provide WGS84 coordinates to comply with the calculation rule of the ExtPar tool. The same argument holds for point source locations, geometric tracks, the center and corner locations of a grid, etc.

2.1.4. Download of Predefined Grids

For fixed domain sizes and resolutions a list of grid files has been pre-built for the ICON model together with the corresponding reduced radiation grids and the external parameters.

The contents of the primary storage directory are regularly mirrored to a public web site for download, see Figure 2.4 for a screenshot of the ICON grid file server. The download server can be accessed via

`http://icon-downloads.mpimet.mpg.de`

The pre-defined grids are identified by a *centre number*, a *subcentre number* and a *numberOfGridUsed*, the latter being simply an integer number, increased by one with every new grid that is registered in the download list. Also contained in the download list is a tree-like illustration which provides information on parent-child relationships between global and local grids, and global and radiation grids, respectively.

Note that the grid information of some of the older grids (no. 23 – 40) is split over two files: The user needs to download the main grid file itself *and* a *grid connectivity* file (suffix `-grfinfo.nc`).

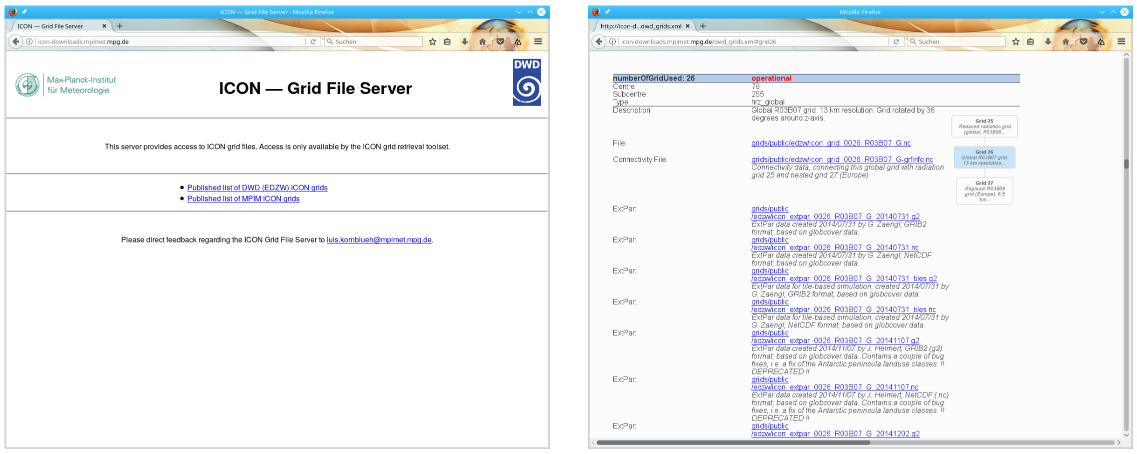
ICON — Grid File Server - Mozilla Firefox
ICON — Grid File Server
icon-downloads.mpimet.mpg.de
Suchen
Max-Planck-Institut für Meteorologie
DWD
Mozilla Firefox
http://icon-d...dwd_grids.xml
icon-downloads.mpimet.mpg.de/dwd_grids.xml#grid26
Grid 25
Reduced radiation grid (global, R03B06...
Grid 26
Global R03B07 grid. 13 km resolution....
Grid 27
Regional R03B08 grid (Europe). 6.5 km...

ICON — Grid File Server

This server provides access to ICON grid files. Access is only available by the ICON grid retrieval toolset.

- Published list of DWD (EDZW) ICON grids
- Published list of MPIM ICON grids

Please direct feedback regarding the ICON Grid File Server to luis.kornblueh@mpimet.mpg.de.

```
numberOfGridUsed: 26      operational
Centre                    78
Subcentre                 255
Type                      hrz_global
Description:              Global R03B07 grid. 13 km resolution. Grid rotated by 36
                          degrees around z-axis.

File:                     grids/public/edzw/icon_grid_0026_R03B07_G.nc

Connectivity File:        grids/public/edzw/icon_grid_0026_R03B07_G-grfinfo.nc
                          Connectivity data, connecting this global grid with radiation
                          grid 25 and nested grid 27 (Europe).

ExtPar:                   grids/public
                          /edzw/icon_extpar_0026_R03B07_G_20140731.g2
                          ExtPar data created 2014/07/31 by G. Zaengl; GRIB2
                          format; based on globcover data.
ExtPar:                   grids/public
                          /edzw/icon_extpar_0026_R03B07_G_20140731.nc
                          ExtPar data created 2014/07/31 by G. Zaengl; NetCDF
                          format; based on globcover data.
ExtPar:                   grids/public
                          /edzw/icon_extpar_0026_R03B07_G_20140731_tiles.g2
                          ExtPar data for tile-based simulation, created 2014/07/31 by
                          G. Zaengl; GRIB2 format; based on globcover data.
ExtPar:                   grids/public
                          /edzw/icon_extpar_0026_R03B07_G_20140731_tiles.nc
                          ExtPar data for tile-based simulation, created 2014/07/31 by
                          G. Zaengl; NetCDF format; based on globcover data.
ExtPar:                   grids/public
                          /edzw/icon_extpar_0026_R03B07_G_20141107.g2
                          ExtPar data created 2014/11/07 by J. Helmert; GRIB2 (g2)
                          format; based on globcover data. Contains a couple of bug
                          fixes, i.e. a fix of the Antarctic peninsula landuse classes. !!
                          DEPRECATED !!
ExtPar:                   grids/public
                          /edzw/icon_extpar_0026_R03B07_G_20141107.nc
                          ExtPar data created 2014/11/07 by J. Helmert; NetCDF (.nc)
                          format; based on globcover data. Contains a couple of bug
                          fixes, i.e. a fix of the Antarctic peninsula landuse classes. !!
                          DEPRECATED !!
ExtPar:                   grids/public
                          /edzw/icon_extpar_0026_R03B07_G_20141202.g2
```

Figure 2.4.: Screenshots of the ICON download server hosted by the Max Planck Institute for Meteorology in Hamburg.

2.1.5. Grid Generator: Invocation from the Command Line

There are (at least) three grid generation tools available for the ICON model: One grid generation tool has been developed at the Max Planck Institute for Meteorology by L. Linardakis[1]. Second, in former releases, the ICON model itself was shipped together with a standalone tool `grid_command`. This program has finally been replaced by another grid generator which is contained in the DWD ICON Tools.

In this section we will discuss the grid generator `icongridgen` that is contained in the DWD ICON Tools, because this utility also acts as the backend for the publicly available web tool. The latter is shortly described in Section 2.1.6. It is important to note, however, that this grid generator is not capable of generating non-spherical geometries like torus grids, see Section 2.1.9.

Minimum version required: Grid files that have been generated by the `icongridgen` tool contain only child-to-parent relations while the parent-to-child relations are computed in the model setup. Therefore these grids only work with ICON versions newer than ~ September 2016.

Grid Generator Namelist Settings

The DWD ICON Tools utility `icongridgen` is mainly controlled using a Fortran namelist.

The command-line option that is used to provide the name of this file and other available settings are summarized via typing

```
icongridgen --help
```

[1]see the repository `https://code.mpimet.mpg.de/projects/icon-grid-generator`.

The Fortran namelist `gridgen_nml` contains the filename of the parent grid which is to be refined and the grid specification is set for each child domain independently. For example (COSMO-EU nest) the settings are

```
dom(1)%region_type  = 3
dom(1)%lrotate      = .true.
dom(1)%hwidth_lon   =   20.75
dom(1)%hwidth_lat   =   20.50
dom(1)%center_lon   =    2.75
dom(1)%center_lat   =    0.50
dom(1)%pole_lon     = -170.00
dom(1)%pole_lat     =   40.00
```

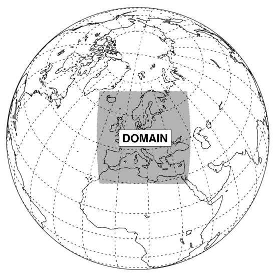

For a complete list of available namelist parameters we refer to the documentation (Prill (2020)).

The `icongridgen` grid generator checks for overlap with concurrent refinement regions, i.e. no cells are refined which are neighbors or neighbors-of-neighbors (more precisely: vertex-neighbor cells) of parent cells of another grid nest on the same refinement level. Grid cells which violate this distance rule are "cut out" from the refinement region. Thus, there is at least one triangle between concurrent regions.

Minimum distance between child nest boundary and parent boundary: A second, less well-known constraint sometimes leads to unexpected (or even empty) result grids: In the case that the parent grid itself is a bounded regional grid, no cells can be refined that are part of the indexing region (of width `bdy_indexing_depth`) in the vicinity of the parent grid's boundary.

Settings for ICON-LAM

When the grid generator `icongridgen` is targeted at a limited area setup (for ICON-LAM), two important namelist settings must be considered:

- *Identifying the grid boundary zone.* In Section 2.3 we will describe how to drive the ICON limited area model. Creating the appropriate boundary data makes the identification of a sufficiently large boundary zone necessary.

  This indexing is enabled through the following namelist setting in `gridgen_nml`: `bdy_indexing_depth = 14`.

  This means that 14 cell rows starting from the nest boundary are marked and can be identified in the ICON-LAM setup, which is described in Section 2.3. See Fig. 2.12 for an illustration of such a boundary zone.

- *Generation of a coarse-resolution radiation grid* (see Section 3.10 for details).

  The creation of a separate (local) parent grid with suffix `*.parent.nc` is enabled through the following namelist setting in `gridgen_nml`:

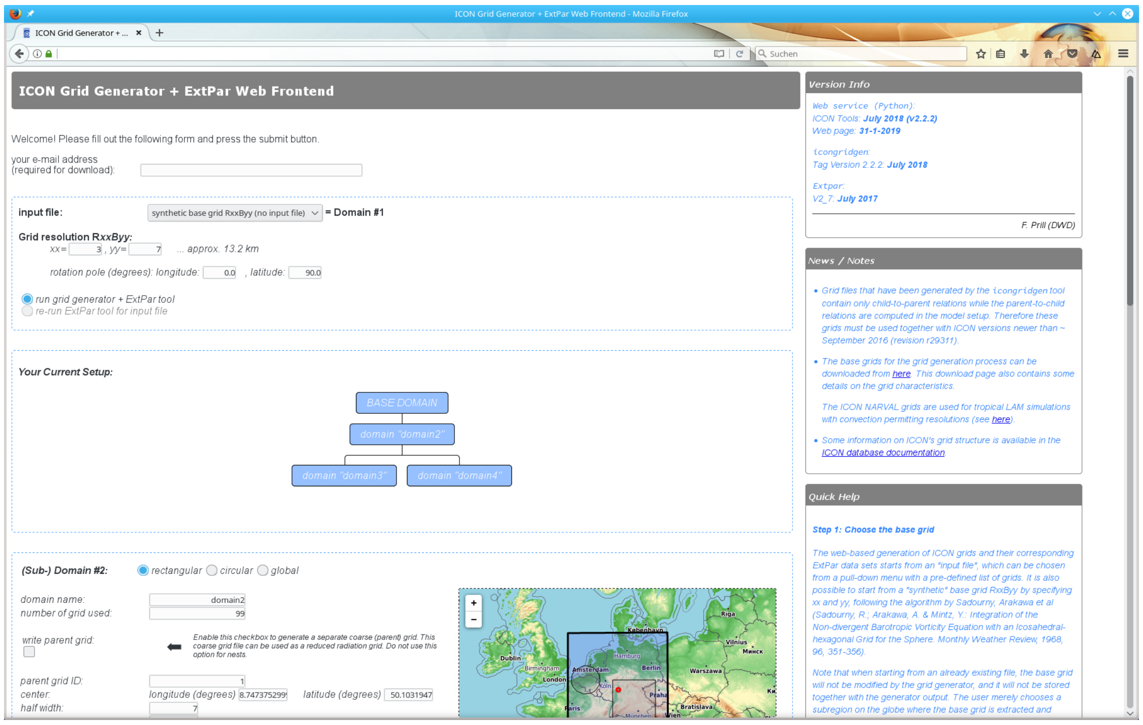

ICON Grid Generator + ExtPar Web Frontend - Mozilla Firefox

ICON Grid Generator + ExtPar Web Frontend

Welcome! Please fill out the following form and press the submit button.

your e-mail address
(required for download):

input file: synthetic base grid RxxByy (no input file) **= Domain #1**

Grid resolution R*xx*B*yy*:
xx= 3 *, yy=* 7 *... approx. 13.2 km*

rotation pole (degrees): longitude: 0.0 *, latitude:* 90.0

[✓ *run grid generator + ExtPar tool*]
re-run ExtPar tool for input file

Your Current Setup:

(Sub-) Domain #2: [✓ *rectangular*] *circular* *global*

domain name: domain2
number of grid used: 99

write parent grid: ☐

Enable this checkbox to generate a separate coarse (parent) grid. This coarse grid file can be used as a reduced radiation grid. Do not use this option for nests.

parent grid ID: 1
center: *longitude (degrees)* 8.747375299 *latitude (degrees)* 50.1031947
half width: 7

Version Info

Web service (Python):
ICON Tools: ***July 2018 (v2.2.2)***
Web page: ***31-1-2019***

icongridgen:
Tag Version 2.2.2: ***July 2018***

Extpar:
V2_7: ***July 2017***

F. Prill (DWD)

News / Notes

- *Grid files that have been generated by the icongridgen tool contain only child-to-parent relations while the parent-to-child relations are computed in the model setup. Therefore these grids must be used together with ICON versions newer than ~ September 2016 (revision r29311).*
- *The base grids for the grid generation process can be downloaded from here. This download page also contains some details on the grid characteristics.*

  The ICON NARVAL grids are used for tropical LAM simulations with convection permitting resolutions (see here).
- *Some information on ICON's grid structure is available in the ICON database documentation.*

Quick Help

Step 1: Choose the base grid

The web-based generation of ICON grids and their corresponding ExtPar data sets starts from an "input file", which can be chosen from a pull-down menu with a pre-defined list of grids. It is also possible to start from a "synthetic" base grid RxxByy by specifying xx and yy, following the algorithm by Sadourny, Arakawa et al (Sadourny, R.; Arakawa, A. & Mintz, Y.: Integration of the Non-divergent Barotropic Vorticity Equation with an Icosahedral-hexagonal Grid for the Sphere. Monthly Weather Review, 1968, 96, 351-356).

Note that when starting from an already existing file, the base grid will not be modified by the grid generator, and it will not be stored together with the generator output. The user merely chooses a subregion on the globe where the base grid is extracted and

Figure 2.5.: Web browser screenshot of the web-based ICON grid generator tool.

```
dom(:)%lwrite_parent = .TRUE.
```

Note that a grid whose child-to-parent indices are occupied by such a coarse grid can no longer be used in a standard feedback-loop together with a global grid.

2.1.6. Grid Generator: Invocation via the Web Interface

A web service has been made available to help users with the generation of custom grid files. After entering grid coordinates through an online form, this web service creates a corresponding ICON grid file together with the necessary external parameter file.

You will need to log in via the user `icon-web`. For the necessary login password – or if you have trouble accessing the web service – please contact `icon@dwd.de`. Then, visit the web page of the grid generator

`https://webservice.dwd.de/cgi-bin/spp1167/webservice.cgi`

The web form is more or less self-explanatory. The settings reflect the namelist parameters of the `icongridgen` grid generator tool that runs as the first stage of the web service. These are explained in the following. The second stage, the ExtPar tool, does not require further settings.

The tool is capable of generating multiple grid files at once. **Please note that the web-based grid generation submits a batch job to DWD's HPC system and takes**

some time for processing! Due to limited computing resources a threshold is imposed: the maximum grid size which can be generated is 3 000 000 cells. Of course, larger grid sizes are allowed when invoking the grid generator from the command line.

Finally all results (and log files) are packed together into a $*$`.tar.gz` archive and the user is informed via e-mail about its FTP download site. Additionally, a web browser visualization of the grids based on *OpenStreetMap* is provided, see Fig. 2.5.

Step 1: Choosing the Base Grid

The web-based generation of ICON grids and their corresponding external parameter (ExtPar) data sets starts from an "input file", which can be chosen from a pull-down menu with a pre-defined list of grids. These grids are identical to those of the download list described in Section 2.1.4.

It is also possible to start from a "synthetic" base grid RnBk by specifying n and k, following the algorithm by Sadourny et al. (1968), see p. 19. Optionally, the location of the grid's pentagon points may be adjusted by a rotation of the base icosahedron, see also Section 2.1.

Note that when starting from an already existing file, the base grid will not be modified by the grid generator, and it will not be stored together with the generator output. The user merely chooses a sub-region on the globe where the base grid is extracted. If, additionally, the subgrid is refined, it will have half of the grid size of the base grid.

Step 2: Specify Global Options

A number of options will be applied to all produced data sets ("global options"):

- **"centre", "subcentre"**
  These numbers are stored in the output meta-data section for the identification of the originating / generating (sub)-center. The values are defined by the WMO, e.g. DWD: 78/0 (see WMO's `Common Code Table C-11` for additional values).
- **"spring dynamics optimization"**
  The ICON grids are based on the spherical icosahedron, but they are post-processed by an iterative algorithm inspired by elastostatics, see the explanation on "spring dynamics optimization" in Section 2.1.
  - **"max. number of iterations"**
    maximum number of pseudo-time stepping steps of the elastostatics model.
  - **"beta factor"**
    stiffness coefficient of the elastostatics model.
  - **"fixed lateral boundary"**
    If this checkbox is set, then the boundary vertices of regional grids are not moved during the optimization. Thus they will still coincide with vertices of the base grid.

Recommended: Do not alter the default settings unless you know the details of the underlying algorithm.

- **"initial refinement"**
  Sometimes the grid region "Domain 1" (or the first level of a grid hierarchy) shall not be refined, because only a cut-out subset of the base grid is needed. Disable this checkbox in order to simply extract the first domain from the base grid.

- **"ASTER" orography**
  In ExtPar the ICON orography will be aggregated from the "GLOBE" or the "ASTER" data set to the target grid. The switch depends on the horizontal resolution of the target grid: spacings below 3 km will be based on the high-resolution, non-global topography "ASTER"; spacings upwards of 3 km will be aggregated from the coarser and global data set "GLOBE".
  Please kindly note that "ASTER" orography data are only available in the latitude range $60°S - 60°N$. Requests with spacings below 3 km and with parts or all of the domain outside this range will fail. To avoid such problems please submit these requests by switching off high-resolution "ASTER" orography by enabling the corresponding checkbox.

- **include base grid**
  This setting is disabled by default but it becomes useful when a global base grid has been created from scratch: In this situation the base grid domain # 0 may not only serve the purpose of being the starting point for the subsequent refinement hierarchy, but it can be used in the ICON simulation itself. Selecting "include base grid" will run the ExtPar process and include this dataset into the resulting zip file.

Step 3: Sub-domain Name and Parent Grid ID

By default, the web form contains only the input fields to specify a single grid. However, more domain specifications can be added to the generator by a click on the "Add another domain" button (or removed by clicking "Remove latest domain").

Numbering: In the web form the base grid is denoted by "#0" while the created domains are denoted by numbers "#1", "#2" and so on.

In the simplest case the domains specify multiple nests on the same refined level. In this case, the "parent grid ID" is always set to "0" (base grid).
Besides, domains can be nested, for example

$$\text{Germany} \rightarrow \text{Europe} \rightarrow \text{Global}.$$

Then, the grid for Germany has "parent grid ID=1", and the Europe grid has "parent grid ID=0".
The currently chosen hierarchy of grids is graphically depicted in the top right corner of the web form.

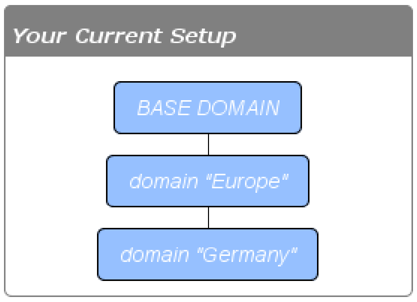

- **"domain name"**
  Each domain requires a name (string) which will be used as a name prefix for the resulting files.

- **“number of grid used”**
  This setting will be written into the grid meta-data. It is part of a GRIB2 mechanism to link data files to their underlying grid files – see also the explanation in Section 2.1.4. For regional domains which are not used operationally, we suggest to choose arbitrary but distinguishable integer numbers.
- **“write parent grid”**
  Enable this checkbox when your grid file is to be used with ICON-LAM and a reduced radiation grid. Note that in this case the grid cannot be used as a nest in standard (non-LAM) mode – see the corresponding remark in Section 2.1.5 above.

Step 4: Specify the Grid Type/Shape

- **“global”**
  In this case, all cells of the base grid are refined, resulting in a grid with $(4\,N)$ triangles if the base grids consists of N triangles. No further settings are required to specify this grid.
- **“rectangular”**
  This specifies a sub-region to be refined by a center latitude/longitude (in degrees) and a size of $2 \times$ “half height” for the latitude and $2 \times$ “half width” in terms of the longitude.
  - **“rotate” / “north-pole”**
    By default, the latitude-longitude coordinates for the rectangular refinement area are based on the standard North Pole 90N 0E. You may use, however, a rotated pole similar to the grids of the COSMO model. This pole rotation value should not be confused with the rotation of the base icosahedron which specifies the location of the grid’s pentagon points.
- **“circular”**
  This defines a circular-shaped refinement region with a given center and radius (in degrees).

Finally, having filled out all necessary fields of the web form, click on the “Proceed” button. The grid generation job is inserted into DWD’s processing queue and you will be informed via e-mail about its completion.

2.1.7. Offline ExtPar Subgrid Extraction

There is a global setting *generate script for ExtPar subset extraction* available in the web form which leads to a fundamentally different grid generation mode: If you prefer to use your own installation of the DWD ICON Tools grid generator, then you can select this option to *prepare* the grid generation in an “offline mode”.

The option requires a local installation of the ICON Tools version $> 2.4.0$, which (besides other changes) contain a utility script

```
icontools/extpar_subset_extraction.py
```

This Python script loads a "config" script (similar to a Fortran namelist) where the user specifies the desired grid parameters:

```
config = {
    "centre"                      : 1,
    "subcentre"                   : 2,
    "initial_refinement"          : ".FALSE.",
    "filename"                    : ["icon_grid_0026_R03B07_G.nc"],
    "dom(1)%outfile"              : ["mydomain"],
    "dom(1)%number_of_grid_used" : 99,
    ...
```

Here is where the web grid generator comes in handy: The configuration is automatically created by the web form option *generate script for ExtPar subset extraction.*

After the Python configuration `config ...` has been generated, the user can execute the `extpar_subset_extraction.py` locally on his own machine:

```
./extpar_subset_extraction.py --config=config.py
```

The necessary base grid and ExtPar data are then automatically determined and downloaded from ICON's public web site. The required grid region is cut out from this data set and no separate run of the ExtPar tool is necessary. If there exists a parent grid (reduced radiation grid), then the corresponding part is extracted, too. The whole operation greatly reduces the computational effort to generate the grid data for a custom ICON run.

As a final remark, the extraction script accepts two optional command-line arguments (which are listed with `extpar_subset_extraction.py --help`:

- The option `--icontoolsdir` allows to specify a directory where the ICON Tools grid generator binary is located.
- The option `--localcopy` greatly accelerates the script execution for large data sets by loading the base grid data from a local directory.

Also note that the `extpar_subset_extraction.py` is not fully "offline", since it requires access to the XML metadata and the base grids available under http://icon-downloads.mpimet.mpg.de.

2.1.8. Which Grid File is Related to My Simulation Data?

ICON data files do not (completely) contain the description of the underlying grid. This is an important consequence of the fact that ICON uses unstructured, pre-generated computational meshes which are the result of a relatively complex grid generation process. Therefore, given a particular data file, one question naturally arises: *Which grid file is related to my simulation data?*

The answer to this question can be obtained with the help of two meta-data items which are part of every ICON data and grid file (either a NetCDF global file attribute or a GRIB2 meta-data key):

- `numberOfGridUsed`
  This is simply an integer number, as explained in the previous sections. The `numberOfGridUsed` helps to identify the grid file in the public download list. If the `numberOfGridUsed` differs between two given data files, then these are not based on the same grid file.
- `uuidOfHGrid`
  This acronym stands for *universally unique identifier* and corresponds to a binary data tag with a length of 128 bits. The UUID can be viewed as a fingerprint of the underlying grid. Even though this is usually displayed as a hexadecimal number string, the UUID identifier is not human-readable. Nevertheless, two different UUIDs can be tested for equality or inequality.

The meta-data values for `numberOfGridUsed` and `uuidOfHGrid` offer a way to track the underlying grid file through all transformations in the scientific workflow, for example in

- external parameter files
- analysis data for forecast input
- data files containing the diagnostic output
- checkpointing files (restarting).

2.1.9. Planar Torus Grids

As a special mode for numerical experiments, ICON allows for planar torus grids. Note that the torus geometry and the corresponding global meta-data (NetCDF attributes) are *not* generated by the "standard grid generator" in Section 2.1.5, but require L. Linardakis' grid generator tool[2].

The torus grid has double periodic boundaries. It consists of equal-sided triangles, with edge length `edge_length`, which is a namelist parameter of the grid generator, and height $\frac{\sqrt{3}}{2}$ `edge_length`, see Fig. 2.6.

The lon-lat parameterization of the torus is

$$(lon, lat) = [0, 2\,\pi] \times [-\texttt{max\_lat}, \texttt{max\_lat}]$$

where `max_lat` $:= \frac{\pi}{18} \equiv 10$ degrees (hard-coded in the torus grid generator). Variables related to the lon-lat parameterization are stored as the data type `t_geographical_coordinates` in the ICON code.

The Cartesian coordinates of the torus grid are: $v = (x, y, 0)$ where

$$(x, y) \in [0, \texttt{domain\_length}] \times [0, \texttt{domain\_height}]$$

The lengths `domain_length`, `domain_height` are stored as global attributes in the grid file. Variables related to the Cartesian mesh are stored as the data type `t_cartesian_coordinates` in the ICON code.

[2]see the repository `https://code.mpimet.mpg.de/projects/icon-grid-generator`

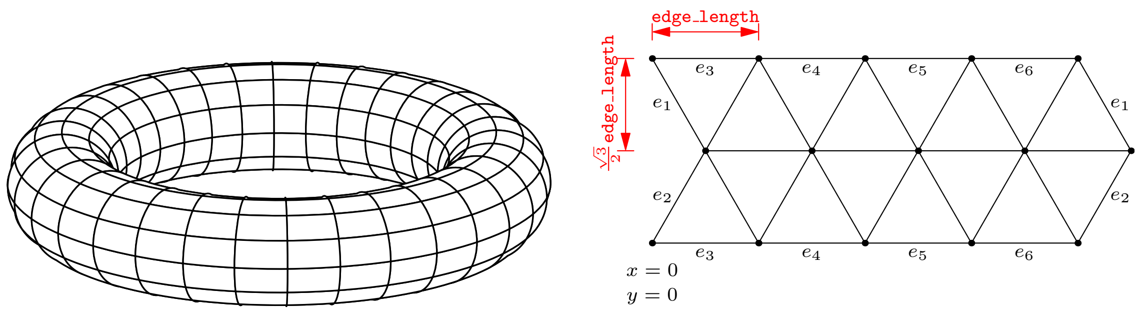

Figure 2.6.: Topological representation of the torus geometry and its triangulation.

2.2. Initial Conditions

Global numerical weather prediction (NWP) is an initial value problem. The ability to make a skillful forecast heavily depends on the accuracy with which the present atmospheric (and surface/soil) state is known. In addition to that, running forecasts with a limited area model requires accurate boundary conditions sampled at regular time intervals.

Initial conditions are usually generated by a process called *data assimilation*[3]. Data assimilation combines irregularly distributed (in space and time) observations with a short term forecast of a general circulation model (e.g. ICON) to provide a "best estimate" of the current atmospheric state. Such *analysis products* are provided by several global NWP centers.

In the following we will present various data sets that can be used to drive the ICON model and explain how these data can be retrieved. In addition we will explain how these data can be remapped to the targeted ICON grid, if necessary. Remapping is one of the basic pre-processing steps which are visualized in Figure 2.7.

Basically, each computational domain, i. e. also a nested domain, requires a separate initial data file. A "workaround" to start a nested simulation without the need to provide initial data for the nest is discussed in Section 5.2.

2.2.1. Obtaining DWD Initial Data

The most straightforward way to initialize ICON is to make use of DWD's analysis products, which are generated operationally every 3 hours and stored in GRIB2 format on the native ICON grid. Deterministic as well as ensemble analysis products are available. Deterministic products are generated by a hybrid Ensemble Variational Data assimilation (En-Var), which combines variational and ensemble methods. Ensemble products are based on a Localized Ensemble Transform Kalman Filter (LETKF) approach. See Chapter 10 for more information on DWD's data assimilation system.

[3]Note that for so-called *idealized test cases* no initial conditions must be read in. All necessary state variables are preset by analytical values.

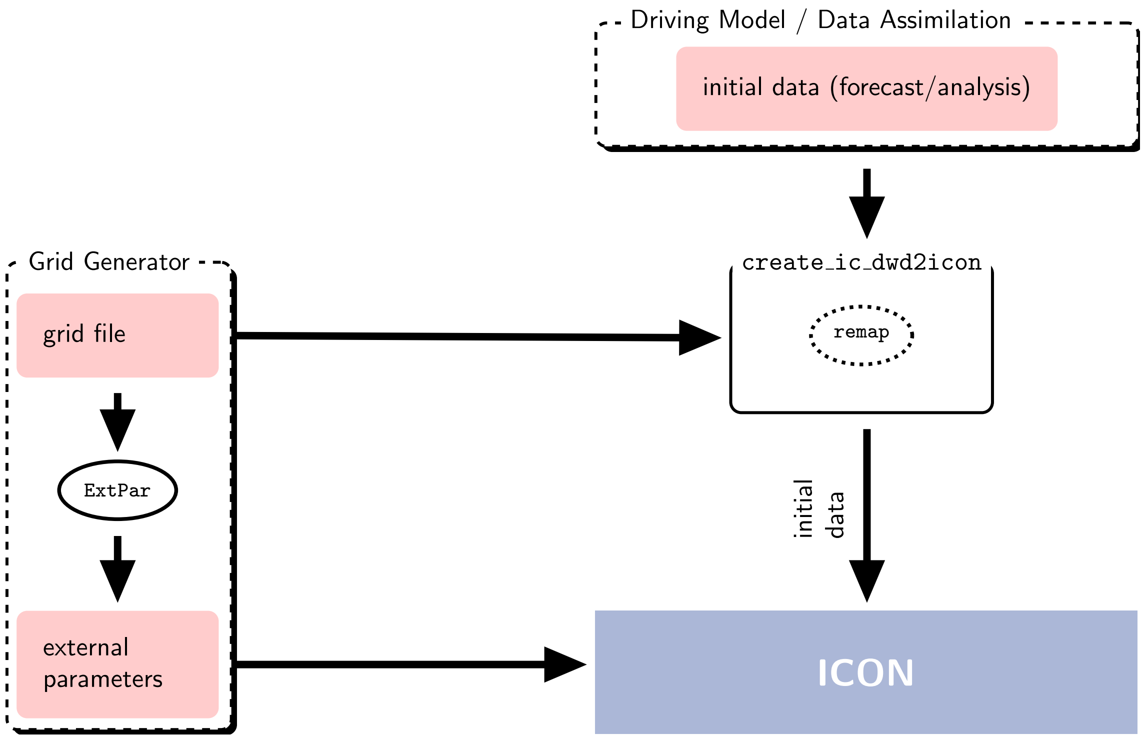

Figure 2.7.: Basic pre-processing steps for ICON (without limited area mode) which include the generation of grids and external parameters as well as the remapping of initial conditions. The grid generation process and the external parameters are described in the Sections 2.1 and 2.4. The initial data processing is covered by Section 2.2.3.

Choosing the Right Product

DWD provides a set of different analysis products. They all constitute a ”best estimate” of the atmospheric state, but differ in some physical and technical aspects. Choosing the right product is crucial and depends on the targeted application.

Some of the analysis products consist of two files: a first guess file and an analysis file. The term *first guess* denotes a short-range forecast of the NWP model at hand, whereas the term *analysis* denotes all those fields which have been updated by the assimilation system.

Several combinations of these files exist, with specific pros and cons:

Uninitialized analysis for IAU
This product consist of a first guess file and an analysis file, with the latter containing analysis *increments* (i.e. the difference between the analysis and the first guess). The validity dates of both files differ. The validity date of the first guess is shifted ahead of the analysis date by 90 min. This product is meant for starting the model in *incremental analysis update* (IAU) mode. IAU is a model internal filtering technique for reducing spurious noise introduced by the analysis (see Section 10.3.1).

While this initialization method performs best in terms of noise reduction, it bears the disadvantage that the corresponding analysis product cannot be interpolated horizontally in a straightforward manner. This prevents its use on custom target grids. The underlying reason is that the analysis product contains tiled surface data. Remapping of tiled data sets makes no sense, since the tile-characteristics can differ significantly between individual source and target grid cells. Only *aggregated* surface fields can safely be remapped (see Section 3.8.11 for more details on the surface tile approach).

A list of included fields can be found in Section 10.3.1.

Plain uninitialized analysis

This product consists of a first guess file and an analysis file, with the latter containing *full* analysis fields instead of increments. The validity date of both files matches the analysis date.

When using this product, the model state is abruptly pulled towards the analyzed state right before the first time integration step. Thus, no noise filtering procedure is included. This conceptually easy approach comes at the price of a massively increased noise level at model start. Due to the lack of tiled surface data, this product can be interpolated horizontally to arbitrary custom target grids without any hassle.

A list of included fields can be found in Section 10.3.2.

Initialized analysis

This product consists of a single file only, containing the analyzed state. First guess and analysis fields have already been merged and filtered by means of an asymmetric IAU. The noise level induced by this product is very moderate. In addition, this product can safely be interpolated to arbitrary custom target grids.

A list of included fields can be found in Section 10.3.3.

The level of spurious noise that emerges from each of these analysis products is compared in Figure 2.8. It shows the area averaged absolute surface pressure tendency as a function of simulation time, which is a measure of spurious gravity-noise induced by spurious imbalances in the initial conditions. It is defined as

$$\begin{aligned}\left\langle\left|\frac{\mathrm{d}p_s}{\mathrm{d}t}\right|\right\rangle &= \frac{1}{A}\sum\nolimits_i \left|\frac{\mathrm{d}p_s}{\mathrm{d}t}\right| \Delta a_i \\ &= \frac{1}{A}\sum\nolimits_i \left(\sum\nolimits_k \left|-g\nabla_h\cdot(\overline{\rho}\hat{\boldsymbol{v}}_h)\,\Delta z_k\right|\right)\Delta a_i\,,\end{aligned}$$

with A denoting the earth's surface and Δa_i denoting the area of the ith cell. The mathematical steps to obtain the pressure tendency equation are discussed at the end of Section 3.3. The blue, green and red curves show results for the *uninitialized analysis for IAU*, the *initialized analysis*, and the *uninitialized analysis*, respectively. It can be seen that for the uninitialized analysis the noise level at simulation start is significantly increased when compared to the other two products. It takes about two days of model forecast for the noise levels to align. The uninitialized analysis for IAU performs best in terms of noise-level, but keep in mind that some data fields cannot easily be interpolated in the

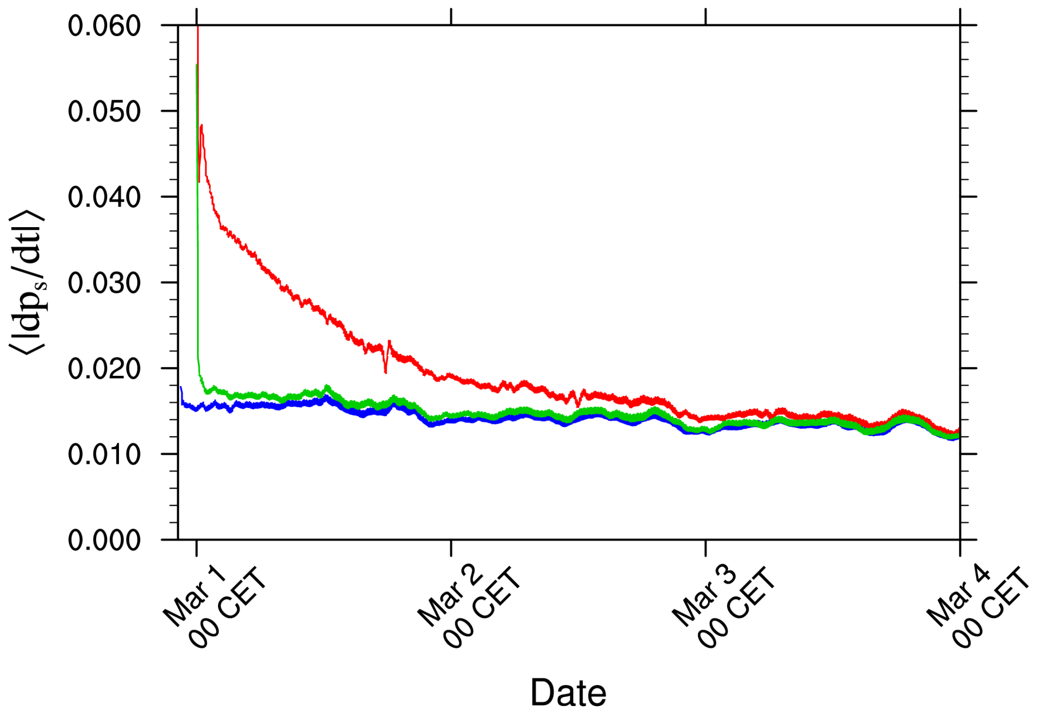

Figure 2.8.: Area averaged absolute surface pressure tendency in hPa as a function of simulation time. Curves differ in terms of the way the model is initialized, with the *uninitialized analysis for IAU* in blue, the *uninitialized analysis* in red and the *initialized analysis* in green.

horizontal, such that the application of this mode is typically restricted to the horizontal grids (13 km/40 km grid spacing) used operationally at DWD.

The specific pros and cons of the different analysis products is summarized in Table 2.1.

Important note: For external users we strongly recommend to use the *initialized analysis* for model initialization, since it constitutes a good compromise between accuracy and practicability.

Downloading Initial Conditions

ICON initial conditions are stored in DWD's meteorological data management system SKY. Here, for better performance, meta and binary data are stored separately: The meta data are stored in a relational database, sorted by data category and time. The binary data are stored temporarily on a hard drive and subsequently moved into the DWD's tape archive using the archiving components in SKY.

A prerequisite for data retrieval is a valid account for the database "roma". The database can be accessed in the following ways:

- If you have access to DWD's Linux cluster `rcnl*`, please contact `klima.vertrieb@dwd.de`, in order to gain additional access to the database.

Table 2.1.: Characteristics of DWD's analysis products. The recommended product for standalone model runs (without data assimilation) is highlighted in blue.

	Uninitialized analysis for IAU	**Uninitialized analysis**	**Initialized analysis**
`# of files`	2	2	1
`noise level`	low	high	moderate
`analysis increments`	yes	no	no
`surface tile information`	yes	no	no
`interpolation possible`	no	yes	yes
`available for det/ens`	yes/yes	yes/yes	yes/yes

Data retrieval will then be possible by using either SKY's query language directly, or by using the PAMORE command-line tool (the latter will be explained below).

- An alternative way to access the database is to use the web-based PAMORE service, see the web page (German description only)

  `https://www.dwd.de/DE/leistungen/pamore/pamore.html`

  It is meant for external users who do not have direct access to DWD's computer systems. It requires a user account. To this end please fill out the registration form

  `Registration form for PAMORE web service`

DWD's operational analysis and forecast products for the ICON model are being stored in the SKY database since 2015-01-20. However, the set of data fields stored is subject to continuous changes and improvements. I. e. the inclusion of additional fields has become necessary with the activation of more advanced physical parameterizations. The set of data fields of the early months is likely to be incomplete with regard to the initialization procedure that is explained in this tutorial: For example, the surface tile approach (see Section 3.8.11) has been activated no earlier than December 2015.

Data retrieval with PAMORE via command-line. PAMORE (*PA*rallel *MO*del data *RE*trieve from Oracle databases) is a high-level tool for the retrieval of (model) data from DWD's meteorological data management system SKY.

A full set of command-line options can be obtained via `pamore -h`. Alternatively, they are accessible on the web via https://webservice.dwd.de/pamore.html

In order to retrieve, for example, initial data on the native ICON grid from February 1, 2019 00 UTC, the following command lines can be used for the different analysis products:

Uninitialized analysis for IAU (deterministic)

Global domain with 13 km grid spacing

`pamore -d` $\underbrace{2019}_{\text{year}}\underbrace{02}_{\text{month}}\underbrace{01}_{\text{day}}\underbrace{00}_{\text{hour}}$ `-lt m -iglo_startdata -iau`

Global domain (13 km) and nested EU domain (6.5 km)

```
pamore -d 2019020100 -lt m -iglo_eu_startdata -iau
```

Note that the EU domain lacks a separate analysis for the atmosphere. If required, it must be interpolated (horizontally) from the global domain.

Uninitialized analysis (deterministic)

Global domain with 13 km grid spacing

```
pamore -d date -lt m -iglo_startdata
```

Global domain (13 km) and nested EU domain (6.5 km)

```
pamore -d date -lt m -iglo_eu_startdata
```

Here, *date* must be replaced by the desired date (see above).

Initialized analysis (deterministic)

Global domain with 13 km grid spacing

```
pamore -d date -hstart 0 -hstop 0 -lt a \
                  -model iglo -iglo_startdata_0
```

Nested EU domain (6.5 km):

```
pamore -d date -hstart 0 -hstop 0 -lt a \
                  -model ieu -iconlam_startdata_0
```

Please note that for the nested domain the optional input field TKE is not available and that Z0 and H_SNOW are only available since 2018-03-14.

Important note for ensemble products: With the additional options

- `-ires r2b06` and
- `-enum` *num*, where *num* specifies an ensemble member (e.g. 3) or a range of ensemble members (e.g. 3 – 8),

analysis products can also be picked from the LETKF analysis ensemble consisting of 40 members with 40/20 km horizontal grid spacing. This does, however, not hold for initialized analysis products.

Initialized analysis products for ICON ensemble members are not archived and, hence, are not available from DWD's database.

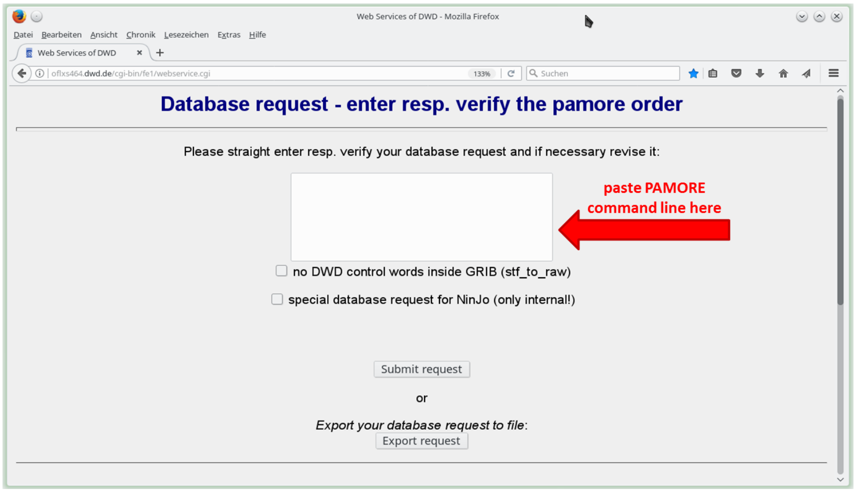
Web Services of DWD - Mozilla Firefox
Datei Bearbeiten Ansicht Chronik Lesezeichen Extras Hilfe
Web Services of DWD
oflxs464.dwd.de/cgi-bin/fe1/webservice.cgi
Suchen

Database request - enter resp. verify the pamore order

Please straight enter resp. verify your database request and if necessary revise it:

paste PAMORE command line here

☐ no DWD control words inside GRIB (stf_to_raw)

☐ special database request for NinJo (only internal!)

Submit request

or

Export your database request to file:
Export request

Figure 2.9.: Screenshot of the PAMORE web service. It shows the HTML form where you can place your PAMORE command line request directly.

Data retrieval with PAMORE via the web form. The PAMORE web service allows the user-defined selection of model fields by navigating through a sequence of HTML forms. Alternatively, the web site offers a plain command-line interface.

For the specific task of retrieving ICON initial data, we strongly suggest to take the latter path. By making direct use of the above PAMORE command-lines and pasting them into the HTML form (see Figure 2.9), you can minimize the risk of missing some fields.

After submitting your database request, the data will be extracted from the database and stored on an FTP server for download. Once your request has been processed, you will receive an e-mail with information about the FTP server address and the path to your data.

2.2.2. Obtaining ECMWF IFS Initial Data

Model runs can also be initialized by "external" analysis files produced by the Integrated Forecast System (IFS) that has been developed and is maintained by the European Centre for Medium-Range Weather Forecasts (ECMWF).

The ICON code contains a script for the automatic request for IFS data from the MARS data base. The Meteorological Archival and Retrieval System (MARS, see `https://software.ecmwf.int/wiki/display/UDOC/MARS+user+documentation`) is the main repository of meteorological data at ECMWF. A full list of recommended IFS analysis fields is provided in Table 2.2.

The script for importing from MARS must be executed on the ECMWF computer system. It is located in the subdirectory

`icon/scripts/preprocessing/mars4icon_smi`

In order to retrieve, for example, T1279 grid data with 137 levels for the July 1, 2013, the following command line is used:

```
./mars4icon_smi -r 1279 -l 1/to/137 -d 2013070100 -O -L 1 -o 20130701.grb -p 5
```

Further options are shown by typing `./mars4icon_smi -h`

Note that prior to 2013-06-25 12 UTC, only 91 instead of 137 vertical levels were used by the operational system at ECMWF. For more information, regarding changes in the ECMWF model, see

https://www.ecmwf.int/en/forecasts/documentation-and-support/changes-ecmwf-model

Table 2.2.: Recommended **IFS analysis fields** on a regular lat-lon grid, as retrieved by the script `mars4icon_smi`. Optional fields are marked in blue. The second column indicates ICON's query name during read in. This is the name which the field must be given to when it is remapped onto the native ICON grid (see also Section 2.2.3).

shortName ECMWF	**shortName ICON**	**Unit**	**Description**
`U, V`	`U, V`	$\mathrm{m\,s^{-1}}$	horizontal velocity components
`OMEGA`	`W`	$\mathrm{Pa\,s^{-1}}$	vertical velocity
`T`	`T`	K	Temperature
`FI`	`GEOP_ML`	$\mathrm{m^2\,s^{-2}}$	model level geopotential (only the surface level is required)
`QV`	`QV`	$\mathrm{kg\,kg^{-1}}$	specific humidity
`CLWC`	`QC`	$\mathrm{kg\,kg^{-1}}$	cloud liquid water content
`CIWC`	`QI`	$\mathrm{kg\,kg^{-1}}$	cloud ice content
`CRWC`	`QR`	$\mathrm{kg\,kg^{-1}}$	rain water content
`CSWC`	`QS`	$\mathrm{kg\,kg^{-1}}$	snow water content
`SST`	`SST`	K	sea surface temperature
`CI`	`CI`	[0,1]	sea-ice cover
`LNSP`	`LNPS`	-	logarithm of surface pressure
`Z`	`GEOP_SFC`	$\mathrm{m^2\,s^{-2}}$	surface geopotential
`TSN`	`T_SNOW`	K	snow temperature
`SD`	`W_SNOW`	m of water eqv.	water content of snow
`RSN`	`RHO_SNOW`	$\mathrm{kg\,m^{-3}}$	density of snow
`ASN`	`ALB_SNOW`	[0,1]	snow albedo
`SKT`	`SKT`	K	skin temperature
`STL[1/2/3/4]`	`STL[1/2/3/4]`	K	soil temperature level 1/2/3/4
`SWVL[1/2/3/4]`	`SMI[1/2/3/4]`	$\mathrm{m^3\,m^{-3}}$	soil moisture index (SMI) layer 1/2/3/4
`SRC`	`W_I`	m of water eqv.	water content of interception storage
`LSM`	`LSM`	[0,1]	land/sea mask

Note that when initializing from "external" analysis files, ICON requires the soil moisture index (`SMI`) and not the volumetric soil moisture content (`SWV`) as input. The conversion of `SWV` to `SMI` is currently performed as part of the MARS request (`mars4icon_smi`). However, this conversion is not reflected in the variable short names. The fields containing `SMI` are still named SWVLx, with x denoting the surface layer index. The ICON model, however, expects them to be named SMIx. Therefore, the proper output name SMIx must be specified explicitly in the namelist `input_field_nml` of `iconremap` (see the example namelist on p. 43).

Besides, when using one of the scripts below in order to generate remapped data in the NetCDF format, other field names must be adjusted as well: In order to read the data with ICON, it is necessary to rename the fields to the ICON-internal short names, according to the second column of Table 2.2.

2.2.3. Remapping Initial Data to Your Target Grid

Often it is desirable to run ICON at horizontal resolutions which differ from those of the initial data. One important application are high-resolution limited area runs, which start from operational ICON forecasts or analysis. Another application is the initialization from IFS analysis, which is provided on a lat-lon grid (see Section 2.2.2). In these cases horizontal remapping of the initial data is necessary. Note that there is no need for vertical interpolation as a separate pre-processing step. The ICON model itself will take care of the interpolation onto the model levels, assumed that the user has provided the height level field HHL and set the appropriate namelist options (see the namelist parameter `init_mode`).

We shortly describe the basic steps of remapping: After the successful download, the analysis data must be interpolated from a regular or triangular grid onto the ICON target grid. To this end, the `iconremap` utility from the DWD ICON Tools will be used in batch mode.

A typical namelist for processing initial data has the following structure:

```
&remap_nml
 in_grid_filename  = INPUT_GRID_FILENAME
 in_filename       = INPUT_FILENAME_GRB
 in_type           = 1                          ! 1: regular grid, 2: ICON grid
 out_grid_filename = ICON_GRIDFILE
 out_filename      = OUTPUT_FILENAME_NC
 out_type          = 2                          ! ICON grid
 out_filetype      = 4                          ! NetCDF format
/

! DEFINITIONS FOR INPUT DATA
!
&input_field_nml  ! temperature
 inputname      = "T"
 outputname     = "T"
/
&input_field_nml  ! horiz. wind comp. U
 inputname      = "U"
 outputname     = "U"
/
&input_field_nml  ! horiz. wind comp. V
 inputname      = "V"
 outputname     = "V"
/
...
```

For each of the variables to be remapped, the script must contain a namelist `input_field_nml` which specifies details of the interpolation methods and the output name. In this example, the 3D temperature field `T` and the horizontal wind components `U`, `V` are remapped from a regular grid onto a triangular ICON grid[4]. Variables are usually accessed through their name (character string), but note that for GRIB1 input data the correct field parameter must be provided with the namelist parameter `code`.

Important note: The remap tool can process files only if they contain a single time step. Furthermore, the tool requires that GRIB records corresponding to a particular variable are stored in contiguous sections. Third, the remapping process fails, if GRIB records are not ordered with respect to levels.

A detailed documentation of the ICON remap command-line options and namelist parameters can be found under `dwd_icon_tools/doc/icontools_doc.pdf`, i. e. Prill (2020). If the DWD ICON tools fail and if the cause of the error does not become clear from the error message, you may increase the output verbosity by setting the command-line options `-v`, `-vv`, `-vvv` etc.

For both, DWD analysis data and ECMWF IFS data, the DWD ICON Tools contain example scripts which generate the required namelists (i.e. `remap_nml` and `input_field_nml`). These scripts are

DWD initial data:
`dwd_icon_tools/icontools/create_ic_dwd2icon`

IFS initial data:
`dwd_icon_tools/example/runscripts/create_ic_ifs2icon`

The scripts contains a machine dependent batch system header and job launch command which must be adapted to the respective target platform.

Some comments are in order for particular data fields:

Soil Moisture Fields `SMI1`, `SMI2`, `SMI3`, `SMI4`. In accordance with the remark in Section 2.2.2, care must be taken to properly rename the fields `SWVL`x to `SMI`x in the case that "external" IFS analysis files are remapped. An example namelist `input_field_nml` is given below:

```
&input_field_nml              ! soil moisture index layer 1
 inputname      = "SWVL1"
 outputname     = "SMIL1"
/
```

[4]Note that in this example, the GRIB2 input *data* file also contains the specification of the input *grid*. Therefore the two namelist parameters *INPUT_GRID_FILENAME* and *INPUT_FILENAME_GRB* are identical!

Wind fields. For the wind fields, the standard remapping would interpolate the samples from each component U, V separately. This approach has been chosen in the example script above. However, the standard method completely decouples the components of the vector fields. It does not take into account the fact that it is a vector-field tangent to the sphere.

Therefore the ICON Tools are also capable of interpolating the edge-normal wind components v_n. See the ICON Tools namelist documentation regarding the interpolation U, V $\leftrightarrow v_n$. A special namelist parameter (RBF shape parameter) must be set for this vector field interpolation with radial basis functions.

Soil water content W_SO. The soil water content W_SO is the prognostic soil moisture variable of ICON. ICON is able to read in either W_SO or SMI, with the latter being converted automatically to W_SO during the initialization phase.

If soil moisture fields need to be remapped, it is strongly recommended to remap SMI instead of W_SO. Remapping of W_SO might lead to nonphysical soil water contents, which is related to the fact that the soil types of the source and target grid points might well differ.

If SMI is unavailable[1] in the initial data, it can be diagnosed from W_SO prior to the remapping step with the help of a small Fortran program named smi_w_so.f90. It ships with the ICON code and can be found in the subdirectory icon/scripts/postprocessing/tools. Note that smi_w_so.f90 requires the soil type field SOILTYP as additional input. It can be extracted from the external parameter file matching the source grid (see Section 2.4) and must then be concatenated with the file containing W_SO.

Masking of surface fields When remapping, it is possible to make use of the land sea mask information of the source grid (var_in_mask="FR_LAND" in input_field_nml) in order to mask out specific points. This can be particularly useful when remapping surface fields. In the example below we mask out water points so that only land points contribute to the interpolation stencil for soil moisture.

```
&input_field_nml             ! soil moisture index layer 1
 inputname       = "SWVL1"
 outputname      = "SMIL1"
 var_in_mask     = "FR_LAND" ! field to be used for masking
 in_mask_threshold = 0.5     ! threshold for masking values of input grid
 in_mask_below   = .TRUE.    ! values <= mask_theshold are masked on input grid
/
```

This feature, however, should be used with caution, as it can lead to uninitialized points on the target grid. It might happen that isolated land points on the target grid (e.g. small islands) do not have a counterpart on the source grid, which then leads to a zero-sized interpolation stencil.

[1]Starting from 2018-03-14 (2018-07-11), DWD's operational forecast products contain the soil moisture index SMI on the EU domain (global domain) (vv=0 output, initialized analysis).

2.3. Boundary Data Preparation for ICON-LAM

When running ICON in limited area mode (LAM), lateral boundary conditions must be provided. In real case applications these are time dependent and must be updated periodically by reading input files. To this end, forecast or analysis data sets from a *driving model* may be used which, however, need to be interpolated horizontally to the ICON grid first.

In this section we briefly describe the process of generating these lateral boundary conditions (LBCs). Again, the basic pre-processing steps for ICON are visualized in Figure 2.10, where the additional pre-processing of boundary data constitutes the main difference to Figure 2.7.

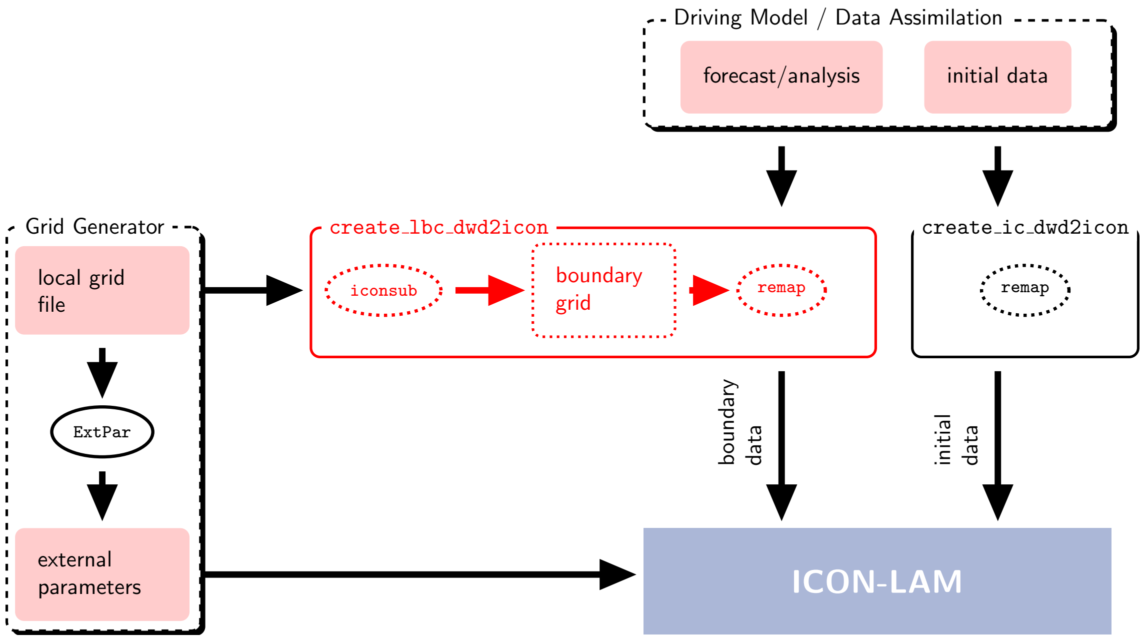

Figure 2.10.: Basic pre-processing steps for ICON-LAM (compare to Fig. 2.7). The grid generation process and the external parameters are described in the Sections 2.1 and 2.4. The initial data processing is covered by Section 2.2.3. Finally, the script `create_lbc_dwd2icon` for extracting the boundary data is described in Section 2.3. This pre-processing step is necessary for the limited area mode ICON-LAM.

Boundary Data Retrieval

The raw data files which are intended to be used as LBCs must contain one of the sets of variables depicted in Figure 2.11, on either a triangular ICON grid, or a regular latitude-longitude grid.

The fact that different sets of variables can be used, provides some flexibility in terms of the driving model. As indicated in Figure 2.11, sets I to III are typical for ICON, COSMO and IFS, respectively.

Set I (e.g. ICON)										
{U, V or VN},		W,	THETA_V,	DEN,	QV,	QC,	QI,	QR,	QS,	HHL
Set II (e.g. COSMO)										
U,	V,	W,	T,	P,	QV,	QC,	QI,	QR,	QS,	HHL
Set III (e.g. IFS)										
U,	V,	OMEGA,	T,	LNSP,	QV,	QC,	QI,	QR,	QS,	FI

Figure 2.11.: Sets of variables that may serve as lateral boundary conditions for ICON-LAM. See Table 2.2 for the requested internal ICON names to which these GRIB2 short names must be mapped. Optional fields are marked in gray. `PS` and `LNSP` denote the surface pressure, or its logarithm, respectively, and `FI` denotes the surface geopotential. Blending of the sets is not allowed. Examples of driving models are given in brackets.

> *Important note:* The 3D field `HHL` (geometric height of model half levels above mean sea level) is constant data. It needs only be contained in the raw data file whose validity date matches the envisaged model start date. In case of set III (IFS) the field `HHL` is computed by ICON during read-in.

Similar to the retrieval of initial conditions in Section 2.2.1, it also possible to download lateral boundary data from the DWD database.

Lateral boundary conditions from deterministic ICON forecasts

The following PAMORE command retrieves lateral boundary conditions from DWD's *forecast* database category:

```
                                                  iglo
pamore -d date -hstart hh -hstop hh -hinc hh -model       -ilam_boundary
                                                  ieu
```

Use `-model iglo`, for retrieving global 13 km forecast data, and `-model ieu` for 6.5 km forecast data on the ICON-EU domain. The meaning of the remaining command line arguments is as follows:

- `-d` *`date`*
  specifies the start date in the format *`YYYYMMddhh`*
- `-hstart` *`hh`* `-hstop` *`hh`*
  specifies the requested time range in hours
- `-hinc` *`hh`*
  specifies the temporal resolution (increments) in hours
- `-ilam_boundary`
  enables the variable set II (see Fig. 2.11) for lateral boundary conditions.

Example: The following example retrieves lateral boundary conditions from the ICON-EU domain for a time range of 36 hours and a temporal resolution of 2 hours, starting at 2020092212:

```
pamore -d 2020092212 -hstart 0 -hstop 36 -hinc 2 -model ieu -ilam_boundary
```

Important note: Please note that ICON forecast data have an expiration date. They are deleted from DWD's data base after 18 months. If you are interested in lateral boundary data which date back longer than 18 months, please use the following PAMORE command:

Lateral boundary conditions from ICON's assimilation cycle

The following PAMORE command retrieves lateral boundary conditions from DWD's *assimilation* database category:

```
                                              iglo
pamore -d date -hstart hh -hstop hh -model         -hindcast_ilam
                                              ieu
```

Use `-model iglo`, for retrieving global 13 km forecast data, and `-model ieu` for 6.5 km forecast data on the ICON-EU domain. Similar to the previous PAMORE command, the parameter `-hindcast_ilam` enables set II (see Fig. 2.11) for lateral boundary conditions. It extracts the data from the assimilation database category, for which there exists no expiration date. The command line argument `-hinc` is not applicable in this case. The temporal resolution is pre-set to 1 hour.

Example: The following example retrieves lateral boundary conditions from the global domain for a time range of 48 hours and a temporal resolution of 1 hour, starting at 2017092200:

```
pamore -d 2017092200 -hstart 0 -hstop 48 -model iglo -hindcast_ilam
```

In particular the above example extracts the 1 h, 2 h, 3 h forecast data from consecutive first guess runs (which are launched every 3 hours in the global assimilation cycle), starting at 2017092200. The final product consists of hourly lateral boundary data spanning the time range $[2017092200, 2017092400]$.

This PAMORE command is particularly useful, if the user wants to perform so called hindcast experiments.

ICON-LAM Pre-Processing Script

The DWD ICON Tools contain a run script `create_lbc_dwd2icon` in the directory `dwd_icon_tools/icontools`, which processes a whole directory of data raw files (script variable "`DATADIR`"), mapping the fields onto the boundary zone of a limited area grid.

The output files are written to the directory specified in the variable `OUTDIR`. The input files are read from `DATADIR`, therefore this directory should not contain other files and should not be identical to the output folder.

The grid file names are specified by

```
INGRID="input_grid_file"  # file name of input grid
LOCALGRID="grid_file.nc"  # file name of limited-area (output) grid
```

After adjusting the necessary filenames `INGRID` and `LOCALGRID` and the input directory name `DATADIR`, this script performs the steps described in the following two sections. The `create_lbc_dwd2icon` script can be submitted to the PBS batch system of DWD's NEC SX-Aurora. In order to run it on other machines, the batch system header and mpirun command must be adapted accordingly.

Step 1: Extract Boundary Region from the Local Grid File

In the first step the above ICON-LAM pre-processing script creates an auxiliary grid file which contains only the cells of the boundary zone. This step needs to be performed only once before generating the boundary data.

Important note: Note that this step is not allowed if vertical boundary nudging is used in addition to lateral boundary nudging. This corresponds to the namelist parameter setting `nudge_type=1` (namelist `nudging_nml`). In this case, boundary data must be provided for the entire local (limited-area) grid, rather than for a boundary strip only, see Section 6.2.

We use the `iconsub` program from the collection of ICON Tools, see Section 1.3, with the following namelist:

```
&iconsub_nml
  grid_filename   = "${LOCALGRID}",
  output_type     = 4,
  lwrite_grid     = .TRUE.,
/
&subarea_nml
  ORDER             = "${OUTDIR}/grid_file_lbc.nc",
  grf_info_file     = "${LOCALGRID}",
  min_refin_c_ctrl = 1
  max_refin_c_ctrl = 14
/
```

Then running the `iconsub` tool creates a grid file *grid_file_lbc.nc* for the boundary strip. The cells in this boundary zone are identified by their value in a special meta-data field, the `refin_c_ctrl` index, e. g. `refin_c_ctrl = 1,...,14`, see Figure 2.12.

The width of the extracted boundary strip in terms of cell rows is specified by the namelist parameters `min_refin_c_ctrl` and `max_refin_c_ctrl`. The maximum allowed value for `max_refin_c_ctrl` is given by `max(refin_c_ctrl) == bdy_indexing_depth`, i. e. the boundary indexing depth that has been chosen when generating the limited area grid (see Section 2.1.5). The width of the extracted boundary strip must be equal or larger than

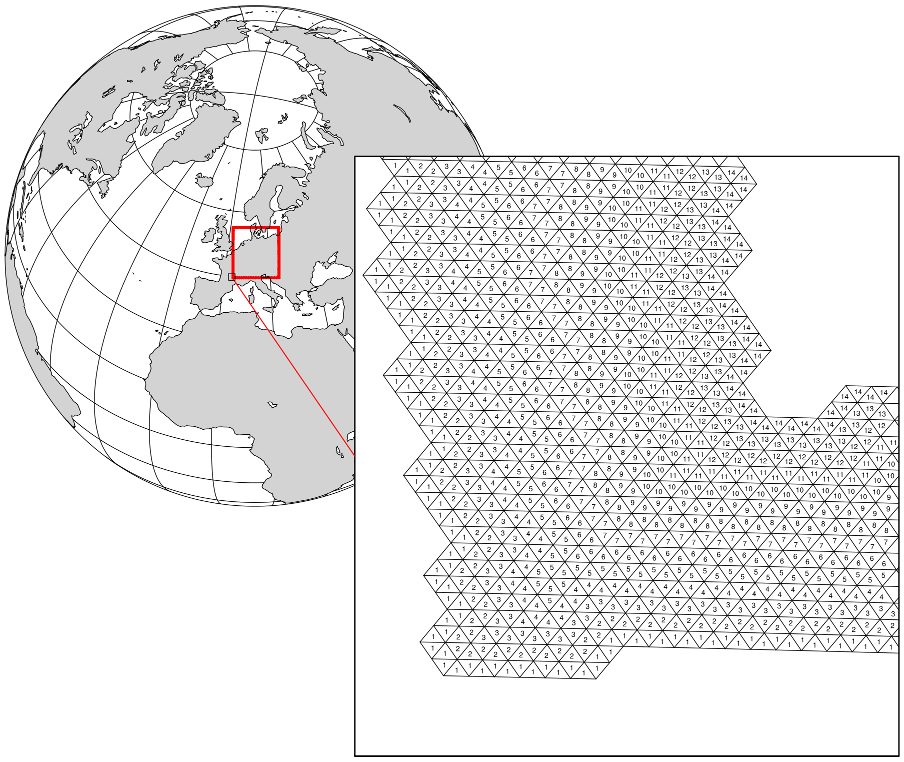

Figure 2.12.: Illustration of the ICON-LAM boundary zone. The cells are identified by their `refin_c_ctrl` index, e. g. `refin_c_ctrl = 1,...,14`.

the width of the lateral nudging zone in the limited-area run for which it is foreseen. A safe setting would be `max_refin_c_ctrl = max(refin_c_ctrl)`, as used in this example.

Reference to the original grid: For a given boundary region file *`grid_file_lbc.nc`* the question may arise, which original grid was used for its creation. This is analogous to the explanation in Section 2.1.8: The boundary region files contain a link to the original grid file in the form of a unique fingerprint `uuidOfOriginalHGrid`.

Step 2: Creating Boundary Data

Any of the data sources explained in the Sections 2.2.1 and 2.2.2 can be chosen for the extraction of boundary data. To be more precise, boundary data originating from ICON, IFS, and COSMO have successfully been used. Data sets from other global or regional models may work as well, but have not been tested yet.

We define the following namelist for the `iconremap` program from the collection of ICON Tools. This happens automatically in our ICON-LAM pre-processing script:

```
&remap_nml
  in_grid_filename  = "${INGRID}"
  in_filename       = "input_data_file"
  in_type           = 2
  out_grid_filename = "${OUTDIR}/grid_file_lbc.nc"
  out_filename      = "${OUTDIR}/data_file_lbc.nc"
  out_type          = 2
  out_filetype      = 4
/
```

Here, the data file *input_data_file* automatically iterates over all files in `${DATADIR}`. The parameters `in_type=2` and `out_type=2` specify that both grids correspond to triangular ICON meshes (`in_grid_filename` and `out_grid_filename`). Additionally, a namelist `input_field_nml` is appended for each of the pre-processed variables.

With respect to the output filename `data_file_lbc.nc` it is a good idea to follow a consistent naming convention. See Section 6.4.1 on the corresponding namelist setup of the ICON model.

Note that the `input_data_file` must contain only a single time step when running the `iconremap` tool. The `iconremap` tool therefore must be executed repeatedly in order to process the whole list of boundary data samples (this is automatically done within the `create_lbc_dwd2icon` script).

After the specification of the filenames, the `create_lbc_dwd2icon` script automatically adds remapping parameters for all variables of the Set I in Fig. 2.11. Regarding the `HHL` field an additional remark is in order: Since this variable needs only be contained in the raw data file whose validity date matches the envisaged model start date (see the remark in Section 2.3), we set this field as optional:

```
&input_field_nml
 inputname      = "HHL"
 outputname     = "z_ifc"
 intp_method    = 3
 loptional      = .TRUE.
/
```

Afterwards, the `create_lbc_dwd2icon` script launches the call to the `iconremap` binary.

In this context the following technical detail may considerably speed up the pre-processing: The `iconremap` tool allows to store and load interpolation weights to and from a NetCDF file. When setting the namelist parameter `ncstorage_file` (character string) in the `iconremap` namelist `remap_nml`, the remapping weights are loaded from a file with this name. If this file does not exist, the weights are created from scratch and then stored for later use. Note that for MPI-parallel runs of the `iconremap` tool multiple files are created. Re-runs require exactly the same number of processes.

2.4. External Parameter Files

External parameter fields describe properties of the Earth's surface and atmosphere, which can be assumed to be invariant during the course of a typical NWP forecast (i. e. a couple of days). Examples are the topography, the land-sea mask, the soil type and atmospheric aerosols. Most of the fields are constant in time while some are available on a monthly basis in order to represent the seasonal cycle. They are read by the model during startup. The full list of external parameter fields is given in Table 2.3.

Table 2.3.: External parameter fields which are requested by ICON during startup (in alphabetical order). Fields marked in blue are not read by ICON in operational NWP runs. In general they are only requested, if the respective depicted namelist parameter is set.

shortName	Description
AER_SS12	Sea salt aerosol climatology (monthly mean) `irad_aero=6,9` (namelist `radiation_nml`)
AER_DUST12	Total soil dust aerosol climatology (monthly mean) `irad_aero=6,9` (namelist `radiation_nml`)
AER_ORG12	Organic aerosol climatology (monthly mean) `irad_aero=6,9` (namelist `radiation_nml`)
AER_SO412	Total sulfate aerosol climatology (monthly mean) `irad_aero=6,9` (namelist `radiation_nml`)
AER_BC12	Black carbon aerosol climatology (monthly mean) `irad_aero=6,9` (namelist `radiation_nml`)
ALB_DIF12	Shortwave ($0.3 - 5.0\,\mu$m) albedo for diffuse radiation (monthly mean) `albedo_type=2` (namelist `radiation_nml`)
ALB_UV12	UV-visible ($0.3 - 0.7\,\mu$m) albedo for diffuse radiation (monthly mean) `albedo_type=2` (namelist `radiation_nml`)
ALB_NI12	Near infrared ($0.7 - 5.0\,\mu$m) albedo for diffuse radiation (monthly mean) `albedo_type=2` (namelist `radiation_nml`)
DEPTH_LK	Lake depth
EMIS_RAD	Surface longwave (thermal) emissivity `itype_lwemiss=1` (namelist `extpar_nml`)
EMISS	Surface longwave (thermal) emissivity derived from satellite measurements (monthly mean) `itype_lwemiss=2` (namelist `extpar_nml`)
FOR_D	Fraction of deciduous forest `ntiles=1` (namelist `lnd_nml`)
FOR_E	Fraction of evergreen forest `ntiles=1` (namelist `lnd_nml`)
FR_LAKE	Lake fraction (fresh water)
FR_LAND	Land fraction (excluding lake fraction but including glacier fraction)
FR_LUC	Land-use class fraction
HSURF	Topographic height at cell centers
LAI_MX	Leaf area index in the vegetation phase `ntiles=1` (namelist `lnd_nml`)

Continued on next page

Table 2.3.: *Continued from previous page*

NDVI_MAX	Normalized differential vegetation index
NDVI_MRAT	Proportion of monthly mean NDVI to yearly maximum (monthly mean)
PLCOV_MX	Plant covering degree in the vegetation phase `ntiles=1` (namelist `lnd_nml`)
ROOTDP	Root depth `ntiles=1` (namelist `lnd_nml`)
RSMIN	Minimum stomatal resistance `ntiles=1` (namelist `lnd_nml`)
SOILTYP	Soil type
SSO_STDH	Standard deviation of sub-grid scale orographic height
SSO_THETA	Principal axis-angle of sub-grid scale orography
SSO_GAMMA	Horizontal anisotropy of sub-grid scale orography
SSO_SIGMA	Average slope of sub-grid scale orography
T_2M_CL	Climatological 2m temperature (serves as lower boundary condition for soil model)
T_2M_CLIM	Climatological 2m temperature (monthly mean) `itype_vegetation_cycle>1` (namelist `extpar_nml`)
TOPO_CLIM	Interpolated topographic height for T_2M_CLIM data `itype_vegetation_cycle>1` (namelist `extpar_nml`)
T_SEA	Sea surface temperature climatology (monthly mean) `sstice_mode=2` (namelist `lnd_nml`)
Z0	Surface roughness length (over land), containing a contribution from subgrid-scale orography `itype_z0=1` (namelist `nwp_phy_nml`)

2.4.1. ExtPar Software

The ExtPar software (ExtPar – External Parameters for numerical weather prediction and climate application) is able to generate external parameters for the different models GME, COSMO, HRM and ICON. Experienced users can run ExtPar on UNIX or Linux systems to transform raw data from various sources into domain-specific data files. For ICON, ExtPar will output the fields given in Table 2.3 in the NetCDF file format and GRIB2 on the native triangular grid. For a more detailed overview of ExtPar, the reader is referred to the *User and Implementation Guide* of ExtPar, Asensio and Messmer (2014), and, additionally Smiatek et al. (2008, 2016).

The ExtPar pre-processor is a COSMO software and not part of the ICON training course release. Still, the ExtPar tool can be accessed via the ICON grid generator web service (see Section 2.1.6). Similar as for the grid files, for fixed domain sizes and resolutions some external parameter files for the ICON model are available for download via

`http://icon-downloads.mpimet.mpg.de`

Topography information: Please note the following remark:

The topography contained in the ExtPar data files is *not identical* to the topography data which is eventually used by the model. This is because at start-up, after reading the ExtPar data, the topography field is optionally filtered by a smoothing operator (`n_iter_smooth_topo >0` in `extpar_nml`). Therefore, for post-processing purposes it is necessary to specify and use the topography height `topography_c` (GRIB2 short name `HSURF`) from the model output (cf. Section 7.1 and Appendix B). The same applies to the fields `DEPTH_LK`, `FR_LAND`, `FR_LAKE`, and `Z0`, which are unconditionally modified by ICON.

2.4.2. Additional Information for Surface Tiles

ExtPar data files are available for download with and without additional information for surface tiles. See Section 3.8.11 for details on the tile approach.

ExtPar files suitable for the tile approach are indicated by the suffix `_tiles`. They are also applicable when running the model without tiles. ExtPar files without the suffix "`_tiles`", however, must only be used when running the model without tiles (`ntiles` = 1, namelist `lnd_nml`).

The data files do not differ in the number of fields, but rather in the way some fields are defined near coastal regions. Without the `_tiles` suffix, various surface parameters (e.g. `SOILTYP`, `NDVI_MAX`) are only defined at so-called dominant land points, i. e. at grid elements where the land fraction exceeds 50%. With the `_tiles` suffix, however, these parameters are additionally defined at cells where the land fraction is below 50%. By this, we allow for mixed water-land points. The same holds for the lake depth (`DEPTH_LK`) which is required by the lake parameterization scheme FLake. For files without the `_tiles` suffix, `DEPTH_LK` is only defined at dominant lake points.

2.4.3. Parameter Files for Radiation

In addition to the ExtPar fields, input fields for radiation are loaded into the ICON model. These constants fields are distributed together with the model code.

RRTM

Input files for the RRTM radiation scheme are located in the folder `icon/data`.

`rrtmg_lw.nc`
: parameters for radiative transfer calculation used for the underlying RRTMG algorithm, thermal radiation.

`ECHAM6_CldOptProps.nc`
: Cloud optical properties for liquid clouds at 30 wavelengths used for the underlying RRTMG algorithm.

On default, ICON expects the RRTMG parameter files to be named as above. Renaming is possible, however the modified name must then be passed into ICON via the namelist parameters `lrtm_filename` and `cldopt_filename` in the namelist `nwp_phy_nml`.

ecRad

Input files for the ecRad radiation scheme are located in the folder `icon/externals/ecrad/data`. The correct folder path must be passed to ICON via the ICON namelist parameter `ecrad_data_path` in the namelist `radiation_nml`.

3. Model Description

Before I came here I was confused about this subject. Having listened to your lecture I am still confused. But on a higher level.

Enrico Fermi

This chapter is devoted to a summary of ICON's model structure. The principal components are illustrated in Fig. 3.1:

Dynamics	The centerpiece of the numerical weather prediction system is the *dynamical core*, which integrates the discrete equations for fluid motion forward in time. ICON's dycore will be shortly described in Sections 3.1–3.5.
Tracer Advection	The dynamical core is followed by the numerical advection scheme, e. g. for humidity and cloud water. Section 3.6 focuses on the different methods available in ICON.
Physics	The former components are then coupled to parameterizations for processes such as convection that occur on scales too small to be resolved directly. We present a comprehensive overview of the physics parameterizations (NWP-mode) in Sections 3.7–3.8.

Finally, the chapter is concluded with the discussion of variable resolution modeling.

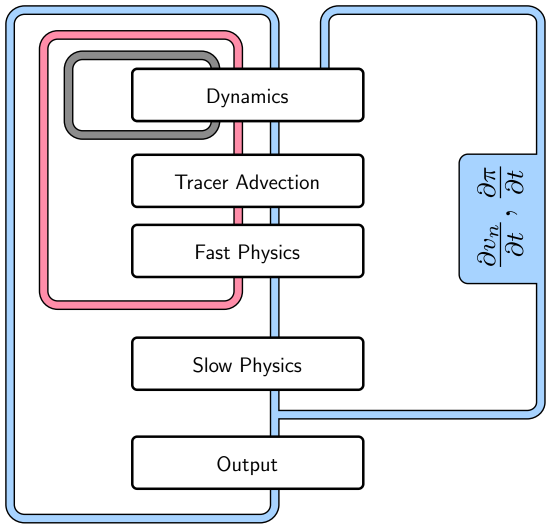
Dynamics
Tracer Advection
Fast Physics
Slow Physics
Output
$\frac{\partial v_n}{\partial t}, \frac{\partial \pi}{\partial t}$

Figure 3.1.: ICON's model structure. This flow chart will be revisited in detail in Fig. 3.8.

3.1. Governing Equations

The equation system of the ICON model is based upon the prognostic variables suggested by Gassmann and Herzog (2008). It describes a two-component system consisting of dry air and water, where water is allowed to occur in all three phases, including precipitating drops and ice particles.

As described in Wacker and Herbert (2003), an equation set for the mixture can be derived by first introducing a reference velocity into the governing equations. The equations for momentum, mass and energy of the mixture, as given below, are then formed as a sum of the constituent-specific equation sets. The specific form of the governing equations for the mixture depends on the choice of the reference velocity.

Here we have chosen the barycentric velocity as reference velocity. It is defined as

$$\boldsymbol{v}_b = \frac{\sum_k \rho_k \boldsymbol{v}_k}{\sum_k \rho_k}\,,$$

with the partial density ρ_k of constituent k and its advective velocity $\boldsymbol{v}_k$. For simplicity, $\boldsymbol{v}_b$ will be denoted as $\boldsymbol{v}$ in the following.

In order to separate turbulent fluctuations from the mean flow, a density weighted averaging (known as Hesselberg averaging) is applied. Every field ϕ is decomposed into a density-weighted mean and a deviation (Hesselberg, 1925)

$$\phi = \widehat{\phi} + \phi''\,,$$

with

$$\widehat{\phi} = \frac{\overline{\rho\phi}}{\overline{\rho}}$$

and subsequent averaging. $\overline{\phi}$ denotes the classical Reynolds average. More details on density-weighted average calculus can be found e.g. in Zdunkowski and Bott (2003).

The basic Hesselberg-averaged equation system, including the shallow atmosphere approximations, reads as follows

$$\frac{\partial \widehat{v}_n}{\partial t} + \frac{\partial \widehat{K}_h}{\partial n} + (\widehat{\zeta} + f)\widehat{v}_t + \widehat{w}\frac{\partial \widehat{v}_n}{\partial z} = -c_{pd}\widehat{\theta}_v \frac{\partial \overline{\pi}}{\partial n} - F(v_n) \tag{3.1}$$

$$\frac{\partial \widehat{w}}{\partial t} + \widehat{\boldsymbol{v}}_h \cdot \nabla \widehat{w} + \widehat{w}\frac{\partial \widehat{w}}{\partial z} = -c_{pd}\widehat{\theta}_v \frac{\partial \overline{\pi}}{\partial z} - g \tag{3.2}$$

$$\frac{c_{vd}c_{pd}}{R_d}\overline{\rho}\widehat{\theta}_v \frac{\partial \overline{\pi}}{\partial t} = c_{pd}\overline{\pi}\frac{\partial \overline{\rho}\widehat{\theta}_v}{\partial t} = -c_{pd}\overline{\pi}\,\nabla \cdot (\overline{\rho}\widehat{\boldsymbol{v}}\widehat{\theta}_v) + \overline{Q} \tag{3.3}$$

$$\frac{\partial \overline{\rho}}{\partial t} + \nabla \cdot (\overline{\rho}\widehat{\boldsymbol{v}}) = \sum\nolimits_k \overline{\sigma}_k^{conv} \tag{3.4}$$

$$\frac{\partial \overline{\rho}\widehat{q}_k}{\partial t} + \nabla \cdot (\overline{\rho}\widehat{q}_k\widehat{\boldsymbol{v}}) = -\nabla \cdot \left(\overline{J}_k^z \boldsymbol{k} + \overline{\rho q_k'' \boldsymbol{v}''}\right) + \overline{\sigma}_k \tag{3.5}$$

Prognostic equations are solved for the horizontal velocity component normal to the triangle edges $\widehat{v}_n$ (3.1), the vertical wind component $\widehat{w}$ (3.2), virtual potential temperature $\widehat{\theta}_v$ (3.3), the total density of the air mixture $\overline{\rho}$ (3.4), with

$$\overline{\rho} = \sum\nolimits_k \overline{\rho}_k \,, \tag{3.6}$$

and mass fractions (3.5)

$$\widehat{q}_k = \widehat{\rho}_k / \overline{\rho} \,. \tag{3.7}$$

The index $k \in \{d, v, c, i, r, s, g\}$ represents a specific constituent of the mixture. We use

$k = d$	for dry air,
$k = v$	for water vapor,
$k = c$	for cloud water,
$k = i$	for cloud ice,
$k = r$	for rain,
$k = s$	for snow, and
$k = g$	for graupel.

Further explanation of symbols and variables is given in Table 3.1. Note that the corresponding data structures containing the physics and dynamics variables are outlined in Section 8.2.

The equation system (3.1)–(3.5) is supplemented by the lower boundary conditions

$$\widehat{w}|_s = \frac{\overline{E}_v - \sum_{k_{prec}} \overline{S}_k|_s}{\overline{\rho}|_s - \sum_{k_{prec}} \overline{\rho}_k|_s} \tag{3.8}$$

$$\overline{J}^z_k|_s = \begin{cases} \overline{E}_k - \overline{\rho}_k \widehat{w}|_s, & \text{if } k \equiv v \\ -\overline{\rho}_k \widehat{w}|_s, & \text{if } k \equiv \text{non-prec. constituent} \\ -\overline{S}_k|_s, & \text{if } k \equiv \text{prec. constituent} \end{cases}$$

and the equation of state

$$\overline{p} = R_d \, \overline{\rho} \, \widehat{T} \, (1 + \alpha) \ ,$$

with

$$\alpha = \left(\frac{R_v}{R_d} - 1 \right) \widehat{q}_v - \sum\nolimits_{k \neq v,d} \widehat{q}_k \,.$$

When expressed in terms of the prognostic variables, the equation of state reads

$$\overline{\pi} = \left(\frac{R_d \overline{\rho} \widehat{\theta}_v}{p_{00}} \right)^{\frac{R_d}{c_{vd}}} \tag{3.9}$$

In contrast to the original formulation by Gassmann and Herzog (2008), we make use of the two-dimensional rather than the three-dimensional Lamb transformation to convert

Table 3.1.: Explanation of symbols in the model equations

Symbol		Description
$\frac{\partial}{\partial n}$		horizontal derivative in edge-normal direction
$\widehat{K}_h$	$= 0.5\left(\widehat{v}_n^2 + \widehat{v}_t^2\right)$	horizontal component of the kinetic energy
$\widehat{\zeta}$	$= (\nabla \times \widehat{\boldsymbol{v}}) \cdot \boldsymbol{k}$	vertical component of relative vorticity
f	$= 2\Omega \sin \phi$	Coriolis parameter
π		Exner function
c_{pd}, c_{vd}		specific heat capacity for dry air at constant pressure/volume
$F(v_n)$		turbulent momentum fluxes
g		acceleration of gravity
$\overline{Q}$		diabatic heat source
$\overline{J}_k^z$	$= \overline{\rho}_k\left(\widehat{w}_k - \widehat{w}\right)$	vertical diffusion flux for constituent k
$\overline{\sigma}_k$		internal conversion rate for kth constituent (i.e. conversion among different phases or particle forms)
$\overline{\sigma}_k^{conv}$		internal conversion rate for kth constituent due to convection only
$\overline{\rho q_k'' \boldsymbol{v}''}$		turbulent flux of kth partial mass fraction
$\overline{E}_v$	$= \overline{\rho q_v'' \boldsymbol{v}''}\vert_s$	surface evaporation flux
$\overline{S}_k$	$= \overline{\rho}\widehat{q}_k\widehat{v}_k^T$	sedimentation flux of kth constituent
$\widehat{v}^T$		terminal fall velocity of kth constituent

the nonlinear momentum advection term into a vector-invariant form. Vector-invariant means that no gradients of vectors appear in this equation, which avoids derivatives of the coordinate basis that would otherwise arise in an arbitrary coordinate frame from the nonlinear momentum advection term.

Note that we do not explicitly solve a prognostic equation for the density of dry air. From Equation (3.6) it becomes clear that the partial density of one constituent (here $\overline{\rho}_d$) can be diagnosed, given that a prognostic equation for the total density and all but one partial densities is solved. The reconstructed tangential velocity component is denoted as $\widehat{v}_t$, and in accordance with the model code, it is assumed here that $(\widehat{v}_t, \widehat{v}_n, \widehat{w})$ form a right-handed system.

From the Equations (3.4), (3.5) for total density and partial densities some important constraints can be derived which must hold in the discretized analogue in order to achieve mass conservation. First of all, the total density is defined as the sum of all partial densities, as shown by Eq. (3.6). From Eq. (3.7) it follows that

$$\textstyle\sum_k \widehat{q}_k = 1\,.$$

Likewise, the prognostic equation for total density (3.4) should be obtained by summing the budget equations (3.5) of all constituents. As a consequence the following constraints hold:

$$\sum\nolimits_k \overline{\boldsymbol{J}}_k = 0\,, \qquad \sum\nolimits_k \overline{\rho q_k'' \boldsymbol{v}''} = 0\,.$$

3.2. The Model Reference State

Dynamics in the atmosphere are characterized by small variations of thermodynamic quantities with respect to some background state. Therefore, like many other modeling frameworks, ICON makes use of an atmospheric reference state, i. e. the thermodynamic variables are defined as the sum of a reference state and a deviation from that. The reference state is assumed to be at rest and horizontally homogeneous, constant in time, dry and hydrostatically balanced.

Any grid-scale thermodynamic variable $\widehat{\psi}$ can then be written as

$$\widehat{\psi}(\lambda, \phi, z, t) = \psi_0(z) + \psi'(\lambda, \phi, z, t)\,.$$

The suffix 0 denotes the reference state while the prime denotes the grid-scale deviation. Thus, for the prognostic thermodynamic variables one gets

$$\begin{aligned} \overline{\rho}(\lambda, \phi, z, t) &= \rho_0(z) &&+ \quad \rho'(\lambda, \phi, z, t) \\ \overline{\pi}(\lambda, \phi, z, t) &= \pi_0(z) &&+ \quad \pi'(\lambda, \phi, z, t) \\ \widehat{\theta}_v(\lambda, \phi, z, t) &= \theta_{v0}(z) &&+ \quad \theta_v'(\lambda, \phi, z, t)\,. \end{aligned}$$

The background state components ρ_0, π_0, and θ_{v0} are related by the equation of state (3.9) and are hydrostatically balanced, i. e.

$$\begin{aligned} \pi_0 &= \left(\frac{R_d \rho_0 \theta_{v0}}{p_{00}}\right)^{\frac{R_d}{c_{vd}}} \\ \frac{\mathrm{d}\pi_0}{\mathrm{d}z} &= -\frac{g}{c_{pd}\theta_{v0}} \end{aligned} \tag{3.10}$$

The actual vertical reference profiles can be obtained by integration of Eq. (3.10) given that suitable boundary values are provided. The reference state in ICON is identical to the state used by the COSMO model.

In a global model like ICON, the local deviation from such a horizontally homogeneous state can be quite substantial. Therefore, no attempt is made to linearize any part of the governing equations with regard to this reference state as it is done in models based on the anelastic assumption. Instead, the main effect of introducing a reference state in a global nonhydrostatic model like ICON is the removal of horizontal base-state pressure gradient terms in the equation of motion, i.e.

$$c_{pd}\theta_v \frac{\partial \overline{\pi}}{\partial n} = c_{pd}\theta_v \frac{\partial \pi'}{\partial n}\,.$$

This reduces the computational error in the calculation of the pressure gradient force in case of sloping coordinate surfaces. Having said that, this effect is of minor importance for ICON, as by default the horizontal pressure gradient is evaluated truly horizontal along surfaces of constant height, rather than in terrain-following coordinates, along sloping coordinate surfaces (Zängl, 2012).

Changing the discretization of the horizontal pressure gradient is possible with the namelist switch `igradp_method` (`nonhydrostatic_nml`), but not recommended. Nevertheless, the reference state is still of some use for ICON. In the standard configuration of ICON, explicit use of the reference state is made when computing the advective horizontal fluxes for ρ and θ_v.

With the base state at hand, the vertical acceleration due to the pressure gradient and gravity in Eq. (3.2) is rewritten as

$$\begin{aligned}
-c_{pd}\widehat{\theta}_v \frac{\partial \overline{\pi}}{\partial z} - g &= -c_{pd}\left(\theta_{v0} + \theta_v'\right)\frac{\partial\left(\pi_0 + \pi'\right)}{\partial z} \\
&= -c_{pd}\left(\theta_v \frac{\partial \pi'}{\partial z} + \theta_v' \frac{\mathrm{d}\pi_0}{\mathrm{d}z}\right) - c_{pd}\theta_{v0}\frac{\mathrm{d}\pi_0}{\mathrm{d}z} - g \\
&\overset{(3.10)}{=} -c_{pd}\left(\theta_v \frac{\partial \pi'}{\partial z} + \theta_v' \frac{\mathrm{d}\pi_0}{\mathrm{d}z}\right)
\end{aligned}$$

The vertical momentum equation finally reads

$$\frac{\partial \widehat{w}}{\partial t} + \widehat{\boldsymbol{v}}_h \cdot \nabla \widehat{w} + \widehat{w}\frac{\partial \widehat{w}}{\partial z} = -c_{pd}\left(\theta_v \frac{\partial \pi'}{\partial z} + \theta_v' \frac{\mathrm{d}\pi_0}{\mathrm{d}z}\right) .$$

The perturbation fields π' and θ_v' are obtained from the predicted full fields and reference fields via $\psi' = \widehat{\psi} - \psi_0$.

3.3. Simplifying Assumptions in the Recent Model Version

The recent model version does not account for mass loss/gain due to precipitation/evaporation. In particular, the following assumptions are made:

The term $\sum_k \overline{\sigma}_k^{conv}$ on the r.h.s. of Eq. (3.4), which describes the net mass tendency of the convection parameterization, is neglected. Thus the model neither accounts for mass loss due to convective precipitation, nor mass re-distribution due to convective motions. The mass continuity equation takes the form

$$\frac{\partial \overline{\rho}}{\partial t} + \nabla \cdot \left(\overline{\rho}\widehat{\boldsymbol{v}}\right) = 0 . \tag{3.11}$$

At the surface, the boundary condition for $\widehat{w}$, Eq. (3.8), is approximated as

$$\overline{\rho}\widehat{w}|_s = \sum\nolimits_k \overline{\rho}_k \widehat{w}_k|_s = 0 , \tag{3.12}$$

which in terrain-following coordinates translates to $\overline{\rho}\widehat{w}|_s = \overline{\rho}\widehat{\boldsymbol{v}}\cdot\nabla h$. h denotes the topography height. Thus, the simulated atmospheric system is assumed to be closed w.r.t. total mass.

The sedimentation fluxes at the surface $\overline{S_k}|_s$ as well as the surface evaporation flux $\overline{E}_v|_s$, which appear in the partial mass continuity equations, are retained. In order for Eq. (3.12) to hold, the (implicit) assumption is that the corresponding mass loss/gain due to sedimentation/evaporation is compensated by a fictitious flux of dry air across the surface.

Away from the surface, the diffusion fluxes of all airborne constituents (except for dry air) are neglected. The diffusive fluxes of all precipitating constituents, however, are taken into account. The continuity equation for the total mass is used in the form (3.11). Since Eq. (3.11) only holds if the constraint $\sum_k \overline{J}_k^z = 0$ holds, again, the (implicit) assumption made is that a fictitious diffusion flux of dry air counteracts the sedimentation fluxes such that the total mass in a volume moving with the barycentric velocity is conserved.

In summary, the simplifying assumptions can be characterized by the following (equivalent) statements:

- The current model version conserves the total air mass instead of the dry air mass.
- The precipitation mass sink and the evaporation mass source are neglected in the total mass budget of the model.
- The net mass gain or loss due to precipitation/evaporation does not affect the surface pressure.

The latter point becomes obvious, when writing down the (hydrostatic) pressure tendency equation and applying the approximations (3.11)–(3.12) (see also Wacker and Herbert (2003)). Starting from the hydrostatic equation $\frac{\partial \overline{p}}{\partial z} = -\overline{\rho} g$ it follows:

$$
\begin{aligned}
\frac{\partial}{\partial t}\int_{\overline{p}_s}^{0} \mathrm{d}p &= -g\frac{\partial}{\partial t}\int_{z_s}^{\infty} \overline{\rho}\,\mathrm{d}z \\
\frac{\partial \overline{p}_s}{\partial t} &= g\int_{z_s}^{\infty} \frac{\partial \overline{\rho}}{\partial t}\,\mathrm{d}z \\
\frac{\partial \overline{p}_s}{\partial t} &= -g\int_{z_s}^{\infty} \nabla\cdot(\overline{\rho}\widehat{\boldsymbol{v}}) - \sum\nolimits_k \overline{\sigma}_k^{conv}\,\mathrm{d}z \\
\frac{\partial \overline{p}_s}{\partial t} &= -g\int_{z_s}^{\infty} \nabla_h\cdot(\overline{\rho}\widehat{\boldsymbol{v}}_h)\,\mathrm{d}z + g\,(\overline{\rho}w)\,|_s + g\overline{P}^{conv}|_s \\
\frac{\partial \overline{p}_s}{\partial t} &= -g\int_{z_s}^{\infty} \nabla_h\cdot(\overline{\rho}\widehat{\boldsymbol{v}}_h)\,\mathrm{d}z + g\cancel{\frac{\overline{\rho}|_s}{\overline{\rho}|_s - \sum_{kprec}\overline{\rho}_k|_s}\left(\overline{E}_v - \sum_{kprec}\overline{S}_k|_s\right)} + \cancel{g\overline{P}^{conv}}|_s\,,
\end{aligned}
$$

with the convective surface precipitation flux

$$
\overline{P}^{conv}|_s = \int_{z_s}^{\infty} \sum\nolimits_k \overline{\sigma}_k^{conv}\,\mathrm{d}z\,.
$$

Thus, dynamical effects of the evaporation/precipitation mass source/sink are neglected. I.e. related pressure changes are ignored.

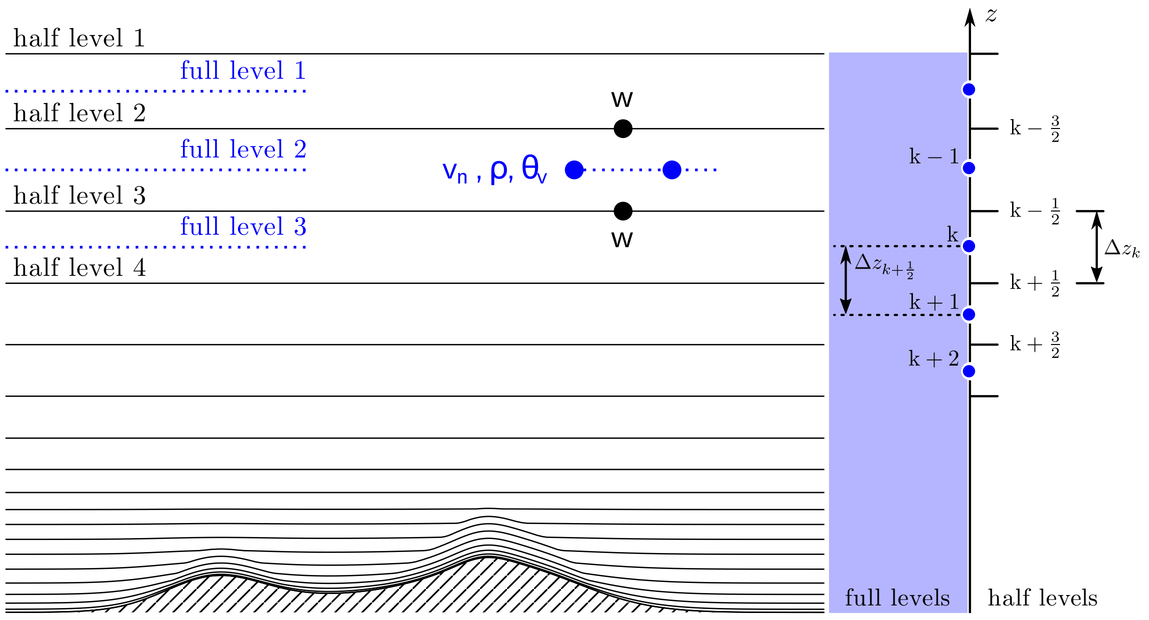

Figure 3.2.: Illustration of ICON's vertical levels. With `num_lev` layers, there are `num_lev` + 1 so-called *half levels*. The half levels $k - 1/2$, $k + 1/2$ enclose layer k at the centers of which are the corresponding full levels k, for $k = 1, \dots,$ `num_lev`. Layer 1 is at the top of the atmosphere and layer n at the bottom of the atmosphere. Half level `num_lev` + 1 coincides with the Earth's surface.

3.4. Vertical Coordinates

In a nonhydrostatic model, a vertical coordinate in terms of pressure does not make sense since it cannot be taken for granted that the pressure is monotonously decreasing with increasing altitude. In general, the air mass of an air column above a certain point can not be calculated from the pressure at that point anymore. Instead, a geometric altitude grid has to be used.

In ICON the choice is a height based coordinate system that follows the terrain and consequently, the top and bottom triangle faces are inclined with respect to the tangent plane on a sphere. Due to the fact that the model levels gradually change into levels of constant height as the distance from the lower boundary increases, top and bottom triangle faces of a grid box are also slightly inclined to each other. The exact altitude of each grid box depends on the geographical position on the globe. The top and bottom faces are called *half levels* of the vertical grid, the center of the box is said to be at the *full level* of the vertical grid, see Fig. 3.2 for an illustration. Note that the numbering of full and half levels is top-down, starting with $l = 1$ for the top half- and full level. A Lorenz-type staggering is used in the vertical, which means that horizontal velocity, virtual potential temperature and density are defined at full levels, whereas vertical velocity is defined at half levels.

When setting up an ICON simulation, the total number of vertical levels has to be specified for each domain via

`num_lev` (namelist `run_nml`, list of integer value)
Comma-separated list of integer values giving the number of vertical full levels for each domain.

If the number of vertical levels is desired to vary between domains, setting the namelist parameter `lvert_nest` (`run_nml`) to `.TRUE.` is required. See Section 3.9.3 for more information on vertical nesting.

Two variants of a height-based terrain-following vertical coordinate are available in ICON. Both of which are briefly described in the following section.

General vertical height coordinate. It will become clear from the description of the terrain-following coordinate below that the exact vertical axis definition depends on a multitude of parameter settings. This makes it virtually impossible to encode the exact vertical coordinate parameters themselves in the appropriate section of the GRIB code. The data sets which are produced by the ICON model therefore contain only a *reference* to a vertical grid. Apart from very basic information like the number of vertical levels, only a number identifying the special vertical grid used is provided. The actual vertical height coordinate is then specified by providing a 3D (GRIB2) field which defines the height of every grid point.

This indirect *reference grid* approach raises the same questions that played a role in the handling of the horizontal grid, see Section 2.1.8: In order to find out if identical vertical coordinate options were used for two given data sets, the GRIB2 data records contain special meta-data items, namely `numberOfVGridUsed` and `uuidOfVGrid`.

3.4.1. Terrain-following Hybrid Gal-Chen Coordinate

The *terrain-following hybrid Gal-Chen coordinate* (Simmons and Burridge, 1981) is an extension of the classic terrain-following coordinate introduced by Gal-Chen and Somerville (1975). As shown by Klemp (2011), it can be expressed in the form

$$\begin{aligned} z(x,y,\eta) &= \frac{(H - B'(\eta)\,h(x,y))}{H}\eta + B'(\eta)\,h(x,y) \\ &= \eta + B'(\eta)\left(1 - \frac{\eta}{H}\right) h(x,y)\,, \end{aligned} \tag{3.13}$$

where z represents the height of the coordinate surfaces η, $h(x,y)$ is the terrain height, and H denotes the domain height. With $B'(\eta) = 1$ the coordinate reverts to the classic formulation by Gal-Chen and Somerville (1975), i.e. the coordinate is terrain-following at the surface ($\eta = 0$) and becomes flat at model top ($\eta = H$). By choosing B' appropriately, a more rapid transition from terrain-following at the surface toward constant height can be achieved. One popular choice is to set

$$B'(\eta)\left(1 - \frac{\eta}{H}\right) = 1 - \frac{\eta}{z_{flat}}, \quad \text{with } z_{flat} < H$$

such that coordinate surfaces become constant height surfaces above $z = z_{flat}$. Sometimes, Equation (3.13) is also written in the discretized form

$$z_h(x,y,k) = A(k) + B(k)\,h(x,y)\,, \quad k = 1, ..., \texttt{num\_lev} + 1 \tag{3.14}$$

where k denotes the vertical level index and z_h is the half level height.

Configuring the Hybrid Gal-Chen Coordinate

The main switch for selecting the Gal-Chen hybrid coordinate is

`ivctype = 1` (namelist `nonhydrostatic_nml`, integer value)

In that case the user has to provide the vertical coordinate table (vct) as an input file. The table consists of the A and B values (see Equation (3.14)) from which the half level heights $z_h(x, y, k)$ can be deduced. A(k)[m] are fixed height values, with $A(1)$ defining the model top height H and $A(\texttt{num\_lev} + 1) = 0\,\mathrm{m}$. The dimensionless values B(k) control the vertical decay of the topography signal, with $B(1) = 0$ and $B(\texttt{num\_lev} + 1) = 1$. Thus, at each horizontal grid point $z_h(x, y, 1)$ is the model top height, while $z_h(x, y, \texttt{num\_lev} + 1)$ is the surface height.

The structure of the expected input file is depicted in Table 3.2. Example files can be found in `icon/vertical_coord_tables`. The file must obey the following naming rule: *atm_hyb_sz_[nlev]*, where [nlev] must be replaced by the total number of full levels. ICON expects the file to be located in the base directory from which the model is started. Note that there is no namelist parameter with which the location and name of the file can be specified. The namelist parameter `vertical_grid_filename` (`grid_nml`), which one might be tempted to use for that purpose, is meant for something slightly different: Its purpose is to read in a vertical grid file (NetCDF format) that has been written to disc by a previous ICON run.

```
# File structure
# --------------
# A and B values are stored in arrays vct_a(k) and vct_b(k).
# The files in text format are structured as follows:
#
#  -------------------------------------
# |    k     vct_a(k) [m]   vct_b(k) [] | <- first line of file = header line
# |    1       A(1)            B(1)     | <- first line of A and B values
# |    2       A(2)            B(2)     |
# |    3       A(3)            B(3)     |
# |    .                                |
# |    .                                |
# | nlev+1     A(nlev+1)       B(nlev+1)| <- last line of A and B values
# |=====================================| <- lines from here on are ignored
# |Source:                              |    by mo_hyb_params:read_hyb_params
# |<some lines of text>                 |
# |Comments:                            |
# |<some lines of text>                 |
# |References:                          |
# |<some lines of text>                 |
#  -------------------------------------
```

Table 3.2.: Structure of vertical coordinate table as expected by the ICON model.

3.4.2. SLEVE Coordinate

In the case of a terrain-following hybrid Gal-Chen coordinate the influence of terrain on the coordinate surfaces decays only linearly with height. The basic idea of the *Smooth Level Vertical* SLEVE coordinate (Schär et al., 2002, Leuenberger et al., 2010) is to increase the decay rate, by allowing smaller-scale terrain features to be removed more rapidly with height. To this end, the topography $h(x, y)$ is divided into two components

$$h(x, y) = h_1(x, y) + h_2(x, y),$$

where $h_1(x, y)$ denotes a smoothed representation of $h(x, y)$, and $h_2(x, y) = h(x, y) - h_1(x, y)$ contains the smaller-scale contributions. The coordinate is then defined as

$$z(x, y, \eta) = \eta + B_1(\eta)\, h_1(x, y) + B_2(\eta)\, h_2(x, y)\,.$$

Different decay functions B_1 and B_2 are now chosen for the decay of the large- and small-scale terrain features, respectively. These functions are selected such that the influence of small-scale terrain features on the coordinate surfaces decays much faster with height than their large-scale (well-resolved) counterparts. The squeezing of the model layers above steep mountains is limited automatically in order to prevent (nearly) intersecting layers that would cause numerical instabilities.

Configuring the SLEVE Coordinate

The main switch for selecting the SLEVE vertical coordinate is

`ivctype = 2` (namelist `nonhydrostatic_nml`, integer value)

This is the default and recommended setting. The vertical grid is constructed during the initialization phase of ICON, based on additional parameters defined in `sleve_nml`. Here we will only discuss the most relevant parameters. For a full list, the reader is referred to the namelist documentation.

Namelist `sleve_nml`:

`top_height` (namelist `sleve_nml`, real value)
Height of model top.

`flat_height` (namelist `sleve_nml`, real value)
Height above which the coordinate surfaces become constant height surfaces.

`min_lay_thckn` (namelist `sleve_nml`, real value)
Layer thickness of lowermost layer.

Note for advanced users: On default, a vertical stretching is applied such that coordinate surfaces become non-equally distributed along the vertical, starting with a minimum thickness of `min_lay_thckn` between the lowermost and second lowermost half-level. If constant layer thicknesses are desired, `min_lay_thckn` must be set to a value ≤ 0. The layer thickness is then determined as `top_height/num_lev`. Control output of the vertical layer distribution is written to `stderr`.

3.5. Temporal Discretization

In this section we will focus on time differencing in isolation and will neglect any complexity due to space differencing. Before we dive into the (nasty) details of ICON's time discretization, let us take a step back and try to grasp the basic idea.

3.5.1. Basic Idea

Consider an arbitrary first-order ordinary differential equation of the form

$$\frac{\mathrm{d}\psi(\vec{x},t)}{\mathrm{d}t} = F(\psi(\vec{x},t),t)\,. \tag{3.15}$$

Here, $\psi : \mathbb{R}^3 \times \mathbb{R} \to \mathbb{R}^q$ is the q-dimensional vector of state variables. In real applications, the vector-valued flux function $F : \mathbb{R}^q \times \mathbb{R} \to \mathbb{R}^q$ might be very complex.

Let t_{n-m} denote some time in the past and t_{n+1} some time in the future. Now we integrate Eq. (3.15) from time t_{n-m} to t_{n+1}, which gives

$$\psi(\vec{x},t_{n+1}) - \psi(\vec{x},t_{n-m}) = \int_{t_{n-m}}^{t_{n+1}} F(\psi(\vec{x},t),t)\,\mathrm{d}t\,.$$

We can try to approximate the integral on the right hand side (r.h.s.) using some weighted average of F at known discrete time levels. In the following we will restrict ourselves to simple two-level time-stepping schemes, i.e. we set $m = 0$ and only make use of F at the discrete times t_n and t_{n+1} (for a general survey of time-differencing schemes, see Randall (2017)). With this restriction we get

$$\frac{\psi(\vec{x},t_{n+1}) - \psi(\vec{x},t_n)}{\Delta t} = \alpha F_{n+1} + \beta F_n\,. \tag{3.16}$$

The coefficients α and β must satisfy the so called *consistency condition*

$$\alpha + \beta = 1\,,$$

such that the r.h.s. of Eq. (3.16) represents some averaged F. Equation (3.16) represents a whole family of simple two-step schemes. For example, by choosing $\alpha = 0$, $\beta = 1$ we arrive at the simple Euler forward scheme, while for $\alpha = 1$, $\beta = 0$ we get the (implicit) Euler backward scheme, both of which are first order accurate. Choosing $\alpha = \beta = 0.5$ leads to the implicit *trapezoidal* scheme, which is of second order accuracy.

One way to avoid the implicity of the trapezoidal scheme while retaining higher order is to switch to iterative schemes, also known as *predictor-corrector* schemes. This is the way pursued in ICON. The key idea of the predictor-corrector scheme is to replace the unwieldy F_{n+1} by an estimate $F^*_{n+1} = F\left(\psi^*_{n+1}, t_{n+1}\right)$ with ψ^*_{n+1} computed by an explicit scheme, e.g. a forward Euler scheme. The full predictor-corrector scheme reads

$$\begin{aligned} \texttt{predictor:} \quad & \psi^*(\vec{x}, t_{n+1}) = \psi(\vec{x}, t_n) + \Delta t F_n \\ \texttt{corrector:} \quad & \psi(\vec{x}, t_{n+1}) \;= \psi(\vec{x}, t_n) + \Delta t \left\{F^*_{n+1},\, F_n\right\}_\alpha \end{aligned} \tag{3.17}$$

Here we have introduced the notation

$$\{x,\, y\}_\alpha := \alpha\, x + (1-\alpha)\, y \;.$$

Note that for $\alpha = 1$, Equation (3.17) is an imitation of the Euler backward scheme (termed Matsuno scheme, (Matsuno, 1966)), while for $\alpha = 0.5$, it is an imitation of the *trapezoidal* scheme (termed *Heun's method*). The Matsuno scheme has first-order accuracy, and Heun's method has second-order accuracy.

In simplified terms, the time integration scheme of ICON can be regarded as a mixture of the Matsuno scheme and the Heun scheme, as the coefficient α used by ICON varies between these two extremes.

3.5.2. Implementation Details

Now, in the terminology of the previous section, in ICON we have

$$\psi(\vec{x}, t) = \left[v_n(\vec{x}, t), w(\vec{x}, t), \rho(\vec{x}, t), \pi(\vec{x}, t)\right]^{\mathsf{T}} .$$

Here, we have omitted the partial densities $\rho\, q_k$ from the vector of state variables. The prognostic equation (3.5) is treated with a different time discretization, as will be explained in Section 3.6.

For the sake of brevity we omit the notation for Reynolds- and Hesselberg averages. The subscripts n, $n+1^*$ and $n+1$ will be used to denote the current time level, the resulting time level of the predictor step and the new time level, respectively. They should not be confused with the subscript n used to denote the normal velocity component v_n, or the horizontal derivative in edge-normal direction $\partial/\partial n$.

The time discretization complies with the explicit two-time level predictor-corrector scheme which was described in the previous section, except for those terms describing vertical sound-wave propagation. These terms, i.e. vertical derivatives of w and π are treated implicitly for reasons of numerical stability and efficiency. Below, the implicit terms are marked in blue .

Predictor step:

$$\frac{v_n^{n+1^*} - v_n^n}{\Delta t} = -\mathrm{adv}(v_n^n) - c_{pd}\theta_v^n \frac{\partial \pi'^{,n}}{\partial n} + F(v_n^n) \tag{3.18}$$

$$\frac{w^{n+1^*} - w^n}{\Delta t} = -\mathrm{adv}(w^n) - c_{pd}\theta_v'^{,n} \frac{\mathrm{d}\pi_0}{\mathrm{d}z} - c_{pd}\theta_v^n \left\{ \frac{\partial \pi'^{,n+1^*}}{\partial z}, \frac{\partial \pi'^{,n}}{\partial z} \right\}_\eta \tag{3.19}$$

$$\frac{\rho^{n+1^*} - \rho^n}{\Delta t} = -\nabla_h \cdot \left(v_n^{n+1^*} \rho^n \right) - \frac{\partial}{\partial z} \left[\left\{ w^{n+1^*}, w^n \right\}_\eta \rho^n \right]$$

$$\frac{\pi^{n+1^*} - \pi^n}{\Delta t} = -\frac{R_d}{c_{vd}} \left(\frac{\pi^n}{\rho^n \theta_v^n} \right) \left[\nabla_h \cdot \left(v_n^{n+1^*} \rho^n \theta_v^n \right) + \frac{\partial}{\partial z} \left[\left\{ w^{n+1^*}, w^n \right\}_\eta \rho^n \theta_v^n \right] \right] + Q^n \tag{3.20}$$

with

$$\mathrm{adv}(v_n^n) = \frac{\partial K_h^n}{\partial n} + (\zeta^n + f)\, v_t^n + w^n \frac{\partial v_n^n}{\partial z}$$
$$\mathrm{adv}(w^n) = \boldsymbol{v}_h^n \cdot \nabla w^n + w^n \frac{\partial w^n}{\partial z}\,.$$

The terms $F(v_n^n)$ and Q^n denote diabatic momentum and Exner pressure tendencies due to *slow physics processes*, i.e. parameterized convection, orographic and non-orographic gravity waves and radiation. See Section 3.7.1 for more details on the distinction between fast and slow physics processes.

The implicitness parameter η (with $0 \le \eta \le 1$) for the vertically implicit sound wave solver has a default value of $\eta = 0.65$ which is usually sufficient to ensure numerical stability in real-case applications. If required, this value can be modified with the namelist parameter `vwind_offctr` (`nonhydrostatic_nml`). Note that `vwind_offctr` presents the off-centering `vwind_offctr` $= \eta - 0.5$ (i.e., the default is `vwind_offctr` $= 0.15$). Its permissible range is given by

$$0 \le \texttt{vwind\_offctr} \le 0.5\,.$$

Corrector step:

$$\begin{aligned}
\frac{v_n^{n+1}-v_n^n}{\Delta t} &= -\left\{\mathrm{adv}(v_n^{n+1^*}),\,\mathrm{adv}(v_n^n)\right\}_\alpha \\
&\quad - c_{pd}\left\{\theta_v^{n+1^*},\,\theta_v^n\right\}_\delta \left\{\frac{\partial \pi'^{,n+1^*}}{\partial n},\,\frac{\partial \pi'^{,n}}{\partial n}\right\}_\delta \\
&\quad - F_d(v_n^{n+1^*}) + F(v_n^n) \qquad (3.21)\\
\frac{w^{n+1}-w^n}{\Delta t} &= -\left\{\mathrm{adv}(w^{n+1^*}),\,\mathrm{adv}(w^n)\right\}_\alpha \\
&\quad - c_{pd}\left\{\theta_v'^{,n+1^*},\,\theta_v'^{,n}\right\}_\delta \frac{\mathrm{d}\pi_0}{\mathrm{d}z} \\
&\quad - c_{pd}\left\{\theta_v^{n+1^*},\,\theta_v^n\right\}_\delta \left\{\frac{\partial \pi'^{,n+1}}{\partial z},\,\frac{\partial \pi'^{,n}}{\partial z}\right\}_\eta \\
\frac{\rho^{n+1}-\rho^n}{\Delta t} &= -\nabla_h\cdot\left(v_n^{n+1}\rho^n\right) - \frac{\partial}{\partial z}\left[\left\{w^{n+1},\,w^n\right\}_\eta\left\{\rho^{n+1^*},\,\rho^n\right\}_\delta\right] \\
\frac{\pi^{n+1}-\pi^n}{\Delta t} &= -\frac{R_d}{c_{vd}}\left(\frac{\pi^n}{\rho^n\theta_v^n}\right)\Bigg[\nabla_h\cdot\left(v_n^{n+1}\rho^n\theta_v^n\right) \\
&\quad + \frac{\partial}{\partial z}\left[\left\{w^{n+1},\,w^n\right\}_\eta\left\{\rho^{n+1^*},\,\rho^n\right\}_\delta\left\{\theta_v^{n+1^*},\,\theta_v^n\right\}_\delta\right]\Bigg] \\
&\quad + Q^n
\end{aligned}$$

The term $F_d(v_n^{n+1^*})$ represents 4th order divergence damping which has been introduced in order to control checkerboard noise.

The parameter α denotes the Matsuno parameter which was introduced in Section 3.5.1. With respect to the velocity, it can be used to make the explicit part of the corrector step resemble either a Matsuno-type scheme ($\alpha \longrightarrow 1$) or Heun's method ($\alpha \longrightarrow 0.5$). The default value of the Matsuno-parameter for velocity is given by $\alpha = 0.75$.

A second Matsuno parameter $0 \le \delta \le 1$ exists for the thermodynamic variables ρ and θ_{v_n}, where the default value of the coefficient is $\delta = 0.4$. The corresponding namelist parameters are named `veladv_offctr` and `rhotheta_offctr` in the namelist `nonhydrostatic_nml`. Note again that both define the off-centering from 0.5 rather than the absolute value.

In order to close the system of equations, for both substeps (predictor and corrector), the quantity θ_v must be calculated from the state variables π and ρ. We explain this in the following, using the notation $\pi^{\mathrm{new}} \equiv \pi^{n+1^*}$ or $\pi^{\mathrm{new}} \equiv \pi^{n+1}$ for the predictor and corrector step.

Once the updated state vector

$$\psi^{\mathrm{new}}(\vec{x},t) = \left[v_n^{\mathrm{new}}(\vec{x},t), w^{\mathrm{new}}(\vec{x},t), \rho^{\mathrm{new}}(\vec{x},t), \pi^{\mathrm{new}}(\vec{x},t)\right]^{\mathsf{T}}$$

is known, the virtual potential temperature θ_v^{new} is diagnosed from the linearized equation of state (3.9)

$$\frac{\pi^{\mathrm{new}}-\pi^n}{\pi^n} = \frac{R_d}{c_{vd}}\frac{(\rho\theta_v)^{\mathrm{new}}-(\rho\theta_v)^n}{(\rho\theta_v)^n}. \qquad (3.22)$$

The rationale behind that is as follows: Multiplying (3.22) by Δt^{-1} and rearranging yields

$$\frac{(\rho\theta_v)^{\text{new}} - (\rho\theta_v)^n}{\Delta t} = \frac{c_{vd}}{R_d}\left(\frac{\rho^n\theta_v^n}{\pi^n}\right)\frac{\pi^{\text{new}} - \pi^n}{\Delta t}\,. \tag{3.23}$$

Thus, diagnosing θ_v^{new} from (3.22) can be interpreted as solving two prognostic equations for the two thermodynamic variables π and θ_v, instead of one prognostic equation for π and the equation of state. By doing so, $\rho\theta_v$ is exactly conserved (in the absence of diabatic terms). The two prognostic equations are constrained by (3.23), i.e. the same flux divergence is used. As a side effect, however, the solution at a particular point in time is not constrained by the equation of state (3.9) – only its time evolution is. This approach was first described by Gassmann (2013).

Pragmatic Simplifications

A potential disadvantage of predictor-corrector schemes as compared to non-iterative schemes is its computational expense. This is because the forcing terms (r.h.s.) must be evaluated twice per time step. Therefore, several terms have been simplified provided that the simplification proved to not degrade the quality of the results significantly. The following pragmatic simplifications have been performed:

- The horizontal and vertical momentum advection at the predictor step is re-used from the corrector step of the preceding time step. With time level n^* denoting $n+1^*$ from the preceding time step this can be written as

  $$\text{Equation (3.18):} \qquad \text{adv}(v_n^n) \simeq \text{adv}(v_n^{n^*})$$
  $$\text{Equation (3.19):} \qquad \text{adv}(w^n) \simeq \text{adv}(w^{n^*})$$

  By this, in each time step the momentum advection needs to be computed only once.

  The first predictor step following the physics step represents an exception. At this time level the momentum advection from the preceding corrector step does not provide a suitable estimate, as the physics step might have changed v_n considerably.

- Another simplification relates to the horizontal pressure gradient term which occurs in the predictor and corrector step of v_n. Using time level n in the predictor and an interpolated value between n and $n+1^*$ in the corrector provides an effective damping mechanism for horizontally propagating sound waves, without significantly impacting gravity waves. A very similar effect can be achieved by using the same horizontal pressure gradient in the predictor and corrector, however, with the pressure being extrapolated in time.

  $$\text{Equation (3.18):} \qquad c_{pd}\theta_v^n\frac{\partial\pi'^{,n}}{\partial n} \simeq c_{pd}\theta_v^n\frac{\partial\pi'^{,\tilde{n}}}{\partial n}$$
  $$\text{Equation (3.21):} \qquad c_{pd}\left\{\theta_v^{n+1^*}, \theta_v^n\right\}_\delta \left\{\frac{\partial\pi'^{,n+1^*}}{\partial n}, \frac{\partial\pi'^{,n}}{\partial n}\right\}_\delta \simeq c_{pd}\theta_v^n\frac{\partial\pi'^{,\tilde{n}}}{\partial n}$$

  By this, in each time step the horizontal pressure gradient needs to be computed only once. The time level $\tilde{n}$ at which the horizontal gradient is taken is an extrapolated time level using the levels n and $n-1$:

  $$\pi'^{,\tilde{n}} = (1+\gamma)\pi'^{,n} - \gamma\pi'^{,n-1}$$

The temporal extrapolation factor is chosen from the range $\gamma \in \left[\frac{1}{3}, \frac{2}{3}\right]$, with the default being $\gamma = 1/3$. The corresponding namelist parameter is named `exner_expol` (`nonhydrostatic_nml`).

Vertically Implicit Solver

The solution to the predictor-corrector scheme described above is mostly straightforward, as the majority of terms are treated in an explicit manner. This, however does not hold for the prognostic equation for vertical wind, since the solution for w^{n+1^*} depends on π^{n+1^*}, which itself depends on w^{n+1^*} (see Equations (3.19) and (3.20)).

Before the exact solution method is derived below, the overall solution strategy can be described as follows: First, π is eliminated from Eq. (3.19) by inserting the prognostic equation (3.20). Then this results in a linear system of equations for the unknown w's in the vertical direction. The derivation for the corrector step is basically identical and differs only w.r.t. the time levels that are used for ρ and θ_v.

We start with the vertical discretization of (3.19) and (3.20). When using basic centered differences, and noting that $\partial\pi/\partial t = \partial\pi'/\partial t$ this leads to

$$w_{k+1/2}^{n+1^*} = Z_{k+1/2}^{w\,\mathrm{expl}} - \Delta t c_{pd} \theta_{v,k+1/2}^{n}\, \eta \frac{\pi_k^{\prime,n+1^*} - \pi_{k+1}^{\prime,n+1^*}}{\Delta z_{k+1/2}} \tag{3.24}$$

$$\pi_k^{\prime,n+1^*} = Z_k^{\pi\,\mathrm{expl}} - \Delta t \frac{R_d}{c_{vd}} \left(\frac{\pi_k^n}{\rho_k^n \theta_{v,k}^n}\right) \eta \frac{(w^{n+1^*}\rho^n\theta_v^n)_{k-1/2} - (w^{n+1^*}\rho^n\theta_v^n)_{k+1/2}}{\Delta z_k}\,, \tag{3.25}$$

with the shorthand notations $Z_{k+1/2}^{w\,\mathrm{expl}}$ and $Z_k^{\pi\,\mathrm{expl}}$ for the explicit parts

$$\begin{aligned} Z_{k+1/2}^{w\,\mathrm{expl}} = w_{k+1/2}^{n} - \Delta t \Bigg[& \mathrm{adv}(w_{n^*})_{k+1/2} + c_{pd} \theta_{v,k+1/2}^{\prime,n} \frac{\mathrm{d}\pi_0}{\mathrm{d}z}\bigg|_{k+1/2} \\ & + c_{pd}\theta_{v,k+1/2}^{n} (1-\eta) \frac{\pi_k^{\prime,n} - \pi_{k+1}^{\prime,n}}{\Delta z_{k+1/2}} \Bigg] \end{aligned}$$

and

$$\begin{aligned} Z_k^{\pi\,\mathrm{expl}} = \pi_k^{\prime,n} - \Delta t \frac{R_d}{c_{vd}} \left(\frac{\pi_k^n}{\rho_k^n \theta_{v,k}^n}\right) \Bigg[& \nabla_h \cdot \left(v^{n+1^*} \rho^n \theta_v^n\right)_k \\ & + (1-\eta) \frac{(w^n\rho^n\theta_v^n)_{k-1/2} - (w^n\rho^n\theta_v^n)_{k+1/2}}{\Delta z_k} \Bigg] + \Delta t\, Q_n^k\,. \end{aligned}$$

$\Delta z_k = z_{k-1/2} - z_{k+1/2}$ denotes the thickness of the k^{th} cell which is bounded by the half levels $k \pm 1/2$, whereas $\Delta z_{k+1/2} = z_k - z_{k+1}$ denotes the thickness of the layer bounded by the full levels k and $k+1$ (see also Figure 3.2).

As an intermediate step, we compute $\pi_k^{\prime,n+1^*} - \pi_{k+1}^{\prime,n+1^*}$ from Eq. (3.25):

$$\begin{aligned}
\pi_k^{\prime,n+1^*} - \pi_{k+1}^{\prime,n+1^*} = Z_k^{\pi\,\mathrm{expl}} - Z_{k+1}^{\pi\,\mathrm{expl}} - \frac{\Delta t R_d}{c_{vd}}\eta \Bigg[& (w^{n+1^*}\rho^n\theta_v^n)_{k-1/2}\frac{\Gamma_k^n}{\Delta z_k} \\
& - (w^{n+1^*}\rho^n\theta_v^n)_{k+1/2}\left(\frac{\Gamma_k^n}{\Delta z_k} + \frac{\Gamma_{k+1}^n}{\Delta z_{k+1}}\right) \\
& + (w^{n+1^*}\rho^n\theta_v^n)_{k+3/2}\frac{\Gamma_{k+1}^n}{\Delta z_{k+1}}\Bigg] .
\end{aligned} \tag{3.26}$$

Here we have introduced Γ_k^n as an abbreviation for

$$\Gamma_k^n = \frac{\pi_k^n}{\rho_k^n \theta_{v,k}^n} .$$

Inserting Eq. (3.26) into Eq. (3.24) and collecting terms proportional to $w_{k-1/2}^{n+1^*}$, $w_{k+1/2}^{n+1^*}$, $w_{k+3/2}^{n+1^*}$ on the left hand side leads to:

$$\begin{aligned}
& - w_{k-1/2}^{n+1^*} \underbrace{\left[\Delta t \frac{c_{pd}\theta_{v,k+1/2}^n}{\Delta z_{k+1/2}} \eta \Delta t \frac{R_d}{c_{vd}} \rho_{k-1/2}^n \theta_{v,k-1/2}^n \eta \frac{\Gamma_k^n}{\Delta z_k}\right]}_{\text{sub-diagonal}} \\
& + w_{k+1/2}^{n+1^*} \underbrace{\left[1 + \Delta t \frac{c_{pd}\theta_{v,k+1/2}^n}{\Delta z_{k+1/2}} \eta \Delta t \frac{R_d}{c_{vd}} \rho_{k+1/2}^n \theta_{v,k+1/2}^n \eta \left(\frac{\Gamma_k^n}{\Delta z_k} + \frac{\Gamma_{k+1}^n}{\Delta z_{k+1}}\right)\right]}_{\text{main diagonal}} \\
& - w_{k+3/2}^{n+1^*} \underbrace{\left[\Delta t \frac{c_{pd}\theta_{v,k+1/2}^n}{\Delta z_{k+1/2}} \eta \Delta t \frac{R_d}{c_{vd}} \rho_{k+3/2}^n \theta_{v,k+3/2}^n \eta \frac{\Gamma_{k+1}^n}{\Delta z_{k+1}}\right]}_{\text{sup-diagonal}} \\
= \quad & Z_{k+1/2}^{w\,\mathrm{expl}} - \Delta t \frac{c_{pd}\theta_{v,k+1/2}^n}{\Delta z_{k+1/2}} \eta \left(Z_k^{\pi\,\mathrm{expl}} - Z_{k+1}^{\pi\,\mathrm{expl}}\right)
\end{aligned} \tag{3.27}$$

Equation (3.27) defines a linear system of equations from which the unknown vertical velocities $w_{k-1/2}^{n+1^*}$ can be computed. The system is tridiagonal and can be solved with the Thomas algorithm (Press et al., 2007, p. 57), given that suitably defined boundary conditions are provided. So far it is assumed that the upper and lower boundary are impermeable w.r.t. to mass, i.e. we set $w_{1/2}^{n+1^*} = w_{\mathrm{nlev}+1/2}^{n+1^*} = 0$. In case of vertical nesting, w at the upper boundary is interpolated from the parent domain.

3.6. Tracer Transport

The transport module is an important building block of any numerical weather prediction (NWP) or climate model, as it predicts the large-scale redistribution of water substances, chemical constituents or aerosols in the atmosphere due to air motion. Mathematically, it solves one of the fundamental laws of physics, namely the equation of tracer mass continuity (3.5). The transport module itself does not take into account tracer sources or sinks. It only predicts its large scale redistribution. Hence, for each tracer the transport module solves the simplified continuity equation

$$\frac{\partial \overline{\rho} \hat{q}_k}{\partial t} + \nabla \cdot (\overline{\rho} \widehat{q}_k \widehat{\boldsymbol{v}}) = 0 \tag{3.28}$$

(compare with Eq. (3.5)). Additional sources and sinks as well as turbulent diffusion are accounted for in the physics interface with a fractional step approach (see Section 3.7).

The numerical solution of Eq. (3.28) is based on so-called space-time finite volume methods. By space-time methods we refer to methods where the temporal and spacial discretizations are combined rather than separated. Space-time methods are also known as *cell-integrated semi-Lagrangian* schemes. As will become clear, such schemes are neither purely semi-Lagrangian, nor Eulerian in the classical sense. They are Eulerian in the sense that the flux of mass through the stationary walls of grid cells is considered. They are, however, semi-Lagrangian in the sense that trajectory calculations are needed for flux computation. In the literature such schemes are sometimes termed *Flux Form Semi-Lagrangian (FFSL)*. The specific implementation in ICON partly builds upon work by Lauritzen et al. (2010, 2011a), Harris and Lauritzen (2010), Skamarock and Menchaca (2010), Miura (2007) for the horizontal and Colella and Woodward (1984), Zerroukat et al. (2006) for the vertical.

As we are dealing with a Finite Volume (FV) discretization, it is worth noting that in the following all scalar variables ψ, whose storage location is at the triangle cell circumcenter, are interpreted as cell averages rather than point values, i.e.

$$\overline{\psi}_i^n = \frac{1}{\Delta V_i} \iiint\limits_{V_i} \psi(x, y, z, t^n) \, \mathrm{d}V \, ,$$

with ΔV_i denoting the volume of the i^{th} prismatic cell (the so-called control volume). Here and in the reminder of this Section, the overbar denotes volume averages rather than Reynolds averages.

3.6.1. Directional Splitting

By integrating the continuity equation (3.28) in space over a prismatic grid cell and in time over the time step Δt, a solution to (3.28) can formally be written as

$$\overline{\rho q}_{i,k}^{n+1} = \overline{\rho q}_{i,k}^{n} + \Delta t \, \left[\mathcal{H}(\overline{q}^n) + \mathcal{V}(\overline{q}^n)\right] \, , \tag{3.29}$$

where $\mathcal{H}$ and $\mathcal{V}$ denote the horizontal and vertical transport operators acting on q^n, and $\overline{\rho q}_{i,k}^{n+1}$ denoting the updated cell averaged partial density of constituent k at the time t^{n+1} (see Reinert, 2020).

Instead of solving this somewhat unwieldy equation in one sweep, a fractional step approach is taken in ICON such that separate equations for horizontal and vertical transport are solved consecutively. Of course, replacing equation (3.29) by some approximation involving the two subproblems

$$\overline{\rho q}_{i,k}^{*} = \overline{\rho q}_{i,k}^{\alpha} + \Delta t \, \mathcal{V}(\overline{q}^{\beta})$$
$$\overline{\rho q}_{i,k}^{**} = \overline{\rho q}_{i,k}^{\gamma} + \Delta t \, \mathcal{H}(\overline{q}^{\delta})$$

will inevitably result in a residual error. This error is known as the *splitting error*. On default, the following approximation to (3.29) is used:

$$\overline{\rho q}^{*}_{i,k} = \overline{\rho q}^{n}_{i,k} + \Delta t\, \mathcal{V}\left(\overline{q}^{n}\right) \tag{3.30}$$

$$\overline{\rho q}^{n+1}_{i,k} = \overline{\rho q}^{*}_{i,k} + \Delta t\, \mathcal{H}\left(\overline{q}^{*}\right) \tag{3.31}$$

In order to maintain $\mathcal{O}\left[\Delta t^2\right]$ accuracy, the order of the operators is reversed on alternate time steps. This might be regarded as a poor man's *Strang splitting* (Strang, 1968). Full Strang-splitting of the form $[\mathcal{V}(\Delta t/2)][\mathcal{H}(\Delta t)][\mathcal{V}(\Delta t/2)]$ has also been tested during the implementation phase. Except for being more expensive (the vertical operator is called twice per time step) no significant impact on the model results has been noted.

A shortcoming of the splitting (3.30), (3.31) is that it does not preserve an initially uniform tracer field (e.g. $q(x, y, z, t_0) = 1$) in a deformational flow since there is not enough information available to correctly do the conversion $\overline{\rho q}^{*} \longrightarrow \overline{q}^{*}$. Tempting candidates for this conversion might be $\overline{\rho}^{n}$ or $\overline{\rho}^{n+1}$ as they are readily available from ICON's dynamical core. Any such attempt, however, will not preserve an initially uniform tracer field. In order to do so, it is necessary to keep track of the changes in partial density ρq that are solely a result of mass convergence/divergence in the directions of splitting. Therefore we follow the method of Easter (1993) wherein the air mass continuity equation (3.5) is simultaneously reintegrated in the same split manner as the continuity equation for tracer mass.

$$\begin{aligned}
\overline{\rho q}^{*}_{i,k} &= \overline{\rho q}^{n}_{i,k} + \Delta t\, \mathcal{V}\left(\overline{q}^{n}\right) \\
\overline{\rho}^{*}_{i,k} &= \overline{\rho}^{n}_{i,k} + \Delta t\, \mathcal{V}\left(1\right) \\
\overline{q}^{*}_{i,k} &= \frac{\overline{\rho q}^{*}_{i,k}}{\overline{\rho}^{*}_{i,k}}
\end{aligned} \tag{3.32}$$

$$\begin{aligned}
\overline{\rho q}^{n+1}_{i,k} &= \overline{\rho q}^{*}_{i,k} + \Delta t\, \mathcal{H}\left(\overline{q}^{*}\right) \\
\overline{\rho}^{n+1}_{i,k} &= \overline{\rho}^{*}_{i,k} + \Delta t\, \mathcal{H}\left(1\right) \\
\overline{q}^{n+1}_{i,k} &= \frac{\overline{\rho q}^{n+1}_{i,k}}{\overline{\rho}^{n+1}_{i,k}}
\end{aligned} \tag{3.33}$$

Changes in partial density solely due to mass convergence/divergence are corrected for in equations (3.32) and (3.33). The key point here is that the intermediate density $\overline{\rho}^{*}$ rather than $\overline{\rho}^{n+1}$ or $\overline{\rho}^{n}$ is used to recover the mass fraction $\overline{q}^{*}$ in (3.32). The re-integration of (3.4) (second and fifth equation above) is rather straightforward, as it relies on pre-computed mass fluxes provided by the dynamical core.

3.6.2. Horizontal Transport

A rigorous derivation of the horizontal transport operator $\mathcal{H}(\overline{q})$ is beyond the scope of this document. We will merely concentrate on the general concept and illustrate graphically how the scheme works. The horizontal transport scheme belongs to the class of so-called **F**lux **F**orm **S**emi-**L**agrangian (FFSL) schemes (Harris and Lauritzen, 2010). In the literature such schemes are sometimes alternatively termed *Incremental remapping schemes* (Lipscomb and Ringler, 2005) or *streamline subgrid integration method* (Yeh, 2007).

Graphical Interpretation

Figure 3.3 provides a graphical interpretation of the FFSL-scheme. Black solid lines show the triangular grid, with thick solid lines highlighting an arbitrary cell with area ΔA_i for which the scheme will be explained. In the following we will refer to this cell as the Eulerian control volume (CV). The basic task is to compute the updated value $\overline{\rho q}_i^{n+1}$ for that cell on the basis of the old values $\overline{\rho q}_i^n$, the cell averages $\overline{q}_i$, and the velocity fields $\boldsymbol{v}^n$ and $\boldsymbol{v}^{n+1}$.

In order to set the stage, let us first take the Lagrangian viewpoint: Assume that the time dependent velocity field is known analytically such that the trajectories for all the air parcels are known, which terminate at the walls of the Eulerian CV at the new time t^{n+1}. As an example, trajectories for air parcels terminating at the CV vertices at t^{n+1} are depicted as gray lines. Accordingly we know the position of these air parcels at time t^n which we will denote as the starting points. By connecting the starting points we can construct the gray shaded area known as the Lagrangian CV. The latter encompasses all air parcels that are transported into the Eulerian CV (i.e. the grid cell) during the time interval $\left[t^n, t^{n+1}\right]$. In a standard semi-Lagrangian scheme the key task is to compute an estimate of the Lagrangian CV (gray shaded), followed by a computation of the total tracer mass contained. Then, the solution $\overline{\rho q_i}^{n+1}$ can easily be deduced from the Lagrangian finite-volume form of the continuity equation (3.28)

$$\overline{\rho q}_i^{n+1} \Delta A_i = \overline{\rho q}_i^n \Delta a_i \,,$$

where ΔA_i and Δa_i denote the area of the Eulerian and Lagrangian CV, respectively (see e.g. Lauritzen et al., 2011b). $\overline{\rho q}_i^n$ is the average tracer mass over the Lagrangian CV area a_i

$$\overline{\rho q}_i^n = \frac{1}{\Delta a_i} \iint_{a_i} \rho^n(x,y) q^n(x,y) \mathrm{d}A \,.$$

As mentioned before, a more Eulerian rather than semi-Lagrangian viewpoint is taken in ICON. Here we keep track of the flux of mass passing the Eulerian cell walls rather than the mass in the Lagrangian CV. This is where the yellow areas in Figure 3.3 enter the game. We will refer to these as *flux areas*. Since the individual edges of the Lagrangian CV pass through the flux areas during $\left[t^n, t^{n+1}\right]$, it is the mass inside the flux areas that is swept across the Eulerian CV walls during one time step. Thus, starting from the mass $\overline{\rho q}_i^n$ in the Eulerian CV and assuming that we know the shape as well as the tracer mass contained in the (yellow) flux areas, we can compute the updated value $\overline{\rho q}_i^{n+1}$.

Mathematically the scheme can be cast into the following flux form:

$$\overline{\rho q}_i^{n+1} = \overline{\rho q}_i^n - \frac{1}{\Delta A_i} \sum_{e=1}^{N_e} s_{ie} \, F_{ie} \quad \text{,with} \quad F_{ie} = \langle \overline{\rho}_i^e \rangle \iint\limits_{a_i^e} q^n(x,y) \, \mathrm{d}a \,, \tag{3.34}$$

where F_{ie} defines the total mass crossing the e^{th} wall during Δt and a_i^e denotes the flux area for the e^{th} wall. $s_i^e = \pm 1$ distinguishes inward and outward directed fluxes.

Note that this Eulerian viewpoint is fully equivalent to the semi-Lagrangian viewpoint. It can be shown (Lauritzen et al., 2011b) that all areas involved in our quasi-Eulerian approach (i.e. the Eulerian CV and the flux areas) sum up to the Lagrangian CV.

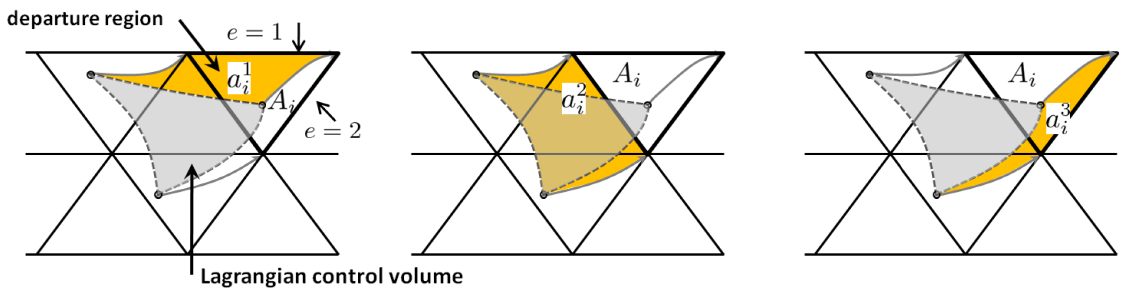

Figure 3.3.: Graphical illustration of the FFSL scheme. Black solid lines show the triangular grid, with thick solid lines highlighting the Eulerian control volume under consideration. Gray area shows the Lagrangian control volume and yellow areas show the flux areas (departure region) for each cell wall.

Basic Algorithm

The numerical algorithm which solves Eq. (3.34) for a single Eulerian CV proceeds in 4 major stages:

1. The flux area a_i^e for each cell wall is reconstructed by means of backward trajectories.
2. For each Eulerian CV the unknown tracer subgrid distribution $q(x, y, t_0)$ is estimated from the known cell averages $\overline{q}_i^n$ of the CV itself and surrounding cells. Several polynomial reconstructions, from linear to cubic, are available.
3. The total mass F_{ie} crossing the e^{th} wall is estimated by numerically evaluating the integral in Eq. (3.34). I.e. the estimated subgrid distribution $q(x, y, t_0)$ is integrated over the approximated flux area a_i^e by means of Gauss quadrature.
4. The sum on the r.h.s. of Eq. (3.34) is evaluated which leads to the solution $\overline{\rho q}_i^{n+1}$.

3.6.3. Vertical Transport

A rigorous derivation of the vertical transport operator $\mathcal{V}(q)$ is beyond the scope of this document. As for the horizontal operator $\mathcal{H}(q)$ we will concentrate on the basic concept.

Piecewise Parabolic Method (PPM)

The vertical transport scheme is based on the Piecewise Parabolic Method (PPM) developed by Colella and Woodward (1984). It is a finite volume scheme and thus inherently mass conserving. It makes use of a piecewise parabolic function for approximating the unknown subgrid distribution of a $1D$ scalar field $q(z)$. The function is forced to be continuous at cell interfaces. Its construction is based on the known cell averages $\overline{q}_k$. The PPM scheme bears some conceptual resemblance to the horizontal FFSL transport scheme. The basic concept is depicted in Figure 3.4 and described below.

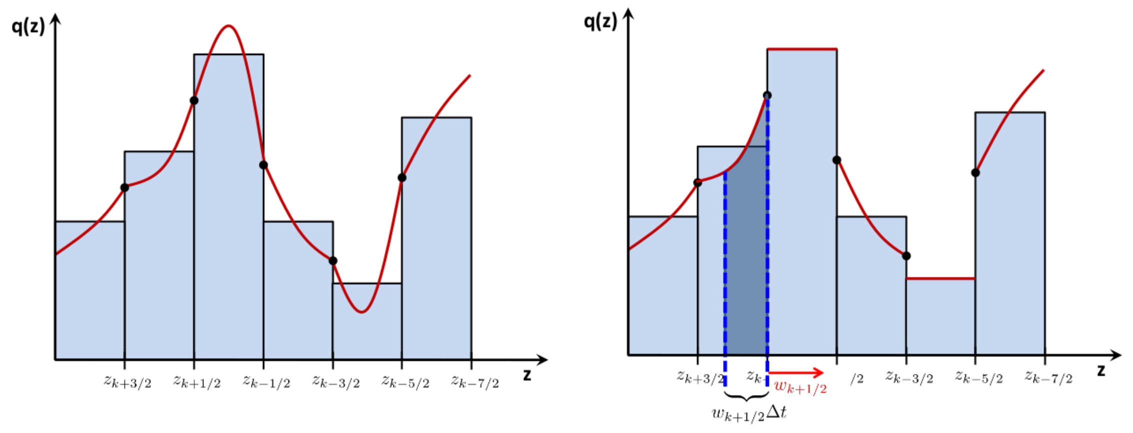

Figure 3.4.: The Piecewise Parabolic Method (PPM). Left: Unknown subgrid distribution $q(z)$ gets approximated by piecewise parabolic interpolants which are $\mathcal{C}^0$ continuous at cell walls. Right: Polynomial reconstruction is filtered (optional) to render the scheme monotonous. Integration step: Sub-grid distribution is integrated over the "area" $w\Delta t$ (dark blue) in order to determine the mass which enters the k^{th} cell during Δt.

Step 1: The subgrid distribution $q(\zeta, k)$ is reconstructed cell-wise in a vertical column by using the parabolic interpolant

$$q(\zeta, k) = a_0 + a_1\zeta + a_2\zeta^2 , \quad \text{with} \quad \zeta = \frac{z - z_{k+1/2}}{\Delta z_k} . \tag{3.35}$$

ζ is a dimensionless coordinate which is 1 at the grid cell top and 0 at its bottom. Specific to the PPM scheme is the way how this parabola is constructed. The unknown coefficients a_i are derived from the three constraints

$$\begin{aligned}
\int_0^1 q(\zeta, k)\mathrm{d}\zeta &= \overline{q}_k , \\
q(\zeta = 1, k) &= q_u = q_{k-1/2} , \\
q(\zeta = 0, k) &= q_l = q_{k+1/2} ,
\end{aligned} \tag{3.36}$$

which, expressed in words, state that the polynomial must be mass conserving, and that the polynomial equals q_u and q_l at its upper and lower end, respectively. q_u and q_l are appropriately reconstructed estimates at the upper and lower half levels and are shared between adjacent cells. By this, continuity of the reconstruction across cells is enforced.

When applying the constraints (3.36) the parabolic interpolant (3.35) can finally be written as a function of the grid scale variables $\overline{q}_k$, $q_{k+1/2}$, $q_{k-1/2}$

$$q(\zeta, k) = \overline{q}_k - \Delta q_k \left(\frac{1}{2} - \zeta\right) - a_{6,k}\left(\frac{1}{6} - \zeta + \zeta^2\right) , \tag{3.37}$$

with

$$\begin{aligned}
\Delta q_k &= q_{k-1/2} - q_{k+1/2} \\
a_{6,k} &= 6\overline{q}_k - 3q_{k-1/2} - 3q_{k+1/2}
\end{aligned}$$

The overall accuracy of the parabolic interpolant (3.37) strongly depends on the accuracy to which the edge values $q_{k\pm1/2}$ are known. Edge value estimates must be of at least third-order in order for the interpolant to exactly reconstruct a parabola. Here we follow Colella and Woodward (1984) and compute fourth-order edge value estimates, as this turned out to be beneficial to the overall accuracy of the scheme (see Lauritzen et al. (2011b, p. 228)).

An in-depth derivation of the edge-values is beyond the scope of this tutorial. Here we simply note that the edge estimate $q_{k+1/2}$ is computed from a cubic polynomial $c(z)$ evaluated at $z_{k+1/2}$. The cubic polynomial is constructed from the constraint that it must be mass conserving in each of the four cells surrounding half level $z_{k+1/2}$ (likewise for $q_{k-1/2}$, see e.g. Zerroukat et al. (2002)).

Step 2: As depicted in Figure 3.4, it is not guaranteed that the reconstruction preserves monotonicity or positive definiteness, especially near strong gradients. The scheme can optionally be made (semi-) monotonic or positive definite by filtering the polynomial reconstruction. The effect of a monotonic filter on the reconstructed parabolas is schematically depicted in Figure 3.4b. The filtering is controlled with the namelist switch `itype_vlimit` (`transport_nml`).

Step 3: In a last step, the mass that is swept across the cell wall during Δt is computed by integrating the subgrid distribution $q(\zeta, k)$ over the (upwind) flux area.

$$F_{k-1/2} = \frac{1}{\Delta t}\int_{z_{k-1/2}-w_{k-1/2}^{n+1/2}\Delta t}^{z_{k-1/2}} \rho(z)q(z)\mathrm{d}z\,, \quad \text{for} \quad w>0 \tag{3.38}$$

Vividly speaking, an estimate of the flux area can be gained by launching a backward trajectory at the given cell wall. In this 1D scheme, the flux area for the cell wall at $z_{k-1/2}$ is simply given as $-w_{k-1/2}^{n+1/2}\Delta t$, where w is the vertical velocity provided by the dynamical core.

For $w>0$ integration of (3.38) finally leads to the time-averaged vertical flux

$$F_{k-1/2} = \rho_{k-1/2}w_{k-1/2}\left[\overline{q}_k + \frac{1}{2}\Delta q_k\left(1-C_{k-1/2}\right) - \frac{1}{6}a_{6,k}\left(1-3C_{k-1/2}+2C_{k-1/2}^2\right)\right]\,,$$

with the Courant number $C_{k-1/2} = w_{k-1/2}\Delta t/\Delta z_k$.

In its standard version, the PPM scheme has a Courant number limitation of $|C|\leq 1$. It can, however, be easily extended to larger Courant numbers by splitting the computation of the mass fluxes (3.38) into so-called integer and fractional fluxes (Lin and Rood, 1996). In its current form in ICON, the PPM scheme is stable up to $|C|=5$.

Parabolic Spline Method (PSM)

As an alternative to PPM, the Parabolic Spline Method (Zerroukat et al., 2006) is available as well. PSM is similar to PPM, as both rely on piecewise parabolic functions for reconstructing the unknown sub-grid distribution in each cell. PSM, however, differs from PPM in terms of the edge-value estimate. The edge values are determined by imposing the following additional constraint on the parabola $q(\zeta, k)$ in (3.35)

$$\frac{1}{\Delta z_{k+1}} \frac{\mathrm{d}q_{k+1}}{\mathrm{d}\zeta}\bigg|_{\zeta=1} = \frac{1}{\Delta z_k} \frac{\mathrm{d}q_k}{\mathrm{d}\zeta}\bigg|_{\zeta=0} , \tag{3.39}$$

which states that the parabola's first derivative must be continuous at cell edges. Hence, while the PPM parabolas are continuous at cell edges, the PSM parabolas are even continuously differentiable. The latter turns the piecewise parabolic function into a parabolic spline. From the condition (3.39) an implicit equation sytem for the unknown edge values $q_{k+1/2}$ can be deduced, which is however beyond the scope of this tutorial (see Zerroukat et al., 2006).

A comparison of PSM and PPM reconstructions for an arbitrary irregular signal is depicted in Figure 3.5a. The signal is taken from Zerroukat et al. (2005) and is defined on the unit interval $z \in [0, 1]$. It is given in terms of cell averages (black dots) on a 1D grid with constant grid spacing. The solid red line depicts the PSM reconstruction, with red circles showing the reconstructed face values. The reconstruction with piecewise parabolics (PPM), is shown in blue.

Both reconstructions result in a third-order accurate and smooth representation of the underlying irregular signal. As expected from the previous discussion, both reconstructions are continuous at cell faces, but exhibit unphysical over and undershoots in the vicinity of strong gradients. Available methods for dealing with spurious over- and undershoots are mentioned in Section 3.6.5. While both reconstructions behave similarly in large parts of the domain, the effect of PPM being only continuous becomes apparent at some points. The fact that PPM slopes exhibit discontinuities at cell faces is clearly visible e.g. at $z = 0.15$ and $z = 0.35$. The PSM reconstruction, on the other hand, has continous slopes throughout the domain, which gives it a more 'natural' appearance. The absolute difference between the PSM and PPM reconstruction is shown in Figure 3.5b. Largest differences occur close to the cell edges.

3.6.4. Reduced Calling Frequency

Given that explicit time stepping is used, the continuity equation for air, the momentum and the thermodynamic equation must obey the time-step restrictions imposed by the fastest waves in the system (i.e. sound waves). While the continuity equation for air is inherently coupled to the momentum equations, tracer transport equations can be solved in isolation given prescribed winds and air densities.

Continuity equations for tracers (like water vapour) lack fast wave modes (sound and gravity waves) and, thus, have less restrictive time step limitations. Given the large number of tracers in state of the art climate and NWP models, significant computational cost savings can be obtained by sub-cycling the solution of the density, momentum and thermodynamic equation with respect to the tracer equations. Stated in another way, the tracer equations can be integrated with a much larger time step. In doing so, care has to be taken in order to maintain tracer-mass consistency.

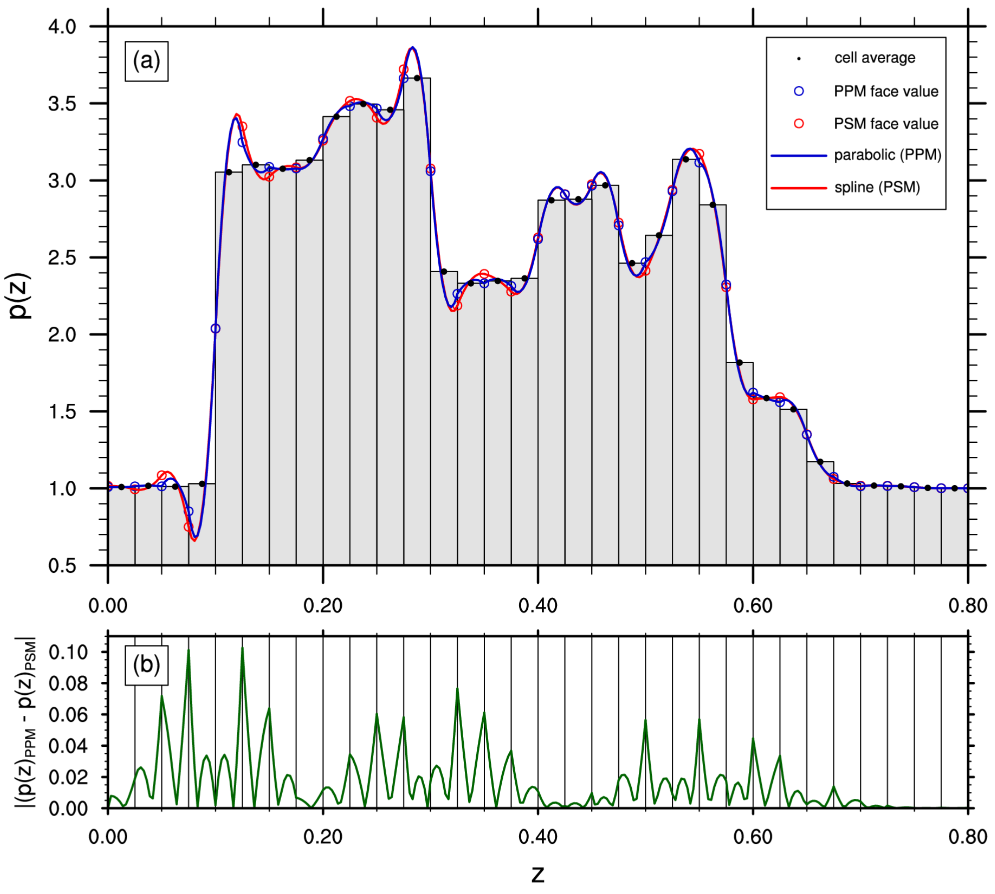

Figure 3.5.: (a) Reconstruction of an irregular 1D signal with piecewise parabolics (blue) and piecewise parabolic splines (red) from known cell averages (black dots) on an equidistant grid. The corresponding reconstructed face values are shown by blue and red circles, respectively. (b) Absolute difference between the piecewise parabolics and piecewise parabolic splines.

In ICON, the number of times by which the integration of the air mass continuity equation (and the entire dynamical core) is sub-cycled with respect to the tracer mass continuity equations is typically 5 (see Section 3.7.1). In order to maintain tracer-mass consistency, the time-averaged rather than the instantaneous mass flux is passed to the transport module. Thus, $\langle \overline{\rho}_i^e \rangle$ in Eq. (3.34) can be expressed in terms of the time-averaged horizontal mass flux $\langle F_{ie}^m \rangle$ as

$$\overline{\rho}_i^e = \langle F_{ie}^m \rangle \Delta t \, l_{ie}$$

with Δt denoting the time step for tracer transport and l_{ie} denoting the length of the e^{th} cell wall.

3.6.5. Some Practical Advice

Here we give some practical guidance on how to configure the tracer transport for standard NWP runs. The most important namelist parameters are discussed along with recommended settings.

The main switch for activating tracer transport is `ltransport` (`run_nml`). Except for specific idealized test cases (see Chapter 4) this switch should generally be set to `.TRUE.`. The namelist `run_nml` contains a second relevant parameter termed `ntracer` which is meant for specifying the total number of tracers that shall be advected. We note, however, that this parameter is important for idealized cases only. In real case runs, ICON takes care of initializing the correct number of tracers based on the selected physics packages. E.g. when selecting the one-moment microphysics scheme without graupel (`inwp_gscp=1`), the number of tracers is automatically set to `ntracer=5`.

The namelist `transport_nml` contains additional parameters for selecting the transport scheme and the type of limiter. This can be done individually for each tracer, for horizontal and vertical directions.

`ihadv_tracer` (namelist `transport_nml`, list of Integer values)

Comma separated list of integer values, specifying the type of the horizontal transport scheme. The i^{th} entry corresponds to the i^{th} tracer in ICON's internal tracer list. Most relevant options are

1	1^{st} order upwind
2	MIURA (Miura (2007)-type with linear reconstruction)
3	MIURA3 (Miura (2007)-type with cubic reconstruction)
4	FFSL with quadratic or cubic reconstruction (depends on `lsq_high_ord` (`interpol_nml`))
5	hybrid MIURA3/FFSL with quadratic or cubic reconstruction
x2	Sub-cycling versions of MIURA ($x = 2$), MIURA3 ($x = 3$), FFSL ($x = 4$) and hybrid MIURA3/FFSL ($x = 5$).

Sub-cycling means that the integration from t^n to t^{n+1} is split into substeps to meet the stability requirements. Sub-cycling is only applied above a certain height defined by `hbot_qvsubstep` (`nonhydrostatic_nml`), see Section 3.8.12. In regions where sub-cycling is applied, the `MIURA` scheme (linear reconstruction) is always used.

FFSL and MIURA3 only differ w.r.t. the way the integration over the flux area is performed. FFSL can cope with slightly larger Courant numbers while being somewhat more expensive. Option 5 tries to combine the improved stability of FFSL with the speed of MIURA3 by calling FFSL only for those edges for which the horizontal Courant number exceeds a threshold.

`ivadv_tracer` (namelist `transport_nml`, list of Integer values)

Comma separated list of integer values, specifying the type of the vertical transport scheme. The i^{th} entry corresponds to the i^{th} tracer in ICON's internal tracer list. Most relevant options are

1	1^{st} order upwind
2	Parabolic Spline Method (PSM)
3	Piecewise Parabolic Method (PPM)

`itype_hlimit` (namelist `transport_nml`, list of Integer values)

Comma separated list of integer values, specifying the type of the horizontal limiter. The i^{th} entry corresponds to the i^{th} tracer in ICON's internal tracer list. Most relevant options are

0	no limiter
3	monotonic Flux Corrected Transport (Zalesak, 1979)
4	positive definite Flux Corrected Transport

`itype_vlimit` **(namelist `transport_nml`, list of Integer values)**

Comma separated list of integer values, specifying the type of the vertical limiter. The i^{th} entry corresponds to the i^{th} tracer in ICON's internal tracer list. Most relevant options are

0	no limiter
1	semi-monotonic reconstruction filter
2	monotonic reconstruction filter
3	positive definite Flux Corrected Transport

Example Settings for a Standard NWP Run

Valid settings for a standard NWP run with one-moment microphysics (i.e. 5 prognostic water tracers) are depicted in Figure 3.6. The (hardcoded) ordering of tracers in ICON and their tracer IDs are listed in Table 3.3. In order to set the transport scheme and limiter for a tracer with `ID` $= i$, the i^{th} entry in the respective namelist parameters must be modified.

```
! transport_nml: tracer transport --------------------------
&transport_nml
 ihadv_tracer  =  52, 2, 2, 2, 2   ! hor. transport selector

 ivadv_tracer  =   3, 3, 3, 3, 3   ! vert. transport selector

 itype_hlimit  =   3, 4, 4, 4, 4   ! hor. limiter

 itype_vlimit  =   1, 1, 1, 1, 1   ! vert. limiter
/
```

Figure 3.6.: Example namelist settings for tracer transport in a standard NWP run with one-moment microphysics without graupel (i.e. 5 tracers q_v, q_c, q_i, q_r, q_s).

This procedure can become unwieldy and error prone if more than a handful of tracers is used. The ART-package alleviates this problem by providing a more elaborate way of configuring tracers based on XML files. Note, however that the configuration via XML files is restricted to ART-specific tracers, only.

`ivadv_tracer, ihadv_tracer:` PPM is the method of choice in the vertical direction for all tracers. In horizontal directions, MIURA is used for all tracers except vapor q_v. A somewhat more accurate (and more expensive) scheme is selected for q_v (hybrid MIURA3/FFSL).

One might wonder why sub-cycling is only activated for q_v. The reason is that with standard NWP settings q_v is the only tracer for which transport is activated all the way up to the model top where the highest wind speeds are typically encountered. For all other water tracers transport is switched off above a certain height defined by

Tracer ID	1	2	3	4	5	6	7
Tracer Name	water vapour q_v	cloud water q_c	cloud ice q_i	rain water q_r	snow q_s	graupel q_g	hail q_h

Table 3.3.: Ordering of water tracers in ICON. The tracer ID indicates the position within ICON's internal tracer data structure. In order to specify transport settings for a tracer with $\texttt{ID} = i$, the i^{th} entry in the respective namelist parameter must be set (see **`ihadv_tracer`**, **`ivadv_tracer`**, **`itype_hlimit`**, **`itype_vlimit`**). Note that this table is incomplete in the sense that additional water tracers for two-moment microphysics schemes (like number concentrations) are omitted. These indices can be taken directly from the source code if required.

`htop_moist_proc`(**`nonhydrostatic_nml`**) (typically around 18 km) such that sub-cycling is not strictly required (see Section 3.8.12).

Note that sub-cycling is activated for q_v. This is crucial for numerical stability!

Furthermore, note that if additional non-water tracers are added (e.g. purely diagnostic passive tracers or chemical tracers), sub-cycling must be activated since **`htop_moist_proc`** is only effective for water tracers.

`itype_hlimit, itype_vlimit:` In terms of limiters, the rule of thumb is that at least a positive definite limiter should be used for all water tracers. Otherwise numerical instabilities will occur due to negative water concentrations. For q_v it is advisable to use a more stringent (albeit more expensive) monotonic limiter in order to reduce spurious condensation/evaporation emerging from nonphysical over-/undershoots in q_v.

3.7. Physics-Dynamics Coupling

3.7.1. ICON Time-Stepping

For efficiency reasons, different integration time steps are applied depending on the process under consideration. In the following, the term *dynamical core* refers to the numerical solution of the dry Navier-Stokes equations, while the term *physics* refers to the diabatic, mostly sub-grid scale, processes that have to be parameterized. In ICON, the following time steps have to be distinguished:

Δt	the basic time step specified via namelist variable `dtime`, which is used for tracer transport, numerical diffusion and the fast-physics parameterizations.
$\Delta\tau$	the short time step used within the dynamical core; the ratio between Δt and $\Delta\tau$ is specified via the namelist variable **`ndyn_substeps`** (namelist **`nonhydrostatic_nml`**, number of dynamics substeps), which has a default value of 5.

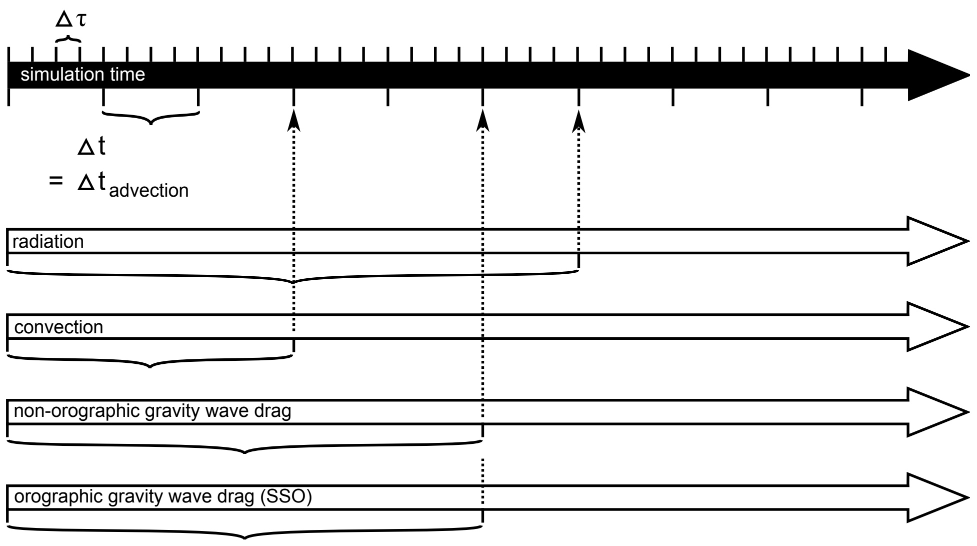
Δτ
simulation time
Δt
= Δt advection
radiation
convection
non-orographic gravity wave drag
orographic gravity wave drag (SSO)

Figure 3.7.: ICON internal time stepping. Sub-cycling of dynamics with respect to transport, fast-physics, and slow-physics. Δt denotes the time step for transport and fast physics and $\Delta\tau$ denotes the short time step of the dynamical core. The time step for slow-physics can be chosen individually for each process.

$\Delta t_{i,slow\_physics}$	the process dependent slow physics time steps; they should be integer multiples of Δt and are rounded up automatically if they are not.

An illustration of the relationship between the time steps can be found in Figure 3.7.

ICON solves the fully compressible nonhydrostatic Navier-Stokes equations using a time stepping scheme that is explicit except for the terms describing vertical sound wave propagation (see Section 3.5). Thus, the maximum allowable time step $\Delta\tau$ for solving the momentum, continuity and thermodynamic equations is determined by the fastest wave in the system – the sound waves. As a rule of thumb, the maximum dynamics time step can be computed as

$$\Delta\tau = 1.8 \cdot 10^{-3}\, \overline{\Delta x}\, \frac{\mathrm{s}}{\mathrm{m}}\,, \tag{3.40}$$

where $\overline{\Delta x}$ is the effective horizontal mesh size in meters (see Equation (2.1)). This implies that the namelist variable `dtime` should have a value of

$$\Delta t = 9 \cdot 10^{-3}\, \overline{\Delta x}\, \frac{\mathrm{s}}{\mathrm{m}}\,,$$

unless `ndyn_substeps` is set to a non-default value.

Historical remark: Note that historically, $\Delta\tau$ rather than Δt was used as basic control variable specified in the namelist, as appears logical from the fact that a universal rule for the length of the time step exists for $\Delta\tau$ only. This was changed shortly before the operational introduction of ICON in 2015 because it turned out that an adaptive reduction of $\Delta\tau$ is needed in rare cases with very large orographic gravity waves in order to avoid numerical instabilities.

> To avoid interferences with the output time control, the long time step Δt was then taken to be the basic control variable, which always remains unchanged during a model integration. The adaptive reduction of $\Delta\tau$ is now accomplished by increasing the time step ratio `ndyn_substeps` automatically up to a value of 8 if the Courant number for vertical advection grows too large.

Additional time step restrictions for Δt arise from the numerical stability of the horizontal transport scheme and the physics parameterizations, in particular due to the explicit coupling between the turbulent vertical diffusion and the surface scheme. Experience shows that Δt should not significantly exceed 1000 s, which becomes relevant when $\overline{\Delta x}$ is larger than about 125 km.

Even longer time steps than Δt can be used for the so-called slow-physics parameterizations, i.e. radiation, convection, non-orographic gravity wave drag, and orographic gravity wave drag. These parameterizations provide tendencies to the dynamical core, allowing them to be called individually at user-specified time steps. The related namelist switches are `dt_rad`, `dt_conv`, `dt_gwd` and `dt_sso` in `nwp_phy_nml`. If the slow-physics time step is not a multiple of the advective time step, it is automatically rounded up to the next advective time step. A further recommendation is that `dt_rad` should be an integer multiple of `dt_conv`, such that radiation and convection are called at the same time[1]. The time-splitting is schematically depicted in Figure 3.7.

3.7.2. Fast and Slow Processes

For efficiency reasons, a distinction is made between so-called *fast-physics processes*, whose time scale is comparable or shorter than the model time step, and *slow-physics processes* whose time scale is considered slow compared to the model time step.

Fast-physics processes are calculated at every physics time step Δt and are treated with time splitting (also known as sequential-update split) which means that (with exceptions noted below) they act on an atmospheric state that has already been updated by the dynamical core, horizontal diffusion and the tracer transport scheme. Each process then sequentially updates the atmospheric variables and passes a new state to the subsequent parameterization.

The calling sequence is saturation adjustment $\longrightarrow$ surface transfer scheme $\longrightarrow$ land-surface scheme $\longrightarrow$ boundary-layer / turbulent vertical diffusion scheme $\longrightarrow$ microphysics scheme, and again saturation adjustment in order to enter the slow-physics parameterizations with an adjusted state. The exceptions from the above-mentioned sequential splitting are the surface transfer scheme and the land-surface scheme. Both take the input at the 'old' time level because the surface variables are not updated in the dynamical core and the surface transfer coefficients and fluxes would be calculated from inconsistent time levels otherwise. The coupling strategy is schematically depicted in Figure 3.8.

[1]This behavior is automatically enforced in the current model version.

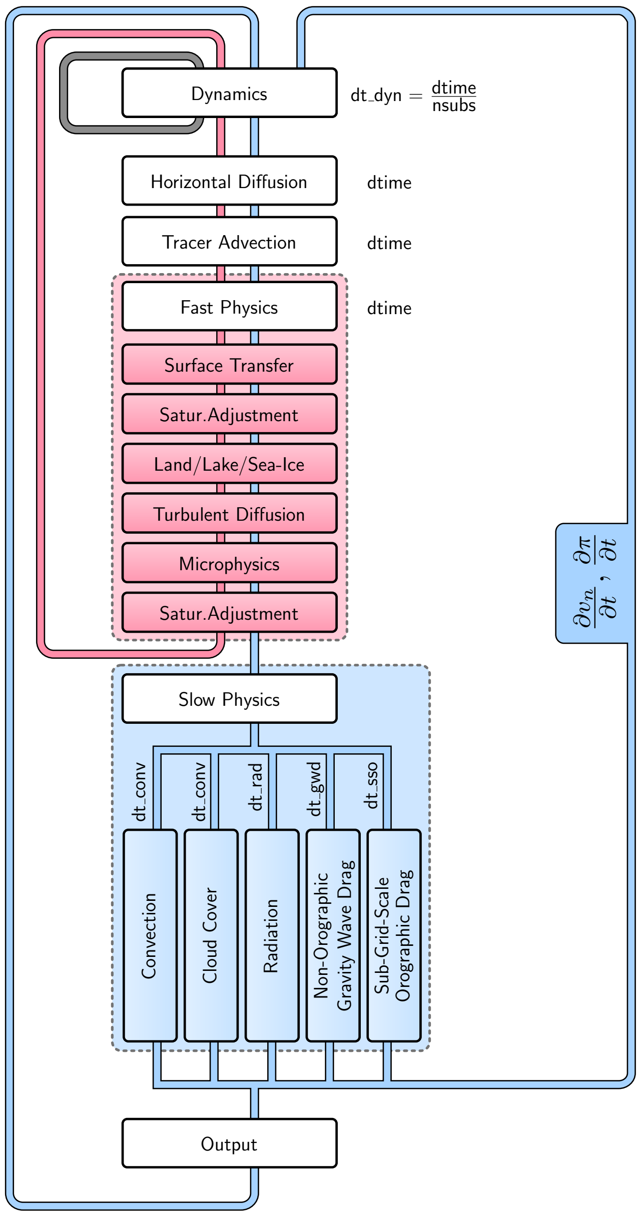

Figure 3.8.: Coupling of the dynamical core and the NWP physics package. Processes declared as fast (slow) are treated in a time-split (process-split) manner.

Note that in the actual ICON code, the surface transfer scheme is called at the very end of the sequence of fast physics processes rather than at the beginning, as depicted in Figure 3.8. In compensation, the input to the surface transfer scheme is the 'new' time level rather than the 'old' one claimed in the text. Without proof, we claim that this is an equivalent implementation of the more natural sequence shown in Figure 3.8. The natural sequence would necessitate the allocation of additional memory for storing the 'old' atmospheric state, as this state is no longer available after the dynamics update due to the inherent substepping. By calling the surface transfer scheme at the end of the previous time step, the allocation of additional memory and related data transfer can be avoided.

Slow-physics processes are treated in a parallel-split manner, which means that they are stepped forward in time independently of each other, starting from the model state provided by the latest fast-physics process. In ICON convection, subgrid-scale cloud cover, radiation, non-orographic and orographic gravity wave drag are considered as slow processes. Typically, these processes are integrated with time steps longer than the (fast) physics time step. The slow-physics time steps can be specified by the user. The resulting slow-physics tendencies $\partial v_n/\partial t$, $\partial T/\partial t$ and $\partial q_x/\partial t$ with $x \in [v, c, i]$ are passed to the dynamical core and remain constant between two successive calls of the parameterization (Figure 3.8). Since ICON solves a prognostic equation for π rather than T, the temperature tendencies are converted into tendencies of the Exner function, beforehand. Rather than treating the moisture tendencies as a forcing term during tracer advection, they are treated in a time-split manner and added to the updated moisture variables thereafter.

3.7.3. Isobaric vs. Isochoric Coupling Strategies

The physics-dynamics coupling in ICON differs from many existing atmospheric models in that it is performed at constant density (volume) rather than constant pressure. This is related to the fact that the total air density ρ is one of the prognostic variables, whereas pressure is only diagnosed for parameterizations needing pressure as input variable. Thus, it is natural to keep ρ constant in the physics-dynamics interface. As a consequence, heating rates arising from latent heat release or radiative flux divergences have to be converted into temperature changes using c_v, the specific heat capacity at constant volume of moist air. Some physics parameterizations inherited from hydrostatic models, in which the physics-dynamics coupling always assumes constant pressure, therefore had to be adapted appropriately.

Moreover, it is important to note that the diagnosed pressure entering into a variety of parameterizations is a hydrostatically integrated pressure rather than a nonhydrostatic pressure derived directly from the prognostic model variables[2]. This is motivated by the fact that the pressure is generally used in physics schemes to calculate the air mass represented by a model layer, and necessitated by the fact that sound waves generated by the saturation adjustment can lead to a local pressure increase with height in very extreme cases, particularly between the lowest and the second lowest model level.

Another important aspect is related to the fact that physics parameterizations traditionally work on mass points (except for three-dimensional turbulence schemes). While the conversion between different sets of thermodynamic variables is reversible except for numerical truncation errors, the interpolation between velocity points and mass points potentially induces errors. To minimize them, the velocity increments, rather than the full velocities, coming from the turbulence scheme are interpolated back to the velocity points and then added to the prognostic variable v_n.

[2]Note that the (surface) pressure available for output is as well the hydrostatically integrated pressure rather than a nonhydrostatic pressure derived directly from the prognostic model variables.

3.8. ICON NWP-Physics in a Nutshell

An in-depth description of the physical parameterization package for NWP is beyond the scope of this document. However, the following section provides a short introduction to the available parameterizations and references for further reading.

Table 3.4 contains a summary of physical parameterizations available in ICON (NWP-mode). In what follows, an outline (executive summary) of the parameterization schemes is given.

3.8.1. Radiation

Section author

S. Schäfer, DWD Physical Processes Division

Radiation is a crucial component that drives weather and climate from microscopical to global scales: Heating by absorption of radiation and cooling by emission determine local and global temperature and gradients, which in turn drive dynamics and physical processes. While some other physical effects occur locally, radiation travels throughout the depth of the atmosphere, therefore the entire atmospheric column has to be considered when calculating local radiative fluxes. Both visible or shortwave radiation from the sun and thermal or longwave radiation emitted within the Earth system interact with atmospheric gases, aerosols, clouds and the surface.

Radiative transfer models for the atmosphere consist of multiple components: optical property parameterizations for each atmospheric component and the surface, and a radiation solver that calculates how radiation travels through the optical medium. The new radiation scheme ecRad (Hogan and Bozzo, 2018; implementation in ICON: Rieger et al., 2019) allows choices for each component individually, while the radiation scheme itself is chosen with `inwp_radiation`=1 for ICON's RRTM radiation scheme and `inwp_radiation`=4 for ecRad (Namelist `nwp_phy_nml`). Using ecRad requires the Compiler-Flag `--enable-ecrad` in the config command before compiling, and setting the namelist parameter `ecrad_data_path` (Namelist `radiation_nml`). The necessary files are contained in '`<ICON-directory>/externals/ecrad/data`'. Since both the whole column and multiple spectral wavelengths have to be considered, the radiation calculation has to be simplified to be practical. Thus, radiation schemes for global weather and climate models neglect horizontal radiative transfer and treat only the vertical dimension. Clouds have a particularly strong radiative effect, and can vary on scales smaller than the model grid-boxes, therefore radiation is calculated once for the clear-sky part of each grid-box and once for the cloudy part.

In the spectral dimension, the strongest variability is due to atmospheric gases, which can absorb and emit radiation of particular, sharply defined wavelengths, according to their molecular properties. The optical properties of cloud particles, aerosol and the surface also depend on the wavelength, but vary more slowly. ICON's RRTM radiation scheme and ecRad both use the RRTM (Rapid Radiative Transfer Model Mlawer et al., 1997) gas optics scheme. The spectral range is divided into 30 spectral bands (16 bands in the longwave spectrum and 14 bands in the shortwave spectrum), and cloud, surface and aerosol optical

Process	Scheme	Settings
Radiation	▨ RRTM (Rapid Radiative Transfer Model) Mlawer et al. (1997), Barker et al. (2003)	`inwp_radiation=1`
	PSRAD Pincus and Stevens (2013)	`inwp_radiation=3`
	ecRad Hogan and Bozzo (2018)	`inwp_radiation=4`
Non-orographic gravity wave drag	▨ Wave dissipation at critical level Orr et al. (2010)	`inwp_gwd=1`
Sub-grid scale orographic drag	▨ Lott and Miller scheme Lott and Miller (1997)	`inwp_sso=1`
Cloud cover	▨ Diagnostic PDF *M. Köhler et al. (DWD)*	`inwp_cldcover=1`
	All-or-nothing scheme (grid-scale clouds)	`inwp_cldcover=5`
Microphysics	▨ Single-moment scheme Doms et al. (2011), Seifert (2008)	`inwp_gscp=1, 2`
	Double-moment scheme Seifert and Beheng (2006)	`inwp_gscp=4`
Convection	▨ Mass-flux shallow and deep Tiedtke (1989), Bechtold et al. (2008)	`inwp_convection=1`
Turbulent transfer	▨ Prognostic TKE (COSMO) Raschendorfer (2001)	`inwp_turb=1`
	EDMF-DualM (Eddy-Diffusivity/Mass-Flux) Köhler et al. (2011), Neggers et al. (2009)	`inwp_turb=3`
	3D Smagorinsky diffusion (for LES)	`inwp_turb=5`
Land	▨ Tiled TERRA Schrodin and Heise (2001), Schulz et al. (2016)	`inwp_surface=1`
	▨ Flake: Mironov (2008)	`llake=.TRUE.`
	▨ Sea-ice: Mironov et al. (2012)	`lseaice=.TRUE.`

Table 3.4.: Summary of ICON's physics parameterizations for NWP, together with the related namelist settings (namelist `nwp_phy_nml`). Parameterizations which are used operationally (at 13 km horizontal grid spacing) are indicated by ▨.

properties are described within each band. The bands are subdivided into sub-intervals with similar gas properties, termed g-points. This so-called correlated-k method strongly reduces computational costs with an accuracy comparable to spectrally more detailed line-by-line models. Since we only consider up- and downwelling radiation, the optical properties are integrated for all angles within a hemisphere, reducing the optical parameters that are needed to optical depth, single scattering albedo and asymmetry factor (of scattering).

Cloud particle optical properties depend on the amount of water or ice, on the particle size and particle shape. Since cloud particles often have sizes similar to the visible or thermal wavelength ranges, scattering by particles varies strongly according to scattering angle and to the ratio of particle size to wavelength (Mie scattering). For given particle shape and size, this complex function can be approximated numerically. Cloud optical property parameterizations have to make an assumption on cloud particle shape. While liquid water particles are spherical, real ice particles can have a variety of shapes, so that ice shape assumptions are uncertain, and vary between parameterizations. Using these assumptions, the cloud optics parameterization provides optical properties depending on particle size (which is parameterized within ICON) and wavelength. In ecRad, several cloud water and ice optics parameterizations are available (namelist parameters `iliquid_scat` and `iice_scat` in `radiation_nml`).

For aerosol, optical properties are directly provided as an input to the radiation scheme. In operational settings, we use fixed global aerosol distributions from climatologies. Similarly, surface optical properties are provided to ICON in an external parameter file, based on satellite observations of the surface.

All of these optical properties are provided to the radiation solver, which calculates reflection, transmission and internal radiation sources in each grid-box and model layer, and the resulting amount of up- and downwelling radiation at each height, for cloudy and clear sky. Vertical overlap of cloudy and clear regions between neighboring layers is parameterized according to overlap assumptions (Hogan and Illingworth, 2000, chosen by namelist parameter `icld_overlap` in `radiation_nml`). Operationally, ICON uses the exponential-random overlap assumption, meaning clouds with clear layers in-between are uncorrelated, while the overlap in continuous clouds decreases exponentially with vertical distance. Since cloud absorption and reflection depend non-linearly on cloud optical depth, the variability of thick and thin cloud in a grid-box also has an effect. Highly variable clouds interact less strongly with radiation than homogeneous clouds that contain the same amount of water. This effect can be parameterized roughly by reducing cloud optical depth to compensate (ICON's RRTM radiation uses a factor of 0.8). In ecRad, the variability is captured by dividing the cloudy region into two or more sub-regions with different cloud optical depths. One method to do this in a numerically efficient way is the Monte Carlo Independent Column Method (McICA, Pincus et al., 2003), which only calculates the radiative transfer for one spectral band in each sub-column. The distribution of the bands over the sub-columns introduces random noise, but no bias. Since this McICA method is comparatively cheap, it is the default method used, However, ecRad also provides a choice of other solvers without random noise: Tripleclouds, and SPARTACUS, which also approximately accounts for sub-grid horizontal transfer. The solver and further namelist parameters specific to ecRad are set in the module `/src/atm_phy_nwp/mo_nwp_ecrad_init` and are described in the ecRad documentation (`https://confluence.ecmwf.int/display/ECRAD`).

From the radiative fluxes, radiative heating and cooling is calculated, which feeds back into dynamics and physics. Despite the simplifying assumptions, radiation is still one of the most expensive parts of the model. Hence, radiation is calculated only on a coarser radiation grid (see Section 3.10) and at a coarse radiation time step `dt_rad` (see Section 3.7.1). However, radiative heating rates are updated more frequently, so that they better represent the diurnal cycle of incoming solar radiation.

3.8.2. Saturation Adjustment

Section author

A. Seifert, DWD Physical Processes Division

In ICON, the atmospheric state which enters the fast physics parameterizations has already been updated by the dynamical core (see Figure 3.8). As a consequence it is no longer guaranteed that vapor and liquid phase are in equilibrium. Hence supersaturated but cloud-free regions might exist, as well as sub- or supersaturated but cloudy ones.

The aim of a saturation adjustment scheme is to adjust the temperature and water vapor mixing ratio to perfect saturation in supersaturated regions. In subsaturated but cloudy regions, cloud water is evaporated until either saturation is reached or all cloud water is evaporated. From a cloud microphysical point of view the saturation adjustment scheme describes the processes of condensation and evaporation of cloud droplets.

In atmospheric models this adjustment process is usually treated isobarically. In ICON, however, it is treated isochorically, which is a consequence of ICON's physics-dynamics coupling strategy.

We start the description of the saturation adjustment scheme with a short derivation of temperature equation emphasizing the difference between the enthalpy (constant pressure) and internal energy (constant volume) formulation and including water vapor and liquid water. For a more complete derivation of the prognostic temperature equation see, e.g., Doms and Baldauf (2018).

To derive the prognostic temperature equation one uses the specific internal energy u or the specific enthalpy $h = u + pv$ as a starting point. While the internal energy is appropriate for processes at constant volume, enthalpy would be chosen for processes at constant pressure. The prognostic temperature equation is derived as an expansion of either h or u as a function of temperature T, mass fractions of dry air q_d, water vapor q_v and liquid water q_ℓ and either specific volume v or pressure p.

$$\frac{dh}{dt} = \left.\frac{\partial h}{\partial p}\right|_{T,\,q_k} \frac{dp}{dt} + \left.\frac{\partial h}{\partial T}\right|_{p,\,q_k} \frac{dT}{dt} + \sum_{k=d,v,\ell} \left.\frac{\partial h}{\partial q_k}\right|_{p,\,T} \frac{dq_k}{dt}$$

$$\frac{du}{dt} = \left.\frac{\partial u}{\partial v}\right|_{T,\,q_k} \frac{dv}{dt} + \left.\frac{\partial u}{\partial T}\right|_{v,\,q_k} \frac{dT}{dt} + \sum_{k=d,v,\ell} \left.\frac{\partial u}{\partial q_k}\right|_{v,\,T} \frac{dq_k}{dt}$$

With

$$c_p = \left.\frac{\partial h}{\partial T}\right|_{p,\,q_k}$$

$$c_v = \left.\frac{\partial u}{\partial T}\right|_{v,\,q_k}$$

and $\sum q_k = 1$ and no phase transitions involving dry air, and therefore $dq_v/dt = -dq_\ell/dt$, we find:

$$\begin{aligned}
\frac{dh}{dt} &= \left.\frac{\partial h}{\partial p}\right|_{T,\,q_k} \frac{dp}{dt} + c_p \frac{dT}{dt} + (h_\ell - h_v)\frac{dq_\ell}{dt} \\
\frac{du}{dt} &= \left.\frac{\partial u}{\partial v}\right|_{T,\,q_k} \frac{dv}{dt} + c_v \frac{dT}{dt} + (u_\ell - u_v)\frac{dq_\ell}{dt}
\end{aligned}$$

Now we use conservation of energy, i.e. $dh = 0$ or $du = 0$, and constant pressure or constant volume respectively, and find:

$$c_p \frac{dT}{dt} = -(h_\ell - h_v)\frac{dq_\ell}{dt} = L_{\ell v} I_\ell, \qquad p = \text{const.} \tag{3.41}$$

$$c_v \frac{dT}{dt} = -(u_\ell - u_v)\frac{dq_\ell}{dt} = \hat{L}_{\ell v} I_\ell, \qquad V = \text{const.} \tag{3.42}$$

The $L_{\ell v}$ or $\hat{L}_{\ell v}$ are the latent heats of vaporization and $I_\ell = dq_\ell/dt$ is the condensation rate and also known as the 'Phasenfluss' (in German). The usual latent heat of vaporization given in most textbooks is the $L_{\ell v}$ or the *enthalpy of vaporization*. At 0°C it has a value of $L_{\ell v,0} = 2.501 \times 10^6$ J kg^{-1}. The corresponding *internal energy of vaporization* $\hat{L}_{\ell v}$ can be derived from $h_k = u_k + pv_k$ and with $v_\ell \ll v_d$ and $pv_v = R_v T$ we find

$$\hat{L}_{\ell v} = L_{\ell v} - pv_v = L_{\ell v} - R_v T$$

Saturation adjustment is a parameterization of condensation which assumes that vapor and liquid phase are in equilibrium, i.e., by saturation adjustment we want to ensure or realize this equilibrium. Therefore we simply assume that the final state with temperature T_1 has a vapor mass fraction of $q_{v,1} = q_{sat}(T_1)$ inside the cloud, i.e., whenever $q_\ell > 0$. From the temperature equation at constant volume (3.42) we find

$$c_{vd}(T_1 - T_0) + \hat{L}_{\ell v}(q_{sat}(T_1) - q_{v,0}) = 0\,.$$

Note that we have now replaced c_v by the specific heat of dry air at constant volume c_{vd} and, hence, made the usual approximation to neglect the differences in the specific heats between dry air, vapor and liquid water in the temperature term. This is justified because q_v and q_l are usually small.

This equation is solved for T_1, e.g., using a Newton iteration

$$T_1^{n+1} = T_1^n - \frac{F(T_1^n)}{F'(T_1^n)}\,,$$

with

$$\begin{aligned}
F(T_1) &= T_1 - T_0 + \hat{L}_{\ell v}\,\frac{q_{sat}(T_1) - q_{v,0}}{c_{vd}} \\
F'(T_1) &= 1 + \frac{\hat{L}_{\ell v}}{c_{vd}} \left.\frac{dq_{sat}}{dT}\right|_{T=T_1}.
\end{aligned}$$

In ICON the iteration is stopped if either $|T_1^{n+1} - T_1^n| < 1\mathrm{E}-3\,\mathrm{K}$, or if the number of iterations exceeds a hard-coded maximum $maxiter = 10$. Regarding the *internal energy of vaporization* $\hat{L}_{\ell v}$ we actually use

$$\hat{L}_{\ell v}(T) = L_{\ell v,0} + (c_{pv} - c_l)(T - T_0) - R_v T \,.$$

Hence, in addition to the $R_v T$ term arising from the Legendre transformation to internal energy as discussed above, we take into account the linear temperature dependency of the latent heat of vaporization according to Kirchhoff's equation[3]

$$\left.\frac{\partial L_{\ell v}}{\partial T}\right|_{p,\,q_k} = \left.\frac{\partial h_v}{\partial T}\right|_{p,\,q_k} - \left.\frac{\partial h_l}{\partial T}\right|_{p,\,q_k} = c_{pv} - c_l \,.$$

This is consistent with the assumption of water vapor as an ideal gas with constant specific heat capacity.

3.8.3. Cloud Microphysics

Section author

A. Seifert, DWD Physical Processes Division

In the exercises for Chapter 8 (see p. 261) we will investigate ICON's physical parameterizations by means of a custom diagnostic quantity. We restrict ourselves to the cloud microphysics parameterization, where some additional background information will be of interest.

Microphysical schemes provide a closed set of equations to calculate the formation and evolution of condensed water in the atmosphere. The most simple schemes predict only the specific mass content of certain hydrometeor categories like cloud water, rain water, cloud ice and snow. This is often adequate, because it is sufficient to describe the hydrological cycle and the surface rain rate, which is the vertical flux of the mass content. Microphysical schemes of this category are called *single-moment schemes*.

In ICON two single-moment schemes are available, one that predicts the categories cloud water, rain water, cloud ice and snow (`inwp_gscp=1` in the namelist `nwp_phy_nml`), and the other that predicts in addition also a graupel category (`inwp_gscp=2`). Graupel forms through the collision of ice or snow particles with supercooled liquid drops, a process called *riming*.

Most microphysical processes depend strongly on particle size and although the mean size is usually correlated with mass content this is not always the case. Schemes that predict also the number concentrations have the advantage that they provide a size information, which is independent of the mass content. Such schemes are called *double-moment schemes*, because both, mass content and number concentration, are statistical moments of the particles size distribution.

ICON does also provide a double-moment microphysics scheme (`inwp_gscp=4`), which predicts the specific mass and number concentrations of cloud water, rain water, cloud

[3]see e.g. http://glossary.ametsoc.org/wiki/Kirchhoff's_equation

ice, snow, graupel and hail. This scheme is most suitable at convection-permitting or convection-resolving scales, i.e., mesh sizes of 3 km and finer. Only on such fine meshes the dynamics is able to resolve the convective updrafts in which graupel and hail form. On coarser grids the use of the double-moment scheme is not recommended.

To predict the evolution of the number concentrations the double-moment scheme includes various parameterizations of nucleation processes and all relevant microphysical interactions between these hydrometeor categories. Currently all choices regarding, e.g., cloud condensation and ice nuclei, particle geometries and fall speeds etc. have to be set in the code itself and can not be chosen via the ICON namelist.

3.8.4. Cumulus Convection

Section author

D. Klocke, DWD Physical Processes Division

Convection is an important process in the atmosphere by contributing to forming the large-scale circulation to local heavy precipitation through thunderstorms. Parameterizations of atmospheric moist convection provide the effect of an ensemble of sub-grid convective clouds on the model column as a function of grid-scale variables. The schemes vertically mix heat, moisture and momentum. They convert available potential energy into kinetic energy and produce precipitation as a result of atmospheric instability.

Three steps are taken. First, it is determined if the grid-scale conditions allow for the occurrence of convection in the column, and a decision is taken if convection is triggered. In the second step, the tendencies of heat, moisture and momentum changes are determined with a *cloud model*, which represents an ascending parcel and its interactions with the environment. Finally the closure decides on the strength of the convection by determining the amount of energy to be converted, which is linked to precipitation amount generated by the convection scheme.

In ICON a bulk mass flux convection scheme is available `inwp_convection=1`(in the namelist `nwp_phy_nml`), which treats three convective cloud types. Only one type - shallow, mid-level or deep convection - can exist at a time in a column, which is decided upon by the trigger function. All three types of convection use a cloud model representing an ascending plume mixing with its environmental air. The cloud base mass flux closure differs between the three convection types, with a CAPE (convective available potential energy) based closure for deep convection, a boundary layer equilibrium closure for shallow convection, and a large-scale omega (vertical velocity in pressure coordinates) based closure for mid-level convection.

The full convection scheme can generally be used for horizontal grids coarser than 5 km, as some resolution dependent adjustments are implemented for grid spacings smaller than 20 km. For convection permitting simulations ($1 - 3$ km horizontal grid spacing) the largest convective clouds can be resolved by the model and the parameterization parts treating deep and mid-level convection can be switched off (`lshallowconv_only=.TRUE.` in the namelist `nwp_phy_nml`).

The implemented scheme represents a branch of the Tiedtke-Bechtold convection scheme used in the IFS model. For further reading we refer to Bechtold et al. (2008), Tiedtke (1989), Bechtold (2017), ECMWF (2017). Similar to the operational IFS scheme it contains an improved CAPE closure for deep convection (Bechtold et al., 2014) in order to improve the representation of the diurnal cycle of convection over land (`icapdcycle>0` in the namelist `nwp_phy_nml`). Note that in the operational ICON scheme the modified closure is only applied over land and latitudinally restricted to the tropics (`icapdcycle=3`).

3.8.5. Cloud Cover

Section author

M. Köhler, DWD Physical Processes Division

To prepare optical properties of clouds for the radiative transfer it is necessary to determine the best estimate of cloud cover, cloud water and cloud ice as well as the precipitation quantities, such as snow, rain and graupel if those are required by the radiation calculation. Note that there are various assumptions in the ICON model on the subgrid distribution of water, such as the up/down/subsidence regions in convection, a uniform distribution in microphysics, and a Gaussian distribution in turbulence.

The aim of the diagnostic cloud cover scheme is to combine information from the different parameterizations mentioned above: turbulence, convection and microphysics. The turbulence scheme provides the sub-grid variability of water due to turbulent motions, the convection scheme detrains cloud into the anvil and the microphysics scheme describes the supersaturation due to ice, in other words, the distribution between ice and vapor in cold situations.

The turbulent variability of water is at the moment prescribed by using a top-hat total water (the sum of water vapor q_v, cloud water q_c, and cloud ice q_i) distribution with a fixed width of 10% of total water. Work is in progress to replace this crude assumption with the total water variance from the turbulence scheme.

The split between water vapor and cloud ice as determined from the microphysics scheme is replicated in the diagnostic cloud scheme for the turbulent component of ice clouds.

The convective anvil is calculated by writing an equation for the evolution of cloud cover that depends on the detrainment of volume (from the convection scheme) and a decay term with a fixed decay time-scale (taken as 30 min). The diagnostic assumption means that we can neglect the tendency term on cloud cover so that we arrive simply at the diagnostic anvil cloud cover that is purely a function of detrainment and decay time-scale. The liquid and ice cloud water is taken also from the convective updraft properties.

In the end the turbulent and convective clouds are combined with a simple maximum function.

To emphasize, the cloud cover scheme takes into account the subgrid variability of water and therefore the associated distribution in water vapor, cloud liquid water and cloud ice (optional 3D diagnostic output variables `tot_qv_dia`, `tot_qc_dia`, `tot_qi_dia` and their vertically integrated counterparts `tqv_dia`, `tqc_dia`, `tqi_dia`). They are not equal to their prognostic grid-scale equivalents (standard output variables `qv`, `qc`, `qi`), yet the sum of all three water quantities is kept the same. This cloud information is then passed to the radiation, where additional assumptions are made on the vertical overlap of clouds.

3.8.6. Turbulent Diffusion

Section authors

M. Köhler and M. Raschendorfer,
DWD Physical Processes Division

TKE Scheme for Turbulence.

The TKE turbulence scheme consists of two components: one describing the free troposphere, and the other for the surface layer.

TURBDIFF. The turbulence scheme TURBDIFF developed by Raschendorfer (2001) is based on a 2^{nd}-order closure on level 2.5 according to Mellor and Yamada (1982) (MY-scheme). In this scheme, all pressure correlation terms and dissipation terms, being present in the system of 2^{nd}-order equations for all the turbulent (co-)variances that can be built from the dynamically active prognostic model variables, are expressed by the standard closure assumptions according to Rotta (1951a,b) and Kolmogorov (1968) valid for quasi-isotropic turbulence. These dynamically active model variables are the horizontal wind components u and v, vertical wind speed w, a variable related to inner energy (like absolute temperature T, potential temperature θ or virtual potential temperature θ_v), specific humidity q_v and at least one cloud water variable q_c (which is a mass fraction and may be split into liquid q_l and frozen q_i cloud water).

Among these 2^{nd}-order moments, only the trace of the turbulent stress tensor, which is twice the Turbulent Kinetic Energy (TKE), is described by a prognostic equation. Each of the remaining 2^{nd}-order equations (for the elements of the remaining trace-less stress tensor and for the other 2^{nd}- order moments) is simplified as diagnostic source term equilibrium being a linear equation in terms of the governing statistical moments.

Further, correlations between any model variable and source terms of scalar model variables are neglected in these equations. However, by choosing quasi-conserved scalar variables (total water content $q_t = q_v + q_c$ and liquid-water potential temperature $\theta_l = \theta - \frac{L_c}{c_{p_d}} q_c$), these correlations are taken into account implicitly as far as local condensation and evaporation within liquid non-precipitating clouds is concerned. Hence, TURBDIFF is a moist turbulence scheme, which includes the effect of these sub-grid scale phase transitions. The required conversion of turbulent fluxes of these conserved variables into those of absolute temperature, specific humidity and liquid water content is performed by means of turbulent saturation adjustment, assuming a Gaussian distribution-function for local saturation-deficiency according to Sommeria and Deardorff (1977).

Finally, application of the horizontal boundary layer approximation reduces the linear system of diagnostic 2nd-order equilibrium equations to a single column scheme with only two equations for two diffusion coefficients (one for horizontal wind components and another for scalar variables), which both are proportional to the square root of TKE and an integral turbulent length scale. This length-scale rises with height above ground according to Blackadar (1962) with a further limitation related to the horizontal grid scale. The desired vertical turbulent fluxes of any prognostic variable can then be calculated by multiplying the (negative) vertical gradient of the latter with the associated diffusion coefficient.

One main extension of TURBDIFF (compared with a moist MY-scheme) is the formal separation of turbulence from a possible non-turbulent part of the subgrid-scale energy spectrum. This separation is related to additional scale-interaction terms in the prognostic TKE equation, which describe additional shear production of TKE by the action of other non-turbulent sub-grid-scale flow patterns (such as wakes generated by sub-grid-scale orography, convective currents or separated horizontal circulations). Through this formalism, the scheme describes Separated Turbulence Interacting with non-turbulent Circulations (STIC), which allows for a consistent application of turbulence closure assumptions, even though other sub-grid-scale processes may be dominant within a grid cell. Due to this extension, the scheme is applicable also above the boundary layer and for very stable stratification. The Eddy Dissipation Rate (EDR) calculated by TURBDIFF can even be used to forecast the intensity of Clear Air Turbulence (CAT).

TURBTRAN. The turbulence scheme TURBDIFF is closely related to the scheme TURBTRAN developed by Raschendorfer (2001) for the surface-to-atmosphere transfer (SAT), which calculates transport resistances for fluxes of prognostic model variables at the surface of the Earth. Figure 3.9 illustrates the corresponding sub layers of the surface layer. In TURBTRAN, a constant flux approximation is applied to the sum of turbulent and laminar vertical fluxes within the transfer layer (between the rigid surface and the lowest atmospheric main level of the model). By application of the turbulence scheme at the top of the lowest atmospheric layer as well as the bottom of this layer (which is the top of the near surface roughness layer being intersected by roughness elements), a vertical interpolation function for the turbulent diffusion coefficient is derived between these two levels and is extrapolated down to the rigid surface. With this preparation, a vertical integration of the flux gradient representation across the transfer layer provides the desired transport resistances for the final bulk representation of SAT fluxes. With this formulation, scale interaction terms considered through STIC in the turbulence scheme also affect the transfer resistances; and hence, some additional mixing is automatically introduced for very large bulk Richardson numbers, as soon as non-turbulent sub-grid-scale motions are present.

Further, with the described procedure, the determination of a specific roughness length for scalars is substituted by a direct calculation of the partial resistance of scalar transfer through the laminar layer and the roughness layer. This partial resistance is dependent on the near-surface model variables, the aerodynamic roughness length and the Surface Area Index (SAI), which is a measure of the surface area enlargement by land use.

TURBDIFF and TURBTRAN are the default schemes for atmospheric turbulence and SAT, respectively, in ICON, and they correspond to `inwp_turb=1` (namelist `nwp_phy_nml`). While TURBTRAN provides the transfer resistances for scalars and horizontal wind components, the final surface fluxes of water vapor and sensible heat are determined in TERRA as a result of updated surface values for q_v and (in case of the upcoming implicit treatment of surface temperature) also for T. Based on these surface fluxes, an implicit equation for vertical diffusion is solved as a final part of TURBDIFF. In this procedure also horizontal momentum and TKE is included, while for these 3 quantities the respective surface concentration is used as a lower boundary condition. Currently, a

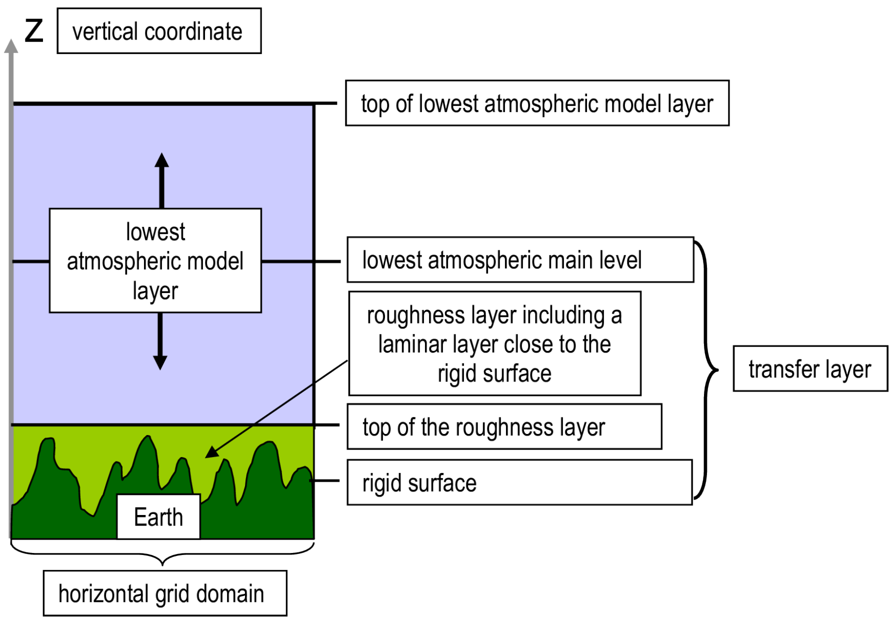
Z
vertical coordinate
top of lowest atmospheric model layer
lowest atmospheric model layer
lowest atmospheric main level
roughness layer including a laminar layer close to the rigid surface
top of the roughness layer
rigid surface
transfer layer
Earth
horizontal grid domain

Figure 3.9.: Surface layer as described in the parameterization TURBTRAN of Raschendorfer (2001).

lower zero-concentration condition is applied for cloud-water and –ice, which is always related to a downward flux for these quantities. For vertical diffusion of passive tracers, the diffusion coefficient for scalars is applied, and the lower boundary condition can be specified individually. Although the effect of local condensation and evaporation is considered in the solution of 2nd –order equations, and hence, can amplify the intensity of turbulent vertical mixing, the direct effect of these additional thermodynamic source-terms in the grid-scale budgets of heat, water vapor and liquid water is not yet considered.

In the namelist `turbdiff_nml` several parameters or selectors for optional calculations related to both schemes can be specified. Through this, TURBDIFF can also be configured as a 3D-turbulence scheme, calculating additionally horizontal shear and providing also horizontal diffusion coefficients. This horizontal shear is the sum of related turbulent shear by the mean flow `itype_sher>0` and (if `ltkeshs=.TRUE.`) of additional shear by larger sub-grid scale non-turbulent horizontal circulations (SHS), which are, for their part, generated by shear of the mean flow, but are formally separated from isotropic turbulence in the framework of STIC. Similarly, each horizontal diffusion coefficient is the sum of the isotropic turbulent diffusion coefficient and an optional additional one related to SHS, provided that this STIC term is active (`ltkeshs=.TRUE.`). However, in ICON, the calculation of horizontal diffusion is not yet connected with these non-isotropic diffusion coefficients from TURBDIFF. Rather, for the time being, isotropic diffusion coefficients calculated by a Smagorinsky formulation are automatically used for 3D diffusion.

DualM EDMF for Turbulence and Shallow Convection

The *Eddy Diffusivity Mass Flux* (EDMF) approach - operational at ECMWF (Köhler et al., 2011) - is based on the decomposition of the turbulent transports proposed by Siebesma and Cuijpers (1995) into eddy diffusivity and mass-flux components. This is based on the idea of unifying the eddy diffusivity and mass-flux concepts that are used in many NWP and climate models within one unified solver. When generalizing to multiple updrafts M_i one arrives at the following equation for the flux of a scalar quantity ϕ:

$$\overline{w'\phi'} = -K\frac{\partial\bar{\phi}}{\partial z} + \sum\nolimits_i M_i(\overline{\phi}_i^u - \bar{\phi}).$$

Here, the mass flux is $M_i = a_i(\overline{w}_i^u - \overline{w})$ and K is the diffusion coefficient. The averaging operators $\overline{\phi}_i^u$ and $\overline{\phi}^e$ act on the updraft and environment fractions, respectively.

To arrive at this equation two assumptions are applied: (i) updraft fraction is small $a \ll 1$ and (ii) the flux within the environment $\overline{w'\phi'_e}^e$ can be approximated by K-diffusion.

The *DualM* framework by Neggers et al. (2009) postulates that two mass-fluxes are sufficient to treat the transition from a dry boundary layer to stratocumulus and shallow cumulus. In particular one dry mass-flux stops at cloud base, while the second moist mass-flux reaches to cloud top. The continuous area partitioning between the dry and moist updraft is a function of moist convective inhibition above the mixed layer top. Updraft initialization is a function of the updraft area fraction and is therefore consistent with the updraft definition. It is argued that the model complexity thus enhanced is sufficient to allow reproduction of various phenomena involved in the cloud–subcloud coupling, namely (i) dry countergradient transport within the mixed layer that is independent of the moist updraft, (ii) soft triggering of moist convective flux throughout the boundary layer, and (iii) a smooth response to smoothly varying forcings, including the reproduction of gradual transitions to and from shallow cumulus convection.

Smagorinsky-Lilly for LES Application

The 3D sub-grid model of Smagorinsky (1963) with the stability correction of Lilly (1962) is implemented for LES applications. This scheme writes the eddy viscosity K_m as

$$K_m = (C_s\Delta)^2\,|S|\,C_B,$$

with the Smagorinsky constant C_s, the filter width Δ, the norm of the strain rate tensor $|S|$ and the stability correction factor C_B.

The filter width is taken to be $\Delta = (\Delta x \Delta y \Delta z)^{\frac{1}{3}}$. The strain rate tensor is defined as

$$S_{ij} = \frac{1}{2}\left(\frac{\partial u_i}{\partial x_j} + \frac{\partial u_j}{\partial x_i}\right),$$

whose calculation requires special care due to the triangular grid in ICON. A metric correction has been developed that treats the horizontal gradients over a sloped orography given a terrain-following coordinate correctly. The norm of S_{ij} is

$$|S| = \sqrt{2 S_{ij} S_{ij}}\,.$$

The stability correction factor C_B is given by

$$C_B = (1 - \mathrm{Ri}\,/\,\mathrm{Pr}_t)^{\frac{1}{2}}$$

with the gradient Richardson number $\mathrm{Ri} = \frac{N^2}{|\bar{S}|}$ and the buoyancy frequency $N^2 = \frac{g}{\theta_0}\frac{\partial\theta_v}{\partial z}$.

The Smagorinsky constant usually has the value of $C_s = 0.1 - 0.2$. In the ICON implementation C_s is set by default to `smag_constant=0.23` (namelist `les_nml`) and the Prandtl number Pr_t to `turb_prandtl=0.333` (namelist `les_nml`).

3.8.7. Sub-grid scale orographic drag

Section authors

J.-P. Schulz, DWD Numerical Models Division
M. Köhler, DWD Physical Processes Division
S. Borchert, DWD Numerical Models Division

ICON treats the entire sub-grid scale orographic drag with one model based on the work of Lott and Miller (1997). Other NWP models treat scales smaller than $\sim 5\,\mathrm{km}$ with different ansatzes, for example with the help of turbulent orographic form drag formulations of the use of an effective roughness length that determines the conductivity of the surface for momentum fluxes between the atmosphere and the Earth.

The motivation for the implementation of a sub-grid scale orographic drag model into ICON traces back to experience with the COSMO model. When the 7-km EU domain of the operational COSMO model at DWD was expanded in order to cover almost all Europe (see Schulz, 2006), it turned out that the surface pressure in the model forecasts became systematically biased. In particular, in wintertime high pressure systems of the model atmosphere tended to develop a positive pressure bias, by 1 to 2 hPa after 48 h, low pressure systems a negative bias ("highs too high, lows too low"). At the same time the wind speed tended to be overestimated by up to $1\,\mathrm{m\,s^{-1}}$ throughout the entire troposphere. The wind direction near the surface showed a positive bias.

The combination of these deficiencies led to the hypothesis that in the model there is too little surface drag, causing an underestimation of the cross-isobar flow in the planetary boundary layer. Consequently, the solution would be to increase the surface drag in the model. This may be accomplished, for instance, by introducing an envelope orography (Wallace et al., 1983, Tibaldi, 1986), but this has unfavorable effects, e.g., for the simulated precipitation. Another option is the inclusion of sub-grid scale orographic (SSO) effects, which were neglected in the COSMO model before. The SSO scheme by Lott and Miller (1997) was selected for this purpose. Its implementation in the COSMO-EU model is described in Schulz (2008), and was later transferred to the ICON model.

The SSO scheme by Lott and Miller (1997) deals explicitly with a low-level flow which is blocked when the sub-grid scale orography is sufficiently high. For this blocked flow separation occurs at the mountain flanks, resulting in a form drag. The upper part of the low-level flow is lead over the orography, while generating gravity waves[4]. In order to describe the low-level flow behavior in the SSO scheme a non-dimensional height H_n of the sub-grid scale mountain is introduced

$$H_n = \frac{NH}{|U|} = Fr^{-1},$$

[4]Propagating, coherent structures consisting of buoyancy and inertial oscillations.

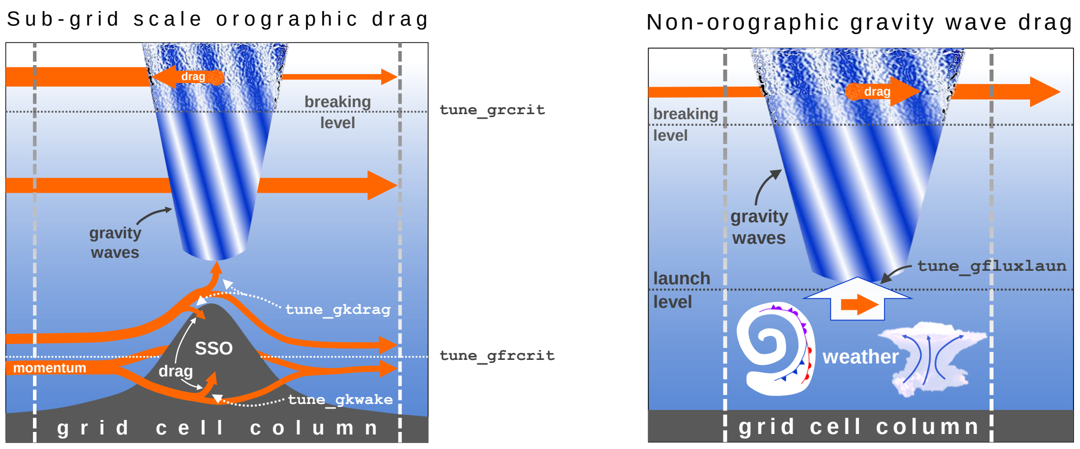

Figure 3.10.: Left: Schematic illustration of the two elements of sub-grid scale orographic drag: First, the low-level blocking, where the horizontal flow (orange) is forced to flow around the sub-grid scale orography (SSO, colored gray). Second, the gravity wave drag on the flow forced to overflow the SSO, and on the flow at higher altitudes, where the radiated gravity waves (white-blue) break. (Following Figure 1 in Lott and Miller (1997).) Right: Schematic illustration of the non-orographic gravity wave drag.

where H is the maximum height of the mountain, $|U|$ is the wind speed and N is the Brunt-Väisälä frequency of the incident flow. The latter is defined by

$$N = \sqrt{\frac{g}{\theta}\frac{\partial\theta}{\partial z}},$$

where θ is the potential temperature, g the acceleration of gravity and z the height coordinate. H_n may be also regarded as an inverse Froude number Fr^{-1} of the system "flow round a mountain".

A small H_n means that there is an unblocked regime, all the flow goes over the mountain and gravity waves (GWs) are forced by the vertical motion of the fluid. A large H_n means that there is a blocked regime, the vertical motion of the fluid is limited and part of the low-level flow goes around the mountain. The SSO scheme requires four external parameters, which are the standard deviation SSO_STDH, the anisotropy SSO_GAMMA, the slope SSO_SIGMA and the geographical orientation SSO_THETA of the sub-grid scale orography. Following Baines and Palmer (1990) these are computed by ExtPar (see Section 2.4.1) from the GLOBE data set (GLOBE-Task-Team, 1999), which has a resolution of approximately 1 km.

Four tuning parameters in the namelist nwp_tuning_nml control the SSO scheme (see Figure 3.10). First, the critical Froude number Fr_c = tune_gfrcrit, which has a twofold effect. The larger its value the higher the likelihood for low-level blocking to occur, since it is activated only where $Fr < Fr_c$. Conversely, where $Fr > Fr_c$ all flow goes over the mountain and the entire stress is associated with GW radiation. In addition, if blocking is active, Fr_c controls the thickness of the blocking layer relative to the mountain height (the larger Fr_c the larger the layer thickness). Its default value is 0.4. Operational simulations with horizontal mesh sizes of 13 km and 40 km use the values 0.333 and 0.425, respectively. Second and third, the magnitudes of the SSO drag and the GW drag are directly proportional to the parameters `tune_gkwake` and `tune_gkdrag`, respectively. The default values are 1.5 and 0.075. Different from this, operational simulations with 13 km horizontal mesh size use `tune_gkwake` = 1.8 and `tune_gkdrag` = 0.09. Finally, the critical Richardson number Ri_c = `tune_grcrit` is a control parameter for the onset of GW breaking. If the Richardson number of the resolved atmospheric state plus the unresolved GWs

$$Ri = \frac{N_{\mathrm{tot}}^2}{|\partial \boldsymbol{u}_{\mathbf{tot}}/\partial z|^2} ,$$

where $\boldsymbol{u}$ denotes the horizontal wind vector, falls below Ri_c, the flow configuration becomes unstable and the GWs break (partly). This process is accompanied by a drag effect on the resolved horizontal flow. Combined with the rule of thumb that Ri decreases with height if GWs are present, this means that the larger the value of Ri_c the lower the altitude where the radiated GWs tend to break and exert a drag. The default value is 0.25.

The scheme computes tendencies of the horizontal wind and the temperature. A detailed description can be found in ECMWF (2018a).

3.8.8. Non-orographic gravity wave drag

Section authors

M. Köhler, DWD Physical Processes Division
S. Borchert, DWD Numerical Models Division

All kinds of (synoptic-scale) atmospheric flow structures (e.g., fronts, convection, jet streams) can develop imbalances that force air parcels to oscillate (vertically) and radiate gravity waves (GWs). The interaction of these non-orographically forced GWs with the atmospheric background flow is assumed to be significant in the middle and upper atmosphere, and is consequently of interest for models that cover this region (e.g., the operational global ICON configuration with its model top at 75 km). If the synoptic scale flow (be it resolved or unresolved by the model) would force GWs, whose horizontal and vertical wave lengths would be smaller than the horizontal and vertical grid mesh sizes, they cannot be resolved by the model. But yet this unresolved part of the GW spectrum could have a significant impact on the resolved flow, and is therefore parameterized (see Figure 3.10).

The parameterization implemented in ICON follows the ansatz of Scinocca (2003) and McLandress and Scinocca (2005), which in turn is based on the work of Warner and McIntyre (1996) to which the simplifying assumption of a hydrostatic, non-rotational atmosphere has been applied. The parameters of this scheme have been optimized following Ern et al. (2006). Details can be found in Orr et al. (2010).

The mechanisms of non-orographic GW forcing can be relatively complex and are not completely understood. For this reason the parameterization assumes a constant source of GWs. The amount of GWs radiated by this idealized source is directly proportional to the namelist parameter `tune_gfluxlaun` (`nwp_tuning_nml`). Its default value is 0.0025 Pa.

The scheme computes tendencies of the horizontal wind and the temperature. A detailed description can be found in ECMWF (2018b).

3.8.9. Lake Parameterization Scheme FLake

Section author
D. Mironov, DWD Physical Processes Division

Lakes significantly affect the structure and the transport properties of the atmospheric boundary layer. The interaction of the atmosphere with the underlying surface strongly depends on the surface temperature.

In numerical weather prediction (NWP), a simplified approach is often taken that amounts to keeping the water surface temperature constant over the entire forecast period. This approach is to some extent justified for ocean and seas. It is hardly applicable to lakes where diurnal variations of the water surface temperature reach several degrees. The situation is even more grave for frozen lakes as the diurnal variations of the ice surface temperature may exceed ten degrees.

Initialization of the NWP model grid boxes that contain water bodies also presents considerable difficulties. When no observational data for some grid boxes are available, those grid boxes are initialized by means of interpolation between the nearest grid-boxes for which the water surface temperature is known (the interpolation procedure may account for some other variables, e.g., two-meter temperature over land). Such procedure is acceptable for sea points where large horizontal gradients of the water surface temperature are comparatively rare, but it is hardly suitable for lakes. Lakes are enclosed water bodies of a comparatively small horizontal extent. The lake surface temperature has little to do with the surface temperature obtained by means of interpolation between the alien water bodies.

In NWP, the lake surface temperature (i.e., the surface temperature of lake water or lake ice) is a major concern. It is this variable that communicates information between the lake and the atmosphere, whereas details of the vertical temperature distribution (e.g., the temperature near the lake bottom) are of minor importance. Therefore, simplified lake models (parameterization schemes), whose major task is to predict the lake surface temperature, the lake freezing and the ice break-up, should be sufficient for NWP and related applications.

The NWP model ICON (as well as COSMO) utilizes the lake parameterization scheme *FLake* (Mironov, 2008, Mironov et al., 2010, 2012). FLake is based on a two-layer parametric representation of the evolving temperature profile. The structure of the stratified layer between the upper mixed layer and the basin bottom, the lake thermocline, is described using the concept of self-similarity (assumed shape) of the temperature-depth curve. The same concept is used to describe the temperature structure of the thermally active upper layer of bottom sediments and of the ice and snow cover. In this way, the problem of solving partial differential equations (in depth and time) for the temperature and turbulence quantities is reduced to solving ordinary differential equations (in time only) for the time-dependent parameters that specify the temperature profile.

The approach is based on what is actually “verifiable empiricism”. However, it still incorporates much of the essential physics and offers a very good compromise between physical realism and computational economy. FLake incorporates the heat budget equations for the four layers in question, viz., snow, ice, water and bottom sediments, developed with due regard for the volumetric character of the solar radiation heating. An entrainment equation is used to compute the depth of a convectively-mixed layer, and a relaxation-type equation is used to compute the wind-mixed layer depth in stable and neutral stratification. Simple thermodynamic arguments are invoked to develop the evolution equations for the ice and snow depths.

Empirical constants and parameters of FLake are estimated, using independent empirical and numerical data. They should not be re-evaluated when the scheme is applied to a particular lake. In this way, the scheme does not require re-tuning, a procedure that may improve an agreement with a limited amount of data but should generally be avoided. Further information about FLake can be found at `http://lakemodel.net`.

FLake is activated within ICON if the namelist parameter `llake` (`lnd_nml`) is set `.TRUE.`, which is the default operational setting at DWD.

FLake requires two external parameter fields. These are the fields of lake fraction (area fraction of a given numerical-model grid box covered by the lake water) and of lake depth. These external parameter fields are generated with the ExtPar software (see Section 2.4) using the Global Lake Database (Kourzeneva, 2010, Kourzeneva et al., 2012, Choulga et al., 2014).

ICON makes use of a tile approach to compute the grid-box mean values of temperature and humidity (and of other scalars) and the grid-box mean fluxes of momentum and scalars. FLake is applied to the ICON grid boxes whose lake fraction exceeds a threshold value; otherwise the effect of sub-grid scale lakes is ignored. Currently, the value of 0.05 is used (see the namelist variable `frlake_thrhld` (`lnd_nml`)).

In the current ICON configuration, the lake depth is limited to 50 m. For deep lakes, the abyssal layer is ignored, a “false bottom” is set at a depth of 50 m, and the bottom heat flux is set to zero. The bottom sediment module is switched off, and the heat flux at the water-bottom sediment interface (or at false bottom) is set to zero. The setting `lflk_botsed_use=.FALSE.` is hard-coded in `mo_data_flake.f90`.

Snow above the lake ice is not considered explicitly. The effect of snow is accounted for in an implicit manner through the temperature dependence of the ice surface albedo with respect to solar radiation Mironov et al. (2012). There is no logical switch to deactivate the snow module of FLake. It is sufficient to set the rate of snow accumulation to zero (hard-coded in `mo_flake.f90`). Without explicit snow layer of the lake ice, the snow depth over lakes is set to zero and the snow surface temperature is set equal to the ice surface temperature.

The attenuation coefficient of lake water with respect to solar radiation is currently set to a default “reference” value for all lakes handled by ICON. It would be advantageous to specify the attenuation coefficient as a global external parameter field. This can be done in the future as the information about the optical properties of lakes becomes available (not the case at the time being).

Generally, no observational data are assimilated into FLake, i.e., the evolution of the lake temperature, the lake freeze-up, and break-up of ice occur freely during the ICON runs. An exception are the Laurentian Great Lakes of North America. Over the Laurentian Great Lakes, the observation data on the ice fraction (provided by the ICON surface analysis scheme) are used to adjust the ice thickness, the ice surface temperature, and (as needed) the water temperature. See the subroutine `flake_init` in `mo_flake.f90` for details. The use of the ice-fraction data over Great Lakes is controlled by the namelist parameter `use_lakeiceana` (`initicon_nml`).

Finally, a word of caution is in order. Running ICON with the lake parameterization scheme switched off (`llake=.FALSE.`) is not recommended as this configuration has never been comprehensively tested at DWD.

3.8.10. Sea-Ice Parameterization Scheme

Section author

D. Mironov, DWD Physical Processes Division

A major task of the sea-ice parameterization scheme for NWP is to predict the existence of ice within a given atmospheric-model grid box and the ice surface temperature. The sea-ice scheme used within ICON NWP accounts for thermodynamic processes only, i.e., no ice rheology is considered (cf. the sea-ice scheme for climate modeling). The horizontal distribution of the ice cover, i.e., the fractional area coverage of sea ice within a given grid box, is governed by the data assimilation scheme. A detailed description of the sea-ice scheme for ICON NWP is given in Mironov et al. (2012), where a systematic derivation of governing equations, an extensive discussion of various parameterization assumptions and of the scheme disposable parameters, and references to relevant publications can be found. Further comments can be found directly in the code, see the module `src/lnd_phy_schemes/mo_seaice_nwp.f90`.

A distinguishing feature of the ICON NWP sea-ice scheme is the treatment of the heat transfer through the ice. As different from many other sea-ice schemes that solve the heat transfer equation on a finite difference grid, the present scheme uses the integral, or bulk, approach (cf. the lake parameterization scheme FLake, Section 3.8.9). It is based on a parametric representation (assumed shape) of the evolving temperature profile within the ice and on the integral heat budget of the ice slab. Using the integral approach, the problem of solving partial differential equations (in depth and time) is reduced to solving ordinary differential equations (in time only) for the quantities that specify the evolving temperature profile. These quantities are the ice surface temperature and the ice thickness.

In the full-fledged scheme outlined in Mironov et al. (2012), provision is made to account for the snow layer above the ice. Both snow and ice are modeled using the same basic concept, that is a parametric representation of the evolving temperature profile and the integral energy budgets of the ice and snow layers (see Mironov (2008) for a detailed discussion of the concept). In the current ICON configuration, snow over sea ice is not considered explicitly. The effect of snow is accounted for implicitly (parametrically) through the ice surface albedo with respect to solar radiation.

A prognostic sea-ice albedo parameterization is used. The sea-ice surface albedo is computed from a relaxation-type rate equation, where the equilibrium albedo and the relaxation (e-folding) time scale are computed as functions of the ice surface temperature. In order to account for the increase of the sea-ice albedo after snowfall events, the ice albedo is relaxed to the equilibrium “snow-over-ice” albedo. The equilibrium snow-over-ice albedo is computed as function of the ice surface temperature, and the relaxation time scale is related to the snow precipitation rate.

The horizontal distribution of the ice cover, i.e., the existence of sea ice within a given ICON grid box and the ice fraction, is governed by the data assimilation scheme (cf. the treatment of lake ice). If an ICON grid box has been set ice-free during the initialization, no ice is created over the forecast period. If observational data indicate open water conditions for a given grid box but there was ice in that grid box at the end of the previous ICON run, ice is removed and the grid box is initialized as ice-free. The new ice is formed instantaneously if the data assimilation scheme indicates that there is sea ice in a given grid box, but there was no ice in that grid box in the previous model run. The newly formed ice has the surface temperature equal to the salt-water freezing point. The thickness of newly formed ice is computed as function of the ice fraction.

ICON utilizes a tile approach to compute surface fluxes of momentum and scalars. For the "sea-water type" grid boxes, the grid-box mean fluxes are computed as a weighted mean of fluxes over ice and over open water, using fractional ice cover f_i and fractional open-water cover $1 - f_i$ as the respective weights. Sea ice in a given ICON grid box is only considered if f_i exceeds its minimum value of 0.015, otherwise the grid box is treated as ice free (see parameter `frsi_min` hard-coded in `mo_seaice_nwp.f90`). Likewise, the open-water fraction less than `frsi_min` are ignored, and the grid box in question is treated as fully ice-covered (f_i is reset to 1). The ice fraction is determined during the model initialization and is kept constant over the entire forecast period. If, however, sea ice melts away during the forecast, f_i is set to zero and the grid box is treated as an open-water water grid box for the rest of the forecast period (prognostic ice thickness is limited from below by a value of 0.05 m, i.e., a thinner ice is removed). The water-surface temperature of that grid box is equal to the observed value from the analysis, or is reset to the salt-water freezing point. The latter situation is encountered when a grid box was entirely covered by ice at the beginning of the forecast, but the ice melts away during the forecast.

In order to run ICON with the sea-ice parameterization scheme switched off, the namelist logical switch `lseaice` (`lnd_nml`) should set equal to `.FALSE.`. This configuration has not been comprehensively tested at DWD and is not recommended.

3.8.11. Land-Soil Model TERRA

Section author

J. Helmert, DWD Physical Processes Division

The soil-vegetation-atmosphere-transfer component TERRA (Schrodin and Heise, 2001, Heise et al., 2006, Schulz et al., 2016) in the ICON model is responsible for the exchange of fluxes of heat, moisture, and momentum between land surface and atmosphere. It establishes the lower boundary-condition for the atmospheric circulation model and considers the energy and water budget at the land surface fractions of grid points. Based on a multi-layer concept for the soil, TERRA considers the following physical processes at each of the tiled land-surface columns, where an uniform soil type with physical properties is assumed:

Radiation

- Photosynthetically active radiation (PAR) is used for plant evapotranspiration

- Solar and thermal radiation budget is considered in the surface energy budget

Biophysical control of evapotranspiration

- Stomatal resistance concept controls the interchange of water between the atmosphere and the plant
- One-layer vegetation intercepts and hold precipitation and dew, which lowers water input to the soil and enhances evaporation
- Roots with root-density profile determines the amount of water available for evapotranspiration in the soil
- Bare-soil evaporation is considered for land-surface fractions without plants.

Heat and soil-water transport

- Implicit numerical methods are used to solve the vertical soil water transport and soil heat transfer between the non-equidistant layers.
- In the operational model version seven layers are used in the soil.
- The lower boundary condition for the heat conduction equation is provided by the climatological mean temperature.
- Surface and sub-surface runoff of water is considered.
- The lower boundary condition is given by a free-drainage formulation.
- A rise of groundwater into the simulated soil column is not represented.
- Soil heat conductivity depends on soil-water content.
- Freezing of soil water and melting of soil ice is considered in hydraulic active soil layers.

Snow

- TERRA offers a one-layer snow model (operational in ICON-NWP) and a multi-layer snow model option (for experiments).
- A prognostic snow density, and snow melting process as well as the time dependent snow albedo are considered
- Surface fractions partly covered with snow are divided in snow-free and snow-covered parts (snow tiles)

Coupling to the atmosphere

- Application of the turbulence scheme at the lower model boundary
- Roughness length for scalars implicitly considered by calculation of an additional transport resistance throughout the turbulent and laminar roughness layer.

TERRA requires a number of external parameter fields, see Section 2.4 for details.

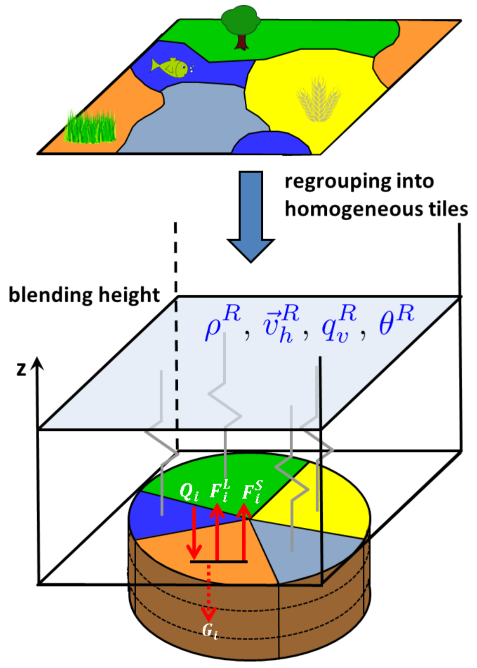
regrouping into homogeneous tiles
blending height
$\rho^R, \vec{v}_h^R, q_v^R, \theta^R$
z
Q_i F_i^L F_i^S
G_i

Figure 3.11.: Tile approach for a grid cell containing various surface types. Patches of the same surface type within a grid box are regrouped into homogeneous classes (tiles) for which the soil and surface parameterizations are run separately.

The Tile Approach

The tile approach addresses the problem of calculating proper cell-averaged surface fluxes in the case of large subgrid variations in surface characteristics. The basic idea following Avissar and Pielke (1989) is depicted in Figure 3.11. If patches of the same surface type occur within a grid box, they are regrouped into homogeneous classes (tiles). The surface energy balance and soil physics are then computed separately for each tile, using parameters which are characteristic of each surface type (roughness length, leaf area index, albedo, . . .). The atmospheric fields which enter the computations, however, are assumed uniform over the grid cell, i.e. the so-called blending height is located at the lowermost atmospheric model level. The contributions from different tiles are then areally weighted to provide the cell-averaged atmospheric forcing. Note that in this approach the geographical distribution of subgrid heterogeneities is not taken into account.

In ICON, the number of surface tiles is specified by the parameter `ntiles` (`lnd_nml`). Setting `ntiles=1` means that the tile approach is switched off, i.e. only the dominant land-surface type in a grid cell is taken into account. Setting `ntiles` to a value $n > 1$, up to n dominant land tiles are considered per grid cell. Note, however, that for $n > 1$ the total number of tiles n_{tot} is implicitly changed to $n_{tot} = n+3$, with three additional "water" tiles classified as "open water" $(n + 1)$, "lake" $(n + 2)$, and "sea-ice" $(n + 3)$. Additional snow-tiles can be switched on by setting `lsnowtile=.TRUE.`. In that case the total number of tiles is further expanded to $n_{tot} = 2 \cdot n + 3$, with the first n tiles denoting the land tiles, the second n tiles denoting the corresponding snow tiles and 3 water tiles as before.

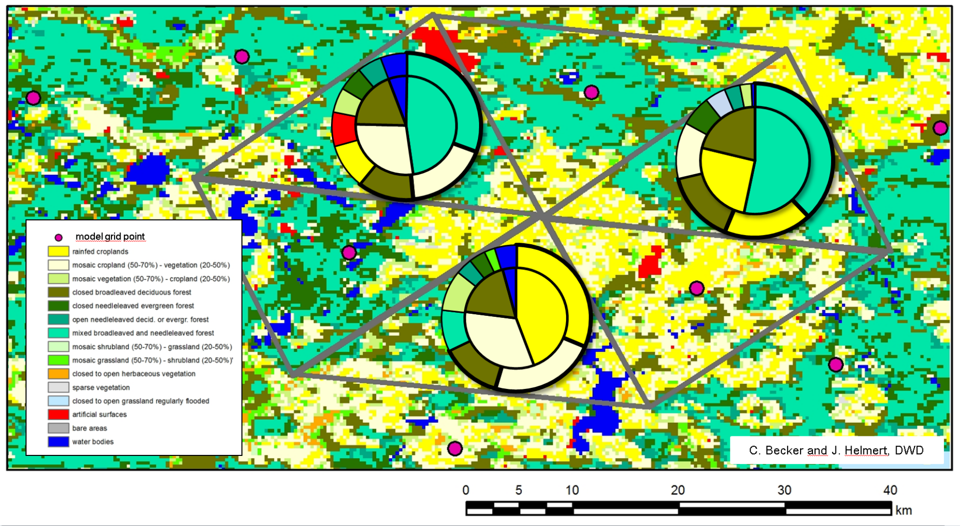
● model grid point
🟨 rainfed croplands
mosaic cropland (50-70%) - vegetation (20-50%)
mosaic vegetation (50-70%) - cropland (20-50%)
closed broadleaved deciduous forest
closed needleleaved evergreen forest
open needleleaved decid. or evergr. forest
mixed broadleaved and needleleaved forest
mosaic shrubland (50-70%) - grassland (20-50%)
mosaic grassland (50-70%) - shrubland (20-50%)'
closed to open herbaceous vegetation
sparse vegetation
closed to open grassland regularly flooded
🟥 artificial surfaces
bare areas
🟦 water bodies
C. Becker and J. Helmert, DWD
0
5
10
20
30
40
km

Figure 3.12.: Tile generation for `ntiles=3`, for the case of a heterogeneous land surface. Outer circles show the fractional areas covered by the respective surface-type for a given grid cell. Inner circles show the selected tiles. Please note the re-scaling of fractional areas in the inner circle.

The process of tile generation in ICON works as follows:
During the setup phase, all land-surface types within a grid box are ranked according to the fractional area f they cover (see Figure 3.12, outer ring). For efficiency reasons, only the `ntiles` (typically about 3) dominating ones are represented by tiles, with the others being discarded (inner ring). If a grid cell contains non-negligible water bodies ($f > 5\%$), up to 3 more tiles are created (i.e. open water, lake, and sea-ice) even if they are not among the dominating ones. By this approach, the surface types represented by tiles can differ from grid cell to grid cell such that the full spectrum of surface types provided by the land cover data set is retained.

If the model is initialized from horizontally interpolated initial data and `ntiles > 1`, a tile coldstart becomes necessary. This can be done by setting `ltile_init=.TRUE.` and `ltile_coldstart=.TRUE.` in the namelist `initicon_nml`. Each tile is then initialized with the same cell averaged value. Note that `ltile_init=.TRUE.` is only necessary, if the initial data come from a model run without tiles.

Important note:
Naive horizontal interpolation of tile-based variables is incorrect, since the dominant tiles and/or their internal ranking will most likely differ between source and target cell. Only aggregated fields can be interpolated!

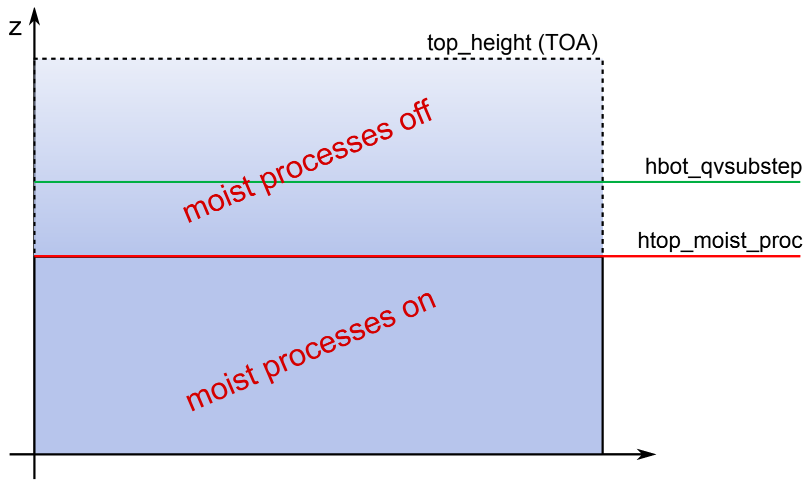

Figure 3.13.: Moist physics are switched off above `htop_moist_proc`, while tracer substepping is switched on above `hbot_qvsubstep`. (Remark: `hbot_qvsubstep` is allowed to be lower than `htop_moist_proc`)

3.8.12. Reduced Model Top for Moist Physics

A notable means for improving the efficiency of ICON is depicted in Figure 3.13. The switch

`htop_moist_proc` (namelist `nonhydrostatic_nml`, floating-point value)

allows to switch off moist physics completely above a certain height. Moist physics include saturation adjustment, grid scale microphysics, convection, cloud cover diagnostic, as well as the transport of all water species but moisture q_v. Of course, moist processes should only be switched off well above the tropopause. The default setting is `htop_moist_proc=22500 m`.

One variant of the implemented horizontal transport scheme for passive scalars is capable of performing internal substepping. This means that the transport time step Δt is split into n (usually 2 or 3) substeps during flux computation. This proves necessary in regions where the horizontal wind speed exceeds a value of about $80\,\mathrm{m\,s^{-1}}$. In real case applications, this mostly happens in the stratosphere and mesosphere. The recommendation for Δt given in Section 3.7.1 then exceeds the numerical stability range of the horizontal transport scheme. To stabilize the integration without the need to reduce the time step globally, transport schemes with and without internal substepping can be combined. The switch

`hbot_qvsubstep` (namelist `nonhydrostatic_nml`, floating-point value)

indicates the height above which the transport scheme switches from its default version to a version with internal substepping. The default value is `hbot_qvsubstep=22500 m`.

Note that substepping is only performed for a particular tracer if a suitable horizontal transport scheme is chosen. The horizontal transport scheme can be selected individually for each tracer via the namelist switch `ihadv_tracer` (`transport_nml`). Variants of the transport scheme with internal substepping are indicated by a two-digit number (i.e. 22, 32, 42, 52). These variants mostly differ w.r.t. the accuracy of the polynomial reconstruction used for the flux estimation. A linear reconstruction is used by the variant 22, whereas 52 uses a cubic reconstruction. See Section 3.6.5 for additional details regarding the transport algorithm.

If moist physics are switched off above 22.5 km (default for NWP applications), internal substepping only needs to be applied for specific humidity q_v, since the advection of all other moisture fields is switched off anyway. However, be aware that you must explicitly enable internal substepping if moisture physics are not switched off, or if other (non-microphysical) tracers are added to the simulation.

3.9. Variable Resolution Modeling

ICON has the capability for static mesh refinement in horizontal directions. This is realized through a *multi-grid approach* which means that one or more additional high resolution (child) domains can be overlaid on coarser (parent) domains. In the following we will make frequent use of the notion *parent* and *child*, in order to illustrate the relationship amongst multiple domains.

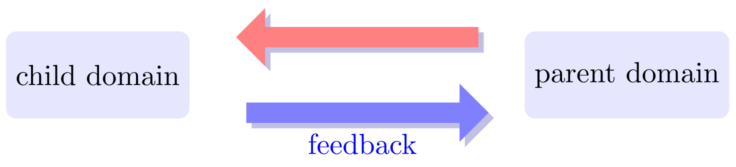

The multi-grid approach easily allows for switching domains on or off at runtime, as well as intertwining one-way and two-way nested domains. two-way as opposed to one-way nesting means that the solution on the child domain is transferred back to the coarser parent domain every time step by means of a feedback mechanism which is described below.

The multi-grid approach closely resembles traditional two-way nesting and has to be distinguished from recent *uni-grid* approaches, where in special areas of interest more cells are added to an existing grid (*h-refinement*). Atmospheric models capable of static h-refinement are e.g. CAM-SE (Zarzycki et al., 2014) and MPAS-A (Skamarock et al., 2012). The basic multi-grid example shown in Figure 3.14 contains one global domain and one regional domain over Europe. It closely resembles the operational setup currently used at DWD.

Since the grids of the different refinement levels are stored in separate files, the usual way to establish a parent-child relationship between these grids is to read the header information from the list of provided grid files, see Section 4.1.2. Then, the parent-child relationships can be inferred from the NetCDF attributes `uuidOfHGrid` and `uuidOfParHGrid`, that have been described in Section 2.1.2.

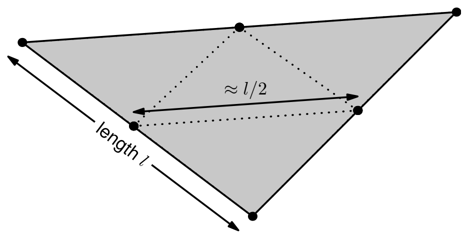

The grid spacing factor between the parent domain and the child domain is fixed to a factor of 2, i.e. each parent triangle is split into 4 child triangles. Correspondingly, in case of nested setups, the time step Δt is multiplied by a factor of 0.5 for each nesting level. Note that the time step Δt needs to be specified for the base (i.e. coarsest) domain only. The (hard-coded) adaption for nested regions is done automatically.

3.9.1. Parent-Child Coupling

This section describes how the exchange of information between a parent and a child domain is realized, and which information (i.e. which fields) is interchanged.

As shown in Figure 3.15, a nested domain can conceptually be split into three areas: A boundary interpolation zone (red), a nudging zone (blue) and a feedback zone (light gray). Prognostic computations are restricted to the latter two. In case of two-way nesting, the nudging zone does not exist and the feedback zone borders on the boundary zone. While the width of the boundary interpolation zone is fixed to 4 cell rows, the width of the nudging zone can be changed with the namelist switch `nudge_zone_width` (`interpol_nml`).

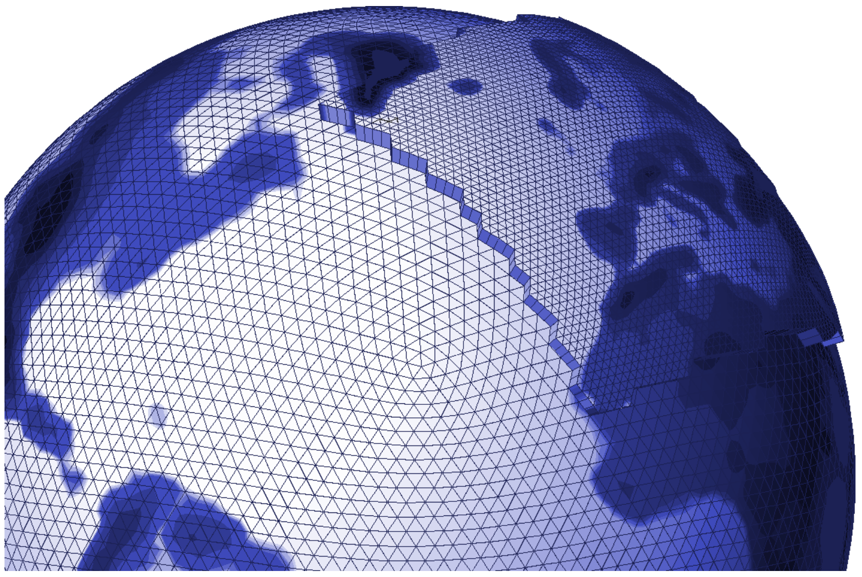

Figure 3.14.: Basic example of a multi-grid setup, consisting of a global ICON domain and a child domain over Europe with half grid spacing. This is similar to the deterministic forecast setup that is operationally used at DWD with a horizontal grid spacing of 13 km globally and 6.5 km in the child domain.

Once the model state on the parent domain $\mathcal{M}_p$ has been updated from time step n to $n+1$, the states $\mathcal{M}_p^n$ and $\mathcal{M}_p^{n+1}$ are used to update the boundary zone on the child domain. By this, the necessary lateral boundary data (forcing) can be provided for integrating the model on the nested domain from state $\mathcal{M}_c^n$ to $\mathcal{M}_c^{n+1}$.

In the feedback zone, the updated model state of the child domain is transferred (interpolated) back to the parent domain. By this, the parent and child domain remain closely coupled, and the simulation on the parent domain can benefit from the high-resolution results of the child domain.

In the nudging zone, which is only active for one-way nesting, upscaled prognostic fields of the child domain are nudged towards the model state of the parent domain. A similar method is applied in limited area mode (LAM). It is further explained in Section 6.2.

Further details on the boundary update and the feedback mechanism are given in the following.

Boundary Update: Parent $\rightarrow$ Child

The overall task of the boundary update mechanism is to provide the child domain with up-to-date lateral boundary conditions at each child time step. Boundary conditions are required for the following set of prognostic variables: v_n, w, ρ, θ_v, q_k. In order to avoid that interpolated values of ρ enter the solution of the continuity equation in the dynamical core, an extended set of variables is used in the boundary update mechanism, namely: v_n, w, ρ, θ_v, q_k, $\langle F_m \rangle$. Here, $\langle F_m \rangle = \langle \rho v_n \rangle$ denotes a temporal average of the mass flux over the dynamic substeps. Since the continuity equation is solved in flux form (see Eq. (3.4)),

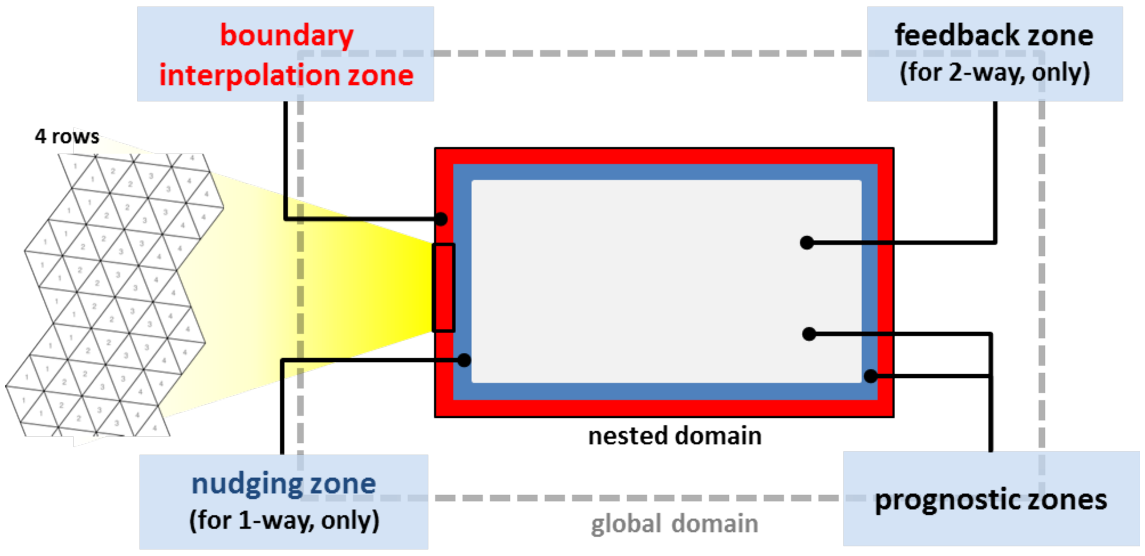
boundary interpolation zone
feedback zone (for 2-way, only)
4 rows
nested domain
nudging zone (for 1-way, only)
global domain
prognostic zones

Figure 3.15.: General structure of a nested domain. Red: boundary interpolation zone consisting 4 cell rows. Blue: nudging zone, which is only active for one-way nesting. Light-gray: feedback zone. Prognostic computations are performed in the feedback and nudging zone.

making use of $\langle F_m \rangle$ implies that interpolated values of ρ are not required for prognosing ρ on the child domain.

In general, the boundary update works as follows: Let ψ_p^n, ψ_p^{n+1} denote any of the above variables on the parent domain at time step n and $n+1$, respectively. Once the model state on the parent domain $\mathcal{M}_p$ has been updated from n to $n+1$, the time tendency

$$\frac{\partial \psi_p}{\partial t} = \frac{\psi_p^{n+1} - \psi_p^n}{\Delta t_p}$$

is diagnosed. Both, ψ_p^n and the tendency $\frac{\partial \psi_p}{\partial t}$ are then interpolated (downscaled) from the parent grid cells/edges to the corresponding cells/edges of the child's boundary zone. With $\mathcal{I}_{p\to c}$ denoting the interpolation operator, we get

$$\psi_c^n = \mathcal{I}_{p\to c}\left(\psi_p^n\right)$$
$$\frac{\partial \psi_c}{\partial t} = \mathcal{I}_{p\to c}\left(\frac{\partial \psi_p}{\partial t}\right)$$

Since the time step on the child domain Δt_c is only half of that on the parent domain, two integration steps are necessary in order to reach the model state $\mathcal{M}_c^{n+1}$. The interpolated tendency is used to update the lateral boundary data after the first physics step and after each dynamics substep. E.g. the lateral boundary conditions for the first and second integration step read ψ_c^n and $\psi_c^n + 0.5\,\Delta t_p \partial\psi/\partial t|_c$, respectively.

Note that in order to reduce interpolation errors above steep orography, for the thermodynamic variables ρ and θ_v perturbations from reference values, rather than the full values are interpolated to the child domain.

Regarding the interpolation operator $\mathcal{I}_{p\to c}$ we distinguish between cell based and edge-based variables. For cell based variables a 2D horizontal gradient is reconstructed at the parent cell center by first computing edge-normal gradients at edge midpoints, followed by a 9-point reconstruction of the 2D gradient at the cell center based on radial basis functions (RBF, Narcovich and Ward (1994)). The interpolated value at the child cell center is then calculated as

$$\psi_c = \psi_p + \nabla\psi_p \cdot \boldsymbol{d}(p,c)\,,$$

with $\nabla\psi_p$ denoting horizontal gradient at the parent cell center, and $\boldsymbol{d}(p,c)$ the distance vector between the parent and child cell center. The same operator is applied to cell based tendencies.

Regarding the interpolation of edge based variables (i.e. $\partial v_n/\partial t$, $\partial F_n/\partial t$, $\langle F_m \rangle$), we distinguish between *outer child edges* that coincide with the edges of the parent cell, and *inner child edges*.

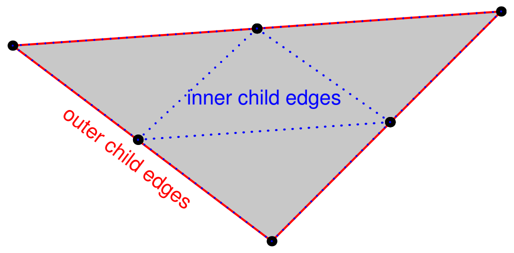

Edge-normal vector components ϕ at the inner child edges are reconstructed by means of a 5-point RBF reconstruction. The 5-point stencil comprises the edges of the two parent cells sharing the edge under consideration.

For the outer child edges a more elaborate reconstruction is applied, in order to assure that the mass flux across the parent edge is equal to the sum of the mass fluxes across the two child edges. To do so, we first reconstruct the vector quantity under consideration at the parent edge vertices using RBF, from which the gradient tangential to parent edge can be computed. The edge-normal vector component at the child edge is then computed as

$$\phi_c = \phi_p + \nabla_t \phi_p \cdot \boldsymbol{d}(p, c)\,,$$

with $\nabla_t \phi_p$ denoting the gradient of the edge-normal vector component tangent to the parent edge, and $\boldsymbol{d}(p, c)$ the distance vector between the parent and child edge midpoints. Since $\boldsymbol{d}(p, c_1) = -\boldsymbol{d}(p, c_2)$ holds on the ICON grid, with c_1, c_2 denoting the child cell's edge midpoints, the above mentioned mass flux consistency is ensured.

The interpolated mass fluxes valid for the current time step can be re-computed from the interpolated average mass flux $\langle F_m \rangle_c$, and the corresponding time tendency. These are prescribed at the outermost edges which separate the boundary zone from the prognostic zone. Since the continuity equation is solved in flux form (see Eq. (3.4)), this implies that interpolated values of ρ are not required for prognosing ρ on the child domain.

Feedback: Child $\rightarrow$ Parent

If two-way nesting is selected (`lfeedback=.TRUE.`, namelist `grid_nml`), the model state $\mathcal{M}_p^{n+1}$ on the parent domain is relaxed towards the updated model state $\mathcal{M}_c^{n+1}$ on the child domain every physics time step. In the following we will refer to this as *relaxation-type feedback*. It is applied to the prognostic variables v_n, w, θ_v, ρ as well as to the prognostic, non-sedimenting mass fractions q_v, q_c, q_i[5]. Let ψ denote any of the above variables. Conceptually, the method can be divided into three major steps:

1. **Upscaling**: The updated field ψ_c^{n+1} on the child domain is interpolated (upscaled) to the parent domain.
2. **Increment computation**: The difference between the solution on the parent domain ψ_p^{n+1} and the upscaled solution $\psi_{c\rightarrow p}^{n+1}$ is computed.
3. **Relaxation**: The solution on the parent domain is relaxed towards the solution on the child domain. The relaxation is proportional to the increment computed in step two.

By way of example, we will mathematically describe the feedback mechanism for the variables ρ and ρq_k. Other variables are handled in a very similar manner.

The feedback mechanism for ρ can be cast into the following form:

$$\rho_p^* = \rho_p^{n+1} + \frac{\Delta t_p}{\tau_{fb}} \left(\mathcal{I}_{c\rightarrow p}(\rho_c^{n+1}) - \rho_p^{n+1} \right) \tag{3.43}$$

[5]Note that when programming ICON the feedback mechanism can easily be switched on for additional tracers by adding the meta-information `lfeedback=.TRUE.` to the corresponding `add_ref`-call, see also Section 8.3.

Here ρ_p^{n+1} denotes the density in the parent cell, which has already been updated by dynamics and physics. The superscript "$*$" indicates the final solution, which includes the increment due to feedback. Δt_p is the fast physics time step on the parent domain, and τ_{fb} is a user-defined relaxation time scale which has a default value of $\tau_{fb} = 10800\,\mathrm{s}$. This value is motivated by the wish to exclude small scale transient features from the feedback, but to capture synoptic-scale features. The relaxation time scale can be adjusted by means of the namelist variable `fbk_relax_timescale` (`gridref_nml`). Finally, $\mathcal{I}_{c\to p}(\rho_c^{n+1})$ denotes a horizontal interpolation operator which upscales the child domain solution to the parent domain.

The interpolation operator is defined as

$$\mathcal{I}_{c\to p}(\rho_c^{n+1}) = \sum\nolimits_{i=1}^{4} \alpha_i \left(\rho_{c,i}^{n+1} - \Delta\rho_{corr}\right) ,$$

with α_i denoting the interpolation weight for the ith child cell. It basically performs a proper weighting of those 4 child cell center values that are connected to the parent cell under consideration. Both bilinear and area-weighted interpolation methods are available, with the former being the default choice. In order to account for differences in the vertical position of the child and parent cell circumcenters, the correction term $\Delta\rho_{corr}$ has been introduced. At locations with noticeable orography, cell circumcenter heights at parent cells can differ significantly from those at child cells. If this is not taken into account, the feedback process will introduce a non-negligible bias in the parent domain's mass field. The correction term is given by

$$\Delta\rho_{corr} = \left(1.05 - 0.005\,\mathcal{I}_{c\to p}(\theta_v'^{\,n+1})\right)\,\Delta\rho_{ref,p} \, ,$$

with the difference in the reference density field

$$\Delta\rho_{ref,p} = \sum\nolimits_{i=1}^{4} (\alpha_i \rho_{ref,c,i}) - \rho_{ref,p} \, ,$$

and the upscaled perturbation value of θ_v denoted by

$$\mathcal{I}_{c\to p}(\theta_v'^{\,n+1}) = \sum\nolimits_{i=1}^{4} \alpha_i \left(\theta_{v,c\,i}^{n+1} - \theta_{v,ref\,i}\right) .$$

The term $\Delta\rho_{ref,p}$, which is purely a function of the parent-child height difference can be regarded as a first order correction term. In order to minimize the remaining mass drift, the empirically determined factor $(1.05 - 0.005\,\mathcal{I}_{c\to p}(\theta_v'^{\,n+1})$ was added, which introduces an additional temperature dependency. Note that the factor 0.005 is close to near surface values of $\frac{\partial\rho}{\partial\theta}$ which can be derived from the equation of state.

Care must be taken to ensure that the feedback process retains tracer and air mass consistency. To this end, feedback is not implemented for tracer mass fractions directly, but for partial densities. In accordance with the implementation for ρ, we get

$$(\rho q_x)_p^* = (\rho q_x)_p^{n+1} + \frac{\Delta t_p}{\tau_{fb}} \left[\mathcal{I}_{c\to p}((\rho q_x)_c^{n+1}) - (\rho q_x)_p^{n+1}\right] \tag{3.44}$$

with

$$\mathcal{I}_{c\to p}((\rho q_x)_c^{n+1}) = \sum\nolimits_{i=1}^{4} \alpha_i \left(\rho_{c,i}^{n+1} - \Delta\rho_{corr}\right) q_{x,c,i}$$

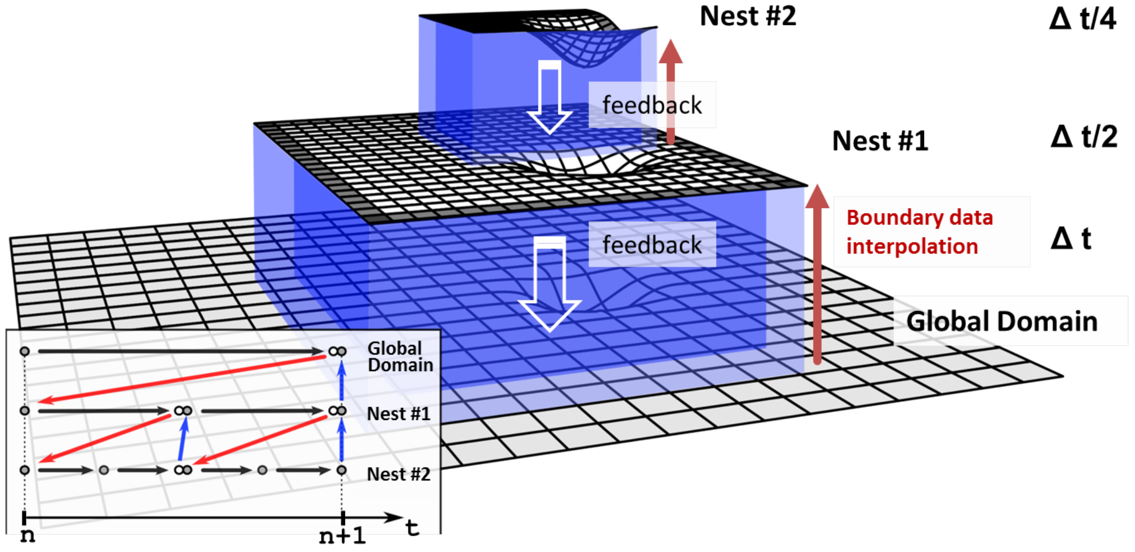

Figure 3.16.: Schematic of a global domain with two two-way nested domains nested into each other. The processing sequence for integrating the model from time step n to $n+1$, is shown in the flowchart at the lower left. Red arrows indicate boundary data interpolation from parent to child, blue arrows indicate the feedback operation from child to parent and black arrows indicate the time integration on the respective domain.

Mass fractions are re-diagnosed thereafter:

$$q_{x,p} = \frac{(\rho q_x)^*_p}{\rho^*_p}$$

When summing Eq. (3.44) over all partial densities, Eq. (3.43) for the total density is recovered. Feedback of other prognostic variables is done in a very similar manner. Note, however, that for θ_v the upscaling is done for the perturbation from the reference state, in order to reduce numerical errors over steep mountains. In the case of v_n some numerical diffusion is added to the resulting feedback increment in order to damp small-scale noise.

3.9.2. Processing Sequence

So far, we concentrated on the information exchange between individual parent and child domains. Nothing has been said about the processing sequence if more than one nested domain, or even repeatedly nested domains are involved. Figure 3.16 provides a common example where a global domain is accompanied by two two-way nested domains nested into each other. The global domain is schematically depicted at the bottom, whereas the nested domains are vertically staggered on top of it. The two blueish regions show the boundary interpolation zone of the nests and the feedback zone. The integration time step on the global domain is Δt, whereas the time step is reduced by a factor of 2 when moving to the next higher grid level.

The processing sequence for integrating the model from time step n to $n+1$ is shown in the flowchart at the lower left. The various domains are ordered top to bottom. The dots indicate the model state $\mathcal{M}_x$ for the different domains, red and blue arrows indicate boundary data interpolation and feedback, respectively, and black arrows indicate time integration.

The basic processing sequence is as follows:

- First, a single time step with Δt is performed on the global domain which results in an updated model state indicated by the white circle.
- It is followed by boundary data interpolation to the first nested domain (red arrow). Then, the model is integrated on nested domain 1 over the time interval $\Delta t/2$.
- Since there exists a second nested domain within nest 1, lateral boundary fields based on the model state $\mathcal{M}_{c1}^{n+1/2}$ are interpolated to the second nested domain. Then, the model is integrated on the nested domain 2 over two times the time interval $\Delta t/4$, resulting in the model state $\mathcal{M}_{c2}^{n+1/2}$.
- Now, feedback is performed from nested domain 2 back to nested domain 1 (blue arrow), which results in an updated model state $\mathcal{M}_{c1}^{n+1/2}$ on nested domain 1 (gray circle). Now, the model is again moved forward in time on nested domain 1 to reach $\mathcal{M}_{c1}^{n+1}$.
- This is followed by a second lateral boundary data interpolation for the nested domain 2. Finally, nested domain 2 is integrated in time again, to reach its final state $\mathcal{M}_{c2}^{n+1}$. As a last step, feedback is performed from nested domain 2 to nested domain 1, followed by feedback from nested domain 1 to the global domain.

An alternative way of visualizing the processing sequence is shown in Figure 3.17. Again, the different grid levels are indicated by horizontal lines with the coarsest grid at the top and the finest one at the bottom. The model state is indicated by a white circle. Every black circle indicates that the model has been integrated in time over one domain-specific time step. Red and blue arrows again denote boundary interpolation and feedback. Note that in cases where only one domain per grid level exists (Figure 3.17a), the processing sequence resembles a W-cycle known from classic multi-grid algorithms for solving elliptic PDEs.

3.9.3. Vertical Nesting

The model top height can be chosen individually for each domain, with the constraint that the height of the parent domain must be larger or at least equal to the height of the child domain. Thereby it is e.g. possible to combine a global domain which extends into the mesosphere with one or several child domains that only extend into the lower stratosphere, see Figure 3.18.

However, it is not possible to choose different vertical level distributions for individual domains. The level distribution is always defined by the global domain. Lower model top heights in child domains are realized by simply neglecting a certain number of levels at the model top. Vertical *refinement* in the sense that vertical resolution is locally increased in a

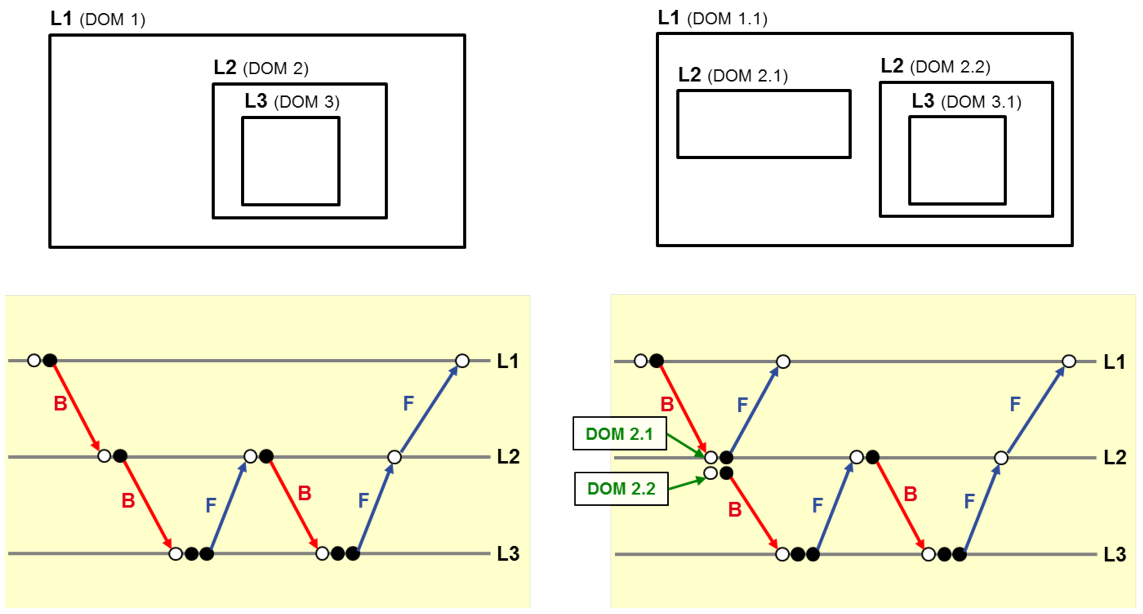

Figure 3.17.: Processing sequence (bottom row) for two generic multi-domain setups (top row). Horizontal lines represent the different grid levels and white circles denote the current model state. A filled black circle, instead, indicates a time integration step. Boundary interpolation and feedback are visualized through red and blue arrows, respectively. Setup (a) is identical to the one shown in Figure 3.16. Setup (b) differs from setup (a) by an additional nested domain on grid level 2.

child domain is so far not possible. One possible workaround might be to repeat the model run with increased vertical resolution in limited area mode (see Chapter 6).

In order to reduce the top height for individual domains, the namelist parameter `num_lev` (`run_nml`), which specifies the number of vertical levels in each domain, must be adapted. In addition, vertical nesting must be enabled by setting `lvert_nest=.TRUE.`. See Section 3.4 for details.

If vertical nesting is activated, boundary conditions are automatically provided for all prognostic variables at the uppermost half level of the nested domain. Several measures are taken in order to avoid excessive reflections of vertically propagating sound and gravity waves from the domain's model top. Further details, however, are beyond the scope of this tutorial.

3.10. Reduced Radiation Grid

In real case simulations, radiation is one of the most time consuming physical processes. It is therefore desirable to reduce the computational burden without degrading the results significantly. One possibility is to use a coarser horizontal grid for radiation than for dynamics.

The implementation is schematically depicted in Figure 3.19:

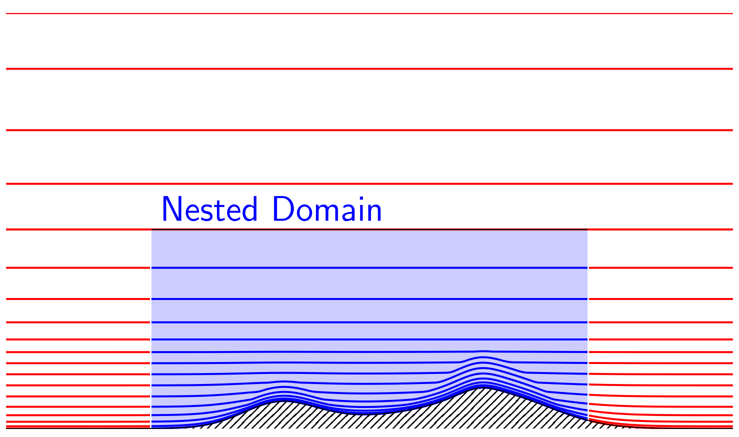

Figure 3.18.: Illustration of ICON's vertical nesting. Note that the nested domain may only have a lower top level height, while the remaining vertical layers must match between the nested and the parent domain. Further note that the parent-nest levels do not coincide in a strict geometrical sense. There exist negligible differences caused by the grid generation process.

Step 1. Radiative transfer computations are usually performed every 30 minutes. Before doing so, all input fields required by the radiation scheme are upscaled to the next coarser grid level.

Step 2. Then the radiative transfer computations are performed and the resulting short wave transmissivities τ^{SW} and longwave fluxes F^{LW} are scaled down to the full grid.

Step 3. In a last step we apply empirical corrections to τ^{SW} and F^{LW} in order to incorporate the high resolution information about albedo α and surface temperature T_{sfc} again. This is especially important at land-water boundaries and the snow line, since here the gradients in albedo and surface temperature are potentially large.

The reduced radiation grid is controlled with the following namelist switches:

`lredgrid_phys= .FALSE./.TRUE.` **(namelist `grid_nml`, logical value)**
If set to `.TRUE.` radiation is calculated on a coarser grid (i.e. one grid level coarser)

`radiation_grid_filename` **(namelist `grid_nml`, string parameter)**
Filename of the grid to be used for the radiation model. Must only be specified for the base domain, since for child domains the grid of the respective parent domain serves as radiation grid. An empty string is required, if radiation is computed on the full (non-reduced) grid.

Note that running radiation on a reduced grid is the standard setting for operational runs at DWD. Using the reduced radiation grid is also possible for the limited area mode ICON-LAM. In this case, both the computational grid and the reduced radiation grid are regional grids. Make sure to create the latter during the grid generation process by setting `dom(:)%lwrite_parent = .TRUE.`, see Section 2.1.5. Internally, the coarse radiation grid is denoted by the domain index 0.

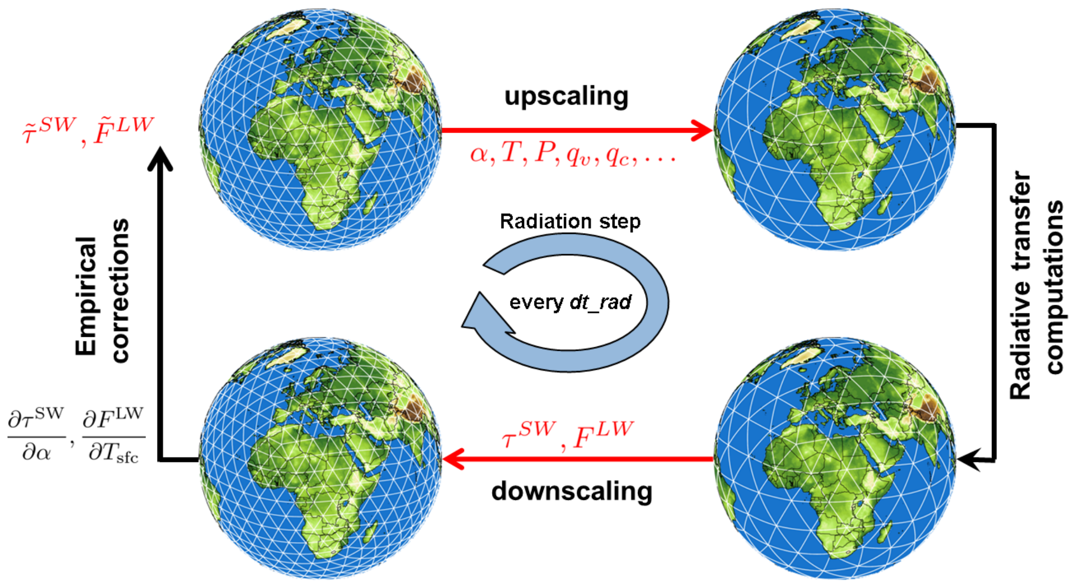

upscaling
$\alpha, T, P, q_v, q_c, \ldots$
Radiation step
every *dt_rad*
Radiative transfer computations
τ^{SW}, F^{LW}
downscaling
$\frac{\partial \tau^{\rm SW}}{\partial \alpha}, \frac{\partial F^{\rm LW}}{\partial T_{\rm sfc}}$
Empirical corrections
$\tilde{\tau}^{SW}, \tilde{F}^{LW}$

Figure 3.19.: Schematic showing how radiation is computed on a reduced (coarser) grid.

4. Running Idealized Test Cases

Idealized test cases typically do not require external parameter or analysis fields for initialization. Initial conditions are usually computed within the ICON model itself, based on analytical functions. These are either evaluated point-wise at cell centers, edges, or vertices, or are integrated over the triangular control volume to provide cell averages.

The ability to run idealized model setups serves as a simple means to test the correctness of particular aspects of the model, either by comparison with analytic reference solutions (if they exist), or by comparison with results from other models. Beyond that, idealized test cases may help the scientist to focus on specific atmospheric processes.

ICON provides a set of pre-defined test cases of varying complexity and focus, ranging from pure dynamical core and transport test cases to "moist" cases, including microphysics and potentially other parameterizations. A complete list of available test cases can be found in the namelist documentation, mentioned in Section 1.1.3.

Individual test cases can be selected and configured by namelist parameters of the namelist **`nh_testcase_nml`**. To run one of the implemented test cases, only a horizontal grid file has to be provided as input. A vertical grid file containing the height distribution of vertical model levels is usually not required, since the vertical grid is constructed within the ICON model itself, based on the set of namelist parameters described in Section 3.4.

From the set of available test cases we choose the Jablonowski-Williamson baroclinic wave test and Straka density current test and walk through the procedure of configuring and running these tests in ICON.

4.1. Main Switches for Idealized Test Cases

This section explains several namelist groups and main switches that are necessary for setting up an idealized model run.

4.1.1. Activating/De-activating Main Model Components

Namelist `run_nml`:

`ltestcase=` `.TRUE./.FALSE.` **(namelist `run_nml`, logical value)**
This parameter must be set to `.TRUE.` for running idealized test cases.

`ldynamics=` `.TRUE./.FALSE.` **(namelist `run_nml`, logical value)**
Main switch for the dynamical core. If set to `.TRUE.`, the dynamical core is

switched on and details of the dynamical core can be controlled via `dynamics_nml`, `nonhydrostatic_nml` and `diffusion_nml`. If set to `.FALSE.`, the dynamical core is switched off completely. This is rarely needed, but can be useful for idealized tests of physical parameterizations with prescribed dynamical forcing.

`ltransport=` `.TRUE./.FALSE.` **(namelist `run_nml`, logical value)**
Main switch for the transport of passive tracers. If set to `.TRUE.`, transport is switched on and details of the transport schemes can be controlled via `transport_nml` (see Section 3.6.5 for additional help). If set to `.FALSE.`, transport of passive tracers is switched off completely.

`iforcing=` `0/2/3` **(namelist `run_nml`, integer value)**
Forcing of dynamics and transport by parameterized processes. If set to 0, forcing is switched off completely (pure dynamical core test case). This implies that all physical parameterizations are switched off automatically. If set to 3, dynamics are forced by NWP-specific parameterizations. Individual physical processes can be controlled via `nwp_phy_nml`, see also Table 3.4. If set to 2, the ECHAM parameterization suite is used. In general, the setting of `iforcing` depends on the selected test case.

`msg_level` **(namelist `run_nml`, integer value)**
You may increase the model output verbosity by setting this namelist parameter to a higher value (≤ 20). This option can be particularly useful if the ICON model run fails and the cause of the error still does not become clear from the error message.

Namelist `dynamics_nml`:

`lcoriolis=` `.TRUE./.FALSE.` **(namelist `dynamics_nml`, logical value)**
Main switch for activation/deactivation of the Coriolis force. In general, the setting depends on the selected test case.

Namelist `extpar_nml`:

`itopo=` `0/1` **(namelist `extpar_nml`, integer value)**
If set to 1, the model tries to read topography data and external parameters from file. If set to `0`, no input file is required for model initialization. Instead, all initial conditions are computed within the ICON model itself. Usually, `itopo` should be set to `0` for running idealized test cases.

4.1.2. Specifying the Computational Domain(s)

ICON's computational domain(s) is/are specified via the following namelist:

Namelist `grid_nml`:

`dynamics_grid_filename` (namelist `grid_nml`, list of string parameters)
Here, the name(s) of the horizontal grid file(s) must be specified. For a global simulation without nests, of course, only a single filename is required. For a global simulation with multiple nests a filename must be specified for each domain. Note that each name must be enclosed by single quotation marks and that multiple names must be separated by a comma (see the examples below).

Namelist `run_nml`:

`num_lev` (namelist `run_nml`, list of integer value)
Comma-separated list of integer values specifying the number of vertical full levels for each domain.

Examples

Assume that the following three horizontal grid files are given

```
icon_grid_0014_R02B05_G.nc
icon_grid_0014_R02B05_N06_1.nc
icon_grid_0014_R02B05_N06_2.nc,
```

which contain a global grid and two nested grids at the same nesting level, respectively (see Figure 4.3). See Section 2.1 for information on the grid file naming convention.

Example 1: Settings for a global run without nest with 40 vertical levels:

```
dynamics_grid_filename = 'icon_grid_0014_R02B05_G.nc'
num_lev = 40
```

Example 2: Settings for a global run with nest number 2 and 40 vertical levels each:

```
dynamics_grid_filename =
'icon_grid_0014_R02B05_G.nc','icon_grid_0014_R02B05_N06_2.nc'
num_lev = 40,40
```

Example 2: Settings for a global run with both nests and 40 vertical levels each:

```
dynamics_grid_filename =
'icon_grid_0014_R02B05_G.nc','icon_grid_0014_R02B05_N06_1.nc',
'icon_grid_0014_R02B05_N06_2.nc'
num_lev = 40,40,40
```

Details regarding the parent-child relationship between different domains/nests, and how ICON knows about these relations can be found in Section 3.9.

4.1.3. Integration Time Step and Simulation Length

The integration time step and simulation length are defined as follows:

Namelist `run_nml`:

`dtime` **(namelist `run_nml`, real value)**
Time step in seconds (for the top-most domain). Note that it is *not* necessary to specify a time step for each domain. For each nesting level, the time step is automatically divided by a factor of two. More details on ICON's time step are given in Section 3.7.1.

`nsteps` **(namelist `run_nml`, integer value)**
Number of time steps. An alternative way for setting the simulation length is to specify the simulation start end end date, see Section 5.1.1.

Output is controlled by the namelist group `output_nml`. It is possible to define more than one output namelist and each output namelist has its own output file attached to it. For example, the run script that is used in Exercise C.4.1 contains three output namelists. The details of the model output specification are discussed in Section 7.1.

4.2. Jablonowski-Williamson Baroclinic Wave Test

In order to activate the Jablonowski-Williamson baroclinic wave test, select:

`nh_test_name='jabw'` **(namelist `nh_testcase_nml`, string parameter)**

The Jablonowski-Williamson baroclinic wave test (Jablonowski and Williamson, 2006) has become one of the standard test cases for assessing the quality of dynamical cores. The model is initialized with a balanced initial flow field. It comprises a zonally symmetric base state with a jet in the mid-latitudes of each hemisphere and a quasi realistic temperature distribution. Overall, the conditions resemble the climatic state of a winter hemisphere. This initial state is in hydrostatic and geostrophic balance, but is highly unstable with respect to baroclinic instability mechanisms. Thus, it should remain stationary if no perturbation is imposed.

To trigger the evolution of a baroclinic wave in the northern hemisphere, the initial conditions are overlaid with a weak (and unbalanced) zonal wind perturbation. The perturbation is centered at $(20°\text{E}, 40°\text{N})$. In general, the baroclinic wave starts growing observably around day 4 and evolves rapidly thereafter with explosive cyclogenesis around model day 8. After day 9, the wave train breaks (see Figure 4.1). If the integration is continued, additional instabilities become more and more apparent especially near the pentagon points (see Section 2.1), which are an indication of spurious baroclinic instabilities triggered by numerical discretization errors. In general, this test has the capability to assess

- the diffusivity of a dynamical core,

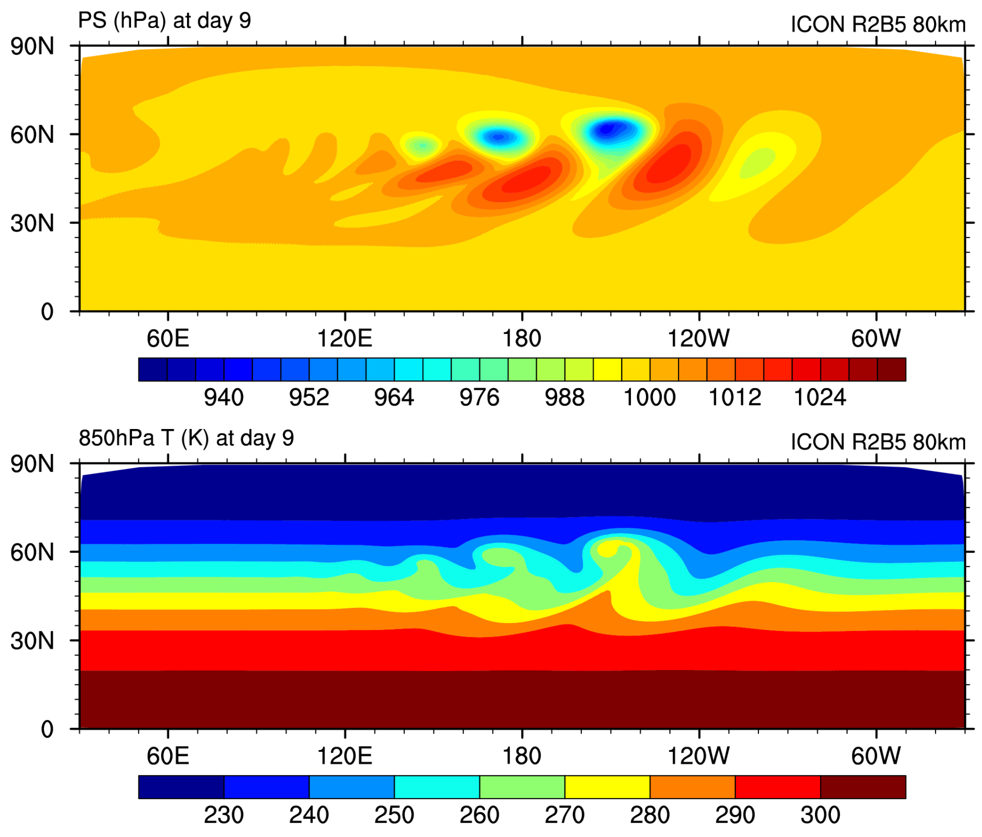

Figure 4.1.: Surface Pressure and 850 hPa Temperature at day 9 for the Jablonowski-Williamson test case on a global R2B5 grid.

- the presence of phase speed errors in the advection of poorly resolved waves,
- the strength of grid imprinting.

In Jablonowski et al. (2008) it is suggested to add a variety of passive tracers to the baroclinic wave test case, in order to investigate the general behavior of the advection algorithm. Questions that could be addressed are

- whether the advection scheme is monotone or positive-definite,
- how accurate or diffusive the advection scheme is,
- whether a constant tracer distribution is preserved (which checks for tracer-air mass consistency).

Four different tracer distributions are implemented, whose initial distributions are depicted in Figure 4.2. See Jablonowski et al. (2008) for further information on the initial distributions.

In Exercise C.4.1 the nested domains depicted in Figure 4.2 will be used to set up and run a nested Jablonowski-Williamson test. A complete list of the recommended namelist settings is given in Table 4.1.

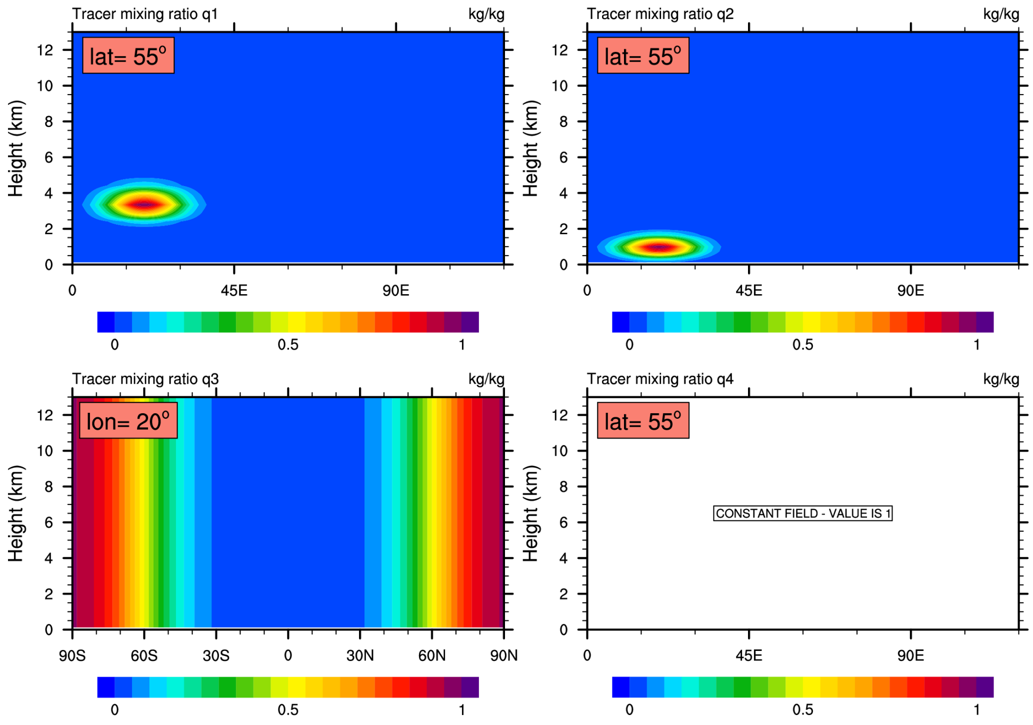

Figure 4.2.: Initial tracer distributions which are available for the Jablonowski-Williamson test case. Tracer $q3$ only depends on the latitudinal position, and tracer $q4$ is constant.

4.2.1. Relevant Namelist Switches in `nh_testcase_nml`:

The following parameters are (in parts) specific to the Jablonowski-Williamson test case. Default values are given in red.

`jw_up`= `1.0` **(namelist `nh_testcase_nml`, real value)**
Amplitude of the u-perturbation in $\mathrm{m\,s^{-1}}$. If this parameter is set to 0, the model's ability to maintain the initial steady state can be tested.

`jw_u0`= `35.0` **(namelist `nh_testcase_nml`, real value)**
Maximum zonal wind in $\mathrm{m\,s^{-1}}$

`jw_temp0`= `288.0` **(namelist `nh_testcase_nml`, real value)**
horizontal-mean temperature at surface in K

`tracer_inidist_list`**(namelist `nh_testcase_nml`, list of integer values)**
Comma-separated list of integer values, choosing from a number of pre-defined initial tracer distributions depicted in Figure 4.2. A value of 1 selects tracer $q1$, 2 selects $q2$, and so on. If this list is empty, no passive tracer will be transported.

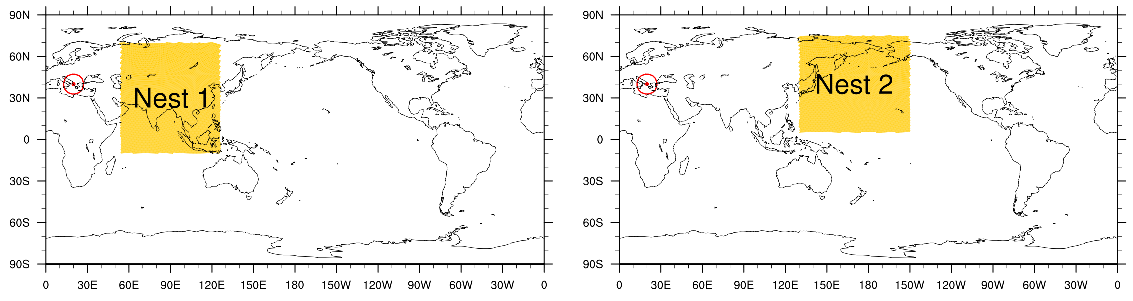

Figure 4.3.: Location of available nests for the baroclinic wave test case (Ex. C.4.1). The perturbation triggering the baroclinic wave is centered at $(20°\mathrm{E}, 40°\mathrm{N})$ (red circle).

Namelist	Parameter	Unit	Value
`nh_testcase_nml`	`nh_test_name`		`'jabw'`
`run_nml`	`ltestcase`		`.TRUE.`
	`ldynamics`		`.TRUE.`
	`ltransport`		`.FALSE.`
	`iforcing`		`0`
	`num_lev`		`40`
	`dtime`	`s`	`576`
	`nsteps`		`1500`
`dynamics_nml`	`lcoriolis`		`.TRUE.`
`extpar_nml`	`itopo`		`0`
`grid_nml`	`dynamics_grid_filename`		`'icon_grid0014_R02B05_G.nc'`
`sleve_nml`	`top_height`	`m`	`35000`
`nonhydrostatic_nml`	`vwind_offctr`		`0.2`
	`damp_height`	`m`	`25000`
	`rayleigh_coeff`		`0.1`

Table 4.1.: Recommended namelist settings for the global Jablonowski-Williamson baroclinic wave test case at a horizontal resolution of $\approx 52\,\mathrm{km}$ (R2B05). See also Ex. C.4.1.

4.3. Straka Density Current Test

Another well known test case for the evaluation and intercomparison of dynamical cores is the nonlinear 2D density current test case described by Straka et al. (1993). See e.g. Gallus and Rančić (1996), Satoh (2002), Skamarock and Klemp (2008), Guerra and Ullrich (2016) for example applications.

In this test case a circular shaped bubble of cold air is initialized a few kilometers above ground in a neutrally stratified ($\theta = 300\,\mathrm{K}$) and hydrostatically balanced atmosphere at rest. The Coriolis force is set to zero. When integrated forward in time, the cold air bubble accelerates towards the ground and forms two symmetric density currents which spread laterally along the bottom boundary and form shear-driven Kelvin-Helmholtz (K-H) instabilities along their top (see Figure 4.5). The simulation is scale limited due to the application of a second order diffusion operator for potential temperature and momentum with constant diffusion coefficients $K_h = K_m = 75\,\mathrm{m^2s^{-1}}$. The resolvable scales are, hence, limited by the viscosity of the simulated medium rather than the spatio-temporal resolution. This enables the computation of a grid-converged reference solution. Straka et al. (1993) showed that for $\Delta x = \Delta z \approx 25\,\mathrm{m}$ the result can be regarded as grid-converged, since any additional resolution increase does not have a noticeable effect. For visual intercomparison Straka et al. (1993) provided reference solutions of various dynamical cores. The $\Delta x = \Delta z \approx 25\,\mathrm{m}$ reference solution of ICON is shown in Figure 4.5.

The computational domain consists of a quasi 2D torus grid (see Section 2.1.9) with doubly-periodic boundary conditions and a width of (at least) 40 km in zonal direction[1]. In meridional direction, the domain consist of 4 cell rows (see Figure 4.4). Due to technical reasons it is not possible to further reduce the number of rows, however, the dynamical core gives identical results for each of these rows. The domain height is set to $H = 6400\,\mathrm{m}$, and the upper and lower boundary are treated as rigid lid (no flux).

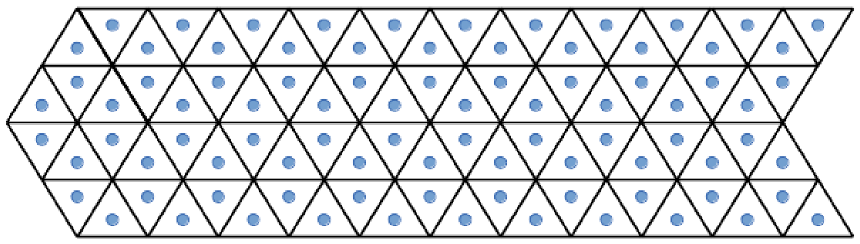

Figure 4.4.: Schematic of the quasi-2D Straka test torus grid, which consists of 4 cell rows in meridional direction. Due to technical reasons it is currently not possible to further reduce the number of rows.

The initial temperature disturbance is applied to the θ field and is given by

$$\Delta T = \begin{cases} 15.0\cos^2\left(\frac{\pi}{2}L\right) & \text{, if} \quad L \leq 1 \\ 0.0 & \text{, if} \quad L > 1\,, \end{cases}$$

with

$$L = \left[\left(\frac{x - x_c}{x_r}\right)^2 + \left(\frac{z - z_c}{z_r}\right)^2\right]^{\frac{1}{2}}.$$

The cold bubble is initially located at $(x_c, z_c) = (0\,\mathrm{km}, 3\,\mathrm{km})$ and has a radius of $(x_r, z_r) = (4\,\mathrm{km}, 2\,\mathrm{km})$.

In general, this test can be used to assess (among other things):

[1]Results are usually compared after $t = 15\,\mathrm{min}$ simulation time, when the wave front has traveled approximately 15 km in both directions. Hence, a domain width of 40 km should be sufficient to avoid significant disturbances along the lateral boundaries.

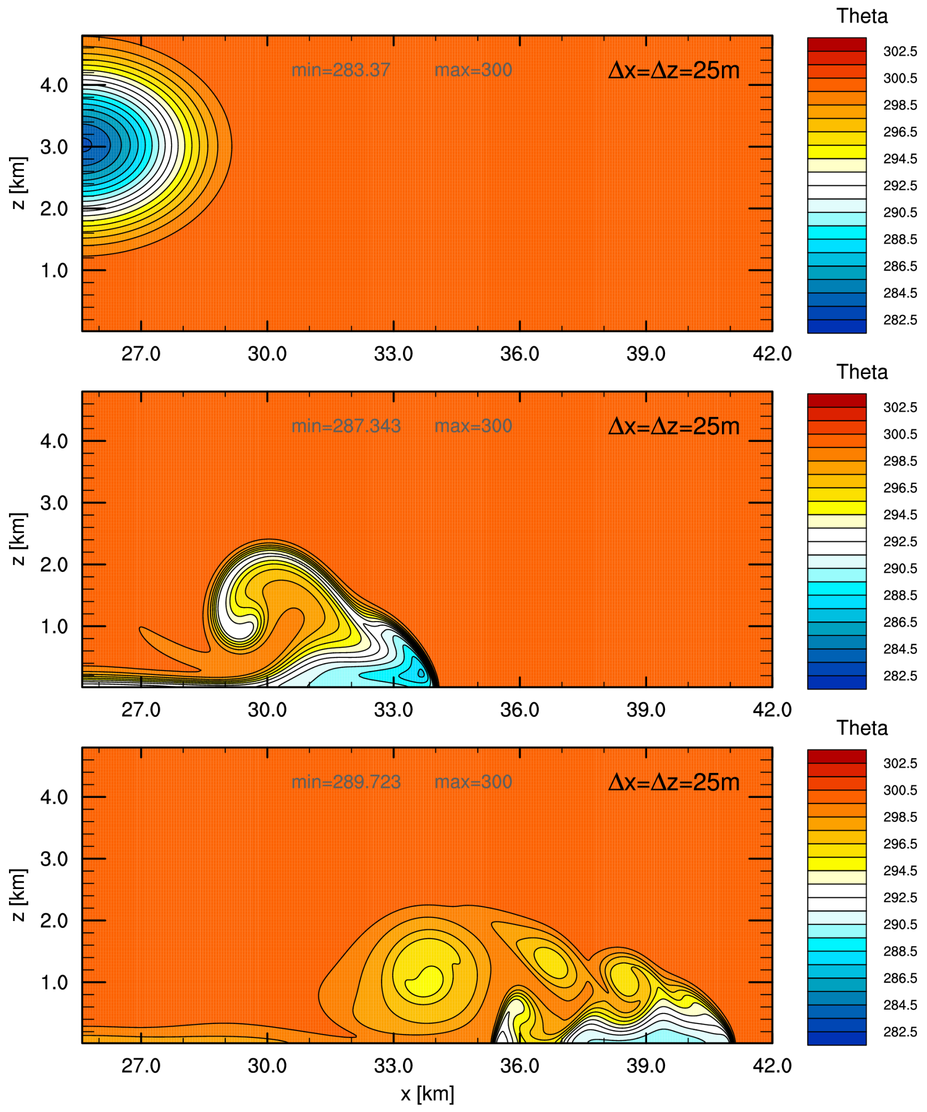

Figure 4.5.: Straka density current test case reference results for ICON with $\Delta x = \Delta z \approx 25\,\mathrm{m}$. Contours show the potential temperature for $t = 0\,\mathrm{min}, 8\,\mathrm{min}, 15\,\mathrm{min}$, respectively. The contour interval is 1 K. Due to the symmetry of the setup only the right moving density current is shown.

- the order of convergence of the dynamical core
- the quality at resolutions much coarser than $\Delta x = \Delta z \approx 25\,\mathrm{m}$. I.e. which resolution is necessary in order to resolve all three K-H rotors?
- the magnitude of phase speed errors. I.e. by adding a nonzero background wind and comparing the right- and left moving currents (see also Skamarock and Klemp (2008)).

A complete list of the recommended namelist settings is given in Table 4.2.

4.3.1. Relevant Namelist Switches in `nh_testcase_nml`:

The following parameters can be used to modify the Straka setup. Default values are given in red. They do not necessarily coincide with the recommended Straka settings (see Table 4.2).

`bub_hor_width`= `1000.0` **(namelist** `nh_testcase_nml`**, real value)**
Horizontal radius of the thermal perturbation in m

`bub_ver_width`= `1400.0` **(namelist** `nh_testcase_nml`**, real value)**
Vertical radius of the thermal perturbation in m

`bubctr_z`= `1400.0` **(namelist** `nh_testcase_nml`**, real value)**
Height of the center of the thermal perturbation in m

`bub_amp`= `2.0` **(namelist** `nh_testcase_nml`**, real value)**
Maximum amplitude of the center of the thermal perturbation in K

`nh_brunt_vais`= `0.01` **(namelist** `nh_testcase_nml`**, real value)**
Initial Brunt-Väisälä frequency (constant with height) in s^{-1}

`nh_u0`= `0.0` **(namelist** `nh_testcase_nml`**, real value)**
Initial constant zonal wind speed. Can be used to break the symmetry of the Straka test case (see Section 4.3).

Namelist	Parameter	Unit	Value
nh_testcase_nml	nh_test_name		'straka93'
	nh_brunt_vais	s^{-1}	0.0
	bubctr_z	m	3000
	bub_hor_width	m	4000
	bub_ver_width	m	2000
	bub_amp	K	-15
run_nml	ltestcase		.TRUE.
	ldynamics		.TRUE.
	ltransport		.FALSE.
	iforcing		3
	num_lev		256
	dtime	s	0.18
	nsteps		6800
dynamics_nml	lcoriolis		.FALSE.
extpar_nml	itopo		0
grid_nml	dynamics_grid_filename		'plane-grid_1600_dx25.0.nc'
	is_plane_torus		.TRUE.
sleve_nml	top_height	m	6400
	min_lay_thckn		0.0
diffusion_nml	hdiff_order		3
	hdiff_efdt_ratio		10
	hdiff_smag_fac		0.12
turbdiff_nml	lconst_z0		.TRUE.
	const_z0	m	0.0003
nwp_phy_nml	inwp_turb		5
les_nml	is_dry_cbl		.TRUE.
	isrfc_type		0
	ufric		0.0
	smag_coeff_type		2
	Km_ext	m^2s^{-1}	75.0
	Kh_ext	m^2s^{-1}	75.0

Table 4.2.: Recommended namelist settings for the Straka density current test case at a horizontal resolution of 25 m on a plane torus grid. Please note that all NWP physics parameterizations except for turbulence (`inwp_turb`) must be switched off.

5. Running Real Data Test Cases

In this chapter you will learn about how to initialize and run the ICON model in a realistic NWP setup. The namelist settings to start from a DWD Analysis and from an IFS Analysis are discussed.

5.1. Model Initialization

The necessary input data to perform a real data run have already been described in Chapter 2. These include

- grid files, containing the horizontal grid information,
- external parameter files, providing information about the Earth's soil and land properties, as well as climatologies of atmospheric aerosols, and
- initial data (analysis) for atmosphere, land and sea.

ICON is capable of reading analysis data from various sources (see Section 2.2), including data sets generated by DWD's Data Assimilation Coding Environment (DACE) and interpolated IFS data. In the following we provide some guidance on how to set up real data runs, depending on the specific data set at hand.

Note that ICON aborts during the setup phase, if any of the required input files has not been found. Therefore, as a first step, check the filenames (and soft links) for the model input files, (see Section 2).

Also make sure that the input data and grid files match. For example, take a look at the global attributes `number_of_grid_used` and `uuidOfHGrid` of the grid file(s). These values have to match the corresponding attributes of the external parameters and initial data file(s), see Section 2.1.8.

5.1.1. Basic Settings for Running Real Data Runs

Most of the main switches, that were used for setting up idealized test cases, are also important for setting up real data runs. As many of them have already been discussed in Chapter 4, we will concentrate on their settings for real data runs. Settings appropriate for the exercises on this subject (see Ex. C.5.1) are highlighted in red.

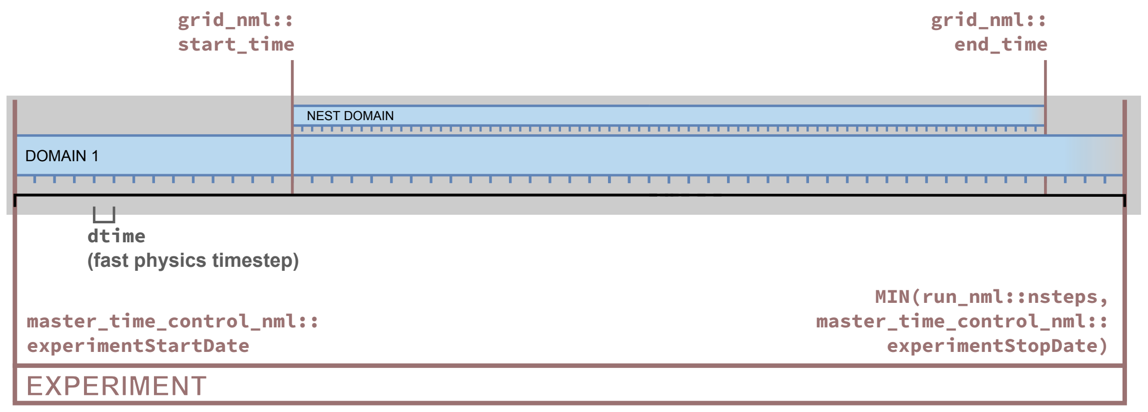

Figure 5.1.: Graphical illustration of the parameters for model start and end. The starting and termination of nested domains is explained in Section 5.2. Please also note Fig. 7.3, in which the program sequence is extended by restart.

Specifying Model Start and End Dates (Namelist `time_nml`)

For real case runs it is important that the user specifies the correct start date and time of the simulation, see Fig. 5.1.

In ICON there coexist two equally usable ways to control the experiment start and end date – without a compelling reason, though. These two alternatives are listed in the following.

Namelist `run_nml`:

time step	`dtime`	`modelTimeStep`

Namelists `time_nml` (left) and `master_time_control_nml` (right):

experiment start	`ini_datetime_string`	`experimentStartDate`
experiment stop	`end_datetime_string`	`experimentStopDate`

Please note that the data types of the above-mentioned namelist parameters differ. The parameters that are listed on the right are consistently based upon the ISO 8601 representations of dates and time spans. However, `dtime` must be specified in seconds.

In the examples of this tutorial, start and end dates are given with `ini_datetime_string` using the ISO8601 format:

`ini_datetime_string= YYYY-MM-DDThh:mm:ssZ` **(namelist `time_nml`)**
 — This must exactly match the validity time of the analysis data set!

Wrong settings lead to incorrect solar zenith angles and wrong external parameter fields. Setting the end date and time of the simulation via `end_datetime_string` is optional. If `end_datetime_string` is not set, the user has to set the number of time steps explicitly in `nsteps` (`run_nml`), which is otherwise computed automatically.

General Settings (Namelist `run_nml`)

`ltestcase= .FALSE.` **(namelist `run_nml`, logical value)**
 This parameter must be set to `.FALSE.` for real case runs.

`iforcing`= 3 **(namelist `run_nml`, integer value)**
A value of 3 means that dynamics are forced by NWP-specific parameterizations.

`ldynamics`= `.TRUE.` **(namelist `run_nml`, logical value)**
The dynamical core must, of course, be switched on.

`ltransport`= `.TRUE.` **(namelist `run_nml`, logical value)**
Tracer transport must be switched on. This is necessary for the transport of cloud and precipitation variables. Details of the transport schemes can be controlled via the namelist `transport_nml` (see Section 3.6.5).

Specifying the Horizontal Grid (Namelist `grid_nml`)

`dynamics_grid_filename` **(namelist `grid_nml`, list of string parameters)**
Here, the name(s) of the horizontal grid file(s) must be specified. For a global simulation without nests, of course, only a single filename is required. For a global simulation with multiple nests, a filename must be specified for each domain. Note that each name must be enclosed by single quotation marks and that multiple names must be separated by a comma (see Section 4.1.2 and the examples therein).

`radiation_grid_filename` **(namelist `grid_nml`, string parameter)**
If the radiative transfer computation should be conducted on a coarser grid than the dynamics (one level coarser, effective mesh size $2\Delta x$), the name of the base grid for radiation must be specified here. See Section 3.10 for further details.

Specifying External Parameters (Namelist `extpar_nml`)

`itopo`= 1 **(namelist `extpar_nml`, integer value)**
For real data runs this parameter must be set to 1. The model now expects one file per domain from which it tries to read topography data and external parameters.

`extpar_filename` **(namelist `extpar_nml`, string parameter)**
Filename(s) of input file(s) for external parameters. If the user does not provide namelist settings for `extpar_filename`, ICON expects one file per domain to be present in the experiment directory, following the naming convention

```
extpar_filename = "extpar_<gridfile>.nc"
```

The keyword *<gridfile>* is automatically replaced by ICON with the grid filename specified for the given domain (`dynamics_grid_filename`). As opposed to the grid-file specification namelist variables (see above), it is not allowed to provide a comma-separated list. Instead, the usage of keywords provides full flexibility for defining the filename structure.

By changing the above setting, the user has full flexibility with respect to the filename structure. The following keywords are allowed for the namelist parameter `extpar_filename`. The keywords are automatically replaced by ICON with the content described in the right column below.

<path>	model base directory (namelist parameter `model_base_dir`, namelist `master_nml`)
<gridfile>	grid filename for the given domain (`dynamics_grid_filename`)
<nroot>	grid root division `R`*x* (single digit)
<nroot0>	grid root division `R`*xx* (two digits)
<jlev>	grid bisection level `B`*yy* (two digits)
<idom>	domain number (two digits).

Specifying the Initialization Mode (Namelist `initicon_nml`)

ICON provides different real data initialization modes which differ in terms of the expected input fields and number of input files. Thereby ICON is able to handle analysis products from different models. The mode in use is controlled via the namelist switch `init_mode`.

`init_mode` (namelist `initicon_nml`, integer value)
It is possible to

- start from (interpolated) *uninitialized* DWD analysis without the IAU procedure: `init_mode = 1`
- start from interpolated IFS analysis: `init_mode = 2`
- start atmosphere from interpolated IFS analysis and soil/surface from interpolated ICON/GME fields: `init_mode = 3`
- start from non-interpolated, *uninitialized* DWD analysis, and make use of the IAU procedure to filter initial noise: `init_mode = 5`
- start from interpolated *initialized* ICON analysis with subsequent vertical remapping: `init_mode=7`

The most relevant modes are mode 1, 2, 5 and 7. They will be explained in more detail below.

ICON supports NetCDF and GRIB2 as input format for input fields. In this context it is important to note that the field names that are used in the input files do not necessarily coincide with the field names that are internally used by the ICON model. To address this problem, an additional input text file is provided, a so-called *dictionary file*. This file translates between the ICON variable names and the corresponding GRIB2/NetCDF short names.

Generally the dictionary is provided via the following namelist parameter:

`ana_varnames_map_file` (namelist `initicon_nml`, string parameter)
Filename of the dictionary for mapping between internal names and GRIB2/NetCDF short names. An example can be found in `icon/run/ana_varnames_map_file.txt`.

5.1.2. Starting from Uninitialized DWD Analysis

This analysis product is rarely the optimal choice for model initialization, as it generates a significant amount of spurious noise during the first few hours of a model run (see Figure 2.8). Nevertheless, this mode is described for completeness. The process of obtaining the uninitialized DWD analysis for non-incremental update is described in Section 2.2.1.

Model initialization is basically controlled by the following three namelist parameters:

`init_mode = 1` (namelist `initicon_nml`, integer value)
To start from uninitialized DWD analysis data (without incremental analysis update), the initialization mode must be set to 1.

In that case the ICON model expects two input files per domain. One containing the ICON first guess (3 h forecast) fields, which served as background fields for the assimilation process. The other contains the analysis fields produced by the assimilation process. See Table 10.2 for a list of variables.

`dwdfg_filename` (namelist `initicon_nml`, string parameter)
Filename of the DWD first guess input file.

`dwdana_filename` (namelist `initicon_nml`, string parameter)
Filename of the DWD analysis input file.

Remember to make sure that the validity date for the first guess and analysis input file is the same and matches the model start date given by `ini_datetime_string`.

Input filenames need to be specified unambiguously, of course. By default, if the user does not provide namelist settings for `dwdfg_filename` and `dwdana_filename`, the filenames have the form

```
dwdfg_filename  = "dwdFG_R<nroot>B<jlev>_DOM<idom>.nc"
dwdana_filename = "dwdANA_R<nroot>B<jlev>_DOM<idom>.nc"
```

This means, e. g., that the first guess filename begins with "`dwdFG_`", supplemented by the grid spacing R*x*B*yy* and the domain number DOM*ii*. Filenames are treated case sensitively.[1]

By changing the above setting, the user has full flexibility with respect to the filename structure. The following keywords are allowed for the namelist parameters `dwdfg_filename`, `dwdana_filename` and `ifs2icon_filename` (for the latter see Section 5.1.5):

<path>	model base directory (namelist parameter `model_base_dir`, namelist `master_nml`)
<nroot>	grid root division R*x* (single digit)
<nroot0>	grid root division R*xx* (two digits)
<jlev>	grid bisection level B*yy* (two digits)
<idom>	domain number (two digits).

[1] More precisely this behavior depends on the file system: UNIX-like file systems are case sensitive, but the HFS+ Mac file system (usually) is not.

5.1.3. Starting from Uninitialized DWD Analysis for IAU

As will be described in Section 10.3.1, IAU is a means to reduce the initial noise which typically results from small scale non-balanced modes in the analysis data set. Combining this analysis product with IAU is the preferred method in cases where the horizontal and vertical grid of the intended forecast run exactly match with that of the analysis. Since no horizontal interpolation is required, the forecast run can make use of the surface tile information which is specific to this analysis product. Moreover, this product exhibits the smallest noise level during model start.

The process of obtaining the uninitialized analysis for IAU is described in Section 2.2.1.

Model initialization is basically controlled by the following namelist parameters:

`init_mode = 5` **(namelist `initicon_nml`, integer value)**
: To start from DWD analysis data with IAU, the initialization mode must be set to 5.

ICON again expects two input files. One containing the ICON first guess, which typically consists of a 1.5 h forecast taken from the assimilation cycle (as opposed to a 3 h forecast used for the non-IAU case). The other file contains the analysis fields (mostly increments) produced by the assimilation process. See Table 10.1 for a full list of variables.

`dwdfg_filename` **(namelist `initicon_nml`, string parameter)**
: Filename(s) of the DWD first guess input file(s) for each domain. See Section 5.1.2 for an explanation of the filename structure.

`dwdana_filename` **(namelist `initicon_nml`, string parameter)**
: Filename(s) of the DWD analysis input file(s) for each domain. See Section 5.1.2 for an explanation of the filename structure.

The behavior of the IAU procedure is controlled via the namelist switches `dt_iau` and `dt_shift`:

`dt_iau = 10800` **(namelist `initicon_nml`, real value)**
: Time interval (in s) during which the IAU procedure (i.e. dribbling of analysis increments) is performed.

`dt_shift = -5400` **(namelist `initicon_nml`, real value)**
: Time (in s) by which the model start is shifted ahead of the nominal model start date given by `ini_datetime_string`. Typically `dt_shift` is set to $-0.5 *$ `dt_iau` such that dribbling of the analysis increments is centered around `ini_datetime_string`.

As explained in Section 10.3.1 and depicted in Figure 5.2, you have to make sure that the first guess is shifted ahead in time by $-0.5 *$ `dt_iau` w.r.t. the analysis. The model start time `ini_datetime_string` must match the validity time of the analysis.

The secret of iterative IAU: Some of you might have heard about an ICON feature named *iterative IAU*, though still wondering what's behind it. The *iterative IAU* combines two model runs which serve two different purposes

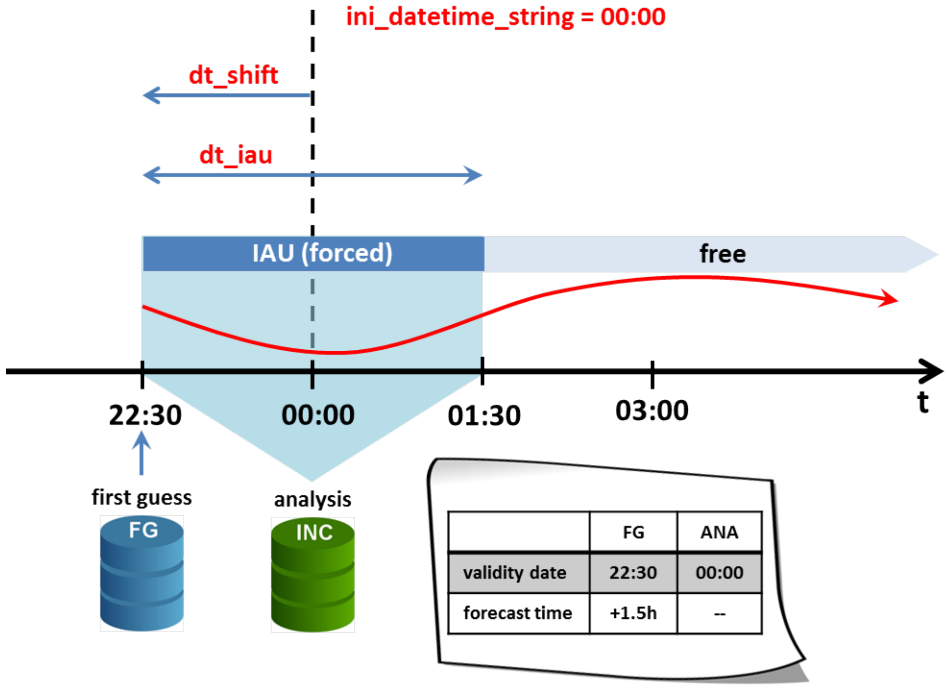

	FG	ANA
validity date	22:30	00:00
forecast time	+1.5h	--

Figure 5.2.: Schematic illustrating typical settings for a global ICON forecast run starting from a DWD analysis **with IAU** at 00 UTC. IAU (i.e. analysis filtering by dribbling of analysis increments) is performed over a 3 h time interval (`dt_iau`), with the model start being shifted ahead of the nominal start date by 1.5 h (`dt_shift`). The validity date of the first guess and analysis is 22:30 UTC and 00 UTC, respectively.

into a single model run. This is achieved by means of an ICON-internal loop structure. It has been implemented for sake of pure convenience.

The first model run is meant to generate a filtered (or initialized) analysis out of the uninitialized analysis for IAU product. To this end an IAU run is launched which, in contrast to the standard IAU run described above, uses a halved asymmetric IAU window of `dt_iau=5400` (asymmetric w.r.t. to the validity time of the analysis increments). The shift of the model start remains unchanged (i.e. `dt_shift=-5400`). The model integration stops after 5400 s (at the nominal start date) and the model state is written to disk. For the example in Figure 5.2 the stop date would be 00 UTC.

During the asymmetric IAU window, the analysis increments have been fully incorporated. The resulting model state is termed *filtered* or *initialized analysis*. It is equivalent to the *initialized analysis product* described in Section 2.2.1.

The second model run is a standard forecast run with a centered IAU window, starting from the uninitialized analysis for IAU product as described earlier in this Section.

The key point is that both runs are performed within a single model run by means of an internal loop structure. After ICON's read-in and initialization procedure, the first loop iteration stores the model's initial state, performs the asymmetric IAU run and saves the resulting initialized analysis to disk. During the second loop iteration, the model resets to the previously stored initial state and performs a standard forecast run with a centered IAU window.

The main benefit of merging these runs into a single model run is that the initial conditions (i.e. first guess and analysis file) have to be read only once, which saves a decent amount of time in the operational forecast cycle.

The iterative IAU is activated by setting `iterative_iau=.TRUE.` in the namelist `initicon_nml`. Given the namelist parameters `dt_shift` and `dt_iau`, they are applied in the following way during iteration 1 and 2:

iteration I:	`0.5 dt_iau`	`dt_shift`
iteration II:	`dt_iau`	`dt_shift`

5.1.4. Starting from Initialized DWD Analysis

The initialized analysis is the product of choice in cases where the horizontal and/or vertical grid of the intended model run differs from that of the analysis. Using the uninitialized analysis for IAU is prohibited in such cases, as the horizontal interpolation of tiled surface fields makes no sense. Moreover, the initialized analysis product is less cumbersome to use, as it consists of a single file per domain, only. When compared to the standard uninitialized analysis product, spurious noise is significantly reduced (see Figure 2.8).

The process of obtaining the initialized analysis is described in Section 2.2.1.

Model initialization is basically controlled by the following namelist parameters:

`init_mode = 7` **(namelist `initicon_nml`, integer value)**
: To start from initialized DWD analysis data, the initialization mode must be set to 7. If the number and or heights of the vertical levels differs between the model and the analysis, the input fields are automatically remapped in the vertical during read-in.

ICON expects a single input file. See Table 10.3 for a full list of variables.

`dwdfg_filename` **(namelist `initicon_nml`, string parameter)**
: Filename(s) of the initialized DWD analysis input file(s) for each domain. Admittedly, the nomenclature "`dwdfg`" is a bit counter intuitive, as the file contains the full analysis rather than the first guess. See Section 5.1.2 for an explanation of the filename structure.

Remember to make sure that the model start time given by `ini_datetime_string` matches the validity date of the input file.

5.1.5. Starting from IFS Analysis

No filtering procedure is currently available when starting off from interpolated IFS analysis data. The model just reads in the initial data from a single file and starts the forecast.

The process of obtaining the IFS analysis and its content is described in Section 2.2.2.

`init_mode= 2` **(namelist `initicon_nml`, integer value)**
: To start from interpolated IFS analysis data, the initialization mode must be set to 2. **Note that for this initialization mode only input data in NetCDF format are supported and the specification of a dictionary file is not possible.**

`ifs2icon_filename` **(namelist `initicon_nml`, string parameter)**
: ICON expects a single file per domain from which interpolated IFS analysis can be read. With this parameter, the filename can be specified. Similar to the namelist parameters `dwdfg_filename` and `dwdana_filename`, which have been explained above in Section 5.1.2, the filenames have the form

```
ifs2icon_filename = "ifs2icon_R<nroot>B<jlev>_DOM<idom>.nc"
```

Remember to make sure that the model start time given by `ini_datetime_string` matches the validity date of the analysis input file.

5.2. Starting or Terminating Nested Domains at Runtime

Starting or terminating nested domains at runtime is possible by means of the namelist parameters `start_time` and `end_time` in the namelist `grid_nml`. Model calculations for the nested domain are performed if the simulation time of the parent domain is greater or equal to `start_time` and less than `end_time`. The settings are graphically illustrated in Fig. 5.1.

`start_time` **(namelist `grid_nml`, list of real values)**
: Comma-separated list of integer values. For each domain, the start time relative to the experiment start date can be specified in seconds. A value of 0 for the ith domain means that it is started at experiment start date which is either defined by `ini_datetime_string` or `experimentStartDate`. If Incremental Analysis Update (IAU) is used, `start_time` must be set equal to `dt_shift` (`initicon_nml`) (i.e. negative), in order for the nested domain to be active from the very beginning.

`end_time` **(namelist `grid_nml`, list of real values)**
: Comma-separated list of integer values. For each domain, the end time relative to the experiment start date can be specified in seconds. I.e. a value of 3600 specified for the ith domain means that it is terminated one hour after experiment start.

As discussed in Section 2.2, initial data files are usually required for each nested domain. With only little loss of forecast skill, this rather tedious procedure can be overcome by starting the nested domain(s) shortly after the global domain. In that case, nested domains are initialized by parent-to-child interpolation of the prognostic fields. Note, however, that surface tile information will be lost. Surface fields on the child domain are initialized with *aggregated* values interpolated from the parent domain.

6. Running ICON-LAM

The most important first: Running the limited area (regional) mode of ICON does not require a separate, fundamentally different executable. Instead, ICON-LAM is quite similar to the other model components discussed so far: It is easily enabled by a top-level namelist switch

Namelist `grid_nml`: `l_limited_area = .TRUE.`

Other namelist settings must be added, of course, to make a proper ICON-LAM setup. This chapter explains some of the details.

Chapter Layout. Some of the pre-processing aspects regarding the regional mode have already been discussed in Section 2.3. Based on these prerequisites the exercises in this chapter (see Ex. C.6.1) will explain how to actually set up and run limited area simulations.

In the following, technical details on the limited area mode are provided, in particular on how to control the read-in of initial data and boundary data.

6.1. Limited Area Mode vs. Nested Setups

In Section 3.9.1 the nesting capability of ICON has been explained. Technically, the same computational grids may be used either for the limited area mode or the nested mode of ICON[1]. Furthermore, both ICON modes aim at simulations with finer grid spacing and smaller scales. They therefore choose a comparable set of options out of the portfolio of available physical parameterizations.

However, there exist some differences between the regional and the one-way nested mode:

- ICON-LAM is driven by externally supplied boundary data which may come from a global model or a coarser resolution LAM that has been run in advance – that's an obvious difference! During the simulation, boundary conditions are updated at regular time intervals by reading input files. Between two lateral boundary data samples the boundary data is linearly interpolated.
- Lateral boundary updates happen (significantly) less frequently compared to one-way nesting.
- The driving model and the limited area model may run on different computer sites. Often they also differ in terms of the governing equations as well as numerical methods used.

[1]Here, we do not take the reduced radiation grid into account, see Section 3.10. This serves to simplify the discussion at this point.

- ICON-LAM allows for a more flexible choice of vertical levels: Nested domains may differ from the global, "driving" grid only in terms of the top level height, but vertical layers must match between the nested and the parent domain (see Section 3.9.3). In contrast to that, the limited area mode performs a vertical interpolation of its boundary data. This is the default namelist parameter setting `itype_latbc=1` in the namelist `limarea_nml`. The level number and the level heights may therefore be chosen independently.

- ICON-LAM allows for a more flexible choice of the horizontal resolution. While for nested setups the increase in horizontal resolution per nesting level is constrained to a factor of 2, the resolution of the limited-area domain can be freely selected. However, resolution jumps much larger than a factor of ~ 5 between the forcing data resolution and the target resolution should be avoided, since it will negatively impact the forecast quality.

6.2. Nudging in the Boundary Region

In order to prevent outward-propagating waves from reflecting back into the domain, a sponge layer is implemented along the lateral boundaries. Within this sponge layer the interior flow is relaxed towards the externally specified boundary data. In addition to this lateral boundary nudging, upper boundary nudging[2] along the model top can be switched on by choosing `nudge_type=1` (namelist `nudging_nml`). The default value is 0, i.e. it is switched off. Figure 6.1 schematically depicts the partitioning of the limited area domain into the *lateral boundary zone*, labeled ⓪, the adjacent *lateral nudging zone* ①, the *upper nudging zone* ②, the *nudging overlap zone* ③ and the *"free" model atmosphere* ④. In the lateral boundary zone ⓪, which has a fixed width of 4 cell rows, externally supplied boundary data are simply prescribed.

The mathematical implementation of the sponge layer in the nudging zones follows the work by Davies (1976, 1983). An additional "forcing" term is added to the right hand side of the prognostic equations for v_n, θ_v, ρ, and q_v:

$$\psi(t) = \psi^*(t) + \alpha_{\text{nudge}} \frac{\Delta t}{\Delta \tau} \underbrace{\left[\psi_{\text{bc}}(t) - \psi^*(t)\right]}_{=\delta\psi},$$

where ψ_{bc} is the externally specified value of the prognostic variable ψ at time t, and α_{nudge} is a relaxation coefficient. The nudging update $\psi - \psi^*$ depends on the time step ratio $\Delta t/\Delta\tau$ ($\rightarrow$ `ndyn_substeps`), but not on the time step itself, so it might be thought of as a

[2] Lateral and upper boundary nudging should not be confused with the Newtonian-relaxation based data assimilation technique which is also named *nudging*. The latter is not available in the ICON model (see Section 10 for available options).

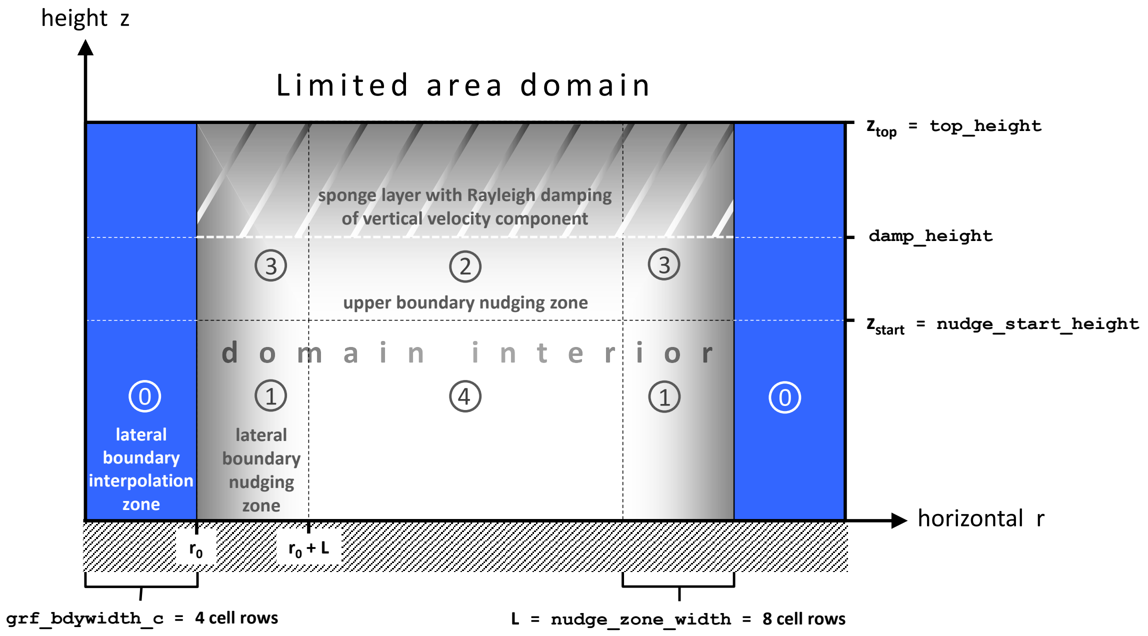
height z
Limited area domain
z_top = top_height
damp_height
z_start = nudge_start_height
sponge layer with Rayleigh damping of vertical velocity component
upper boundary nudging zone
domain interior
lateral boundary interpolation zone
lateral boundary nudging zone
horizontal r
r_0
r_0 + L
grf_bdywidth_c = 4 cell rows
L = nudge_zone_width = 8 cell rows

Figure 6.1.: Schematic illustration of the lateral boundary zone (blue) and the lateral and upper boundary nudging zones (gray) in the limited-area mode.

kind of state "shift" from ψ^* to ψ. The nudging coefficient α_{nudge} gradually decreases with increasing distance from the boundary and is of the form

$$\alpha_{\text{nudge}} = \begin{cases} A_0 \exp\left(-\frac{|r-r_0|}{\mu}\right), & \text{if } |r-r_0| \leq L \text{ (region ① in Fig. 6.1)} \\ B_0 \left(\frac{z-z_{\text{start}}}{z_{\text{top}}-z_{\text{start}}}\right)^2, & \text{in region ②} \\ \max\left\{A_0 \exp\left(\cdots\right), B_0\left(\cdots\right)^2\right\}, & \text{in region ③} \\ 0, & \text{in region ④} \end{cases},$$

with A_0 the maximum relaxation coefficient in the lateral nudging zone, L the width of the lateral nudging zone given in units of cell rows, μ the e-folding width given in units of cell rows, r the actual cell row index beginning with 1 in the outermost cell row of the boundary zone, and r_0 the cell row index at which the nudging zone starts (typically `grf_bdywidth_c+1`, see Figure 6.1). The parameters L, μ, and A_0 can be specified via `nudge_zone_width`, `nudge_efold_width`, and `nudge_max_coeff` in the namelist `interpol_nml`. The nudge zone width should at least comprise 8 (better 10) cell rows in order to minimize boundary artifacts. For the variables v_n and q_v the parameter A_0 is multiplied by the factor 0.5.

B_0 is the maximum nudging coefficient in the upper boundary nudging zone between the model top at height z_{top} (`sleve_nml`: `top_height`) and the nudging start height z_{start} (`nudging_nml`: `nudge_start_height`). The value of B_0 is controlled by `max_nudge_coeff_vn` (`nudging_nml`) for the horizontal wind v_n, and `max_nudge_coeff_thermdyn` for θ_v and ρ.

Note that positive water vapor increments $\delta\psi = \delta q_v > 0$ are cut to zero in supersaturated regions ($q_c > 0$) in the lateral boundary nudging zone, in order to avoid an undesirable positive feedback on the growth of the amount of cloud water. In addition, water vapor is not subject to nudging in the upper boundary nudging zone. If the nudging data from the driving model contain hydrostatic variables (i.e. hydrostatic pressure), it might be more consistent to formulate the nudging in terms of the basic hydrostatic variables: pressure and temperature. This option is controlled by the namelist switch `nudge_hydro_pres` (`limarea_nml`), which applies to both lateral and upper boundary nudging. If set to `.TRUE.` (default), nudging increments of the hydrostatic pressure and the temperature, δp and δT, are computed and transformed into virtual potential temperature and density increments following the linear mapping

$$\begin{aligned}\delta\rho &= X_\rho \delta p + Y_\rho \delta T + Z_\rho \delta q_v \\ \delta\theta_v &= X_{\theta_v} \delta p + Y_{\theta_v} \delta T + Z_{\theta_v} \delta q_v\,,\end{aligned}$$

which is motivated by the total differential of the thermodynamic state equations. The factors X, Y and Z are determined by the state before the nudging (ψ^*). Note again that water vapor increments are nonzero only in the lateral boundary nudging zone.

Important note: Independent of the upper boundary nudging is the treatment of the vertical velocity component w along the model top: w and corresponding vertical mass fluxes are set to zero at the uppermost half level of the computational domain. Starting from the height specified by `damp_height` (`nonhydrostatic_nml`), the vertical velocity is damped towards zero following the method proposed by Klemp et al. (2008).

If upper boundary nudging is switched on (`nudging_nml`: `nudge_type=1`), “lateral boundary” data (the driving data for the nudging) have to be provided for the entire limited area domain rather than the lateral boundary region, only. This mode requires the namelist parameter `latbc_boundary_grid` (`limarea_nml`) defining the grid file on which the lateral boundary data are defined to be empty, i.e. `latbc_boundary_grid=" "`.

In multi-domain simulations upper boundary nudging is restricted to the primary limited area domain. On nests within this nudging type is not applied.

Running the model in regional mode is quite often accompanied by choosing a lower model top height compared to global simulations. In these cases, the neglected air mass above model top can have a noticeable impact regarding the attenuation of the incoming solar irradiance and can be the source of a small but noticeable amount of downward long-wave irradiance. To account for that in a rather ad hoc manner, an additional model layer above model top can be added by setting `latm_above_top=.TRUE.` (namelist `nwp_phy_nml`). It is used by the radiation scheme, only. The additional layer has a (hard-coded) thickness of 1.5 times the thickness of the uppermost model layer. Currently, temperature is linearly extrapolated, assuming a vertical gradient of $-5\,\mathrm{K\,km^{-1}}$. For ozone, aerosols and cloud fields, a simple no-gradient condition is assumed. Despite this rather ad hoc solution, it is suggested to activate the additional layer. Please note that this option works only in combination with a reduced radiation grid.

6.3. Model Initialization

The necessary input data to perform a limited area run are basically identical to those required for a global run (i.e. horizontal grid(s), initial conditions, external parameter; see Section 5.1), with the exception that lateral boundary data are required in addition in order to drive the model.

Technically it is possible to combine initial- and boundary data from different sources (e.g. one might take boundary data from IFS and initial data from ICON). In general, however, it is better to use boundary and initial data from the same source.

Dependent on the available initial data, the following initialization modes can be used in limited area mode:

`init_mode` **(namelist** `initicon_nml`**, integer value)**

`init_mode = 2`	initialize from **IFS data**. This mode has already been described in Section 5.1.5 in the context of reading IFS analysis data.
`init_mode = 3`	initialize from **IFS atmospheric** and **ICON surface data**. This mode is of special interest for operational weather services who want to perform cold starts with IFS atmospheric data.
`init_mode = 7`	initialize from **ICON data**. This mode has already been described in Section 5.1.4 in the context of reading in DWD's initialized analysis product.

These modes have in common that the read-in process is followed by a vertical interpolation of the input fields to the target vertical grid. Thus the target vertical grid can be chosen independent of the vertical grid on which the input is defined. Note that in case of `init_mode = 7` the vertical interpolation requires that the field `HHL` (vertical half level heights) is contained in the initial data.

Specifics of `init_mode=2`

- Only input data in NetCDF format are supported.
- A single input file per domain is expected, containing the analysis (or, more generally, the initial state). The filename must be provided for `ifs2icon_filename` (see also Section 5.1.5).
- The required input fields are depicted in Figure 6.2.

Specifics of `init_mode=7`

- A single input file per domain is expected, containing the analysis (or, more generally, the initial state). The filename must be specified with the parameter `dwdfg_filename(initicon_nml)`.

Atmosphere

$\left\{\begin{matrix}\texttt{U, V}\\ \text{or}\\ \texttt{VN}\end{matrix}\right\}$, `W`, `T`, `LNPS`, `GEOP_ML`, `QV`, `QC`, `QI`, `QR`, `QS`

Soil/Surface

`SMIL1`, `SMIL2`, `SMIL3`, `SMIL4`, `STL1`, `STL2`, `STL3`, `STL4`, `LSM`, `CI`, `GEOP_SFC`, `ALB_SNOW`, `SST`, `SKT`, `T_SNOW`, `W_SNOW`, `RHO_SNOW`, `W_I`

Figure 6.2.: Required variable set when initializing ICON-LAM from IFS data, i.e. `init_mode=2`. Optional fields are marked in gray. Please note that although the field is called `W` (vertical velocity) ICON expects the content of this field to be `OMEGA` (vertical wind in a pressure based coordinate system) in case of `init_mode=2`!

- As we do not make use of a second input file containing explicit analysis information, it is good practice to indicate this via the following namelist parameter.

  `lread_ana` **(namelist** `initicon_nml`**, logical value)**
  By default, this namelist parameter is set to `.TRUE.`. If `.FALSE.`, a separate analysis file is not required. The filename of the first guess file is specified via the `dwdfg_filename` namelist option, see Section 5.1.2.

  Note that in the recent ICON version `lread_ana=.FALSE.` is set automatically for `init_mode= 7`, if it has been forgotten by the user.

- The required input fields are listed in Table 10.3. A valid option is to use DWD's initialized analysis product for initialization. See Section 2.2.1 for ways to obtain it.

Specifics of `init_mode=3`

- Two files are needed, `dwdfg_filename` containing the surface fields and `ifs2icon_filename` including the atmospheric fields (both in `initicon_nml`).

- For the atmospheric data the same procedures are used internally as for `init_mode=2`. As a consequence, the same set of atmospheric variables is required (see Figure 6.2) and the data needs to be in NetCDF format.

- Internally, the same procedures are used for the surface data as for `init_mode=7`. Hence, the same surface fields are required (see Table 10.3).

- Initially, this `init_mode` was designed to combine IFS atmospheric data with GME surface data. As there is no fundamental difference between the ICON and GME surface parameterizations, this `init_mode` can be used for both.

6.4. Reading Lateral Boundary Data

The read-in of lateral boundary data is fortunately less cumbersome than the read-in of initial data, as it is based on a decision tree. The user is no longer required to select a specific mode which (hopefully) fits the data at hand. Instead, ICON scans the boundary data file and, dependent on its content, ICON diagnoses additional fields so as to obtain the internally required set of variables. The decision tree is depicted in Figure 6.3. If the provided data set does not match any of the trees, an error is thrown. As a result, ICON can handle variable sets from hydrostatic models (e.g. IFS) as well as non-hydrostatic models (e.g. COSMO, ICON) without the assistance of the user.

As apparent from the decision tree, three different variable sets can be handled. See Figure 2.11 for its specific content.

> *Important note:* Boundary data sets originating from a non-hydrostatic model with height based vertical coordinates (e.g. COSMO or ICON) must contain the field HHL (vertical half level heights). It is required by the vertical interpolation procedure. Note, however, that the field only needs to be present in the boundary data set whose validity date equals the model start date.

> *Troubleshooting:* The usage of a decision tree as depicted in Figure 6.3 has consequences when searching for the cause of an error. For example, a wrong specification of HHL in `latbc_varnames_map_file` leads to the following error behavior: ICON does not find HHL, so it erroneously takes the right branch of the decision tree. ICON then looks for the geopotential `GEOSP` (or alternatively `GEOP_ML`). This is also not found which results in the error that the geopotential was not found.

Read-in of boundary data is controlled by the following namelist parameters:

The type of lateral boundary conditions is specified by

`itype_latbc` (namelist `limarea_nml`, Integer value)

If set to 1 time-dependent boundary conditions are used. ICON then tries to read external data files at regular time intervals from a particular location specified by `latbc_filename` and `latbc_path` (see below).
If set to 0, time-constant lateral boundary conditions are used which are derived from the initial conditions.

Boundary data is read at regular time intervals. This is specified by the following namelist parameter:

`dtime_latbc` (namelist `limarea_nml`, floating-point value)

Time difference in seconds between two consecutive boundary data sets. At intermediate times, boundary conditions are computed by linear interpolation in time.

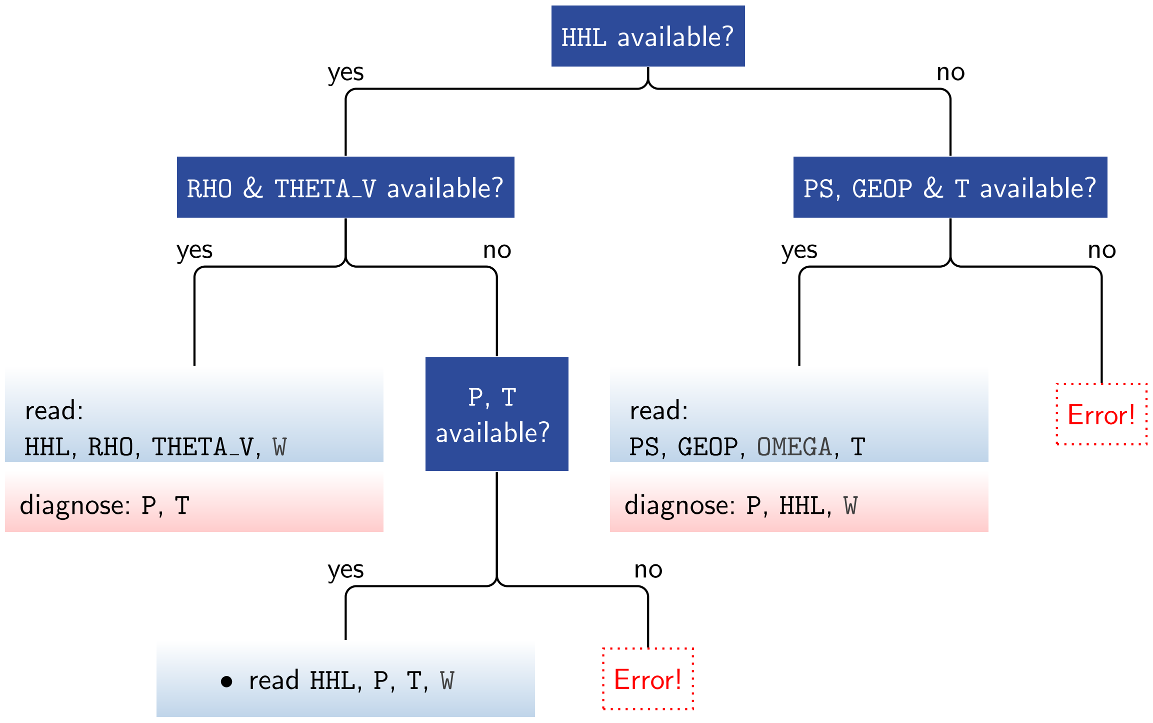

Figure 6.3.: Read-in of lateral boundary data. Based on this decision tree, ICON investigates the data file contents and diagnoses additional fields.
The following fields are read additionally from file: velocity fields `VN` (or `U`, `V`) and mixing ratios `QV`, `QC`, `QI` (optional: `QR`, `QS`). The fields `W` and `OMEGA` are optional; if they are unavailable, the vertical wind is initialized with zero.
For the input from a pressure based coordinate system (right branch), note that ICON expects the field `OMEGA` under the name `W`.

6.4.1. Naming Scheme for Lateral Boundary Data

Naturally, the sequence of lateral boundary data files must satisfy a consistent naming scheme. It is a good idea to consider this convention already during the pre-processing steps (see Section 2.3).

Filenames: `latbc_filename`, `latbc_path` **(string parameters,** `limarea_nml`**)**
By default, the filenames are expected to have the following form:

"prepiconR*<nroot>*B*<jlev>*_*<y><m><d><h>*.nc"

Here, several keywords are used which are further explained below. This naming scheme can be flexibly altered via the namelist parameter `latbc_filename` (namelist `limarea_nml`) using the available keywords. The absolute path to the boundary data can be specified with `latbc_path` (string parameter, `limarea_nml`).

By changing the above setting, the user has full flexibility with respect to the filename structure. The following keywords are allowed for the namelist parameter `latbc_filename`:

<nroot>	grid root division R*x* (single digit)
<nroot0>	grid root division R*xx* (two digits)
<jlev>	grid bisection level B*yy* (two digits)
<dom>	domain number (two digits)
<y>	year (four digits)
<m>	month (two digits)
<d>	day in month (two digits)
<h>	hour (UTC) (two digits)
<min>	minutes (UTC) (two digits)
<sec>	seconds (UTC) (two digits)
<ddhhmmss>	elapsed days, hours, minutes and seconds since `ini_datetime_string` or `experimentStartDate` (each two digits)
<dddhh>	elapsed days and hours since `ini_datetime_string` or `experimentStartDate` (three digits day, two digits hours).

Field names: `latbc_varnames_map_file` **(namelist** `limarea_nml`**, string)**
ICON supports NetCDF and GRIB2 as input format for boundary fields. Field names in input files do not necessarily coincide with internal ICON field names. Hence, an additional input text file (*dictionary file*) can be provided. This two-column file translates between the ICON variable names and the corresponding DWD GRIB2 short names or NetCDF variable names.

Specifying a valid dictionary file is currently mandatory, if pre-fetching of boundary data is selected `num_prefetch_proc=1` (see below).

Boundary grid: `latbc_boundary_grid` **(namelist** `limarea_nml`**, string)**
As it has been explained in Section 2.3, the lateral boundary data can be defined on an auxiliary grid, which contains only the cells of the boundary zone for optimization purposes.
If this is the case for the applied boundary data, the filename of this grid file must be specified with this namelist parameter.

6.4.2. Pre-Fetching of Boundary Data (Mandatory)

Pre-fetching strives to avoid blocking of the computation due to reading of boundary data. The term denotes the reading of files ahead of time, i.e. the next input file will be processed simultaneously with the preceding compute steps. This avoids waiting for the I/O processes during the time consuming procedure of opening, reading and closing of the input files.

`num_prefetch_proc= 1` **(namelist** `parallel_nml`**, integer value)**
If this namelist option is set to `1`, one MPI process will run exclusively for asynchronously reading boundary data during the limited area run. This setting, i.e. the

number of pre-fetching processors, can be zero or one.

Enabling the pre-fetching mode is **mandatory** for the described LAM setup.

6.5. Tropical Setup

The tropical setup namelist configuration of the COSMO model was and still is applied by many users of the COSMO model. As ICON is a global model, it is routinely applied to a wider range of conditions than a limited-area only model like the COSMO model. Nevertheless, when choosing an area close to the equator some namelist parameters have to be adapted compared to mid-latitude high-resolution limited-area setups. For some of these parameters, the necessary adaptions are quite straight forward. Other parameters require rigorous testing and tuning of the configuration in order to find a good combination for these parameters.

Parameter	Mid-Latitudes	Tropical Setup	Description
`tune_zvz0i` (`nwp_tuning_nml`)	`1.25`	test & tune	Terminal fall velocity of ice, meaningful range for tuning between `1.` and `3.5`
`rat_sea` (`turbdiff_nml`)	`7.`	test & tune	Ratio of laminar scaling factors over sea and land, meaningful range for tuning between `1.` and `20.`
`inwp_convection` `lshallowconv_only` (`nwp_phy_nml`)	`1` `.true.`	test & tune	Convection parameterization, `inwp_convection=1` and `lshallowconv_only=.true.` for shallow convection only, `inwp_convection=0` for no convection parameterization
`top_height` (`sleve_nml`)	`22000.`	`30000.`	Model top height (only for `ivc_type=2`, see Section 3.4)
`damp_height` (`nonhydrostatic_nml`)	`12250.`	`18000.`	Height at which Rayleigh damping of vertical wind starts

Table 6.1.: List of namelist parameters that are sensitive to the choice of the limited-area domain location. Values that are listed in the table are suitable for setups around 2.5 km effective grid spacing.

Table 6.1 provides an overview on namelist parameters that are sensitive to the choice of the domain location. For the terminal fall velocity of ice (`tune_zvz0i`) literature suggests higher values than used in current ICON setups (e.g., Heymsfield and Donner (1990) suggest a value which is higher by a factor of 3). Such literature values are derived under certain conditions (e.g., particle shape, temperature range). Hence, the value which is required by a model in order to get good results can differ. This value has a strong impact on the radiative properties of ice clouds and can be used to compensate biases. In summary,

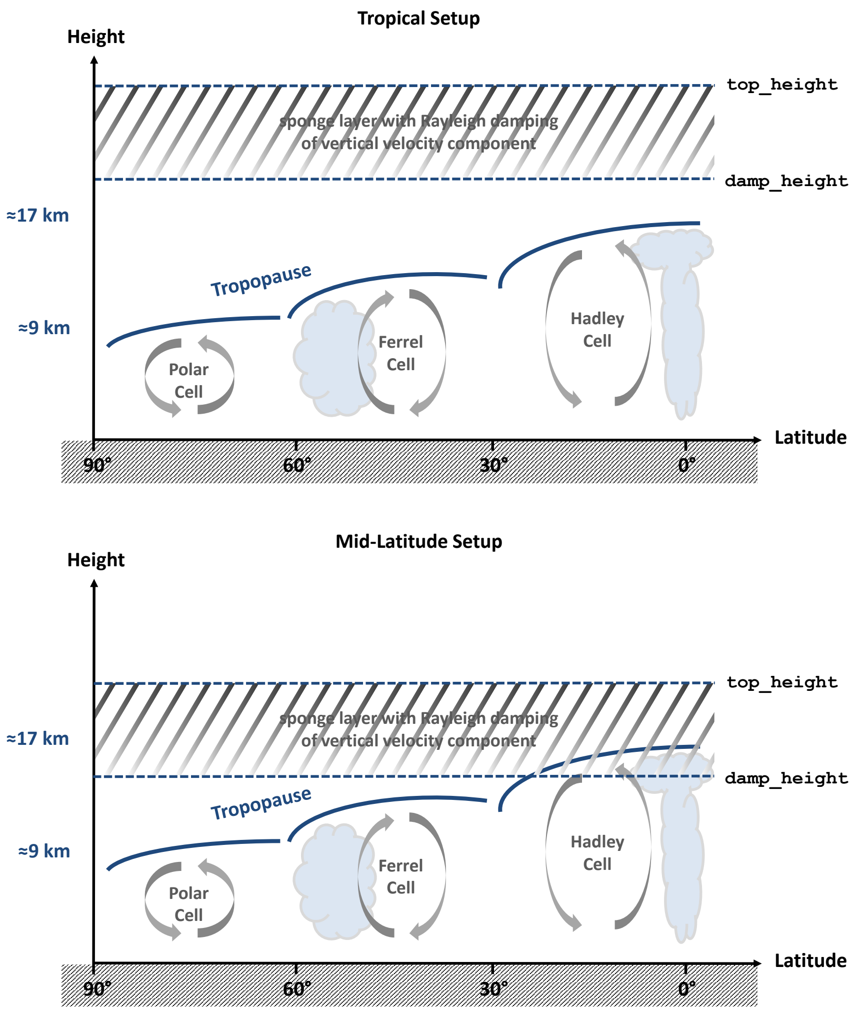

Figure 6.4.: Schematic illustration of the choice of the namelist parameters `damp_height` and `top_height` for tropical and mid-latitude setups.

`tune_zvz0i` is a tuning parameter worth investigating if there are biases in radiation under cloudy conditions.

The namelist parameter `rat_sea` increases the thickness of the laminar sublayer over sea. Larger values mean larger laminar sublayers, i.e. less heat and moisture fluxes over sea. For example, tuning this parameter to lower values might be beneficial if there is too little ocean-atmosphere exchange in case of tropical cyclones. This parameter can only have an impact if a significant part of the model is covered by ocean.

At effective grid spacings of 5 km or less, deep convection is resolved explicitly. The namelist switch `lshallowconv_only` allows to turn off the deep convection parameterization but keeping the shallow convection parameterization active. However, especially for arid regions at effective grid spacings of <3 km it can be beneficial to turn off convection completely by setting `inwp_convection=0`. Otherwise the already sparsely available water vapor is lifted by the shallow convection parameterization from the boundary layer into the free atmosphere. This can lead to a too strong cloud formation inhibition in arid regions.

The probably most important change for tropical setups is depicted schematically in Figure 6.4. The model top height (`top_height`) and the height above which the Raleigh damping of the vertical velocity becomes active (`damp_height`) have to be chosen such that convection is not inhibited by the Rayleigh damping. The tropical tropopause reaches to higher altitudes than the mid-latitude and polar tropopause. While it is sufficient for mid-latitude setups to choose the model top at 22 km and start the damping layer at about 12 km, the tropical tropopause is typically located at an altitude of 17 km. Hence, the relaxation of the vertical velocity would in this case inhibit deep convection. It can be easily avoided by extending the vertical extent of the model simulation to, for example, `top_height=30000.0` and `damp_height=18000.0`. This requires a sufficient number of vertical levels (e.g., `num_lev=65`).

7. Parallelization and Output

In this chapter we describe advanced settings for the namelist controlled model output.

In particular, the ICON model offers several options for internal post-processing, such as the horizontal remapping of the prognostic output onto regularly spaced ("longitude-latitude") grids and vertical interpolation, for example on pressure levels. Another type of output products is ICON's checkpointing feature which allows to restart the execution from a pre-defined point using the data stored in a file.

The chapter is concluded by an overview of the different mechanisms for parallel execution of the ICON model. These settings become important for performance scalability when increasing the model resolution and core counts.

7.1. Settings for the Model Output

Model output is enabled via the namelist `run_nml` with the main switch `output`. By setting this string parameter to the value `"nml"`, the output files and the fields requested for output can be specified by special namelists. In the following, this procedure will be described in more detail.

In general the user has to specify five individual quantities to generate output of the model. These are:

a) The time interval between two model outputs.

b) The name of the output file.

c) The name(s) of the variable(s) to output.

d) The type of the vertical output grid, e. g., pressure levels or model levels.

e) The type of the horizontal output grid, i. e. ICON grid or geographical coordinates.

All of these parameters are set in the namelist `output_nml`. Multiple instances of this namelist may be specified for a single model run, where each `output_nml` creates a separate output file. The options d) and e) require an interpolation step. They will be discussed in more detail in Section 7.1.1.

In the following, we give a short explanation for the most important namelist parameters:

`output_filename` (namelist `output_nml`, string parameter)
This namelist parameter defines a prefix for the output filename (which may include the directory path). The domain number, level type, file number and file format extension will be appended to this prefix.

`output_bounds` (namelist `output_nml`, three floating-point values)
This namelist parameter defines the start time and the end time for the model output and the interval between two consecutive write events. The three values for this parameter are separated by commas and, by default, they are specified in seconds.

`ml_varlist` (namelist `output_nml`, character string list)
This parameter is a comma-separated list of variables or variable groups (the latter are denoted by the prefix "`group:`"). The `ml_varlist` corresponds to model levels, but all 2D variables (for example surface variables) are specified in the `ml_varlist` as well. It is important to note that the variable names follow an ICON-internal nomenclature. The temperature field, for example, is denoted by the character string "temp". A list of available output fields is provided in Appendix B.

Users can also specify the variable names in a different naming scheme, for example "T" instead of "temp". To this end, a translation table (a two-column ASCII file) can be provided via the parameter `output_nml_dict` in the namelist `io_nml`. An example for such a dictionary file can be found in the source code directory: `run/dict.output.dwd`.

`m_levels` (namelist `output_nml`, character string)
This character string specifies a list of model levels for which the variables and groups should be written to output. Level ordering does not matter.
Allowed is a comma- (or semicolon-) separated list of integers, and of integer ranges like "`10...20`". One may also use the keyword "`nlev`" to denote the maximum integer (or, equivalently, "`n`" or "`N`"). Furthermore, arithmetic expressions like "`(nlev-2)`" are possible.
Basic example: `m_levels = "1,3,5...10,20...(nlev-2)"`

`dom` (namelist `output_nml`, integer values, comma-sep.)
Related to setups with nests, i.e. multiple domains: This namelist parameter sets the domains for which this namelist is used. If not specified (or specified as -1), this namelist will be used for all domains.

`remap` (namelist `output_nml`, integer value: `0/1`)
This namelist parameter is related to the horizontal interpolation of the output to regular grids, see Sections 7.1.1 and 7.1.2.

`filetype` (namelist `output_nml`, integer value: `2/4`)
ICON offers the possibility to produce output either in NetCDF or GRIB2 format. This can be chosen by the namelist parameter `filetype` of the namelist `output_nml`. Here, the value `filetype=2` denotes the GRIB2 output, while the value `filetype=4` denotes the NetCDF file format.

The namelist parameter `output_filename` provides only partial control over the resulting filename, namely its prefix. Complete control over the resulting filename can be achieved with the namelist parameter `filename_format` (namelist `output_nml`, character string). By default, `filename_format` is set to:

"*<output_filename>*_DOM*<physdom>*_*<levtype>*_*<jfile>*"

The following keywords are allowed for `filename_format` (the list is incomplete and shows only the most important options):

<path>	model base directory (namelist parameter `model_base_dir`, namelist `master_nml`)
<physdom>	domain number (two digits)
<levtype>	Level type (`ML`, `PL`, `HL`, `IL`)
<datetime>	ISO-8601 date-time stamp in format `YYYY-MM-DDThh:mm:ss.sssZ`
<ddhhmmss>	elapsed days, hours, minutes and seconds since `ini_datetime_string` or `experimentStartDate` (each two digits)
<datetime2>	ISO-8601 date-time stamp in format `YYYYMMDDThhmmssZ`
<jfile>	Consecutive file id.

As it has been stated before, each `output_nml` creates a separate output file. To be more precise, there are a couple of exceptions to this rule. First, multiple time steps can be stored in a single output file, but they may also be split up over a sequence of files (with a corresponding index in the filename), see the namelist parameter `steps_per_file`. Second, an instance of `output_nml` may also create more than one output file if grid nests have been enabled in the model run together with the global model grid, see the namelist parameter `dom`. In this case, each of the specified model domains is written to a separate output file. Finally, model output is often written on different vertical axes, e. g., on model levels and on pressure levels. The specification of this output then differs only in the settings for the vertical interpolation. Therefore it is often convenient to specify the vertical interpolation in the same `output_nml` as the model level output, which again leads to multiple output files.

7.1.1. Output on Regular Grids and Vertical Interpolation

Many diagnostic tools, e. g., to create contour maps and surface plots, require a regularly spaced distribution of the data points. Therefore, the ICON model has a built-in output module for the interpolation of model data from the triangular mesh onto a regular longitude-latitude grid. Further information on the interpolation methods can be found in the database documentation Reinert et al. (2020), see Section 0.3.

The relevant namelist parameters for the *horizontal* interpolation of the output fields are set in the namelist `output_nml`. As it was already mentioned in Section 7.1, multiple instances of this namelist may be specified for a single model run, where each `output_nml` creates a separate output file.

`remap` **(namelist** `output_nml`**, integer value** `0=triangular / 1=lon-lat`**)**
Set this namelist parameter to the value `1` to enable horizontal interpolation onto a regular grid. This option needs to be defined combination with `reg_lat_def` / `reg_lon_def`.

`reg_lat_def` / `reg_lon_def` **(namelist** `output_nml`**)**
Latitudes and longitudes for the regular grid points are each specified by three values:

start, increment, end value; given in degrees. Alternatively, the user may set the number of grid points instead of an increment.

Users of the COSMO model are familiar with *rotated lat-lon grids*: Here, the computational spherical coordinate system is rotated in such a way that a pole problem is avoided and minimal convergence of the meridians is achieved. To some extent, this output can be reproduced by the ICON model:

`north_pole` **(namelist `output_nml`)**
: Definition of the north pole for rotated lat-lon grids (`[longitude, latitude]`). The default is `north_pole = 0,90`.

Note, however, that the "COSMO output" is in detail not quite what the COSMO user expects, especially with regard to wind speeds `U`, `V`: First, the basis vectors, i.e. the meridional and longitudinal directions, are not rotated. Second, in COSMO these speeds are defined on horizontally and vertically shifted grids ("staggered grids"). This is not the case with ICON and especially difficult to detect in data sets.

Furthermore, the model output can be written on a different *vertical* axis, e. g., on pressure levels, height levels or isentropes. In the following we will describe how to specify these options in the namelist `output_nml`. The relevant namelist parameters for the vertical interpolation of the output fields are:

`hl_varlist` / `pl_varlist` / `il_varlist` **(character string lists)**
: Similar to the namelist parameter `ml_varlist` mentioned above, these parameters are comma-separated lists of variables or variable groups. While the `hl_varlist` sets the output for height levels, `pl_varlist` defines variables on pressure levels and `il_varlist` specifies output on isentropic levels.

`h_levels` / `p_levels` / `i_levels` **(floating point values, comma-sep.)**
: Comma separated list of height, pressure, and isentropic levels for which the variables and groups specified in the above mentioned variable lists should be output. Height levels must be given in m, pressure levels in Pa and isentropes in K. Level ordering does not matter.

ICON's interpolation on pressure levels is extrapolating into the topography. This has the simple reason that contour plots, e.g. for 850hPa, usually do not show missing values over regions like Antarctica. There is no option to change this behavior in ICON. If needed, this has to be accounted for in the post-processing.

7.1.2. Remarks on the Horizontal Interpolation

First of all, it should be noted that all explanations in this section also apply to the `iconremap` tool, which interpolates ICON data as a pre-processing step.

ICON supports several numerical methods for interpolating data horizontally from the native triangular grid onto a regular lat-lon grid (or, in the `iconremap` case, to the interpolation between different triangular grids):

- Radial basis functions (RBF)
- Barycentric interpolation
- Nearest-neighbor interpolation

The concrete interpolation procedure depends on the variable and its physical characteristics. It is prescribed for the output module as indicated in the output product tables of ICON's database description, see Reinert et al. (2020). For the `iconremap` tool the interpolation method is set explicitly by the user for each field.

First, a small number of output fields is treated with a *nearest-neighbor interpolation*. The nearest neighbor algorithm selects the value of the nearest point and does not consider the values of neighboring points at all, yielding a piecewise-constant interpolant.

Barycentric interpolation is a two-dimensional generalization of linear interpolation. This method uses just three near-neighbors to interpolate and avoids over- and undershoots, since extremal values are taken only in the data points. This interpolation makes sense for fields where the values change in a roughly piecewise linear way.

Barycentric interpolation needs to be enabled with the following namelist setting (otherwise it is replaced by a fallback interpolation):

`support_baryctr_intp = .FALSE.` (namelist `interpol_nml`, logical value)

The `icondelaunay` tool: The DWD ICON Tools contain the `icondelaunay` binary, which processes existing ICON grid files. It appends a Delaunay triangulation of the cell circumcenters to the grid file. This auxiliary triangulation can be used then to speed up the interpolation process.

Note that this way of pre-processing the ICON grid files is mandatory for DWD's NEC SX-Aurora platform where the spherical Delaunay algorithm has not been vectorized.

Most of the output data on regular grids is processed using an *RBF-based interpolation method*. The algorithm approximates the input field with a linear combination of radial basis functions (RBF) located at the data sites, see, for example, Ruppert (2007). RBF interpolation typically produces over- and undershoots at position where the input field exhibits steep gradients. This behavior is illustrated in Fig. 7.1. Therefore, the internal interpolation algorithm performs a cut-off by default. Note that RBF-based interpolation is *not conservative*.

The *shape parameter* (or *scale parameter*) is an important parameter which affects the quality of the RBF interpolation. The core of the interpolation method are the *radial basis functions* which are for the ICON tools chosen to be of Gaussian type, i. e.

$$f(x) := \mathrm{e}^{-\left(\frac{x}{a}\right)^2} , \quad a > 0 ,$$

with shape parameter a.

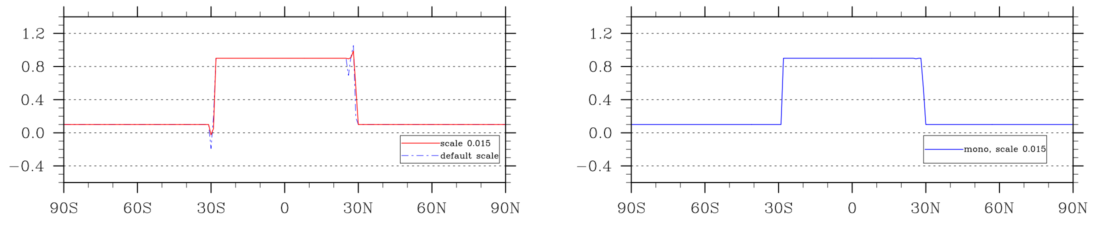

Figure 7.1.: *Left:* Examples for over- and undershoots for an RBF-based interpolation. *Right:* RBF interpolant with cut-off applied.

When we choose a smaller value for a then the RBF basis functions approach the Dirac delta function, which yields an almost-nearest-neighbor interpolation. Larger values for a generally reduce the interpolation error, but there exists a (grid specific) bound where the Cholesky decomposition of certain dense matrices fails, that are necessary for the RBF weight computation (see the info box below). The ICON tools provide a heuristic which estimates a proper RBF shape parameter for which the Cholesky decomposition succeeds in floating-point arithmetic. This estimation method is applied when the user does not provide a specific value via the namelist.

For the latter case, see ICON's namelist documentation for the namelist parameter `rbf_scale` (`output_nml`).

Cholesky Decomposition Fails: The Cholesky decomposition of the RBF interpolation weight computation may fail with an error message of the following kind:

```
# mo_math_utilities:choldec: error in matrix inversion, nearly singular matrix
mo_remap_rbf_errana::rbf_error: Cholesky decomposition failed!
```

This may happen for example when a bad value for the shape parameter has been chosen manually. However, the *automatic* shape parameter estimation may fail as well: This algorithm estimates largest-as-possible shape parameter by extrapolation from a number of sample (test) decompositions. When it fails to compute these samples, even the automatic estimator may abort with the above error message,

In these cases, please adjust the shape parameter manually (which may require several trial-and-error steps).

7.1.3. Output Rank Assignment

When a large number of different output files is written during the simulation, the task of formatting and writing may put an excessive load on the output processes. The number of output processes which share this output load can be increased by setting the `num_io_procs` (`parallel_nml`) namelist parameter, see Section 7.4.1. If there exist multiple groups (e.g. output files, different variable sets, output intervals, interpolation grids) then these so-called *streams* will be distributed automatically over the available output processes.

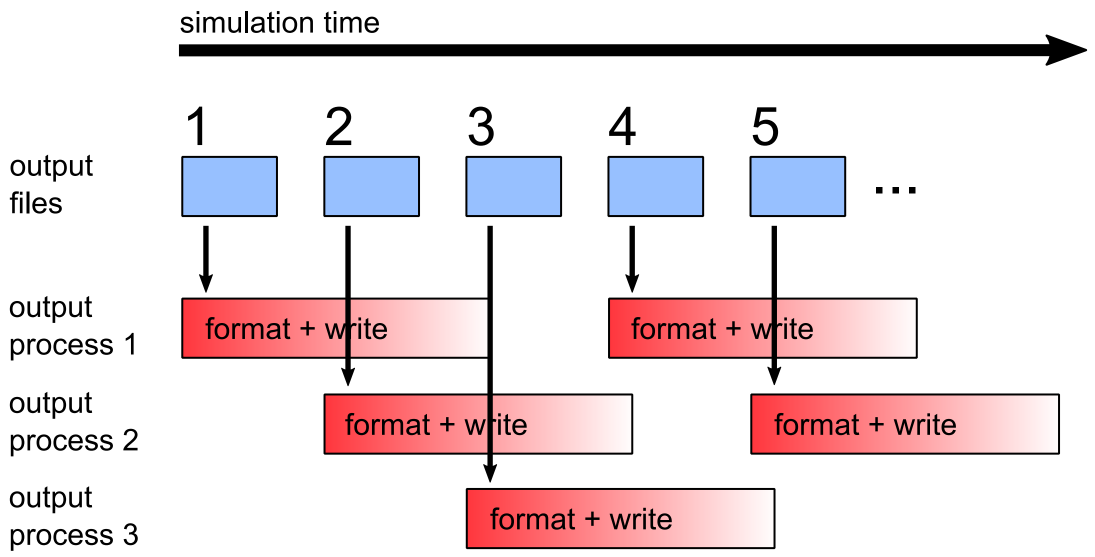

Figure 7.2.: Schematic illustrating the distribution of output load onto three output processes, using `num_io_procs=3` and `stream_partitions_ml=3`.

`stream_partitions_ml` **(namelist** `output_nml`**, integer)**
It may be even useful to spread the files of a *single* stream over multiple output processes. For example, when each output file is relatively large, then the subsequent file of this stream can be written by a different output process in order to diminish the risk of congestion. Please use the namelist parameter `stream_partitions_ml` to set the number of output processes among which the output files should be divided.

The distribution of output load using `stream_partitions_ml` is illustrated in Fig. 7.2.

`pe_placement_ml` **(namelist** `output_nml`**, integer array)**
This array is related to the namelist parameters `num_io_procs` and `stream_partitions_ml` and allows for an even more fine-tuned distribution of the output workload. At most `stream_partitions_ml` different ranks can be specified, ranging between `0` ... (`num_io_procs` - 1). This explicitly assigns the output streams to specific PEs and facilitates a load balancing with respect to small and large output files.

7.2. Checkpointing and Restart

There are many reasons why a simulation execution may be interrupted prematurely or unexpectedly. The checkpoint/restart option can save you from having to start the ICON model over from the beginning if it does not finish as expected. It allows you to restart the execution from a pre-defined point using the data stored in a checkpoint file.

Activating the restart. The checkpoint/restart functionality is controlled by the following namelist parameters, which are also illustrated in Fig. 7.3.

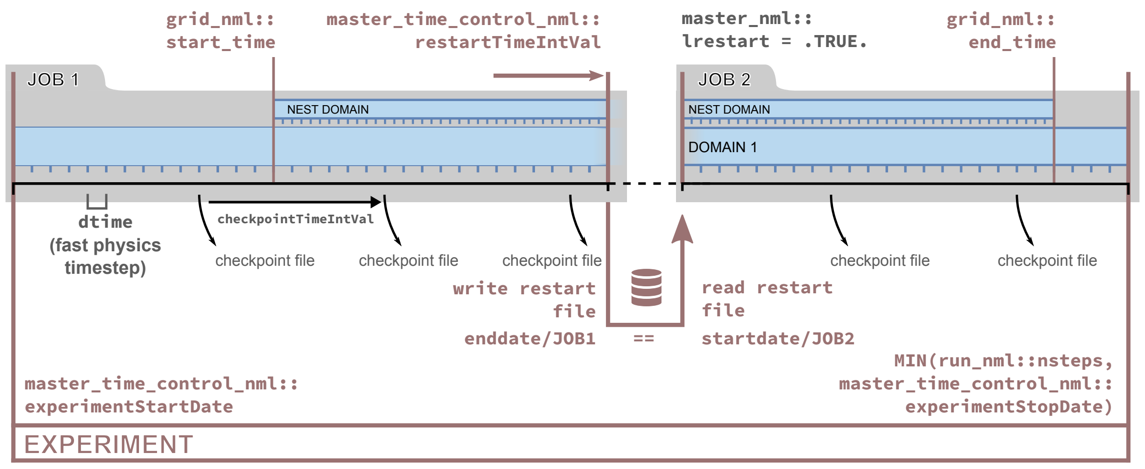

Figure 7.3.: Specifying experiment restart; compare this illustration to Fig. 5.1. The namelist parameters are explained in Section 7.2. Here we prefer the ISO8601 date-time specification (e. g. `checkpointTimeIntVal`) over the over the older settings (e. g. `dt_checkpoint`).

`dt_checkpoint` **(namelist** `io_nml`**, floating-point value)**

This parameter specifies the time interval for *writing* restart files. The restart files are written in NetCDF format, and their names are specified by the namelist parameter `restart_filename`, see below.

Note that if the value of `dt_checkpoint` resulting from the model default or user's specification is larger than `dt_restart` (see below), then it will be automatically reset to `dt_restart`, s. t. at least one restart file is generated during the restart cycle.

Similar to the namelist parameters described in 5.1.1, which specify the model start and end dates, there exist character string replacements for `dt_checkpoint` and `dt_restart`:

- `restartTimeIntVal` (namelist `master_time_control_nml`, ISO8601, character string)
- `checkpointTimeIntVal` (namelist `master_time_control_nml`, ISO8601, character string)

`lrestart` **(namelist** `master_nml`**, logical value)**

If this namelist parameter is set to `.TRUE.` then the current experiment is resumed from a restart file.

Instead of searching for a specific data filename, the model reads its restart data always from a file with name `restart_atm_DOM01.nc` (analogously for nested domains). It is implicitly assumed that this file contains the newest restart data, because during the writing of the checkpoints this file is automatically created as a symbolic link to the latest checkpoint file.

`restart_filename` **(namelist** `run_nml`**, string parameter)**

This namelist parameter defines the name(s) of the checkpointing file(s). By default, the checkpoint files (not the symbolic link) have the form `*gridfile*_restart_atm_*restarttime*.nc`

`dt_restart` (namelist `time_nml`, floating-point value)

This parameter is in some ways related to the `dt_checkpoint` parameter: It specifies the length of a restart cycle in seconds, i. e. it specifies how long the model runs until it saves its state to a file *and stops*. Later, the model run can be resumed, s. t. a simulation over a long period of time can be split into a chain of restarted model runs.

Similar to the asynchronous output module, the ICON model (see Section 7.4) also offers the option to reserve a dedicated MPI task for writing checkpoint files. This feature can be enabled by setting the parameter `num_restart_procs` in the namelist `parallel_nml` to an integer value larger than 0.

Restart modes. Different restart write modes are available, which allow for a distributed writing and read-in of restart files, depending on the parallel setup. These different restart modes are controlled via the namelist parameter `restart_write_mode` (`io_nml`).

Allowed settings for `restart_write_mode` (character strings!) are:

`"joint procs multifile"`

All worker processes write restart files to a dedicated directory. Therefore, the directory itself represents the restart data set. The information is stored in a way that it can be read back into the model independent from the processor count and the domain decomposition.

Read-in: All worker processes read the data in parallel.

`"dedicated procs multifile"`

In this case, all the restart data is first transferred to memory buffers in dedicated restart writer processes. After that, the work processes carry on with their work immediately, while the restart writers perform the actual restart writing asynchronously. Restart processes can parallelize over patches and horizontal indices.

Read-in: All worker processes are available to read the data in parallel (though this is usually limited by the number of restart files).

`"sync"`

'Old' synchronous mode. Process # 0 reads and writes restart files. All other processes have to wait.

`"async"`

'Old' mode for asynchronous restart writing: Dedicated processes (`num_restart_proc > 0`) write restart files while the simulation continues. Restart processes can only parallelize over different patches.

Read-in: Processes # 0 reads while other processes have to wait.

`" "`

Fallback mode.
If `num_restart_proc` (`parallel_nml`) is set to `0`, then this behaves like `"sync"`, otherwise like `"async"`.

7.3. Meteogram Output

The ICON model also features a special output product called *meteograms*, containing the model variables with respect to time for a particular location, i. e. at single grid points.

ICON's built-in meteograms are intended for *non-operational use*. They should be seen as a by-product of the usual data output, rather for the purpose of error detection during development. Meteogram data files are written in the NetCDF data format, where an example of the (non-standard) file structure is given below. The output is enabled via the namelist setting `output = 'nml'` (namelist `io_nml`) in combination with a special namelist, `meteogram_output_nml`:

```
&meteogram_output_nml
    lmeteogram_enabled = .TRUE.
    n0_mtgrm           = initial time step for meteogram output
    ninc_mtgrm         = output interval (in time steps)
    stationlist_tot    = 50.050, 8.600, 'Frankfurt-Flughafen',
                         40.74153, -73.98537, 'New York City',
    ...
```

In addition to the namelist parameters in the example above, the following settings are worth mentioning:

`max_time_stamps` (namelist `meteogram_output_nml`, integer value)
: number of output time steps to record in memory before flushing to disk

`zprefix` (namelist `meteogram_output_nml`, character string)
: string with file name prefix for output file

`var_list` (namelist `meteogram_output_nml`, list of character strings)
: Optional positive-list of variables. Only variables contained in this list are included in the meteogram. If the default list is not changed by this user setting, then all available variables are added to the meteogram.

During the model simulation, one of the asynchronously running output processes (see Section 7.4) collects the meteogram buffers from the compute processes and writes the data to a file. Meteograms do not use ICON's variable list infrastructure (see Section 8.3). However, the output can be easily extended to sample of additional model variables. To this end, see the extensive comments in the source code, `src/io/atmo/mo_mtgrm_output.f90`.

For basic textual output, there exists an auxiliary NCL script

```
scripts/postprocessing/tools/mtgrm_cosmo.ncl
```

For an introduction to the NCAR Command Language NCL see Section 9.3.2. This script can be applied to a data file with the following command:

```
ncl -n mtgrm_cosmo.ncl DataFileName='"METEOGRAM.nc"' itime=0;
```

The same directory also contains scripts for plotting meteogram data with NCL.

File format description. As mentioned before, the NetCDF meteogram output has a non-standard file structure. We list the most important file entries in the following:

meteogram station info:

`station_name`, `station_lon`, `station_lat`, `station_hsurf`,
and `station_idx`, `station_blk`: global triangle adjacent to meteogram station

sample date info:

`date` (sample dates) and `time_step` (plain time step indices).

info and value buffer for surface (2D) variables, `1,...,nsfcvars`:

`sfcvar_name`, `sfcvar_long_name`, `sfcvar_unit`,
`sfcvalues(time, nsfcvars, nstations)`: value buffer

info and value buffer for 3D variables `1,...,nvars`:

`var_name`, `var_long_name`, `var_unit`,
`heights(max_nlevs, nvars, nstations)`: level heights,
`var_levels`: plain level indices,
`values`: value buffer

7.4. Parallelization and Performance Aspects

As mentioned in Section 1.2.1, ICON can use two different mechanisms for parallel execution:

a) *OpenMP* – Multiple threads are run in a single process and share the memory of a single machine.
An implementation of OpenMP ships with your Fortran compiler. OpenMP-parallel execution therefore does not require the installation of additional libraries.

b) *MPI* – Multiple ICON processes (*processing elements*, PEs) are started simultaneously and communicate by passing messages over the network. Each process is assigned a part of the grid to process.

These mechanisms are not mutually exclusive. A *hybrid* approach is also possible: Multiple ICON processes are started, each of which starts multiple threads. The processes communicate using MPI. The threads communicate using OpenMP.

7.4.1. Settings for Parallel Execution

Several settings must be adjusted to control the parallel execution:

Namelist `parallel_nml`

First, we focus on some namelist settings for the distributed-memory MPI run. Processors are divided into

Worker PEs	this is the majority of MPI tasks, doing the actual work
I/O PEs	dedicated output server tasks[1]
Restart PEs	for asynchronous restart writing (see Section 7.2)
Prefetch PE	for asynchronous read-in of boundary data in limited area mode (see Section 6.4.2)
Test PE	MPI task for verification of MPI parallelization (debug option)

The configuration settings are defined in the namelist `parallel_nml`. To specify the number of output processes, set the namelist parameter `num_io_procs` to a value larger than 0, which reserves a number of processors for output. While writing, the remaining processors continuously carry out calculations. Conversely, setting this option to 0 forces the worker PEs to wait until output is finished. For the writing of the restart checkpoints (see Section 7.2), there exists a corresponding namelist parameter `num_restart_procs`.

During start-up, the model prints out a summary of the processor partitioning. This is often helpful to identify performance bottlenecks. First of all, the model log output contains a one-line status message:

```
Number of procs for
           test: xxx, work: xxx, I/O: xxx, Restart: xxx, Prefetching: xxx
```

Afterwards, the sizes of grid partitions for each MPI process are summarized as follows:

```
 Number of compute PEs used for this grid: 118
 #         prognostic cells: max/min/avg    xxx   xxx   xxx
```

Given the case that the partitioning process would fail, these (and the subsequently printed) values would be grossly out of balance.

Batch queuing system

Apart from the namelist settings, the user has to specify the computational resources that are requested from the compute cluster. In addition to the number of MPI tasks and OpenMP threads, here the user has to set the number of cluster-connected *nodes*.

Increasing the number of nodes allows to use more computational resources, since a single compute node comprises only a limited number of PEs and OpenMP threads. On the other hand, off-node communication is usually more expensive in terms of runtime performance.

The computer platform at DWD, the NEC SX-Aurora, uses the batch system `PBS` to control the requested resources. When using the `qsub` command to submit a script file, the batch system `PBS` allows for specification of options at the beginning of the file prefaced by the `#PBS` delimiter followed by `PBS` commands.

Finally the user has to set the correct options for the application launcher, which is the `mpirun` command on the NEC SX-Aurora platform. The Appendix A contains a description of the most important settings.

Best Practice for Parallel Setups

ICON employs both distributed memory parallelization and shared memory parallelization, i.e. a “hybrid parallelization”. Only the former type actually performs a decomposition of the domain data, using the de-facto standard MPI. The shared memory parallelization, on the other hand, uses OpenMP directives in the source code. In fact, nearly all `DO` loops that

[1]The notation “I/O” is justified by historical arguments. In the current version of ICON, these MPI processes exclusively operate as *output* servers.

iterate over grid cells are preceded by OpenMP directives. For reasons of cache efficiency the `DO` loops over grid cells, edges, and vertices are organized in two nested loops: "`jb` loops" and "`jc` loops"[1] Here the outer loop ("`jb`") is parallelized with OpenMP.

There is no straight-forward way to determine the optimal hybrid setup, except for the extreme cases: If only a single node is used, then the global memory facilitates a pure OpenMP parallelization. Usually, this setup is only feasible for very small simulations. If, on the other hand, each node constitutes a single-core system, a multi-threaded (OpenMP) run would not make much sense, since multiple threads would interfere on this single core. A pure MPI setup would be the best choice then.

In all of the other cases, the parallelization setup depends on the hardware platform and on the simulation size. In practice, 4 threads/MPI task have proven to be a good choice on x86-based systems. This should be combined with the *hyper-threading* feature, i.e. a feature of the x86 architecture where one physical core behaves like two virtual cores.

Starting from this number of threads per task the total number of MPI tasks is then chosen such that each node is used to an equal extent and the desired time-to-solution is attained – in operational runs at DWD this is $\sim 1\,\mathrm{h}$. In general one should take care of the fact that the number of OpenMP threads evenly divides the number of cores per CPU socket, otherwise inter-socket communication might impede the performance.

Finally, there is one special case: If an ICON run turns out to consume an extraordinarily large amount of memory (which should not be the case for a model with a decent memory scaling), then the user can resort to "investing" more OpenMP threads than it is necessary for the runtime performance. Doing so, each MPI process would have more memory at its disposal.

7.4.2. Mixed Single/ Double Precision in ICON

To speed up code parts strongly limited by memory bandwidth, an option exists to use single precision for variables that are presumed to be insensitive to computational accuracy – primarily the dynamical core and the tracer advection.

This affects most local arrays in the dynamical core routines, some local arrays in the tracer transport routines, the metrics coefficients, arrays used for storing tendencies or differenced fields (gradients, divergence etc.), reference atmosphere fields, and interpolation coefficients. Prognostic variables and intermediate variables affecting the accuracy of mass conservation are still treated in double precision.

To activate the mixed-precision option, the pre-processor flags `-D__MIXED_PRECISION` and `-D__MIXED_PRECISION_2` need to be specified in the configuration settings used for generating the Makefile. The latter flag is used for physics tendencies.

There exists a configure option which enables the above pre-processor flags:

```
./configure --enable-mixed
```

Note that interpolation to a latitude-longitude grid is not supported for single-precision variables; if you desire to output physics tendency fields on a regular grid for diagnostic purposes, do not set `-D__MIXED_PRECISION_2`.

[1]This implementation method is known as *loop tiling*, see also Section 8.3.

7.4.3. Bit-Reproducibility

Bit-reproducibility refers to the feature that running the same binary multiple times should ideally result in bit-wise identical results. Depending on the compiler and the compiler flags used this is not always true if the number of MPI tasks and/or OpenMP threads is changed in between. Usually compilers provide options for creating a binary that offers bit-reproducibility, however this is often payed dearly by strong performance losses. With the NEC SX-Aurora compiler, it is however possible to generate an ICON binary offering bit-reproducibility with only little performance loss. The ICON binary used in this workshop gives bit-reproducible results (will be checked in Exercise C.5.7).

Bit-reproducibility is generally an indispensable feature for debugging. It is helpful

- for checking the MPI/OpenMP parallelization of the code. If the ICON code does not give bit-identical results when running the same configuration multiple times, this is a strong hint for an OpenMP race condition. If the results change only when changing the processor configuration, this is a hint for an MPI parallelization bug.
- for checking the correctness of new code that is supposed not to change the results.

7.4.4. Basic Performance Measurement

The ICON code contains internal routines for performance logging for different parts (setup, physics, dynamics, I/O) of the code. These may help to identify performance bottlenecks. ICON performance logging provides timers via the two namelist parameters `ltimer` and `timers_level` (namelist `run_nml`).

Note for advanced users: The built-in timer output is rather non-intrusive. It is therefore advisable to have it enabled also in operational runs.

With the following settings in the namelist `run_nml`,

```
ltimer                = .TRUE.
timers_level          =    10
```

the user gets a sufficiently detailed output of wall clock measurements for different parts of the code:

```
---------------------------  -------           -------------  -------------
name                         # calls           total min (s)  total max (s)
---------------------------  -------           -------------  -------------
total                        237       ...          903.085        903.089
 L integrate_nh              170640    ...          884.128        892.143
    L nh_solve               5972400   ...          401.055        428.694
       L nh_solve.veltend    7166880   ...           36.469         51.376
 ...
physics                      49678     ...          103.107        104.759
```

```
L nwp_radiation              10030      ...          40.402          42.985
   L radiation               220674     ...          31.845          34.963
...
model_init                   711        ...          59.875          59.876
...
```

Note that some of the internal performance timers are nested, e.g. the timer log for `radiation` is contained in `physics`, indicated by the “`L`” symbol. For correct interpretation of the timing output and computation of partial sums one has to take this hierarchy into account.

- The column ”`total max (s)`” contains the maximum timing in seconds (maximum over all MPI tasks, OpenMP master thread).
- The row ”`model_init`” contains the measurements for the model setup (allocation, read-in, etc.).
- The row ”`total`” contains the model run-time, *excluding* the initialization and finalization phase.

8. Programming ICON

Just because something doesn't do what you planned it to do doesn't mean it's useless.

Thomas Edison

The previous chapters' topics have been guided by questions of how to run ICON simulations in various settings and how to control and understand the model's characteristics. In this short chapter, instead, we will introduce ICON's inner workings, i.e. the code layout and the most important data structures.

The description is detailed enough to make it relatively easy for the reader to modify the code. We exemplify this in Section 8.3 by implementing an own simple diagnostic.

8.1. Representation of 2D and 3D Fields

We begin with a suitable representation of two- and three-dimensional fields. Here, we refer to a discrete variable as a *2D field* if it depends on the geographical position only. A *3D field*, in addition, contains a vertical dimension, associated with the grid column.

Indexing. Recalling the unstructured nature of ICON's computational grids (see Section 2.1) there is no obvious order of the cells in a 2D array like indexing them according to longitudes and latitudes. Instead, we just order the cells in a deliberate way and index them in this order with ascending integer numbers. This means that our 2D field becomes a 1D array, referenced by the cell indices as subscript values.

Most arrays are associated with the centers of the triangular grid cells, but we do that in a similar way for the edges and vertices of the triangles. An extension to 3D fields, i. e. including a vertical dimension, results in 2D arrays, the first index being the cell (or edge or vertex) index, the second index being the height level.

Blocking. For reasons of cache efficiency nearly all `DO` loops over grid cells, edges, and vertices are organized in two nested loops: "`jb` loops" and "`jc` loops". Often, the outer loop ("`jb`") is parallelized with OpenMP.

With respect to the data layout, this means that the long vector is split into several chunks of a much smaller length `nproma` (this is a run-time parameter, defined in the namelist `parallel_nml`). We store the long vector in a 2D array, the first index counting the elements

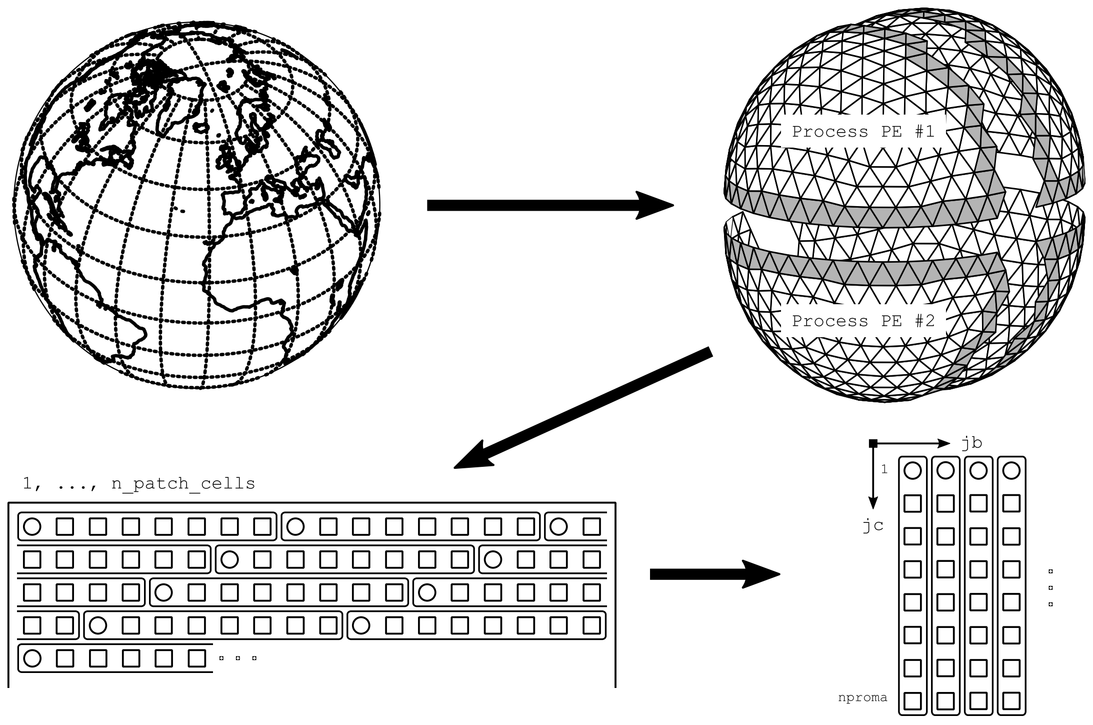

Figure 8.1.: Illustration of the 2D field representation. The original spherical domain is decomposed (light-gray: halo region). Afterwards, the long vector of grid cells is split into several chunks of a much smaller length `nproma`.

in a block (*line index*), the second index counting the blocks. The last block may be shorter since `nproma` is not necessarily a divisor of the number of cells. The blocking procedure is illustrated in the lower half of Figure 8.1. There exist auxiliary functions `idx_no`, `blk_no` and `idx_1d`, which help to calculate the blocked indices from the 1D array index and vice versa (declared in the module `mo_parallel_config`).

Finally, let us consider the 3D fields that were stored in 2D arrays, with the cell index as the first dimension and the second being the vertical coordinate. With index blocking, these fields will be stored in 3D arrays with the first index counting the elements in a block, the second index counting the levels and the third index counting the blocks. The reason is that the blocks are often passed one by one to some subprograms which are called in a loop over the blocks. Since Fortran stores arrays in column-major order, the data for a single `jb` is stored contiguously in memory. Thus we can pass this chunk of data to the subprograms without any reshaping of the arrays.

Domain decomposition. Domain decomposition is, naturally, a prerequisite for scalability on modern parallel computers. For large scale realistic ICON setups and with operational core counts in the range of tens of thousands, the use of persistent global-sized arrays is unacceptable. Each model domain is therefore distributed onto several processors[1]. This means that we have only certain regions of a domain on each processor.

[1]In the following, we will use the generic term "Processing Element" (PE).

Each processor's region consists of an inner portion and a lateral boundary portion. The latter may be either a lateral boundary for the entire domain or a *halo region*, i. e. a lateral boundary of the partial domain which is overlaid with neighboring partial domains. The halo region (which is also known as a *ghost-cell region*) is illustrated in the upper half of Figure 8.1.

The programmer is responsible for the distribution of the data among the processors and the correct communication through MPI calls. This means that all halo regions have to be updated by the neighboring partial domains. We will sketch this synchronization process in Section 8.2.4 below.

> Keep in mind that it is the width of the halo region which defines a size limit for your stencil calculations: It is not possible to include cells in a stencil which extend beyond the halo region!

Index ordering. After the domain decomposition, which takes place in the model initialization phase, each PE performs a sorting of its locally allocated cells (and edges and vertices). This *local* index ordering is determined by the `refin_`*`xxx`*`_ctrl` index which counts the distance from the lateral boundary in units of cell/edge/vertex rows. In particular, note the `refin_c_ctrl` array which already played a role for the preparation of lateral boundary input data, see Section 2.3. Portions of the triangular cells correspond to different values of `refin_c_ctrl`, which allows a sorting into the following categories: the cell rows at the lateral boundary, the nudging zone, the inner cells, and the halo region. Of course, for a global domain only the two latter categories exist.

The upper part of Figure 8.2 schematically shows the different parts of a computational domain, subdivided between two PEs: Each PE "owns" a subset of interior cells and part of the lateral boundary. The halo region is shared between the PEs.

The lower part of Figure 8.2 visualizes the ordering of the grid portions in the index vector. It can be seen that the leftmost indices (i. e. the smallest subscripts) correspond to the lateral boundary region, followed by the prognostic cells. The sorting of these prognostic cells with respect to their cell row stops after the first cell row (denoted by "sorted" vs. "unsorted" in Fig. 8.2).

Thus the indices are ordered in such a way that typical iterations over grid portions like prognostic cells, lateral boundary points etc. can be realized without conditional statements. Each portion is annotated by its start index, where the subscript corresponds to the `refin_c_ctrl` value. For convenience, there exists the auxiliary function `get_indices_c` (declared in the module `mo_loopindices`) which helps to adjust the loop iteration accordingly: For a given value of `refin_c_ctrl` and a specific block index we get the start and end indices to loop over.

Only the halo cells deserve some further remark (note the comment *"when not overlapping with lateral boundary"* in Fig. 8.2): In the special case, when no lateral boundary is present (for a global grid, say, or when a PE operates only on an inner portion of the domain), the halo cells are stored in a contiguous fashion at the end of the index vector. When a lateral boundary is present, however, there exist some halo cells which also belong to the

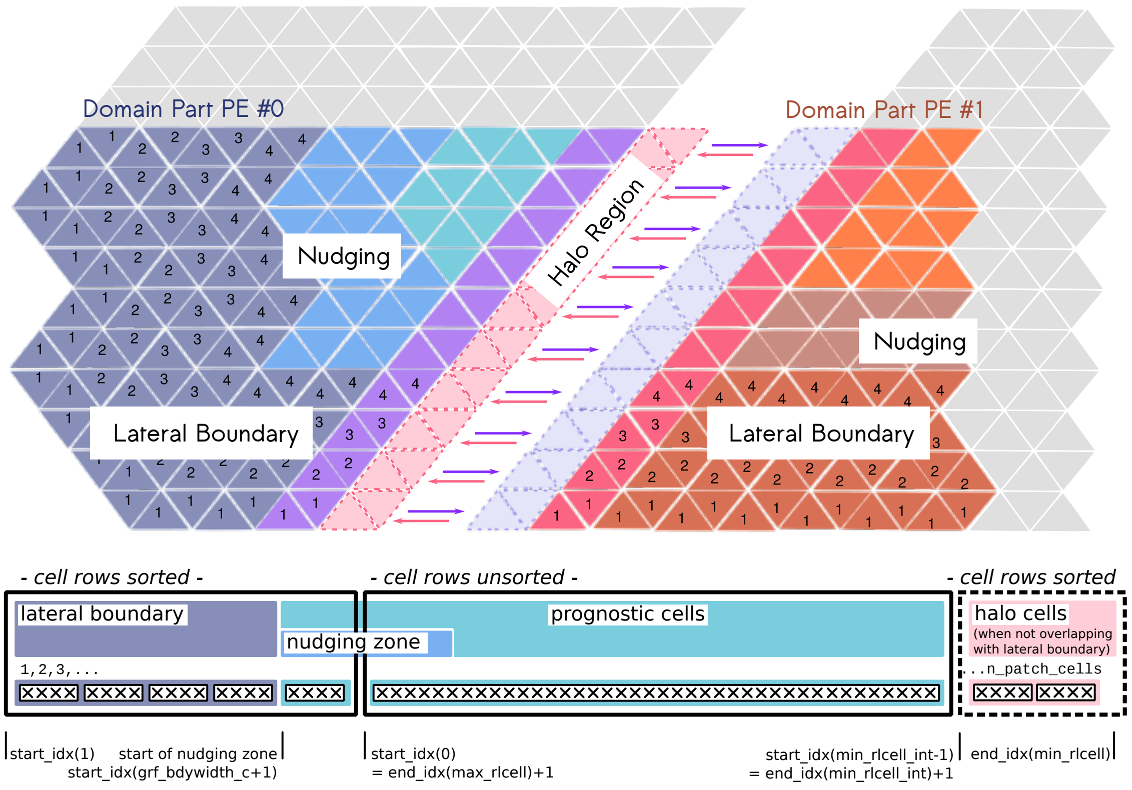

Figure 8.2.: Schematic illustration of ICON's index ordering (grid cells).
The upper part schematically shows the different portions of a computational domain, subdivided between two PEs. The lower part of the illustration depicts the index vector for PE #0, see the explanation in the text.
Both PEs "own" a subset of interior cells and part of the lateral boundary. The halo region that surrounds each partition is used to exchange data between the PEs (dashed): The halo-exchange operation copies the contents of the cells on the partition border (violet, pink) to the halo cells of the adjacent process (light violet, light pink).
(Note: The sizes of the regions shown differ from the real situation.)

lateral boundary. These cells are then sorted into the leading part of the index array, since the ability to address boundary cells in a contiguous fashion is much more important in practice. A possibility to distinguish between prognostic cells and halo points is provided by the `decomp_domain` data structure and the "owner info" field, see the following section.

8.2. Data Structures

8.2.1. Description of the Model Domain: `t_patch`

The `t_patch` data structure contains all information about the grid coordinates and topology, as well as parallel communication patterns and decomposition information. It is declared in `src/shr_horizontal/mo_model_domain.f90` as an array of length (# domains), where the coarsest base grid is denoted by the index 1, while the refined domains are denoted by numbers 2, 3 and so on.

All contained data arrays and indices relate to the index/block ordering described in Section 8.1 and non-existent indices are denoted by `-1`. The most important contents of the `t_patch` data structure are

`t_patch`

`grid_filename`	character string, containing grid file name
`ldom_active`	indicator if current model domain is active, see Section 5.2
`parent_id`	domain ID of parent domain
`child_id(1:n_childdom)`	list of child domain ID's
`n_patch_cells/edges/verts`	number of locally allocated cells, edges ...
`n_patch_XXXX_g`	global number of cells, edges and vertices
`nblks_c/e/v`	number of blocks
`npromz_c/e/v`	chunk length in last block
`cells / edges / verts`	grid information, see below
`comm_pat_c/e/v`	halo communication patterns, see Section 8.2.4
	⋮

The data members `cells`, `edges`, and `verts`, which are of the types `t_grid_cells`, `t_grid_edges`, and `t_grid_vertices`, respectively, give us information about the grid cells themselves, in particular about their geographical coordinates. For example,

`t_grid_cells`

`center(:,:)`	longitude and latitude of cell circumcenters, dimensions: `[1:nproma, 1:nblks_c]`
`neighbor_idx(:,:,:)`	line indices of triangles next to each cell, dimensions: `[1:nproma, 1:nblks_c, 1:3]`
`decomp_info`	information on domain decomposition
	⋮

Essentially, all data arrays which are contained in the grid files and which are described in Section 2.1.1 have a counterpart in this derived data type.

Besides, the data member `decomp_info` which separately exists for cells, edges and vertices, deserves additional comments. Its data type `t_grid_domain_decomp_info` is declared in `/src/parallel_infrastructure/mo_decomposition_tools.f90`:

`t_grid_domain_decomp_info`

`glb_index(:)`	global index of local cell, dimension: `1:n_patch_cells`
`decomp_domain(:,:)`	domain decomposition flag, `0`: owned (for cells), dimensions: `[1:nproma, 1:nblks_c]`
	⋮

The global index (`glb_index`) is particularly useful to perform operations (or write out data) which must not depend on the parallel domain decomposition of the model run. The "owner info" (`decomp_domain`) can be used to distinguish between prognostic cells and halo points whose values are just copied from adjacent PEs.

8.2.2. Date and Time Variables

When installing own processes within ICON's time loop, the question for the current (simulation) time naturally arises. All global date and time variables are contained in the data structure `time_config`, which is of the derived data type `t_time_config` and declared in `src/configure_model/mo_time_config.f90`. The dates are initialized with the corresponding namelist parameters given in Section 5.1.1.

`t_time_config`

`tc_exp_startdate`	experiment start (`tc` means "time control")
`tc_exp_stopdate`	experiment stop
`tc_startdate`	start of current simulation. In case of restart this is the date at which the simulation has been continued.
`tc_stopdate`	end of single run
`tc_current_date`	current model date
	⋮

The dates and time spans make use of the `mtime` calendar library[2] which is precise up to milliseconds without round-off errors. The `mtime` library resides in the directory `externals/mtime`. It is written in C and has a Fortran interface (module `mtime`).

We motivate the use of the `mtime` module by two examples. First, we perform a date calculation, adding a time span of 1 day to a given date. We make use of two variables: `mtime_date` (`TYPE(datetime)`, `POINTER`) and `mtime_td` (`TYPE(timedelta)`, `POINTER`).

```
mtime_td   => newTimedelta("P01D")
mtime_date => newDatetime("2014-06-01T00:00:00")

mtime_date = mtime_date + mtime_td
CALL datetimetostring(mtime_date, dstring)
```

[2]The NWP mode uses the *proleptic* Gregorian calendar that is a backward extension of the Gregorian calendar to dates before its introduction October 15, 1582.

```
WRITE (*,*) "2014-06-01T00:00:00 + 1 day = ", TRIM(dstring)

CALL deallocateDatetime(mtime_date)
CALL deallocateTimedelta(mtime_td)
```

As a second example, we demonstrate the `mtime` event mechanism which may be used to start certain processes in the program. An event (`TYPE(event), POINTER`) is defined by a start date, a regular trigger interval and an end date. Besides, let `RefDate` denote the event *reference date* (anchor date) in our example. Then the event triggers every `RefDate` $+\, k *$ `interval`, but only within the bounds given by `startDate` and `endDate`.

```
advectionEvent => newEvent('advection', RefDate, startDate, &
  &                          endDate, interval)
IF (isCurrentEventActive(advectionEvent, current_date)) THEN
    WRITE (*,*) 'Calculate advection!'
ENDIF
CALL deallocateEvent(advectionEvent)
```

8.2.3. Data Structures for Physics and Dynamics Variables

On each model domain we need the same collection of 2D and 3D fields in order to describe the state of the atmosphere. These fields are collected in the data structure `t_nh_state`. This derived type and the following types are declared in `src/atm_dyn_iconam/mo_nonhydro_types.f90`.

First, the prognostic fields, which are integrated over time, are collected in the data structure `t_nh_prog`. Elements of `t_nh_prog` are allocated for each time slice that is needed for the time integration. For the nonhydrostatic time integration, the number of time slices is two, time t for the current time and $t + \Delta t$ for the prediction.

`t_nh_prog`

`w`	orthogonal vertical wind [$\mathrm{m\,s^{-1}}$]
`vn`	orthogonal normal wind [$\mathrm{m\,s^{-1}}$]
`rho`	density [$\mathrm{kg\,m^{-3}}$]
`exner`	Exner pressure
`tke`	turbulent kinetic energy [$\mathrm{m^2\,s^{-2}}$]
`tracer`	tracer concentration [$\mathrm{kg\,kg^{-1}}$]
	$\vdots$

A global variable `p_nh_state` of type `t_nh_state` is instantiated in the module `/src/atm_dyn_iconam/mo_nonhydro_state.f90`. This is an array whose index corresponds to the model domain. The density of the atmosphere as state variable of the nonhydrostatic dynamical core is therefore given as

```
p_nh_state(domain)%prog(time slice)%rho(index,level,block)
```

Regarding the *`time slice`* argument, we briefly comment on ICON's handling of the two-time-level scheme and the mechanism to avoid reallocation or unnecessary data copies:

For each prognostic variable in the two-time-level scheme, two arrays are pre-allocated:

```
p_nh_state%prog(1)%field(:,:)
p_nh_state%prog(2)%field(:,:)
```

Additionally, we introduce two global `INTEGER` index variables `nnow` and `nnew` which we initialize at model start with

```
nnow = 1
nnew = 2
```

The result values of the integration scheme (time slice $t + \Delta t$) are stored on the `nnew` time level. We therefore access the data on this time level by

```
p_nh_state%prog(nnew)%field(:,:)
```

While the calculations in the dynamical core fill this array with values, the prognostic state of the "old" time step can be accessed by

```
p_nh_state%prog(nnow)%field(:,:)
```

Then, at the end of each dynamic (sub-)step, the time step `n+1` becomes the "old" one, while the time step `n` is freed and can be used as the new working array for the time stepping. This operation does not require any copying but merely exchanges the roles of `nnow` and `nnew`:

```
CALL swap(nnow, nnew)
```

Alas, the whole process is complicated by the following two facts: First, `nnow`, `nnew` are defined for each domain separately. The above examples therefore require the domain index `jg`, i. e. `nnow(jg)`, `nnew(jg)`. Second, as it has been explained in Section 3.7.1, different integration time steps are applied for efficiency reasons. A separate `nnow_rcf/nnew_rcf` accounting is required for the basic time step which is used for tracer transport, numerical diffusion and the fast-physics parameterizations, to distinguish it from the short time step used within the dynamical core[3].

The data type `t_nh_diag` (defined in `src/atm_dyn_iconam/mo_nonhydro_types.f90`) contains a collection of diagnostic fields, determined by all prognostic variables, boundary conditions and the compositions of the atmosphere.

`t_nh_diag`

`u`	zonal wind [$\mathrm{m\,s^{-1}}$]
`v`	meridional wind [$\mathrm{m\,s^{-1}}$]
`temp`	temperature [K]
`pres`	pressure [Pa]
	⋮

Similar to the prognostic fields, the domain-wise data of type `t_nh_diag` can be accessed via `p_nh_state(domain)%diag`.

[3]Here, the suffix `rcf` stands for "reduced calling frequency".

8.2.4. Parallel Communication

To simplify the data exchange between neighboring domain portions, ICON contains synchronization routines `exchange_data`, defined in the module

`src/parallel_infrastructure/mo_communication.f90`.

These take the specific halo region as an argument (data type `t_comm_pattern`) and several exchange patterns are pre-defined for each domain (see the derived data type `t_patch`). For example, `comm_pat_c`, defines the halo communication for *cells* which are owned by neighboring processes. The subroutine call

```
CALL exchange_data(patch%comm_pat_c, array)
```

would perform a typical synchronization of the halo regions.

As it has been noted in Section 7.4.1, there exist different process groups in ICON: I/O, restarting and computation. These groups are related to MPI communicators which are defined in the module `src/parallel_infrastructure/mo_mpi.f90`. Probably the most important MPI communicator in the ICON code is `p_comm_work` (which is identical to the result of a call to `get_my_mpi_work_communicator()`). This is the MPI communicator for the *work group*.

The work group has a total size of `num_work_procs`, where each process may inquire about its rank by calling `get_my_mpi_work_id()`. On a non-I/O rank, its work group comprises all processes which take part in the prognostic calculations. It is therefore used by the `exchange_data` synchronization routine.

A final remark is related to the everlasting chit-chat of the status log (screen) output: The `process_mpi_stdio_id` is always the 0th process of the MPI communicator `process_mpi_all_comm`, which is the MPI communicator containing all PEs that are running this model component. A typical code line for printing out a message to screen would be

```
IF (my_process_is_stdio()) write (0,*) "Hello world!"
```

With this, the message print-out would be suppressed on all PEs 1, 2, ...

Of course, there already exists an auxiliary subroutine `message()` in ICON, whose exact purpose is what we achieved manually above:

```
CALL message('caller', 'message text')
```

The `message()` subroutine is located in the module `mo_exception` and restricts the print-out to PE #0. It takes the caller's subroutine name as an additional argument.

8.3. Implementing Own Diagnostics

A thorough description of how to modify the ICON model and implement one's own diagnostics would certainly be a chapter in its own right. Here, we try to keep things as simple and short as possible with a view to the exercise Ex. C.8.3.

Adding new fields. ICON keeps so-called *variable lists* of its prognostic and diagnostic fields. This global registry eases the task of memory (de-)allocation and organizes the field's meta-data, e.g., its dimensions, description and unit. The basic call for registering a new variable is the `add_var` command (module `mo_var_list`). Its list of arguments is rather lengthy and we will discuss them step by step.

First, we need an appropriate **variable list** to which we can append our new variable. For the sake of simplicity, we choose an existing diagnostic variable list, defined in the module `mo_nonhydro_state`:

```
p_diag_list  =>  p_nh_state_lists(domain)%diag_list
```

The corresponding type definition can be found in the module `mo_nonhydro_types`. There, in the derived data type `TYPE(t_nh_diag)`, we place a **2D variable pointer**

```
REAL(wp), POINTER  ::  newfield(:,:)
```

which we can afterwards access as `p_nh_state(domain)%diag%newfield`.

Note that we did not allocate the variable so far.

Each ICON variable must be accompanied by appropriate **meta-data**. In this example we need to initialize GRIB and NetCDF variable descriptors for a variable located in the cell circumcenters (mass points). To keep this presentation as short as possible we have omitted the necessary `USE` statements:

```
cf_desc    = t_cf_var("newfield", "unit", "long name", DATATYPE_FLT32)
grib2_desc = grib2_var(discipline, parameterCategory, parameterNumber, &
                       DATATYPE_PACK16, GRID_UNSTRUCTURED, GRID_CELL)
```

The derived types `t_cf_var` and `t_grib2_var` are defined in the modules `mo_cf_convention` and `mo_grib2`, respectively. The expression `grib2_var` is actually a call to a constructor function, also defined in `mo_grib2`, which takes a triple of integers (*discipline*, *parameterCategory*, *parameterNumber*) as the field specifier.

Let us create an `INTEGER` array of length 2 with the name `shape2d_c`, denoting the **dimensions** of the new variable. The dimensions of a 2D field will be explained below. Here we take them as given:

```
shape2d_c = (/ nproma, nblks_c /)
```

Now, with the essential ingredients at hand, we define our new field by the following call. We will place it at the very end of the subroutine `new_nh_state_diag_list` in the module `mo_nonhydro_state`.

```
CALL add_var( p_diag_list, 'newfield',                              &
       p_nh_state(domain)%diag%newfield,                            &
       GRID_UNSTRUCTURED_CELL, ZA_SURFACE,                          &
       cf_desc, grib2_desc,                                         &
       ldims=shape2d_c, lrestart=.FALSE. )
```

The INTEGER parameters GRID_UNSTRUCTURED_CELL and ZA_SURFACE define the type of the horizontal grid and the (trivial) vertical axis. From now on the new field can be specified in the output namelists that were described in Section 7.1:

```
&output_nml
  ...
  ml_varlist = 'newfield'
/
```

The **extra_2d** *and* **extra_3d** *fields:* When debugging the model code, it is often advantageous to be able to output intermediate results and ad hoc calculated diagnostic fields. However, it would be an unnecessary effort to define and allocate new variables especially for these test situations. ICON has a special mechanism for this purpose:

By setting the namelist parameter `inextra_2d` (namelist `io_nml`, INTEGER value) or `inextra_3d` (namelist `io_nml`, INTEGER value), respectively, a number of 2D or 3D cell-based floating-point arrays with the names `extra_2d1`, `extra_2d2`, . . ., and `extra_3d1`, `extra_3d2`, . . . is automatically created. Inside the model code, these can be accessed as

```
p_nh_state(domain)%diag%extra_2d_ptr(1)%p_2d(:,:)
```

and similar. Note that all extra variables are actually stored in common buffers

```
p_nh_state(domain)%diag%extra_2d(:,:,1:inextra_2d)
p_nh_state(domain)%diag%extra_3d(:,:,:,1:inextra_3d)
```

The fields can be used as output buffers for the temporary output data then.

Looping over the grid points. Of course, the newly created field '*newfield*' still needs to be filled with values. As explained in Section 8.1 above, nearly all DO loops that iterate over grid cells are organized in two nested loops: "jb loops" and "jc loops". Here the outer loop ("jb") is parallelized with OpenMP and limited by the *cell block number* `nblks_c`. The innermost loop iterates between 1 and the block length `nproma`.

Since the ICON model is usually executed in parallel, we have to keep in mind that each process can perform calculations only on a portion of the decomposed domain. Moreover, some of the cells between interfacing processes are duplicates of cells from neighboring sub-domains (so-called *halo cells*). Often it is not necessary to loop over these halo points, since they will be updated by the next parallel synchronization call.

The auxiliary function `get_indices_c` (declared in the module `mo_loopindices`) helps to adjust the loop iteration accordingly:

```
i_startblk = p_patch(domain)%cells%start_block(grf_bdywidth_c+1)
i_endblk   = p_patch(domain)%cells%end_block(min_rlcell_int)

DO jb = i_startblk, i_endblk
```

```
                          IN                    IN   IN            IN         OUT  OUT
    CALL get_indices_c(p_patch(domain), jb, i_startblk, i_endblk, is, ie, &
                          IN                    IN
                          grf_bdywidth_c+1, min_rlcell_int)
    DO jc = is, ie
      p_nh_state(domain)%diag%newfield(jc,jb) = ...
    END DO
  END DO
```

The constants `grf_bdywidth_c` and `min_rlcell_int` can be found in the modules `mo_impl_constants_grf` and `mo_impl_constants`, respectively. Note that these constants have to be inserted in `start_block`, `end_block` and also in the argument list of `get_indices_c`. A graphical interpretation of these constants is provided by Figure 8.2. The loop example therefore iterates over all prognostic cells (denoted by the blue area).

Loop exchange: The special pre-processor flag `__LOOP_EXCHANGE` can be found in numerous places of the ICON model code. It causes a loop interchange in many performance critical loops: If applied, the variable used in the inner loop switches to the outer loop.

Usually, this means that the loop over the vertical levels becomes the fastest running loop, compared to the iteration indices for the horizontal location. When arrays do not contain vertical levels, access to array elements may take advantage of the CPU cache.

Placing the subroutine call. Having encapsulated the computation together with the `DO` loops in a custom subroutine, we are ready to place this subroutine call in between ICON's physics-dynamics cycle.

Let us take a look at Figure 3.8: The outer loop "Dynamics → Physics → Output" is contained in the core module `mo_nh_stepping` inside the `TIME_LOOP` iteration. For diagnostic calculations it is important to have all necessary quantities available for input. On the other hand the result must be ready before the call to the output module,

```
CALL write_name_list_output(jstep)
```

The fail-safe solution here is to place the call immediately above this call.

Having inserted the call to the diagnostic field computation, we are done with the final step. Recompile the model code and you are finished!

Style recommendations: When writing your own extensions to ICON it is always a good idea to keep an eye on the quality of your code.

Make sure that there is **no duplicate functionality** and try to improve the readability of your subroutines through **indentation**, **comments** etc. This will make it easier for other developers to understand and assimilate. Better

> introduce own **modules** with complete interfaces and avoid `USE`s and `PUBLIC` fields.
>
> A good starting point for your own project are the **template files**, given in the subdirectory `src/templates` of the ICON source code. These provide examples for modules, functions and subroutines.

Additional remarks: 3D fields, accumulated quantities. For the sake of brevity, only the simple case of two-dimensional fields has been discussed so far.

Three-dimensional fields would have an additional dimension for the **column levels**:

```
shape3d_c = (/ nproma, nlev, nblks_c /)
```

This information needs to be provided to the constructor `add_var(...)`, together with an `INTEGER` parameter which indicates the type of the vertical axis:

Usually, the ICON generates its vertical axis on-the-fly, i. e. during the model setup. The user may choose between the hybrid Gal-Chen coordinate and the (more common) SLEVE coordinate via namelist parameters, see Section 3.4. However, it is practically impossible to encode the exact vertical coordinate parameters themselves in the data sets which are produced by the ICON model. Apart from very basic information like the number of vertical levels, only a number identifying the special vertical grid used is provided. This indirect approach is indicated by the parameter `ZA_REFERENCE`.

Finally, it is often necessary to **reset accumulated quantities** in regular intervals. This can be achieved by

```
action_list = actions(new_action(ACTION_RESET,interval))
```

For example, by setting *`interval`* `= "PT06H"`, the respective field would be reset to zero every 6 hours.

```
CALL add_var( p_diag_list, 'newfield',                          &
      p_nh_state(domain)%diag%newfield,                         &
      GRID_UNSTRUCTURED_CELL, ZA_REFERENCE,                     &
      cf_desc, grib2_desc,                                      &
      action_list=actions(new_action(ACTION_RESET,interval)),   &
      ldims=shape3d_c, lrestart=.FALSE. )
```

8.4. NWP Call Tree

All of ICON's NWP and infrastructure modules, however numerous they may be, can roughly be classified into an initialization phase, the time integration loop and the clean-up phase. In Figure 8.3 we restrict ourselves to the most important subprograms.

These are listed together with a short description of their location and purpose, which, of course, change gradually between released versions. We recommend to compare this to the flow chart of processes in the physics-dynamics coupling, see Fig. 3.8.

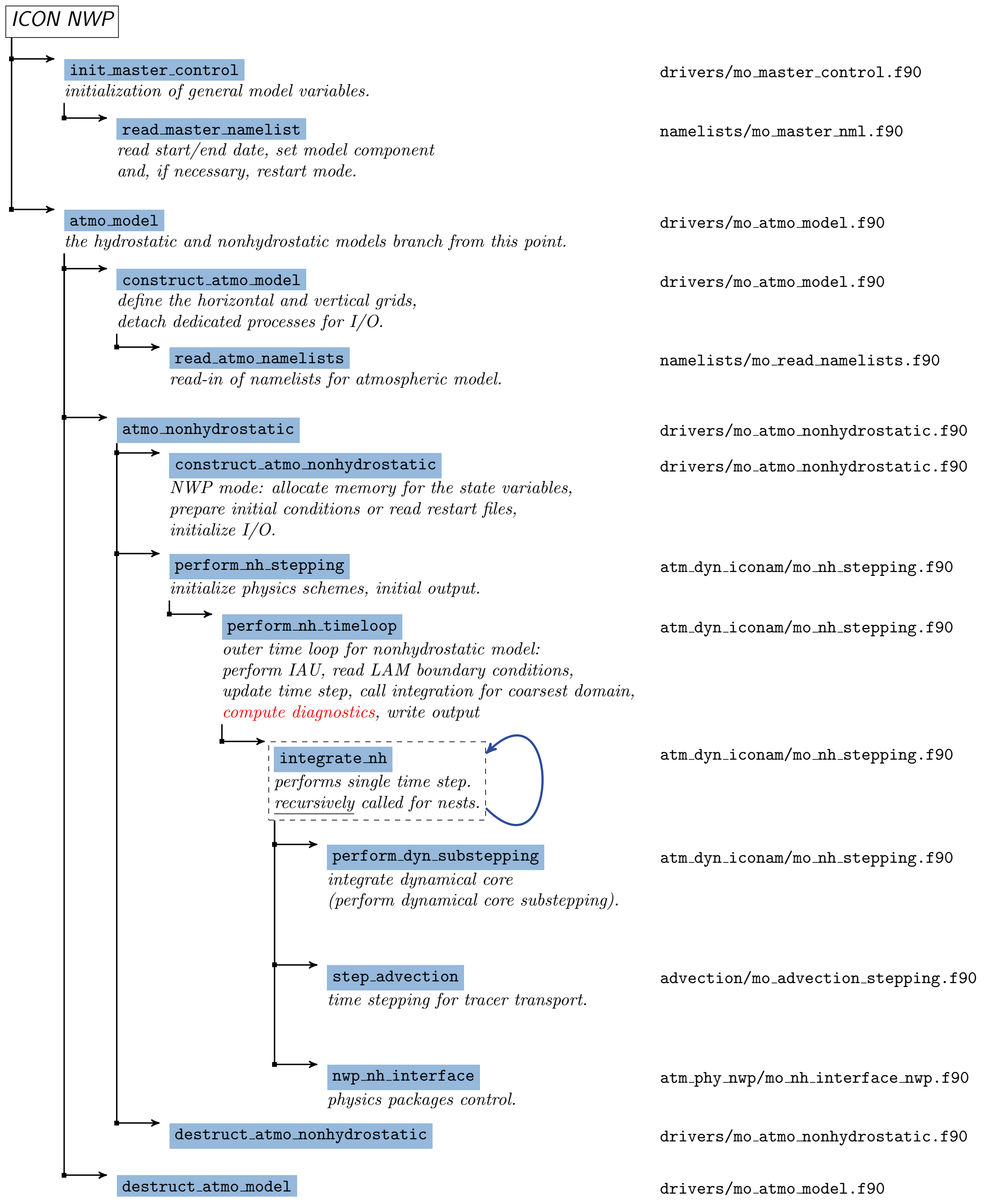
ICON NWP
init_master_control
initialization of general model variables.
drivers/mo_master_control.f90
read_master_namelist
read start/end date, set model component and, if necessary, restart mode.
namelists/mo_master_nml.f90
atmo_model
the hydrostatic and nonhydrostatic models branch from this point.
drivers/mo_atmo_model.f90
construct_atmo_model
define the horizontal and vertical grids, detach dedicated processes for I/O.
drivers/mo_atmo_model.f90
read_atmo_namelists
read-in of namelists for atmospheric model.
namelists/mo_read_namelists.f90
atmo_nonhydrostatic
drivers/mo_atmo_nonhydrostatic.f90
construct_atmo_nonhydrostatic
NWP mode: allocate memory for the state variables, prepare initial conditions or read restart files, initialize I/O.
drivers/mo_atmo_nonhydrostatic.f90
perform_nh_stepping
initialize physics schemes, initial output.
atm_dyn_iconam/mo_nh_stepping.f90
perform_nh_timeloop
outer time loop for nonhydrostatic model: perform IAU, read LAM boundary conditions, update time step, call integration for coarsest domain, compute diagnostics, write output
atm_dyn_iconam/mo_nh_stepping.f90
integrate_nh
performs single time step. recursively called for nests.
atm_dyn_iconam/mo_nh_stepping.f90
perform_dyn_substepping
integrate dynamical core (perform dynamical core substepping).
atm_dyn_iconam/mo_nh_stepping.f90
step_advection
time stepping for tracer transport.
advection/mo_advection_stepping.f90
nwp_nh_interface
physics packages control.
atm_phy_nwp/mo_nh_interface_nwp.f90
destruct_atmo_nonhydrostatic
drivers/mo_atmo_nonhydrostatic.f90
destruct_atmo_model
drivers/mo_atmo_model.f90

Figure 8.3.: Call tree of ICON's NWP component (note that this list has been restricted to the most important subroutines).

9. Post-Processing and Visualization

Oh my God! Look at that picture over there! There's the Earth coming up. Wow, is that pretty.

W. Anders, Apollo 8

ICON offers the possibility to produce output either in NetCDF or GRIB2 format. Many visualization environments such as GrADS, Matlab or R now include packages with which NetCDF data files can be handled. The GRIB format, which is also commonly used in meteorology, can be processed with these tools as well. However, since the standardization of unstructured GRIB records is relatively new, many post-processing packages offer only limited support for GRIB data that has been stored on the triangular ICON grid.

Since the visualization of *regular* (lat-lon) grid data is relatively straightforward, we limit ourselves in our description to a very simple program, `ncview`, which does not have a large functionality but is an easy-to-use program for a quick view of NetCDF output files. It is therefore very useful for a first impression.

Model data that has been stored on the *triangular* ICON grid can be visualized with the Python programming language, the NCL scripting language, R or the Generic Mapping Tools (GMT). Section 9.3 contains some examples how to visualize NetCDF data sets without the need of an additional regridding.

9.1. Retrieving Data Set Information

We begin with command-line utilities which provide a textual description of the data sets. For a quick overview of dimensions and variables, the command-line utility `ncdump` can be used. This program will shortly be described first. More sophisticated tools exist, for cutting out subsets of data, e. g., and producing averages or time series. One of these tools are the `cdo` utilities.

9.1.1. The ncdump Tool

The tool `ncdump` comes with the NetCDF library as provided by Unidata and generates a text representation of a NetCDF file on standard output. The text representation is in a form called CDL (network Common Data form Language). `ncdump` may be used as a simple browser for NetCDF data files, to display the dimension names and sizes, variable names, types and shapes, attribute names and values, and optionally, the data values themselves for all or selected variables in ASCII format. For example, to investigate the structure of a NetCDF file, use

```
ncdump -h data-file.nc
```

With this command, dimension names and sizes, variable names, dependencies and values of dimensions will be displayed. To show the type version of a NetCDF file, type

```
ncdump -k data-file.nc
```

This gives information about the NetCDF base format of a specific file, for example NetCDF Classic Format, NetCDF 64-bit Offset Format or NetCDF-4 Format.

NetCDF data can also be redirected to a text file with

```
ncdump -b c data-file.nc > data-file.cdl
```

This produces an annotated CDL version of the structure and the data in the NetCDF file *data-file.nc*. You can also save data for specified variables to text files just using:

```
ncdump -v variable data-file.nc > data-file.txt
```

For further information on working with `ncdump` see

http://www.unidata.ucar.edu/software/netcdf/ ···
docs/netcdf_utilities_guide.html#ncdump_guide

9.1.2. CDO – Climate Data Operators

The CDO (Climate Data Operators) are a collection of command-line operators to manipulate and analyze NetCDF and GRIB data. The CDO package is developed and maintained at the MPI for Meteorology in Hamburg. Source code and documentation are available from

https://code.mpimet.mpg.de/projects/cdo

The tool includes more than 400 operators to print information about data sets, copy, split and merge data sets, select parts of a data set, compare data sets, modify data sets, arithmetically process data sets, to produce different kind of statistics, to detrend time series, for interpolation and spectral transformations. The CDOs can also be used to convert from GRIB to NetCDF or vice versa, although some care has to be taken there.

In particular, the "operator" `cdo infov` writes information about the structure and contents of all input files to standard output. By typing

```
cdo infov data-file.nc
```

in the command-line for each field the following elements are printed: date and time, parameter identifier and level, size of the grid and number of missing values, minimum, mean and maximum. A variant of this CDO operator is

```
cdo sinfov data-file.nc
```

which prints out short information of each field.

Remapping to regular grids with the CDOs. The CDO are, by the way, also capable of remapping data to regular grids. Basically, two steps are necessary to process the ICON output files:

- In the first call of the CDO ("`gencon`"), 1st order conservative remap weights are generated and stored to a separate file:

  ```
  cdo gencon,lat-lon_grid_description  icon_grid  coefficient_file
  ```

  The generation of the interpolation weights may take some time.

- Afterwards, the interpolation is done with

  ```
  cdo remap,grid_description,coefficient_file  in_file out_file
  ```

Here, the file *icon_grid* is a NetCDF file which contains the topological and geometric information about the triangular ICON grid. This grid information must correspond to the data set *in_file* and it is not part of the data set itself. Instead, it must be downloaded separately from the web. See `http://icon-downloads.mpimet.mpg.de/dwd_grids.xml` for the list of "official" DWD ICON grids[1].

With respect to datasets with "missing values" the above CDO workflow with pre-calculated weights fails. The following remark applies, for example, to the ICON-D2 datasets:

Since the "missing values" are not part of the source grid definition, the CDOs detect the masking only when reading the data file. Then, to avoid the risk of using undefined values for the interpolation stencils, the whole process is aborted in this case. A workaround when interpolating a single file is to do the weight calculation simultaneously with the interpolation:

```
cdo remapcon,grid_description -setgrid,icon_grid:2  in_file out_file
```

In this example we have also set the source grid index explicitly to 2 to distinguish between the cell grid, edge grid, and the vertex grid in the *icon_grid* file. The concrete index can be obtained from the output of `cdo sinfov` *data-file.nc*.

DWD OpenData Documentation: A valuable web resource in this context is DWD's OpenData website. Here, ICON data sets are made freely available to the public and the whole procedure of remapping ICON data with the CDO tool is also described.
OpenData information on ICON forecast data:

`https://www.dwd.de/DE/leistungen/opendata/hilfe.html`

Furthermore, there even exists a Docker software container in which all necessary packages for the CDO and the ecCodes are combined:

`https://github.com/deutscherwetterdienst/regrid`

[1] Currently in operational use is the global grid #26 with 13 km horizontal grid spacing (`http://icon-downloads.mpimet.mpg.de/grids/public/edzw/icon_grid_0026_R03B07_G.nc`).

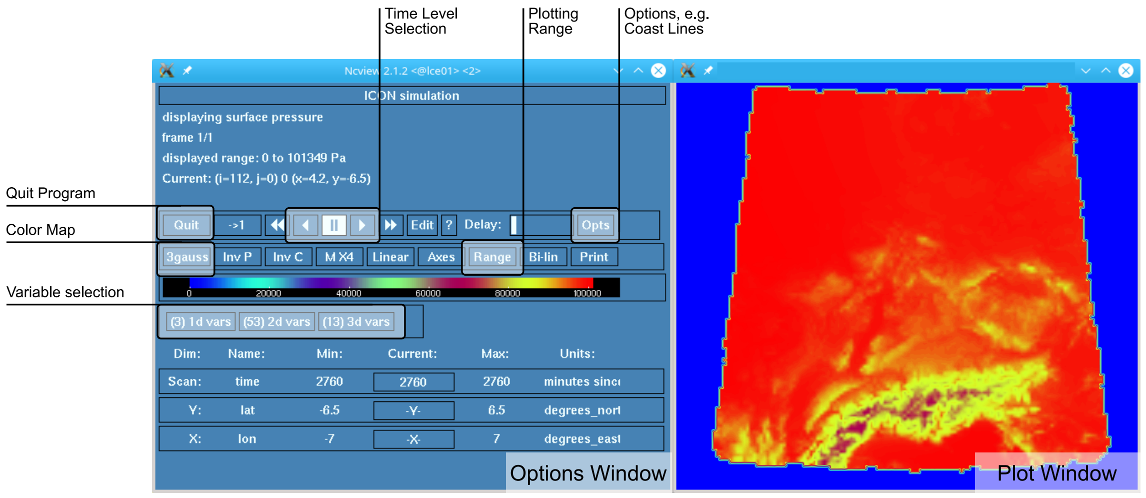

ICON simulation

displaying surface pressure
frame 1/1
displayed range: 0 to 101349 Pa
Current: (i=112, j=0) 0 (x=4.2, y=-6.5)

Dim:	Name:	Min:	Current:	Max:	Units:
Scan:	time	2760	2760	2760	minutes sinc
Y:	lat	-6.5	-Y-	6.5	degrees_nort
X:	lon	-7	-X-	7	degrees_east

Figure 9.1.: Screenshot of the `ncview` NetCDF plotting tool.

The structure of the lon-lat grid description file is explained in the CDO documentation[2]. A global regular grid, for example, would be defined as

```
gridtype =  lonlat
xsize    =    1440
ysize    =     721
xfirst   =    0.00
xinc     =    0.25
yfirst   =  -90.00
yinc     =    0.25
```

Caveat: Alas, the CDO do not handle the entire set of GRIB2 meta-data correctly. Some meta-data items, for example those which regard ensemble runs, still remain unsupported. However, this limitation does not matter if the desired output format is NetCDF and not GRIB2, or if the processed data fields are rather standard. Alternatives for remapping ICON data sets to lon-lat grids are the *fieldextra* software (which is a COSMO software) or the DWD ICON Tools, which are internally used at DWD but lack official support.

9.2. Plotting Data Sets on Regular Grids: `ncview`

`ncview` is a visual browser for NetCDF format files developed by David W. Pierce. Using `ncview` you can get a quick and easy look at *regular* grid data in your NetCDF files.

To install `ncview` on your local platform, see the `ncview` website:
`http://meteora.ucsd.edu/~pierce/ncview_home_page.html`

You can run the program by typing:

```
ncview data-file.nc
```

[2]Appendix D, `https://code.mpimet.mpg.de/projects/cdo/embedded/index.html`.

which will open a new window with the display options. It is possible to view simple movies of data, view along different dimensions, to have a look at actual data values at specific coordinates, change color maps, invert data, etc., see the screenshot in Fig. 9.1.

If *data-file.nc* contains wildcards such as '*' or '?' then all files matching the description are scanned, if all of the files contain the same variables on the same grid. Choose the variable you want to view. Variables which are functions of longitude and latitude will be displayed in two-dimensional images. If there is more than one time step available you can easily view a simple movie by just pushing the forward button. The appearance of the image can be changed by varying the colors of the displayed range of the data set values or by adding/removing coastlines. Each one- or two-dimensional subset of the data can be selected for visualization. `ncview` allows the selection of the dimensions of the fields available, e.g. longitude and height instead of longitude and latitude of 3D fields.

The pictures can be sent to Postscript (`*.ps`) output by using the function `print`. Be careful that whenever you want to close only a single plot window to use the `close` button, because clicking on the ⊠-icon on the top right of the window will close all `ncview` windows and terminate the entire program!

9.3. Plotting Data Sets on the Triangular Grid

Let us now focus on ICON's original computational mesh, the triangular grid. In this section we will sketch several approaches for the visualization of data sets based on the triangular cells.

By now there is quite a number of scripting languages and visualization tools available for this task. We will present quick start examples for the Python programming language, NCL, R, and GMT. All these approaches have in common that the NetCDF grid file must be read in together with the data file.

9.3.1. Visualization with Python

The Python module *PyNGL* (pronounced "pingle") is a Python language module for generating high-quality, 2D visualizations of scientific data. *PyNIO* is a Python module used for reading and writing NetCDF, GRIB, and HDF.

PyNGL is developed by the Computational and Information Systems Lab at the National Center for Atmospheric Research (NCAR), see

`https://www.pyngl.ucar.edu`

In the following we will explain the basic usage of PyNGL in a step-by-step tutorial.

PyNGL Installation

PyNGL and PyNIO can be installed on Linux and MacOS systems via *conda*[3], or its slimmed-down version *miniconda*:

First, download the *miniconda* installer script to your machine. In our example we will install the stable release version for Linux x86 architectures. Visit the *conda* web page to find out which version is the right one for your platform.

```
wget https://repo.anaconda.com/miniconda/Miniconda3-latest-Linux-x86_64.sh
bash Miniconda3-latest-Linux-x86_64.sh
source $HOME/miniconda3/etc/profile.d/conda.sh
```

Once *miniconda* is installed, we use the `conda` command to install the *PyNGL* and *PyNIO* Python packages:

```
conda create  --name pyn_env --channel conda-forge numpy pyngl pynio
```

Now, you can activate Python environment via

```
conda activate pyn_env
```

and the newly installed packages *PyNGL* and *PyNIO* are ready to use.

NumPy and threading issues: On some platforms (like DWD's `rcl.dwd.de`) you may encounter a SegFault when using the *NumPy* package in Python+conda. A similar problem occurs when using the packages *PyNGL* and *PyNIO*. This problem, which is related to the multi-threaded BLAS library, can be avoided by setting in your shell environment

```
export OMP_NUM_THREADS=1
```

PyNGL Step-by-step Tutorial

In the following we provide a detailed step-by-step tutorial for producing graphics from an ICON data set. To this end, we create a file `visualization_tutorial.py` where a sequence of commands can be stored and executed with

```
python visualization_tutorial.py
```

We begin by loading some Python modules which provide high-level functions for plotting and numerical computations

```
# load Python modules for plotting
import Ngl, Nio, numpy
```

These lines also contain a comment. Comment lines in Python are preceded by the hash sign '#'.

[3] *Conda* is an open source package management system see https://conda.io.

Step 1: Reading grid coordinates from file. Since the ICON model uses an unstructured grid topology, we open and read such a topology file, stored in NetCDF format, by the following commands:

```
gridfile = Nio.open_file("gridfile.nc")
print(gridfile)
```

The `print` command lists all variables that have been found in the NetCDF file as textual output. For the ICON grid, the vertex positions of the grid triangles are of special interest. They are stored as longitude/latitude positions in the `vlon`, `vlat` fields (this is explained in more detail in Section 2.1.1, page 21). For PyNGL we convert from steradians to degrees:

```
vlon = numpy.rad2deg( gridfile.variables["vlon"][:] )
vlat = numpy.rad2deg( gridfile.variables["vlat"][:] )
```

Additionally, we load the vertex indices for each triangle edge of the icosahedral mesh.

```
edge_vertices = gridfile.variables["edge_vertices"][:]
```

The indices are stored in the grid file data set `edge_vertices` and reference the corresponding vertices from `vlon`, `vlat`,

$$\text{edge } \#i: \qquad (\texttt{vlon}[q_1], \texttt{vlat}[q_1]) \text{ --- } (\texttt{vlon}[q_2], \texttt{vlat}[q_2])$$

where

$$q_{1/2} := \texttt{edge\_vertices}[1/2, i] - 1$$

Note that by subtracting 1 we take the 0-based array indexing of Python into account.

Step 2: Creating a plot of the triangular grid. Producing graphics with PyNGL requires the creation of a so-called *workstation*, i.e. a description of the output device. In this example, this "device" will be an image file `plot.png`, but we could also define a different output format, e.g. PostScript `"ps"` instead.

```
wks = Ngl.open_wks("png","plot")
```

Then the map settings have to be defined and we collect these specifications in a "resource data structure" named `config1`. First of all, we disable the immediate drawing of the map image, since the ICON icosahedral grid plot will consist of two parts: the underlying map and the grid lines. We do so by setting the resource attributes `bglFrame` and `nglDraw` to `False`.

We then define an orthographic projection centered over Europe. It is important that grid lines are true geodesic lines, otherwise the illustration of the ICON grid would contain graphical artifacts, therefore we set the parameter `mpGreatCircleLinesOn`.

```
config1 = Ngl.Resources()
config1.nglFrame              = False
config1.nglDraw               = False

config1.mpProjection          = "Orthographic"
config1.mpGreatCircleLinesOn  = True
config1.mpCenterLonF          = 10
config1.mpCenterLatF          = 50
```

Having completed the setup of the `config1` data structure, we can create an empty map by the following command:

```
map = Ngl.map(wks,config1)
```

Now, the edges of the ICON grid must be added to the plot. As described before, we convert the indirectly addressed `edge_vertices` into an explicit list of geometric segments with dimension $2 *$ `nedges`:

```
ecx = numpy.ravel( vlon[ edge_vertices-1 ], order='F' )
ecy = numpy.ravel( vlat[ edge_vertices-1 ], order='F' )
```

This operation deserves additional comments: First of all, since the PyNGL plotting function below will expect one-dimensional lists for its interface, we use the auxiliary function `numpy.ravel` for reshaping the array of lines. Second, with `order='F'` we define the array ordering of `vlon`, `vlat` to be “Fortran-style”. Compared to Python (numpy) this is the transpose memory layout.

Now, there exists an PyNGL high-level command for plotting lines, `Ngl.add_polyline`.

```
lines_cfg = Ngl.Resources()
lines_cfg.gsSegments = numpy.arange(0, edge_vertices.size, 2)
poly = Ngl.add_polyline(wks, map, ecx, ecy, lines_cfg)
```

The whole plotting process is then triggered by the command

```
Ngl.draw(map)
Ngl.frame(wks)
Ngl.end()
```

Here, the call to `Ngl.end()` terminates the PyNGL script. The first of the resulting image files `plot.000001.png` will contain an illustration similar to Fig. 9.2 (left part).

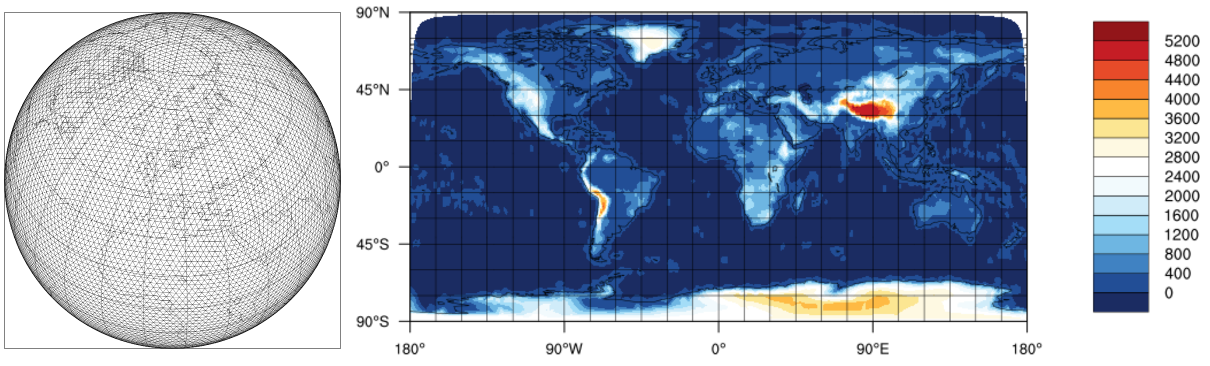

Figure 9.2.: The two plots generated by the Python example script in Section 9.3.1.

Step 3: Loading a data set from a second file. We now assume that the data sets produced by the ICON model have been stored in NetCDF format. This allows to visualize the unstructured data without additional Python packages. As a second file we open such a NetCDF data set `datafile.nc` in read-only mode and investigate its data set `topography_c`:

```
datafile = Nio.open_file("datafile.nc")
topo = datafile.variables["topography_c"]
print(topo)
```

The final step of this exercise is the creation of a contour plot from the data contained in `datafile`. As it has been stated by the previous call to `print`, the data sites for the field `topography_c` are the triangle circumcenters, located at `clon`, `clat`.

```
clon  = numpy.rad2deg( gridfile.variables["clon"][:] )
clat  = numpy.rad2deg( gridfile.variables["clat"][:] )
```

For a basic contour plot, a cylindrical equidistant projection with automatic adjustment of contour levels will do. It is important to specify the two additional arguments `sfXArray` and `sfYArray`.

```
config2 = Ngl.Resources()
config2.mpProjection          = "CylindricalEquidistant"
config2.cnFillOn              = True
config2.cnLinesOn             = False
config2.cnLineLabelsOn        = False
config2.sfXArray              = clon
config2.sfYArray              = clat
```

Afterwards, we generate the plot (image file `plot.000002.png`) with a call to `Ngl.contour_map`.

```
map = Ngl.contour_map(wks,topo,config2)
```

Note that this time it is not necessary to launch additional calls to `draw` and `frame`, since the default options in `config2` are set to immediate drawing mode.

You may wonder why the plot has a rather smooth appearance without any indication of the icosahedral triangular mesh. What happened is that PyNGL generated its own Delaunay triangulation building upon the cell center coordinates provided via `clon`, `clat`. Thus, we are unable to locate and investigate individual ICON grid cells. In order to visualize individual cells, we need to additionally load the vertex coordinates of each triangle into PyNGL. This information is also available from the grid file and is stored in the fields `clon_vertices`, `clat_vertices`.

```
clonv  = numpy.rad2deg( gridfile.variables["clon_vertices"][:] )
clatv  = numpy.rad2deg( gridfile.variables["clat_vertices"][:] )
config2.sfXCellBounds          = clonv
config2.sfYCellBounds          = clatv
config2.cnFillMode             = "CellFill"
```

By choosing the `CellFill` mode, it is ensured that every grid cell is filled with a single color.

Afterwards we generate the plot once more with a call to `Ngl.contour_map`.

```
map = Ngl.contour_map(wks,topo,config2)
```

Do you see the difference?

9.3.2. NCL – NCAR Command Language

The NCAR Command Language (NCL) is an interpreted language designed specifically for scientific data analysis and visualization. It is built on top of the same ”resource model” used in the PyNGL Python package.

NCL allows convenient access to data in a variety of formats such as NetCDF and GRIB1/2, among others. It has many features common to modern programming languages, such as types, variables, operators, expressions, conditional statements, loops, and functions and procedures, see `https://www.ncl.ucar.edu` for details.

Besides an interactive mode, NCL allows for script processing (recommended). NCL scripts are processed on the command-line by typing

```
ncl filename.ncl
```

For visualizing ICON data on the native triangular grid, we recommend using NCL 6.2.0 or higher.

Note that NCAR has recently made the decision to adopt Python as the scripting language platform of choice for future development of analysis and visualization tools. NCL's graphics routines will have continued development through the PyNGL Python package.

NCL Quick-Start Example

The following example script creates a temperature contour plot with NCL (see Figure 9.3):

```
begin

; Open model level output file
 File = addfile( "JABW_DOM01_ML_0001.nc", "r" )

; read grid information (i.e. coordinates of cell centers and vertices)
 rad2deg = 45./atan(1.)          ; radians to degrees
 clon = File->clon * rad2deg            ; cell center, lon (ncells)
 clat = File->clat * rad2deg            ; cell center, lat (ncells)

 vlon = File->clon_bnds * rad2deg   ; cell vertices, lon (ncells,3)
 vlat = File->clat_bnds * rad2deg   ; cell vertices, lat (ncells,3)

; read data
;
 temp_ml = File->temp(:,:,:)   ; dims: (time,lev,cell)
 print("max T " + max(temp_ml) )
 print("min T " + min(temp_ml) )

; create plot
;
 wks = gsn_open_wks("ps","outfile")
 gsn_define_colormap(wks,"testcmap")      ; choose colormap

 ResC                       = True
 ResC@sfXArray              = clon        ; cell center (lon)
 ResC@sfYArray              = clat        ; cell center (lat)
 ResC@sfXCellBounds         = vlon        ; define triangulation
 ResC@sfYCellBounds         = vlat        ; define triangulation
 ResC@cnFillOn              = True        ; do color fill
 ResC@cnFillMode            = "cellfill"
 ResC@cnLinesOn             = False       ; no contour lines

; plot temperature level
 plot = gsn_csm_contour_map(wks,temp_ml(0,80,:),ResC)

end
```

To open a data file for reading, the function **addfile** returns a file variable reference to the specified file. Second, for drawing graphics, the function **gsn_open_wks** creates an output resource, where the “ps”, “pdf” or “png” format are available. Third, the command **gsn_csm_contour_map** creates and draws a contour plot over a map.

Loading the coordinates of the triangle cell centers into NCL (resources **sfXArray** and **sfYArray**) is essential for visualizing ICON data on the native grid. Loading the vertex coordinates of each triangle (resources **sfXCellBounds** and **sfYCellBounds**), however, is optional. If not given, a Delaunay triangulation in the 2D plane will be performed by

NCL, based on the cell center information. If given, the triangles defining the mesh will be deduced by sorting and matching vertices from adjacent cell boundaries. If you are interested in the correct representation of individual cells, the resource `sf[X/Y]CellBounds` should be set.

Creating a plot can get very complex depending on how you want to look at your data. Therefore we refer to the NCL documentation that is available online under

`http://www.ncl.ucar.edu`

Note that there is another NCL example contained in the course material, which very closely resembles the steps explained in the PyNGL tutorial in Section 9.3.1. For the exercises in this tutorial we refer to the prepared NCL scripts. These files are stored in the subdirectory `test_cases/case`*xx* together with the model run scripts.

9.3.3. Visualization with R

Section authors

J. Förstner and M. Köhler,
DWD Physical Processes Division

R is a free software environment for statistical computing and graphics. R is available as free software under the terms of the Free Software Foundation's GNU General Public License. More Information can be found here:

`https://www.r-project.org`

To start R in an interactive mode simply type

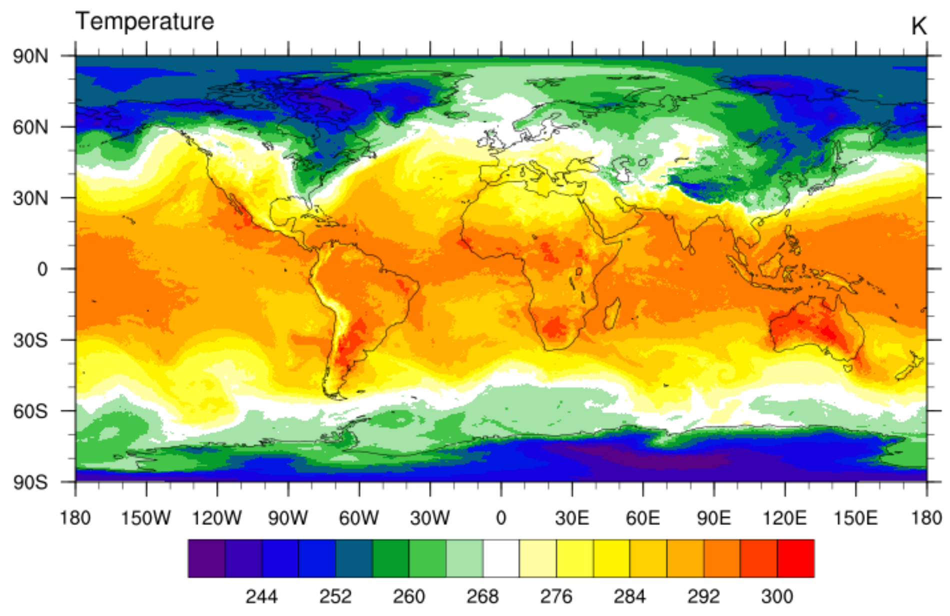

Figure 9.3.: ICON temperature field on a specific model level produced with the above NCL script.

```
R
```

on the command line. Afterwards R commands can be entered, which are then interpreted line by line. R can be extended (easily) via packages. Additional packages have to be installed via the R command

```
install.packages("package_name")
```

For the compilation of some packages it might be necessary to provide specific (development) libraries on the system and to give information about the include and library paths as additional arguments to that command.
Most packages are available through the CRAN family of internet sites. An exception to this is the `gribr` package, which is used in the example script below to read in GRIB2 data:

https://github.com/nawendt/gribr

This package uses and therefore needs a recent installation of ecCodes (it is not working with the GRIB API). Additional information about (other) prerequisites and the installation of the package can be found on the given website.

Installation of R on the DWD computer system: The R software has been preinstalled on DWD's `rcl.dwd.de` as a software module, where `R/3.6.2` is the current default (for which the below example has been tested). Further modules have to be loaded as well, see the comment in the following example.

Besides an interactive mode, R allows for script processing (recommended). R scripts are processed on the command-line by typing

```
Rscript filename.R
```

As default a PDF named `Rplots.pdf` will be created.

R Quick-Start Example

The following example script `icon_native_4_tutorial.R` can be found in the tarball directory `scripts`. It creates a global temperature contour plot with R (see Figure 9.4):

```
# ... on DWD's RCL, as a prerequisite issue the following commands:
# module load netcdf4 oracle
# module load R
# module load gribr

# ---------------------------------------------------------------

# load necessary libraries
 library(gribr)
 library(RNetCDF)
```

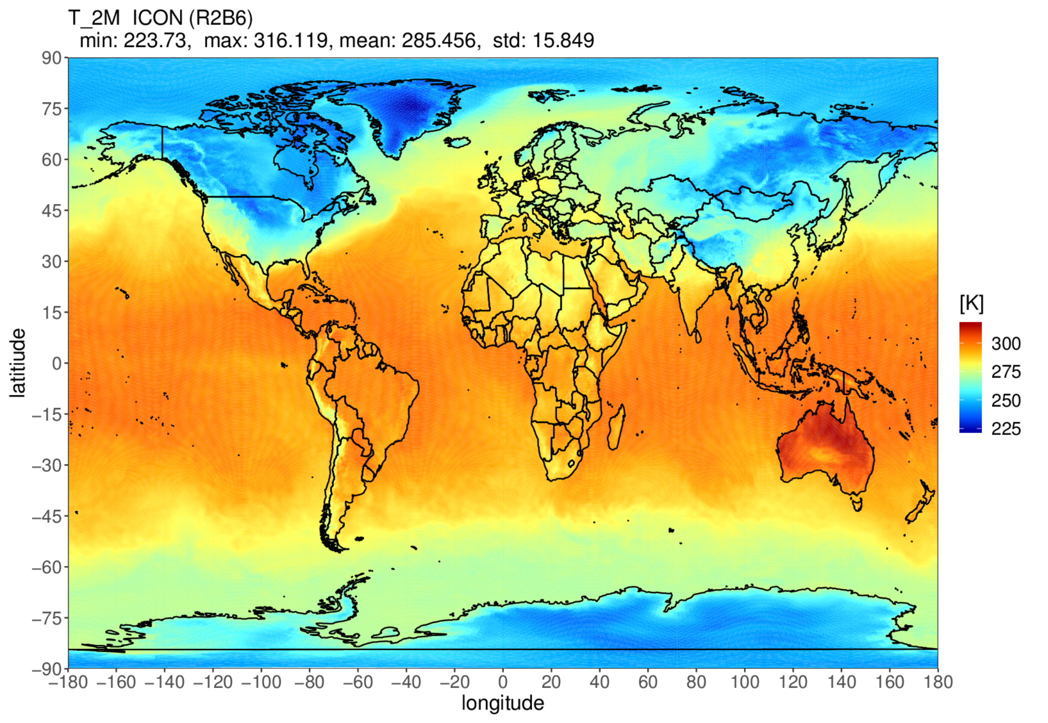

Figure 9.4.: ICON 2 m temperature field produced with the given example script for R.

```
 library(data.table)
 library(ggplot2)
 library(dplyr)
 library(colorRamps)

# --- setup ----------------------------------------------------

shortName <- "T_2M"
title     <- paste(shortName," ICON (R2B6)\n")

# data file names
grid <- "./icon_grid_0024_R02B06_G.nc"
data <- "./T_2M.R2B06_ICON_global.grb"

# --- icon grid ------------------------------------------------

 ncHandle <- open.nc(grid)

# function to convert coordinates in degress
 rad2deg <- function(rad) {(rad * 180) / (pi)}

# get longitudes and latitudes of triangle vertices of a cell
 vlon <- rad2deg(var.get.nc(ncHandle,"clon_vertices"))
 vlat <- rad2deg(var.get.nc(ncHandle,"clat_vertices"))
 close.nc(ncHandle)

# --- icon data ------------------------------------------------

 gribHandle <- grib_open(data)

# select the grib record based on a given list of keys
 gribRecord <- grib_select(gribHandle, list(shortName = shortName))

 grib_close(gribHandle)

# create a data table with data to plot - ids and values are tripled
 DT <- data.table(lon = as.vector(vlon),
                  lat = as.vector(vlat),
                  id  = rep(1:(dim(vlon)[2]) , each=3),
                  var = rep(gribRecord$values, each=3))

# --- domain and edges -----------------------------------------

# Global
 xrange <- c(-180.,  180.)
 yrange <- c( -90.,   90.)

# select the subset of ids in the domain
 usedIDs <- unique(DT[lon%between%xrange & lat%between%yrange]$id)

# use only the respective subset of the data
 DT <- DT[id %in% usedIDs]

# special treatment for the cells near the date line
# ... when the 3 corners on opposite sides of the date line move one corner
 IDsR = DT[,list( (max(lon)-min(lon))>200 & mean(lon)>0.0 ), by=id][V1==T]$id
 IDsL = DT[,list( (max(lon)-min(lon))>200 & mean(lon)<0.0 ), by=id][V1==T]$id
 DT[id %in% IDsR & lon < 0.0, lon := lon + 360.0]
 DT[id %in% IDsL & lon > 0.0, lon := lon - 360.0]
# ... copy triangles by 360deg to fill holes near date line
 DTT    <- DT[id%in%IDsR]
 DTT[lon > 0.0, lon := lon - 360.0]
 DTT$id <- DTT$id + max(DT$id)
 DT     <- rbind(DT, DTT)
 DTT    <- DT[id%in%IDsL]
 DTT[lon < 0.0, lon := lon + 360.0]
 DTT$id <- DTT$id + max(DT$id)
 DT     <- rbind(DT, DTT)

# --- plot data using ggplot2 with geom_polygon ----------------

# landscape mode
 pdf(paper="a4r", width=11.692, height=8.267)

# create the plot object
 pp <- ggplot() +
      geom_polygon(data = DT, aes(x = lon, y = lat, group = id, fill = var)) +
       borders(colour = "black", xlim = xrange, ylim = yrange)             +
       scale_fill_gradientn(colours = matlab.like(100))                    +
       coord_cartesian(xlim = xrange,ylim = yrange, expand = FALSE)        +
       scale_x_continuous(breaks = seq(xrange[1], xrange[2],20))           +
       scale_y_continuous(breaks = seq(yrange[1], yrange[2],15))           +
       theme_bw()                                                          +
       labs(x="longitude", y="latitiude", fill="[K]")                      +
       theme(axis.text    = element_text(size=14),
             axis.title   = element_text(size=16),
             plot.title   = element_text(size=16, hjust=0),
             legend.title = element_text(size=16),
             legend.text  = element_text(size=14))                         +
       ggtitle(paste0(title,
               "  min: ", round(min (DT$var, na.rm=TRUE),3), ", ",
               " max: " , round(max (DT$var, na.rm=TRUE),3), ", ",
               "mean: " , round(mean(DT$var, na.rm=TRUE),3), ", ",
               " std: " , round(sd  (DT$var, na.rm=TRUE),3)))

# issue the plot object
 pp
```

9.3.4. GMT – Generic Mapping Tools

GMT is an open source collection of command-line tools for manipulating geographic and Cartesian data sets and producing PostScript illustrations ranging from simple x-y plots via contour maps to 3D perspective views. GMT supports various map projections and transformations and facilitates the inclusion of coastlines, rivers, and political boundaries. GMT is developed and maintained at the University of Hawaii, and it is supported by the National Science Foundation.

To install GMT on your local platform, see the GMT website:

https://www.generic-mapping-tools.org

Since GMT is comparatively fast, it is especially suited for visualizing high resolution ICON data on the native (triangular) grid. It is capable of visualizing individual grid cells and may thus serve as a helpful debugging tool. So far, GMT is not capable of reading ICON NetCDF or GRIB2-output offhand. However, CDO can be used to convert your data to a format readable by GMT.

From your NetCDF output, you should first select your field of interest and pick a single level at a particular point in time:

```
cdo -f nc selname,VNAME -seltimestep,ITIME -sellevidx,ILEV \
    ICON_OUTPUT.nc ICON_SELECTED.nc
```

Now this file must be processed further using the `outputbounds` command from CDO, which finally leads to an ASCII file readable by GMT.

```
cdo -outputbounds ICON_SELECTED.nc >  ICON_SELECTED.gmt
```

The output looks as follows:

```
# Generated by CDO version 1.6.3
#
# Operator = outputbounds
# Mode     = horizonal
#
# File  = NWP_DOM01_ML_0006_temp.nc
# Date  =  2012-01-04
# Time  = 00:00:00
# Name  = temp
# Code  = 0
# Level = 80
#
> -Z254.71
   -155.179  90
   36  89.5695
   108  89.5695
   -155.179  90
> -Z255.276
   36  89.5695
   36  89.1351
   72  89.2658
   36  89.5695
...
```

For each triangle, it contains the corresponding data value (indicated by `-Z`) and vertex coordinates.

As a starting point, a very basic GMT script is added below. It visualizes the content of `test.gmt` on a cylindrical equidistant projection including coastlines and a colorbar. An example plot based on this script is given in Figure 9.5.

```
#!/bin/bash

# Input filename
INAME="test.gmt"

# Output filename
ONAME="test.ps"

# generate color palette table (min/max/int)
makecpt -Cpolar -T"235"/"305"/"5" > colors.cpt

# draw triangle and take fill color from colors.cpt
psxy ${INAME} \
-Rd -Jq0/1:190000000 -Ccolors.cpt -X3.2 -Y4. -K > ${ONAME}

# visualize coastlines
pscoast       -Rd -Jq0/1:190000000 -Dc -W0.25p,black -K -O >> $ONAME
```

```
# plot colorbar
psscale -D11c/14c/18c/1.0ch -Ccolors.cpt -E -B:"T":/:K: -U -O>> $ONAME
```

Note: In order to get filled polygons, the `-L` option must be added to `psxy`. The purpose of `-L` is to force closed polygons, which is a prerequisite for polygon filling. However, in some recent releases of GMT (5.1.2) adding this option results in very large output files whose rendering is extremely slow. Thus, the `-L` option was omitted here so that only triangle edges are drawn and colored.

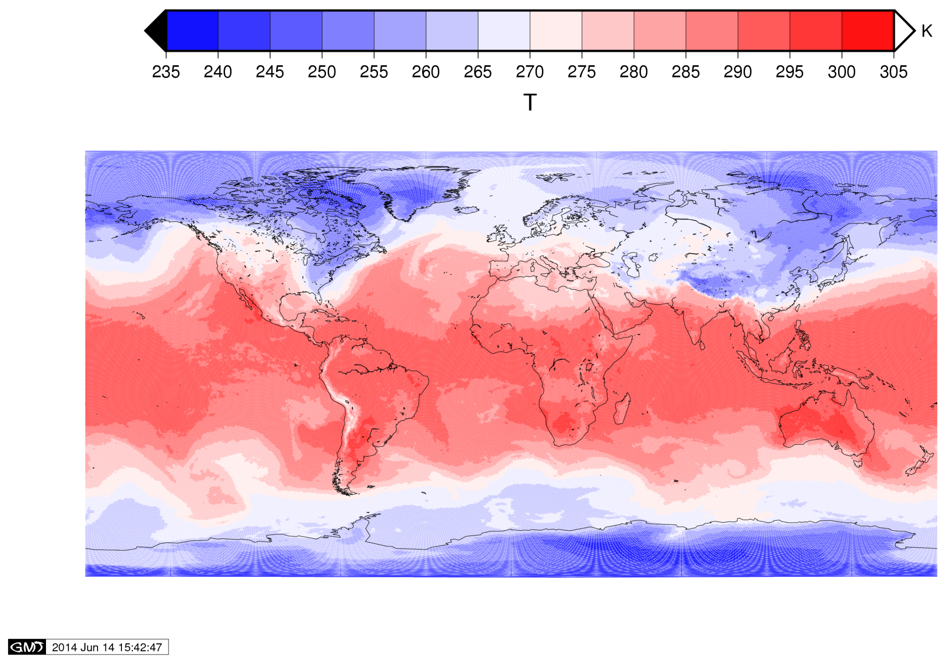

Figure 9.5.: ICON temperature field on a specific model level produced with the above GMT script.

10. ICON's Data Assimilation System and Analysis Products

In this chapter you will get to know basic components of the ICON data assimilation system. It consists of a whole collection of programs and modules both for the atmospheric variables of the model as well as for soil, snow, ice and sea surface, all collected into the *Data Assimilation Coding Environment* (DACE). The analysis products of this software package are discussed in Section 10.3.

10.1. Data Assimilation

Numerical weather prediction (NWP) is an initial value problem. The ability to make a skillful forecast heavily depends on an accurate estimate of the present atmospheric state, known as *analysis*. In general, an analysis is generated by combining, in an optimal way, all available observations with a short term forecast of a general circulation model (e.g. ICON).

Stated in a more abstract way, the basic idea of data assimilation is to fit model states x to observations y. Usually, we do not observe model quantities directly or not at the model grid points. Here, we work with *observation operators* H which take a model state and calculate a simulated observation $y = H(x)$. In terms of software, these model operators can be seen as particular modules, which operate on the ICON model states. Their output is usually written into so-called feedback files, which contain both the real observation y_{meas} with all its meta data (descriptions, positioning, further information) as well as the simulated observation $y = H(x)$.

However, data assimilation cannot be treated at one point in time only. The information passed on from the past is a crucial ingredient for any data assimilation scheme. Thus, *cycling* is an important part of data assimilation. It means that we

1. Carry out the core data assimilation component 3D-VAR to calculate the so-called *analysis* $x^{(a)}$, i.e. a state which best fits previous information and the observations y,
2. Propagate the analysis $x_k^{(a)}$ to the next analysis time t_{k+1}. Here, it is called *first guess* or *background* $x_{k+1}^{(b)}$.
3. Carry out the next analysis by running the core data assimilation component, generating $x_{k+1}^{(a)}$, then cycling the steps.

See Figure 10.1 for a schematic of the basic assimilation process.

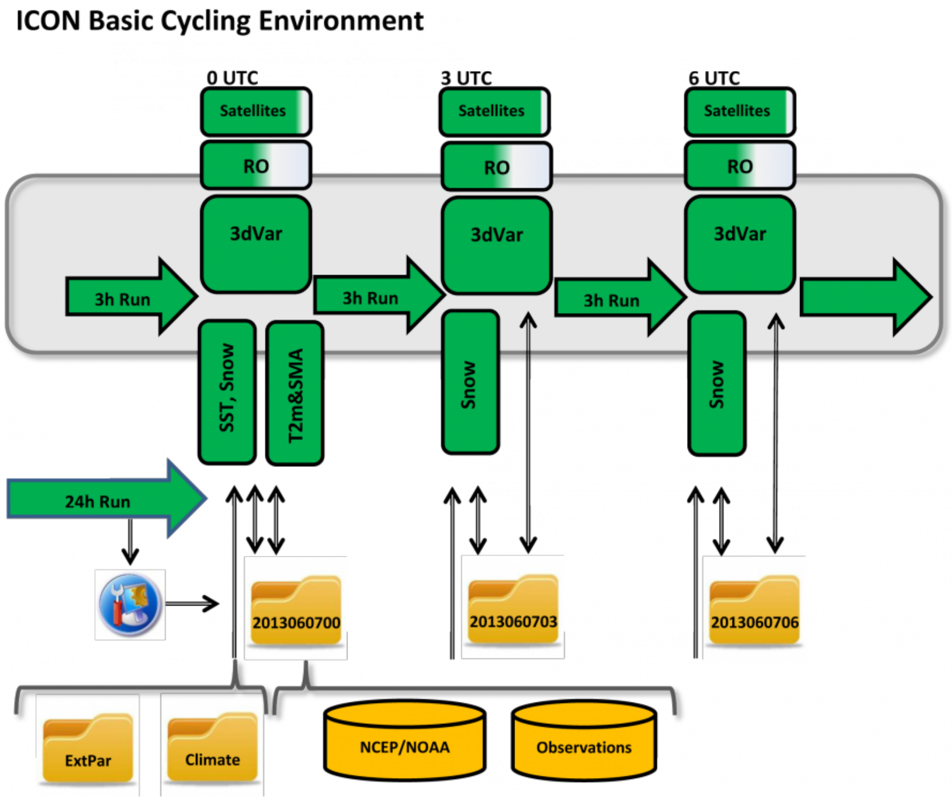

Figure 10.1.: Basic ICON cycling environment using 3D-VAR. Observations are merged with a background field taken from a 3 h forecast (first guess) of the ICON model. *Courtesy of R. Potthast, DWD.*

10.1.1. Variational Data Assimilation

The basic 3D-VAR step minimizes the functional

$$\mu(x) := \|x - x^{(b)}\|^2_{B^{-1}} + \|y - H(x)\|^2_{R^{-1}}, \tag{10.1}$$

where B is the background state distribution *covariance matrix* which is making sure that the information which is available at some place is distributed into its neighborhood properly, and R is the error covariance matrix describing the error distribution for the observations. The minimizer of (10.1) is given by

$$x^{(a)} = x^{(b)} + BH^T(R + HBH^T)^{-1}(y - H(x^{(b)}). \tag{10.2}$$

The *background* or *first guess* $x^{(b)}$ is calculated from earlier analysis by propagating the model from a state x_{k-1} at a previous analysis time t_{k-1} to the current analysis time t_k. In the data assimilation code, the minimization of (10.1) is not carried out explicitly by (10.2), but by a conjugate gradient minimization scheme, i.e. in an iterative manner, first solving the equation

$$(R + HBH^T)z_k = y - H(x_k^{(b)})$$

in observation space calculating z_k at time t_k, then projecting the solution back into model space by

$$\delta x_k = x_k^{(a)} - x_k^{(b)} = BH^T z_k.$$

We call δx_k the *analysis increment*.

The background covariance matrix B is calculated from previous model runs by statistical methods. We employ the so-called NMC method initially developed by the US weather bureau. The matrix B thus contains statistical information about the relationship between different variables of the model, which is used in each of the assimilation steps.

10.1.2. Ensemble Kalman Filter

To obtain a better distribution of the information given by observations, modern data assimilation algorithms employ a dynamical estimator for the covariance matrix (B-matrix). Given an ensemble of states $x^{(1)}, ..., x^{(L)}$, the standard stochastic covariance estimator calculates an estimate for the B-matrix by

$$B = \frac{1}{L-1} \sum\nolimits_{\ell=1}^{L} (x_k^{(\ell)} - \overline{x}_k)(x_k^{(\ell)} - \overline{x}_k)^T, \tag{10.3}$$

where $\overline{x}$ denotes the mean defined by

$$\overline{x}_k = \frac{1}{L} \sum\nolimits_{\ell=1}^{L} x_k^{(\ell)}, \quad k \in \mathbb{N}.$$

This is leading us to the *Ensemble Kalman Filter* (EnKF), where an ensemble is employed for data assimilation and the covariance is estimated by (10.3). Here, we use the name EnKF (ensemble Kalman filter) as a generic name for all methods based on the above idea.

In principle, the EnKF carries out cycling as introduced above, just that the propagation step carries out propagation of a whole *ensemble* of L atmospheric states $x_k^{(a,\ell)}$ from time t_k to time t_{k+1}, and the analysis step has to generate L new analysis members, called the *analysis ensemble* based on the *first guess* or *background ensemble* $x^{(b,\ell)}$, $\ell = 1, ..., L$.

Usually, the analysis is carried out in observation space, where a transformation is carried out. Also, working with a low number of ensemble members as it is necessary for large-scale data assimilation problems, we need to suppress spurious correlations which arise from a naive application of Eq. (10.3). This technique is known as *localization*, and the combined transform and localization method is called *localized ensemble transform Kalman filter* (LETKF), first suggested by Hunt et al. (2007).

The DWD data assimilation coding environment (DACE) provides a state-of-the-art implementation of the LETKF which is equipped with several important ingredients such as different types of covariance *inflation*. These are needed to properly take care of the *modeling error*. The original Kalman filter itself does not know what error the model has and thus by default under-estimates this error, which is counter-acted by a collection of tools.

10.1.3. Hybrid Data Assimilation

The combination of variational and ensemble methods provides many possibilities to further improve the state estimation of data assimilation. Based on the ensemble Kalman filter

LETKF the data assimilation coding environment provides a *hybrid system EnVar*, the *ensemble variational* data assimilation.

The basic idea of EnVar is to use the dynamical flow dependent ensemble covariance matrix B as a part of the three-dimensional variational assimilation. Here, localization is a crucial issue, since in the LETKF we localize in observation space, but 3D-VAR employs B in state space. Localization is carried out by a *diffusion*-type approximation in DACE.

The cycling for the EnVar needs to cycle both the ensemble $x^{(\ell)}$, $\ell = 1, ..., L$ and one deterministic state x_{det}. The resolution of the ensemble can be lower than the full deterministic resolution. By default we currently employ a 40 km grid spacing for the ensemble and a 13 km global grid spacing for the deterministic state. The ensemble B matrix is then carried over to the finer deterministic resolution by interpolation. See Section 10.2 for more details on the operational assimilation system at DWD.

10.1.4. Surface Analysis

DACE provides additional modules for Sea Surface Temperature (SST) analysis, Soil Moisture Analysis (SMA) and snow analysis. Characteristic time scales of surface and soil processes are typically larger than those of atmospheric processes. Therefore, it is often sufficient to carry out surface analysis only every 6 to 24 hours.

10.2. Assimilation Cycle at DWD

The *assimilation cycle* iterates the steps described in Section 10.1: updating a short-range ICON forecast (first guess) using the observations available for that time window to generate an analysis, from which then a new updated first guess is started.

The core assimilation for atmospheric fields is based on a hybrid system (EnVar) as described in Section 10.1.3. At every assimilation step (every 3 h) an LETKF is ran using an ensemble of ICON first guesses. Currently, the ensemble consists of 40 members with a horizontal grid spacing of 40 km and a 20 km nest over Europe. A convex linear combination of the 3D-VAR climatological and the LETKF's (flow dependent) covariance matrix is then used to run a deterministic 3D-VAR analysis at 13 km horizontal grid spacing.

In addition, the above mentioned surface modules are run: Sea Surface Temperature (SST) analysis, Soil Moisture Analysis (SMA) and snow analysis.

Note that for the ICON-EU nest no assimilation of atmospheric fields is conducted. Instead the necessary atmospheric analysis increments are interpolated from the underlying global grid. Together with the available first guess fields on the nest they form the nest analysis. A separate surface analysis, however, is conducted.

The deterministic as well as the ensemble analysis is generated 8 times a day. Based on the former, deterministic forecasts are launched at approx. 13 km horizontal grid spacing globally with a 6.5 km nest over Europe. The maximum forecast time of the whole system is limited to +30 h lead time at 03/09/15/21 UTC. Otherwise, the system is integrated up to +120 h while at 00/12 UTC the integration on the global domain (only) is prolonged to +180 h lead time.

Since the beginning of 2018 ICON ensemble forecasts are conducted as well. On the basis of the analysis ensemble 40 short to medium forecasts at 40 km globally and 20 km nested over Europe are run 8 times a day. The maximum forecast times are equivalent to those of the deterministic system (see above). The primary purpose of the ensemble forecasts is to estimate the forecast uncertainty, which arises due to uncertainties in the initial conditions and the model error.

The input, output and processes involved in the assimilation cycle are briefly described below:

Atmospheric Analysis

Fields modified by the atmospheric analysis: (see Appendix B for a description of each variable) `t`, `p`, `u`, `v`, `qv`.

Grid(s) on which it is performed: global

Carried out at every assimilation time step (3 h) using the data assimilation algorithms described in the previous sections.

Main input: First guess, observations, previous analysis error, online bias correction files.

Main output: Analysis of the atmospheric fields, analysis error, bias correction files, feedback files with information on the observation, its departures to first guess and analysis.

The system can make use of the following observations: radiosondes, weather stations, buoys, aircraft, ships, radio occultations, AMV winds and radiances. Available general features of the module are variational quality control and (variational) online bias correction. Regarding EnKF specifics, different types of inflation techniques, relaxation to prior perturbations and spread, adaptive localization, SST perturbations and SMA perturbations are available.

Snow Analysis

Fields modified by the snow analysis: (see Appendix B for a description of each variable) `freshsnow`, `h_snow`, `rho_snow`, `t_snow`, `w_i`, `w_snow`.

Grid(s) on which it is performed: global, EU-nest

Carried out at each assimilation time step (3 h).

Main input: SYNOP snow depth observations if the coverage is sufficient. If this is not the case, more sources of information are looked for until the number of observations is high enough, namely (and in this order), precipitation and 2 m temperature, direct observations (wwreports) and the NCEP external snow analysis.

Main output: Analysis of the snow fields.

Sea Surface Temperature Analysis

Fields modified by the SST analysis: (see Appendix B for a description of each variable) `fr_seaice`, `h_ice`, `t_ice`, `t_so`.

Grid(s) on which it is performed: global, EU-nest

Carried out only once a day, at 0 UTC.

Main input: NCEP analysis from the previous day (which uses satellite, buoy and ship observations, to be used as a first guess), ship and buoy observations available since the time of the NCEP analysis.

Main output: Sea surface temperature analysis and estimated error.

Soil Moisture Analysis

Fields modified by the SMA analysis: (see Appendix B for a description of each variable) `w_so`.

Grid(s) on which it is performed: global, EU-nest

Carried out only once a day, at 0 UTC.

Main input: Background fields for relevant fields at every hour since last assimilation, 2 m-temperature analysis (see below) to be used as observations.

Main output: Soil moisture analysis and estimated error.

2m Temperature Analysis

Although carried out only at 0 UTC, it is run for several time steps in between to provide the output (2 m temperature) needed by the SMA analysis. Uses observations from SYNOP stations on land and METAR information from airports.

10.3. Analysis Products

This section provides an overview of DWD's analysis products.

10.3.1. Uninitialized Analysis for IAU

In the *incremental analysis update* (IAU) method (Bloom et al., 1996, Polavarapu et al., 2004) the analysis increment is not added completely at a particular time step, but it is embedded into the model integration and added to the model states $x_k^{(b)}$ during an interval Δt, which by default is $\Delta t = 3\,\mathrm{h}$ for global forecasts. This method of tentatively pulling the model from its current state (first guess) towards the analyzed state acts as a low pass filter in the frequency domain on the analysis increments, such that small scale unbalanced modes are effectively filtered.

In the following, let us assume that we want to start a model forecast at 00 UTC. Technically, the application of the IAU method has some potential pitfalls, which the user should be aware of:

- The analysis file has to contain analysis increments (i.e. deviations from the first guess) instead of full fields, with validity time 00 UTC. The only exceptions are `FR_ICE` and `T_SEA` (or alternatively `T_SO(0)`), which must be full fields (see Table 10.1).
- The model must be started from a first guess which is shifted back in time by 1.5 h w.r.t. the analysis. Thus, in the given example, the validity time of the first guess must be 22:30 UTC of the previous day. This is because "dribbling" of the analysis increments is performed over the symmetric 3 h time window [00 UTC − 1.5h, 00 UTC + 1.5h]. See Section 5.1.3 for an illustration of this process.

Table 10.1 provides an overview of the fields contained in the *uninitialized analysis product for IAU* for 00 UTC. Columns 1 to 3 show DWD's GRIB2 shortName, the unit and a short description of the fields, respectively. Columns 4 and 5 indicate, whether the field is part of the first guess file and/or analysis file. The marker ⊗ highlights analysis increments as opposed to full fields. First guess fields which are optional for starting the model with IAU are highlighted in blue, with their scope being indicated in the description. If one or more of these fields are unavailable, a cold-start of these fields is performed given that the parameterizations for which they are needed are activated.

As explained in Section 10.2, the atmospheric analysis is performed more frequently than the surface analysis. Therefore, the analysis product at times different from 00 UTC usually contains only a subset of the fields provided at 00 UTC. Consequently, Table 10.1 will look different for non-00 UTC runs in such a way that the fields

`FR_ICE`	`T_SEA`	`W_SO`	`T_2M`

will not be provided in the analysis file. The first three fields of this list will be contained in the first guess file instead.

Table 10.1.: Content of the **uninitialized analysis product for IAU**, separated into first guess (FG) and analysis (ANA). Optional fields for model initialization are marked in blue. The marker ⊗ indicates analysis increments as opposed to full fields. Analysis fields highlighted in red are only available for 00 UTC. The validity date of the first guess is shifted back by 1.5 h w.r.t. the start date.

shortName	**Unit**	**Description**	**Source**	
			FG	**ANA**
`DEN`	$\mathrm{kg\,m^{-3}}$	air density	×	
`P`	Pa	pressure		⊗

Continued on next page

Table 10.1.: *Continued from previous page*

QC	$\mathrm{kg\,kg^{-1}}$	cloud liquid water mass fraction	×	
QI	$\mathrm{kg\,kg^{-1}}$	cloud ice mass fraction	×	
QR	$\mathrm{kg\,kg^{-1}}$	rain water mass fraction	×	
QS	$\mathrm{kg\,kg^{-1}}$	snow mass fraction	×	
QV	$\mathrm{kg\,kg^{-1}}$	water vapor mass fraction	×	⊗
T	K	air temperature		⊗
THETA_V	K	virtual potential temperature	×	
TKE	$\mathrm{m^2\,s^{-2}}$	turbulent kinetic energy	×	
U, V	$\mathrm{m\,s^{-1}}$	horizontal velocity components		⊗
VN	$\mathrm{m\,s^{-1}}$	edge normal velocity component	×	
W	$\mathrm{m\,s^{-1}}$	vertical velocity	×	
ALB_SEAICE	%	sea ice albedo scope: `lprog_albsi=.TRUE.` (namelist `lnd_nml`)	×	
C_T_LK	1	shape factor w.r.t. temp. profile in the thermocline)	×	
EVAP_PL	$\mathrm{kg\,m^{-2}}$	evaporation of plants (integrated since "nightly reset") scope: `itype_trvg=3` (namelist `lnd_nml`)	×	
FRESHSNW	1	age of snow indicator	×	⊗
FR_ICE	1	sea/lake ice fraction		×
H_ICE	m	sea ice depth	×	
H_ML_LK	m	mixed-layer thickness	×	
H_SNOW	m	snow depth	×	⊗
HSNOW_MAX	m	maximum snow depth reached within current snow-cover period scope: `itype_snowevap=3` (namelist `lnd_nml`)	×	
QV_S	$\mathrm{kg\,kg^{-1}}$	surface specific humidity	×	
RHO_SNOW	$\mathrm{kg\,m^{-3}}$	snow density	×	
SKT	K	skin temperature scope: `itype_canopy=2` (namelist `lnd_nml`)	×	
SNOAG	d	duration of current snow-cover period scope: `itype_snowevap=3` (namelist `lnd_nml`)	×	
SNOWC	%	snow cover	×	
T_BOT_LK	K	temperature at water-bottom sediment interface	×	
T_G	K	surface temperature	×	

Continued on next page

Table 10.1.: *Continued from previous page*

T_ICE	K	sea ice temperature	×	
T_MNW_LK	K	mean temperature of the water column	×	
T_SEA	K	sea surface temperature		×
T_SNOW	K	snow temperature	×	
T_WML_LK	K	mixed-layer temperature	×	
W_I	$\mathrm{kg\,m^{-2}}$	water content of interception layer	×	
Z0	m	surface roughness length	×	
T_SO	K	soil temperature	×	
T_2M	K	2 m temperature bias scope: `itype_vegetation_cycle=3` (namelist `extpar_nml`)		⊗
T_2M_FILTBIAS	K	Time-filtered T_2M bias scope: `itype_vegetation_cycle=3` (namelist `extpar_nml`)	×	
W_SO	$\mathrm{kg\,m^{-2}}$	soil water content (liq. + ice)	×	⊗
W_SO_ICE	$\mathrm{kg\,m^{-2}}$	soil ice content	×	

Please note that all GRIB2-keys of the fields `T_2M` and `T_2M_FILTBIAS` are identical, except for the key *typeOfGeneratingProcess*. In order to decode `T_2M_FILTBIAS` correctly and to distinguish it from `T_2M`, it is recommended to make use of the most recent DWD-specific GRIB definition files (see Section 1.1.2).

10.3.2. Uninitialized Analysis

The *uninitialized analysis* without IAU can be used if, for some reason, the model should be started without any noise filtering procedure. The first guess and analysis file are read in and merged by the model, i.e. the model state is abruptly pulled towards the analyzed state right before the first time integration step. This conceptually easy approach comes at the price of a massively increased noise level at the beginning of the simulation.

The validity time of the *first guess* and *analysis* must match the model's start date. Table 10.2 provides an overview of the fields contained in the *uninitialized analysis product* for 00 UTC. Columns 4 and 5 again indicate, whether a specific field is contained in the first guess file and/or analysis file. Fields which are optional for starting the model are highlighted in blue, with their scope being indicated in the description. If one or more of these fields are unavailable, a cold-start of these fields is performed given that the parameterizations for which they are needed are activated.

As already explained in the previous section, the analysis at times different from 00 UTC will only contain a subset of the fields provided at 00 UTC. Table 10.2 will differ for non-00 UTC runs in the way that the fields

FR_ICE H_ICE T_ICE T_SEA W_SO

will not be available from the analysis file but from the first guess file.

Table 10.2.: Content of the **uninitialized analysis product**, separated into first guess (FG) and analysis (ANA). Optional fields for model initialization are marked in blue. Analysis fields highlighted in red are only available for 00 UTC.

shortName	Unit	Description	Source	
			FG	ANA
DEN	$\mathrm{kg\,m^{-3}}$	air density	×	
P	Pa	pressure		×
QC	$\mathrm{kg\,kg^{-1}}$	cloud liquid water mass fraction	×	
QI	$\mathrm{kg\,kg^{-1}}$	cloud ice mass fraction	×	
QR	$\mathrm{kg\,kg^{-1}}$	rain water mass fraction	×	
QS	$\mathrm{kg\,kg^{-1}}$	snow mass fraction	×	
QV	$\mathrm{kg\,kg^{-1}}$	water vapor mass fraction		×
T	K	air temperature		×
THETA_V	K	virtual potential temperature	×	
TKE	$\mathrm{m^2\,s^{-2}}$	turbulent kinetic energy	×	
U, V	$\mathrm{m\,s^{-1}}$	horizontal velocity components		×
VN	$\mathrm{m\,s^{-1}}$	edge normal velocity component	×	
W	$\mathrm{m\,s^{-1}}$	vertical velocity	×	
ALB_SEAICE	%	sea ice albedo scope: `lprog_albsi=.TRUE.` (namelist `lnd_nml`)	×	
C_T_LK	1	shape factor w.r.t. temp. profile in the thermocline)	×	
EVAP_PL	$\mathrm{kg\,m^{-2}}$	evaporation of plants (integrated since "nightly reset") scope: `itype_trvg=3` (namelist `lnd_nml`)	×	
FRESHSNW	1	age of snow indicator		×
FR_ICE	1	sea/lake ice fraction		×
H_ICE	m	sea ice depth		×
H_ML_LK	m	mixed-layer thickness	×	
H_SNOW	m	snow depth		×
HSNOW_MAX	m	maximum snow depth reached within current snow-cover period scope: `itype_snowevap=3` (namelist `lnd_nml`)	×	
QV_S	$\mathrm{kg\,kg^{-1}}$	surface specific humidity	×	

Continued on next page

Table 10.2.: *Continued from previous page*

RHO_SNOW	kg m^{-3}	snow density	×	
SNOAG	d	duration of current snow-cover period scope: `itype_snowevap=3` (namelist `lnd_nml`)	×	
T_BOT_LK	K	temperature at water-bottom sediment interface	×	
T_G	K	surface temperature	×	
T_ICE	K	sea ice temperature		×
T_MNW_LK	K	mean temperature of the water column	×	
T_SEA	K	sea surface temperature		×
T_SNOW	K	snow temperature		×
T_WML_LK	K	mixed-layer temperature	×	
W_I	kg m^{-2}	water content of interception layer	×	
W_SNOW	kg m^{-2}	snow water equivalent	×	
Z0	m	surface roughness length	×	
T_SO	K	soil temperature	×	
W_SO	kg m^{-2}	soil water content (liq. + ice)		×
W_SO_ICE	kg m^{-2}	soil ice content	×	

10.3.3. Initialized Analysis

The *initialized analysis* is strongly related to the *uninitialized analysis for IAU*. It is a by-product of starting the model from the latter. E.g. the *initialized analysis* at 00 UTC is generated by starting the model from the 22:30 UTC first guess, and adding the analysis increments over an asymmetric time window of 1.5 h width until 00 UTC. Therefore the noise level of the initialized analysis product is comparable to that of the *uninitialized analysis product for IAU*.

For model initialization the validity time of the *initialized analysis product* must match the model's start date. Table 10.3 provides an overview of the fields contained in the *initialized analysis product* for 00 UTC. Fields which are optional for starting the model are highlighted in blue. If one or more of these fields are unavailable, a cold-start of these fields is performed given that the parameterizations for which they are needed are switched on.

Note that this product is also suitable for initializing COSMO limited area simulations. To this end it contains the atmospheric fields `T`, `P`, `U`, `V` rather than ICON's set of prognostic atmospheric variables, i.e. `THETA_V`, `RHO`, `VN`. For ICON, the necessary transformation is performed automatically during startup.

For recent analysis dates (say August 2018 and later) this analysis product contains both `SMI` and `W_SO`. For previous analysis dates only `W_SO` is available. ICON can read any of them, however `SMI` is preferred and `W_SO` is the fallback. Whenever this analysis product needs to be remapped and `SMI` is not available, it is strongly recommended to manually convert `W_SO` to `SMI` beforehand, since interpolating `W_SO` can lead to strong numerical artifacts. See Section 2.2.3 for more details.

Table 10.3.: Content of the **initialized analysis product**. Fields which are optional for model initialization are marked in blue.

shortName	Unit	Description
`P`	Pa	pressure
`QC`	$\mathrm{kg\,kg^{-1}}$	cloud liquid water mass fraction
`QI`	$\mathrm{kg\,kg^{-1}}$	cloud ice mass fraction
`QR`	$\mathrm{kg\,kg^{-1}}$	rain water mass fraction
`QS`	$\mathrm{kg\,kg^{-1}}$	snow mass fraction
`QV`	$\mathrm{kg\,kg^{-1}}$	water vapor mass fraction
`T`	K	air temperature
`TKE`	$\mathrm{m^2\,s^{-2}}$	turbulent kinetic energy
`U, V`	$\mathrm{m\,s^{-1}}$	horizontal velocity components
`W`	$\mathrm{m\,s^{-1}}$	vertical velocity
`ALB_SEAICE`	%	sea ice albedo scope: `lprog_albsi=.TRUE.` (namelist `lnd_nml`)
`C_T_LK`	1	shape factor w.r.t. temp. profile in the thermocline)
`EVAP_PL`	$\mathrm{kg\,m^{-2}}$	evaporation of plants (integrated since "nightly reset") scope: `itype_trvg=3` (namelist `lnd_nml`)
`FRESHSNW`	1	age of snow indicator
`FR_ICE`	1	sea/lake ice fraction
`H_ICE`	m	sea ice depth
`H_ML_LK`	m	mixed-layer thickness
`H_SNOW`	m	snow depth
`HSNOW_MAX`	m	maximum snow depth reached within current snow-cover period scope: `itype_snowevap=3` (namelist `lnd_nml`)
`QV_S`	$\mathrm{kg\,kg^{-1}}$	surface specific humidity
`RHO_SNOW`	$\mathrm{kg\,m^{-3}}$	snow density
`SNOAG`	d	duration of current snow-cover period scope: `itype_snowevap=3` (namelist `lnd_nml`)

Continued on next page

Table 10.3.: *Continued from previous page*

`T_BOT_LK`	K	temperature at water-bottom sediment interface
`T_G`	K	surface temperature
`T_ICE`	K	sea ice temperature
`T_MNW_LK`	K	mean temperature of the water column
`T_SNOW`	K	snow temperature
`T_WML_LK`	K	mixed-layer temperature
`W_I`	$\mathrm{kg\,m^{-2}}$	water content of interception layer
`W_SNOW`	$\mathrm{kg\,m^{-2}}$	snow water equivalent
`Z0`	m	surface roughness length
`SMI`	1	soil moisture index
`T_SO`	K	soil temperature
`W_SO`	$\mathrm{kg\,m^{-2}}$	soil water content (liq. + ice)
`W_SO_ICE`	$\mathrm{kg\,m^{-2}}$	soil ice content
`HHL`	m	vertical coordinate half level heights

Please note that in contrast to the Uninitialized Analysis for IAU product (Table 10.1) the Initialized Analysis product does not contain the skin temperature `T_SKT` and the time-filtered 2 m temperature bias `T_2M_FILTBIAS`. If the skin temperature parameterization is activated (`itype_canopy=2`) but an initial `T_SKT` is missing, `T_SKT` is initialized with the surface temperature `T_S`. It is nevertheless recommended to switch on the skin temperature parameterization. The lack of initial conditions for `T_SKT` does only have a marginal effect on the forecast quality.

Similarly, if the enhanced vegetation cycle parameterization is activated (`itype_vegetation_cycle=3`) but `T_2M_FILTBIAS` is missing, `T_2M_FILTBIAS` is initialized with zero (which effectively resembles `itype_vegetation_cycle=2`).

A. The Computer System at DWD

Available Platforms at DWD

The NEC SX-Aurora supercomputer system at DWD is one of our main platforms for the execution of the ICON-NWP model. This system consists of numerous compute nodes with corresponding cross-compilation nodes.

- `rcl.dwd.de` → `rcnl100`, `rcnl101`:
  These are the cross-compilation nodes (x86 AMD "Rome", 32 cores, 2.5 GHz), which run a Red Hat Enterprise Linux.

  They are used for **compiling and linking**, preparation of data and basic editing work. Tools for the **visualization of meteorological fields** (CDO, NCL, `ncview`) are also available here.

  The `rcl.dwd.de` nodes are not used for running parallel NWP simulations, but ICON jobs can be submitted to the NEC SX-Aurora compute nodes `vh`*`XXX`* (vector computer) or the `rcn`*`XXX`* (Linux cluster). Note that there are also big memory nodes `rcb`*`XXX`* available with a memory limit of 192G for each process.

  To compile and link applications on the routine cluster use either the `intel` or the `gnu` compiler. To compile and link targeting the NEC SX-Aurora platform the `nfort` NEC compiler must be used.

- **NEC SX-Aurora**:
  The NEC SX-Aurora research cluster has 232 **x86 vector hosts**, where each node is equipped with 8 **NEC SX-Autora 1 TSUBASA Type 10AE vector engine CPUs**. The vector hosts are AMD EPYC "Rome" processors with 24 cores, 2.8GHz, and 256 GiB memory. [1] Each vector engine achieves ca. 2.15 TFLOPS double precision peak performance and 8 computational cores. The vector nodes cannot be accessed interactively, but only by **PBS batch jobs** together with the queuing system NQSV from NEC.

  Such jobs can use up to 24 GB of main memory per vector engine.

There is a common file system across all nodes and every user has three different main directories:

- `/hpc/uhome/`*`username`* (`$HOME`)
  Directory for storing source code and scripts to run the model. This is a GPFS file system suitable for many small files.

[1]Note that 8 of these 24 x86 cores are reserved for the vector engine OS.

- `/hpc/uwork/`*`username`* (`$WORK`)
  Directory for storing larger amounts of data. For the `$WORK` (Lustre) file system there is a common quota for every user of 7.9 TBytes.
- `/hpc/gtmp/`*`username`* (Lustre file system, contains `$TMPDIR`)
  Temporary directory for storing larger amounts of data.

The Batch System for the NEC SX-Aurora

Jobs for the NEC SX-Aurora system have to be submitted from the login nodes `rcl.dwd.de`, `rcnl100`, `rcnl101` with the batch system `PBS`. Together with the source code of the programs we provide some run scripts in which all necessary batch commands are set.

Here are the most important commands for working with the `PBS`:

`qsub` *`job_name`*	submit a batch job to `PBS`.
`qstat`	query the status of all batch jobs on the NEC SX-Aurora. You can see whether jobs are `Q` (queued) or `R` (running). You have to submit jobs to the queue `sx_norm`.
`qstat -u` *`user`*	query the status of all your batch jobs on the machine.
`qdel` *`job_nr`*`@`*`machine`*	cancel your job(s) from the batch queue of a machine. The *job_nr* is given by `qstat -w`.
`qcat -o -f` *`job_nr`*`@`*`machine`*	follow stdout and stderr interactively.

For the vector engines you have to use the queue `sx_norm`. Here are some important PBS options.

`#PBS -q` *`queue`*	define the queue
`#PBS -T necmpi`	necessary for MPI jobs
`#PBS -l cpunum_job=1`	No. of Xeon cores used on VH
`#PBS -l elapstim_req=3600`	Time limit 1 hour
`#PBS -l coresz_prc=0`	limit on max. core file size
`#PBS --venum-lhost=8`	No. of VE per logical host; max is 8
`#PBS -b` *`#logical hosts`*	Number of logical hosts
`#PBS --use-hca=2`	necessary (no. host channel adapters per logical host)
`#PBS -v` *`N1=var1,N2=var2`*	define environment variables

In your run scripts, execution begins in your home directory, regardless of what directory your script resides in or where you submitted the job from. You can use the `cd` command to change to a different directory. The environment variable `$PBS_O_WORKDIR` makes it easy to return to the directory from which you submitted the job:

```
cd $PBS_O_WORKDIR
```

To start a parallel executable, the `mpirun` command has to be used:

```
mpirun -nn #nodes -ve 0-7 -np #PEs /path/to/application
```

Here the options have the following meaning:

`-nn`	number of vector hosts
`-ve`	number of vector engines used: here all 8 vector engines of a node are used
`-np`	total number of processing elements.

More detailed information and documentation to the NEC SX-Aurora and related software can be found on the NEC web pages: `https://www.hpc.nec/documentation`

A. DWD HPC System

B. Table of ICON Output Variables

The following table contains the NWP variables available for output[1]. Please note that the field names are following an ICON-internal nomenclature, see Section 7.1 for details. The list also contains tile-based fields (suffix _t_1, _t_2, ...) which are summarized as _t_*.

By "ICON-internal" variable names, we denote those field names that are provided as the string argument `name` to the subroutine calls `CALL add_var(...)` and `CALL add_ref(...)` inside the ICON source code. These subroutine calls have the purpose to register new variables, to allocate the necessary memory, and to set the meta-data for these variables.

Variable Name	GRIB2 Name	Description
acdnc	ndcloud	Cloud droplet number concentration
adrag_u_grid		Zonal resolved surface stress mean since model start
adrag_v_grid		Meridional resolved surface stress mean since model start
aer_bc	aer_bc	Black carbon aerosol
aer_du	aer_dust	Total soil dust aerosol
aer_or	aer_org	Organic aerosol
aer_ss	aer_ss	Sea salt aerosol
aer_su	aer_so4	Total sulfate aerosol
aercl_bc		Black carbon aerosol climatology
aercl_du		Total soil dust aerosol climatology
aercl_or		Organic aerosol climatology
aercl_ss		Sea salt aerosol climatology
aercl_su		Total sulfate aerosol climatology
alb_dif	alb_dif	Shortwave albedo for diffuse radiation
alb_si	alb_seaice	Sea ice albedo (diffuse)
albdif_t_*	alb_rad	Tile-based shortwave albedo for diffusive radiation
albdif	alb_rad	Shortwave albedo for diffuse radiation
albni_dif	alb_ni	Near IR albedo for diffuse radiation
albnirdif_t_*	alb_ni	Tile-based near IR albedo for diffuse radiation
albnirdif	alb_ni	Near IR albedo for diffuse radiation
albnirdir	alnip	Near IR albedo for direct radiation
albuv_dif	alb_uv	UV visible albedo for diffuse radiation
albvisdif_t_*	alb_uv	Tile-based UV visible albedo for diffusive radiation
albvisdif	alb_uv	UV visible albedo for diffuse radiation
albvisdir	aluvp	UV visible albedo for direct radiation
alhfl_bs	alhfl_bs	Latent heat flux from bare mean since model start
alhfl_pl	alhfl_pl	Latent heat flux from plantmean since model start
alhfl_s	alhfl_s	surface latent heat flux mean since model start
aqhfl_s	evapt	surface moisture flux mean since model start
ashfl_s	ashfl_s	Surface sensible heat flux mean since model start

Continued on next page

[1]The Table B.1 in this Appendix is based on the revision state `77cdb449` (2019-02-27).

Table B.1 – *Continued from previous page*

Variable Name	GRIB2 Name	Description
asob_s	asob_s	Surface net solar radiation mean since model start
asob_t	asob_t	TOA net solar radiation mean since model start
asobclr_s	nswrfcs	Clear-sky surface net solar radiation mean since model start
asod_s	asod_s	Surface down solar rad. mean since model start
asod_t	sodt_rad	Top down solar radiation mean since model start
asodifd_s	aswdifd_s	Surface down solar diff. rad. mean since model start
asodifu_s	aswdifu_s	Surface up solar diff. rad. mean since model start
asodird_s	aswdir_s	Surface down solar direct rad.mean since model start
asou_t	uswrf	Top up solar radiation mean since model start
astr_u_sso	lgws	Zonal sso surface stress mean since model start
astr_v_sso	mgws	Meridional sso surface stress mean since model start
aswflx_par_sfc	apab_s	Downward PAR flux mean since model start
athb_s	athb_s	Surface net thermal radiation mean since model start
athb_t	athb_t	TOA net thermal radiation mean since model start
athbclr_s	nlwrcs	Clear-sky surface net thermal radiation mean since model start
athd_s	athd_s	Surface down thermal radiationmean since model start
athu_s	athu_s	Surface up thermal radiation mean since model start
aumfl_s	aumfl_s	U-momentum flux flux at sumean since model start
avg_qc	tqc_dia	Tci specific cloud water content (diagnostic) avg
avg_qi	tqi_dia	Tci specific cloud ice content (diagnostic) avg
avg_qv	tqv_dia	Column integrated water vapour (diagnostic) avg
avmfl_s	avmfl_s	V-momentum flux flux at sumean since model start
bvf2		Square of Brunt-Vaisala frequency
c_t_lk	c_t_lk	Shape factor (temp. profile in lake thermocline)
cape_ml	cape_ml	Cape of mean surface layer parcel
cape	cape_con	Conv avail pot energy
ceiling	ceiling	Ceiling height
cin_ml	cin_ml	Convective inhibition of mean surface layer parcel
clch	clch	High level clouds
clcl	clcl	Low level clouds
clcm	clcm	Mid level clouds
clct_avg	clct	Total cloud cover time avg
clct_mod	clct_mod	Modified total cloud cover for media
clct	clct	Total cloud cover
clc	clc	Cloud cover
cldepth	cldepth	Modified cloud depth for media
cloud_num		Cloud droplet number concentration
con_gust		Convective contribution to wind gust
cosmu0	uvcossza	Cosine of solar zenith angle
dbz_850	dbz_850	Reflectivity in approx. 850 hPa
dbz_cmax	dbz_cmax	Column maximum reflectivity
dbz_ctmax	dbz_ctmax	Column and time maximum reflectivity during the last 01H
dbz	dbz	Radar reflectivity in dBZ
ddqz_z_full_e		Metrics functional determinant (edge)

Continued on next page

Table B.1 – *Continued from previous page*

Variable Name	**GRIB2 Name**	**Description**
ddqz_z_full		Metrics functional determinant
ddqz_z_half		Metrics functional determinant
ddt_adv_q*		Advective tracer tendency
ddt_exner_phy		Exner pressure physical tendency
ddt_grf_q*		Tracer tendency for grid refinement
ddt_pres_sfc	dpsdt	Surface pressure tendency
ddt_qc_conv		Convective tendency of cloud water mass density
ddt_qc_gscp		Microphysics tendency of specific cloud water
ddt_qc_turb		Turbulence tendency of specific cloud water
ddt_qg_gscp		Microphysics tendency of graupel
ddt_qi_conv		Convective tendency of cloud ice mass density
ddt_qi_gscp		Microphysics tendency of specific cloud ice
ddt_qi_turb		Turbulence tendency of specific cloud ice
ddt_qr_conv		Convective tendency of rain mass density
ddt_qr_gscp		Microphysics tendency of rain
ddt_qs_conv		Convective tendency of snow mass density
ddt_qs_gscp		Microphysics tendency of snow
ddt_qv_conv		Convective tendency of absolute humidity
ddt_qv_gscp		Microphysics tendency of specific humidity
ddt_qv_turb	qtendt	Turbulence tendency of specific humidity
ddt_temp_drag	ttends	Sso + gwdrag temperature tendency
ddt_temp_dyn		Dynamical temperature tendency
ddt_temp_gscp		Microphysical temperature tendency
ddt_temp_pconv	dt_con	Convective temperature tendency
ddt_temp_radlw	thhr_rad	Long wave radiative temperature tendency
ddt_temp_radsw	sohr_rad	Short wave radiative temperature tendency
ddt_temp_turb	ttendts	Turbulence temperature tendency
ddt_tke_hsh	dtke_hsh	TKE tendency horizonzal shear production
ddt_tke_pconv	dtke_con	TKE tendency due to sub-grid scale convection
ddt_tke	tketens	Tendency of turbulent velocity scale
ddt_u_gwd	ewgd	GWD tendency of zonal wind
ddt_u_pconv	du_con	Convective tendency of zonal wind
ddt_u_sso	du_sso	Sso tendency of zonal wind
ddt_u_turb	utendts	Turbulence tendency of zonal wind
ddt_v_gwd	nsgd	GWD tendency of meridional wind
ddt_v_pconv	dv_con	Convective tendency of meridional wind
ddt_v_sso	dv_sso	Sso tendency of meridional wind
ddt_v_turb	vtendts	Turbulence tendency of meridional wind
ddt_vn_adv		Advective normal wind tendency
ddt_vn_phy		Normal wind physical tendency
ddt_w_adv		Advective vertical wind tendency
ddxn_z_full		Terrain slope in normal direction
ddxt_z_full		Terrain slope in tangential direction
depth_lk	depth_lk	Lake depth
dgeopot_mc	fi	Geopotential difference between half levels
div_ic		Divergence at half levels
div	rdiv	Divergence
dp_bs_lk		Depth of thermally active layer of bot. sediments.

Continued on next page

Table B.1 – *Continued from previous page*

Variable Name	GRIB2 Name	Description
dpres_mc		Pressure thickness
drag_u_grid		Zonal resolved surface stress
drag_v_grid		Meridional resolved surface stress
dtheta_v_ic_ubc		Potential temperature at child upper boundary
dvn_ie_int		Normal velocity at parent interface level
dvn_ie_ubc		Normal velocity at child upper boundary
dw_ubc		Vertical velocity at child upper boundary
dwdx		Zonal gradient of vertical wind
dwdy		Meridional gradient of vertical wind
dyn_gust		Dynamical gust
eai		(evaporative) earth area index
echotopinm	echotopinm	Maximum height of exceeding radar reflectivity threshold during the last 01H
echotop	echotop	Minimum pressure of exceeding radar reflectivity threshold during the last 01H
emis_rad	emis_rad	Longwave surface emissivity
exner_dyn_incr		Exner dynamics increment
exner_pr	exner	Exner perturbation pressure
exner_ref_mc		Reference atmosphere field exner
exner	exner	Exner pressure
fetch_lk	fetch_lk	Wind fetch over lake
fis	fis	Geopotential (s)
for_d	for_d	Fraction of deciduous forest
fr_glac		Fraction glacier
fr_lake	fr_lake	Fraction lake
fr_land	fr_land	Fraction land
fr_seaice	fr_ice	Fraction of sea ice
frac_t_*	fr_luc	Tile point area fraction list
freshsnow_t_*	freshsnw	Indicator for age of snow in top of snow layer
freshsnow	freshsnw	Weighted indicator for age of snow in top of snow layer
gamso_lk		Attenuation coefficient of lake water with respect to sol. rad.
geopot_agl_ifc	fi	Geopotential above groundlevel at cell center
geopot_agl	fi	Geopotential above groundlevel at cell center
geopot	fi	Geopotential at full level cell centre
graupel_gsp_rate	prg_gsp	Gridscale graupel rate
graupel_gsp	grau_gsp	Gridscale graupel
grf_tend_mflx		Normal mass flux tendency (grid refinement)
grf_tend_rho		Density tendency (grid refinement)
grf_tend_thv		Virtual potential temperature tendency (grid refinement)
grf_tend_vn		Normal wind tendency (grid refinement)
grf_tend_w		Vertical wind tendency (grid refinement)
gust10	vmax_10m	Gust at 10 m during the last 01H
gz0_t_*	z0	Tile-based roughness length times gravity
gz0	z0	Roughness length
h_b1_lk	h_b1_lk	Thickness of the upper layer of the sediments
h_ice	h_ice	Sea/lake-ice depth

Continued on next page

Table B.1 – *Continued from previous page*

Variable Name	GRIB2 Name	Description
h_ml_lk	h_ml_lk	Mixed-layer thickness
h_snow_lk		Depth of snow on lake ice
h_snow_si		Depth of snow on sea ice
h_snow_t_*	h_snow	Snow height
h_snow	h_snow	Weighted snow depth
hbas_con	hbas_con	Height of convective cloud base
hbas_sc	hbas_sc	Cloud base above msl, shallow convection
hdef_ic		Deformation
hfl_q*		Horizontal tracer flux
hmo3		Height of O3 maximum (Pa)
htop_con	htop_con	Height of convective cloud top
htop_dc	htop_dc	Height of top of dry convection
htop_sc	htop_sc	Cloud top above msl, shallow convection
hzerocl	hzerocl	Height of 0 deg C level
k400		Level index corresponding to the HAG of the 400hPa level
k700		Level index corresponding to the HAG of the 700hPa level
k800		Level index corresponding to the HAG of the 800hPa level
k850		Level index corresponding to the HAG of the 850hPa level
k950		Level index corresponding to the HAG of the 950hPa level
ktype		Type of convection
l_pat		Effective length scale of circulation patterns
lai	lai	Leaf Area Index
lc_class_t_*	luc	Tile point land cover class
lhfl_bs_t_*		Tile-based latent heat flux from bare soil
lhfl_bs		Latent heat flux from bare soil
lhfl_pl_t_*		Tile-based latent heat flux from plants
lhfl_pl		Latent heat flux from plants
lhfl_s_t_*	lhfl_s	Tile-based surface latent heat flux
lhfl_s	lhfl_s	Surface latent heat flux
lpi_max	lpi_max	Lightning potential index, maximum during the last 01H
lpi	lpi	Lightning potential index (LPI)
lw_emiss	emis_rad	Longwave surface emissivity
lwflx_dn_clr		Longwave downward clear-sky flux
lwflx_dn		Longwave downward flux
lwflx_up_clr		Longwave upward clear-sky flux
lwflx_up		Longwave upward flux
lwflxall	nlwrf	Longwave net flux
mask_mtnpoints_g		Mask field for mountain points
mask_mtnpoints		Mask field for mountain points
mass_fl_e_sv		Storage field for horizontal mass flux at edges
mass_fl_e		Horizontal mass flux at edges
ndvi_max		NDVI yearly maximum
ndviratio	ndviratio	(monthly) proportion of actual value/maximum NDVI (at init time)
o3	o3	Ozone mixing ratio
omega_z	relv	Vertical vorticity

Continued on next page

Table B.1 – *Continued from previous page*

Variable Name	GRIB2 Name	Description
omega	omega	Vertical velocity
parcelfreq2		Square of air parcel oscillation frequency
pat_len		Length scale of sub-grid scale roughness elements
plcov_t_*	plcov	Plant covering degree in the vegetation phase
plcov	plcov	Plant covering degree in the vegetation phase
prec_con_rate_avg	cprat	Convective precip rate, time average
prec_con	prec_con	Convective precip
prec_gsp_rate_avg	lsprate	Gridscale precip rate, time average
prec_gsp	prec_gsp	Gridscale precip
pref_aerdis		Reference pressure used for vertical distribution of aerosol optical depths
pres_ifc	p	Pressure at half level
pres_msl	pmsl	Mean sea level pressure
pres_sfc	ps	Surface pressure
pres	p	Pressure
psl_m	pmsl	Mean sea level pressure (time mean)
pv	pot_vortic	Potential vorticity
q_int*		Q at parent interface level
q_sedim	q_sedim	Specific content of precipitation particles
q_ubc*		Q at child upper boundary
qcfl_s		Surface cloud water deposition flux due to diffusion
qc	qc	Specific cloud water content
qg	qg	Specific graupel content
qhfl_s_t_*	evapt	Tile based surface moisture flux
qhfl_s	evapt	Surface moisture flux
qifl_s		Surface cloud ice deposition flux due to diffusion
qi	qi	Specific cloud ice content
qr	qr	Rain mixing ratio
qs	qs	Snow mixing ratio
qv_2m	qv_2m	Specific water vapor content in 2m
qv_s_t_*	qv_s	Specific humidity at the surface
qv_s	qv_s	Specific humidity at the surface
qv	qv	Specific humidity
rain_con_rate_3d	prr_con	3d convective rain rate
rain_con_rate	prr_con	Convective rain rate
rain_con	rain_con	Convective rain
rain_gsp_rate	prr_gsp	Gridscale rain rate
rain_gsp	rain_gsp	Gridscale rain
rain_upd		Rain in updroughts
rcld		Standard deviation of the saturation deficit
rh_2m_land	relhum_2m_l	Relative humidity in 2m over land fraction
rh_2m	relhum_2m	Relative humidity in 2m
rho_ic	den	Density at half level
rho_ref_mc		Reference atmosphere field density
rho_ref_me		Reference atmosphere field density
rho_snow_t_*	rho_snow	Snow density
rho_snow	rho_snow	Weighted snow density

Continued on next page

Table B.1 – *Continued from previous page*

Variable Name	**GRIB2 Name**	**Description**
rho	den	Density
rh	relhum	Relative humidity
rootdp	rootdp	Root depth of vegetation
rsmin	rsmin	Minimal stomata resistence
rstom	rstom	Stomatal resistance
runoff_g_t_*	watr	Soil water runoff; sum over forecast
runoff_g	runoff_g	Weighted soil water runoff; sum over forecast
runoff_s_t_*	watr	Surface water runoff; sum over forecast
runoff_s	runoff_s	Weighted surface water runoff; sum over forecast
sai		Surface area index
sdi2	sdi_2	Supercell detection index (SDI2)
shfl_s_t_*	shfl_s	Tile-based surface sensible heat flux
shfl_s	shfl_s	Surface sensible heat flux
skinc	skc	Skin conductivity
slope_angle		Slpe angle
slope_azimuth		Slpe azimuth
smi	smi	Soil moisture index
snow_con_rate_3d	prs_con	3d convective snow rate
snow_con_rate	prs_con	Convective snow rate
snow_con	snow_con	Convective snow
snow_gsp_rate	prs_gsp	Gridscale snow rate
snow_gsp	snow_gsp	Gridscale snow
snowfrac_lc_t_*	snowc	Tile-based snow-cover fraction
snowfrac_lcu_t_*		Tile-based snow-cover fraction
snowfrac_lc	snowc	Snow-cover fraction
snowfrac_t_*		Local tile-based snow-cover fraction
snowfrac		Snow-cover fraction
snowlmt	snowlmt	Height of snow fall limit above MSL
sob_s_t_*	sobs_rad	Tile-based shortwave net flux at surface
sob_s	sobs_rad	Shortwave net flux at surface
sob_t	sobt_rad	Shortwave net flux at TOA
sobclr_s	nswrfcs	Net shortwave clear-sky flux at suface
sod_t	sodt_rad	Downward shortwave flux at TOA
sodifd_s	swdifds_rad	Shortwave diffuse downward flux at surface
soiltyp	soiltyp	Soil type
sou_s	swdifus_rad	Shortwave upward flux at surface
sou_t	uswrf	Shortwave upward flux at TOA
sp_10m	sp_10m	Wind speed in 10m
sso_gamma	sso_gamma	Anisotropy of sub-gridscale orography
sso_sigma	sso_sigma	Slope of sub-gridscale orography
sso_stdh_raw		Standard deviation of sub-grid scale orography
sso_stdh	sso_stdh	Standard deviation of sub-grid scale orography
sso_theta	sso_theta	Angle of sub-gridscale orography
str_u_sso	lgws	Zonal sso surface stress
str_v_sso	mgws	Meridional sso surface stress
swflx_dn_clr		Shortave downward clear-sky flux
swflx_dn		Shortave downward flux
swflx_par_sfc	pabs_rad	Downward photosynthetically active flux at surface

Continued on next page

Table B.1 – *Continued from previous page*

Variable Name	GRIB2 Name	Description
swflx_up_clr		Shortave upward clear-sky flux
swflx_up		Shortave upward flux
t_2m_land	t_2m_l	Temperature in 2m over land fraction
t_2m	t_2m	Temperature in 2m
t_b1_lk	t_b1_lk	Temperature at the bottom of the upper layer of the sediments
t_bot_lk	t_bot_lk	Temperature at the water-bottom sediment interface
t_bs_lk		Clim. temp. at bottom of thermally active layer of sediments
t_cl	t_2m_cl	CRU near surface temperature climatology
t_g_t_*	t_g	Weighted surface temperature
t_g	t_g	Weighted surface temperature
t_ice	t_ice	Sea/lake-ice temperature
t_mnw_lk	t_mnw_lk	Mean temperature of the water column
t_s_t_*	t_s	Temperature of ground surface
t_seasfc	t_sea	Sea surface temperature
t_sk_t_*	skt	Skin temperature
t_sk	skt	Skin temperature
t_snow_lk		Temperature of snow on lake ice
t_snow_si		Temperature of snow on sea ice
t_snow_t_*	t_snow	Temperature of the snow-surface
t_snow	t_snow	Weighted temperature of the snow-surface
t_so_t_*	t_so	Soil temperature (main level)
t_so	t_so	Weighted soil temperature (main level)
t_s	t_s	Weighted temperature of ground surface
t_tilemax_inst_2m	t_2m	Instantaneous temperature in 2m, maximum over tiles
t_tilemin_inst_2m	t_2m	Instantaneous temperature in 2m, minimum over tiles
t_wml_lk	t_wml_lk	Mixed-layer temperature
tai		Transpiration area index
tch_t_*	tch	Tile-based turbulent transfer coefficients for heat
tch	tch	Turbulent transfer coefficients for heat
tcm_t_*	tcm	Tile-based turbulent transfer coefficients for momentum
tcm	tcm	Turbulent transfer coefficients for momentum
tcond10_max	tcond10_mx	Total column-integrated condensate above z(T=-10 degC), max. during the last 01H
tcond_max	tcond_max	Total column-integrated condensate, max. during the last 01H
td_2m_land	td_2m_l	Dew-point in 2m over land fraction
td_2m	td_2m	Dew-point in 2m
temp_ifc	t	Temperature at half level
tempv	vtmp	Virtual temperature
temp	t	Temperature
tfh		Factor of laminar transfer of scalars
tfm		Factor of laminar transfer of momentum
tfv_t_*	nswrs	Tile-based laminar reduction factor for evaporation
tfv		Laminar reduction factor for evaporation
thb_s_t_*	thbs_rad	Tile-based longwave net flux at surface
thb_s	thbs_rad	Longwave net flux at surface

Continued on next page

Table B.1 – *Continued from previous page*

Variable Name	GRIB2 Name	Description
thb_t	thbt_rad	Thermal net flux at TOA
thbclr_s	nlwrcs	Net longwave clear-sky flux at suface
theta_ref_ic		Reference atmosphere field theta
theta_ref_mc		Reference atmosphere field theta
theta_ref_me		Reference atmosphere field theta
theta_v_ic	theta_v	Virtual potential temperature at half levels
theta_v	theta_v	Virtual potential temperature
thu_s	thus_rad	Longwave upward flux at surface
tke	tke	Turbulent kinetic energy
tkr_t_*		Tile-based turbulent reference surface diffusion coefficient
tkred_sfc		Reduction factor for minimum diffusion coefficients
tkr		Turbulent reference surface diffusion coefficient
tkvh	tkvh	turbulent diffusion coefficients for heat
tkvm	tkvm	turbulent diffusion coefficients for momentum
tmax_2m	tmax_2m	Max 2m temperature
tmin_2m	tmin_2m	Min 2m temperature
topography_c	hsurf	Geometric height of the earths surface above sea level
tot_prec_rate_avg	tot_pr	Total precip rate, time average
tot_prec	tot_prec	Total precip
tot_qc_dia	qc_dia	Total specific cloud water content (diagnostic)
tot_qi_dia	qi_dia	Total specific cloud ice content (diagnostic)
tot_qv_dia	qv_dia	Total specific humidity (diagnostic)
tqc_dia	tqc_dia	Total column integrated cloud water (diagnostic)
tqc	tqc	Total column integrated cloud water
tqg	tqg	Total column integrated graupel
tqi_dia	tqi_dia	Total column integrated cloud ice (diagnostic)
tqi	tqi	Total column integrated cloud ice
tqr	tqr	Total column integrated rain
tqs	tqs	Total column integrated snow
tqv_dia	tqv_dia	Total column integrated water vapour (diagnostic)
tqv	tqv	Total column integrated water vapour
tracer_vi_avg*		Average of vertically integrated tracers
trsolall		Shortwave net tranmissivity
tsfc_ref		Reference surface temperature
tsfctrad		Surface temperature at trad
tvh_t_*		Tile-based turbulent transfer velocity for heat
tvh		Turbulent transfer velocity for heat
tvm_t_*		Tile-based turbulent transfer velocity for momentum
tvm		Turbulent transfer velocity for momentum
twater	twater	Total column integrated water
u_10m_t_*	u_10m	Tile-based zonal wind in 2m
u_10m	u_10m	Zonal wind in 10m
uh_max	uh_max	Updraft helicity, max. during the last 01H
umfl_s_t_*	umfl_s	U-momentum flux at the surface
umfl_s	umfl_s	U-momentum flux at the surface
u	u	Zonal wind
v_10m_t_*	v_10m	Tile-based meridional wind in 2m

Continued on next page

Table B.1 – *Continued from previous page*

Variable Name	GRIB2 Name	Description
v_10m	v_10m	Meridional wind in 10m
vfl_q*		Vertical tracer flux
vio3	tozne	Vertically integrated ozone amount
vmfl_s_t_*	vmfl_s	V-momentum flux at the surface
vmfl_s	vmfl_s	V-momentum flux at the surface
vn_ie	vn	Normal wind at half level
vn	vn	Velocity normal to edge
vor_u	vortic_u	Zonal component of relative vorticity
vor_v	vortic_v	Meridional component of relative vorticity
vorw_ctmax	vorw_ctmax	Maximum rotation amplitude during the last 01H
vor	relv	Vorticity
vt	vt	Tangential-component of wind
vwind_expl_wgt		Explicit weight in vertical wind solver
vwind_impl_wgt		Implicit weight in vertical wind solver
v	v	Meridional wind
w_concorr_c		Contravariant vertical correction
w_ctmax	w_ctmax	Maximum updraft track during the last 01H
w_i_t_*	w_i	Weighted water content of interception water
w_i	w_i	Weighted water content of interception water
w_snow_t_*	w_snow	Water equivalent of snow
w_snow	w_snow	Weighted water equivalent of snow
w_so_ice_t_*	w_so_ice	Ice content
w_so_ice	w_so_ice	Ice content
w_so_t_*	w_so	Total water content (ice + liquid water)
w_so	w_so	Total water content (ice + liquid water)
wap_m	omega	Vertical velocity (time mean)
ww	ww	Significant weather
w	w	Vertical velocity
z_ifc	hhl	Geometric height at half level center
z_mc	h	Geometric height at full level center

List of ICON Variable Groups

The "group:" keyword for the namelist parameters ml_varlist, hl_varlist, pl_varlist (namelist output_nml) can be used to activate a set of common variables for output at once. The following lists contain the variables for each of these groups (empty groups and groups with only a single entry are omitted).

Group ADDITIONAL_PRECIP_VARS
cape, clct, clct_mod, prec_con_rate_avg, prec_gsp_rate_avg, tqc_dia, tqi_dia, tqv_dia

Group ATMO_DERIVED_VARS
div, omega, omega_z, vor

Group ATMO_ML_VARS
pres, qc, qg, qi, qr, qs, qv, temp, tke, u, v, w

Group ATMO_PL_VARS
qc, qg, qi, qr, qs, qv, temp, tke, u, v, w

Group ATMO_TIMEMEAN
psl_m, wap_m

Group ATMO_ZL_VARS
pres, qc, qg, qi, qr, qs, qv, temp, tke, u, v, w

Group CLOUD_DIAG
clc, tot_qc_dia, tot_qi_dia, tot_qv_dia

Group DWD_FG_ATM_VARS
pres, pres_sfc, qc, qg, qi, qr, qs, qv, rho, t_2m, td_2m, temp, theta_v, tke, u, u_10m, v, v_10m, vn, w, z_ifc

Group DWD_FG_SFC_VARS
alb_si, c_t_lk, fr_land, fr_seaice, freshsnow, gz0, h_ice, h_ml_lk, h_snow, qv_s, rho_snow, snowfrac_lc, t_bot_lk, t_g, t_ice, t_mnw_lk, t_seasfc, t_sk, t_snow, t_so, t_wml_lk, w_i, w_snow, w_so, w_so_ice

Group DWD_FG_SFC_VARS_T
freshsnow_t_*, h_snow_t_*, qv_s_t_*, rho_snow_t_*, snowfrac_lc_t_*, t_g_t_*, t_sk_t_*, t_snow_t_*, t_so_t_*, w_i_t_*, w_snow_t_*, w_so_ice_t_*, w_so_t_*

Group ICON_LBC_VARS
pres, qc, qi, qr, qs, qv, temp, tke, u, v, w, z_ifc

Group LAND_TILE_VARS
h_snow_t_*, qv_s_t_*, rho_snow_t_*, snowfrac_lc_t_*, snowfrac_t_*, t_g_t_*, t_s_t_*, t_sk_t_*, t_snow_t_*, t_so_t_*, w_i_t_*, w_snow_t_*, w_so_ice_t_*, w_so_t_*

Group LAND_VARS
qv_s, rho_snow, snowfrac, snowfrac_lc, t_g, t_snow, t_so, w_i, w_snow, w_so, w_so_ice

Group LATBC_PREFETCH_VARS
pres, pres_sfc, qc, qg, qi, qr, qs, qv, rho, temp, theta_v, u, v, vn, w, z_ifc

Group MODE_COMBINED_IN
fr_seaice, freshsnow, h_ice, h_snow, qv_s, rho_snow, t_g, t_ice, t_snow, t_so, w_i, w_snow, w_so

Group MODE_COSMO_IN
alb_si, freshsnow, h_ice, qv_s, rho_snow, t_g, t_ice, t_snow, t_so, w_i, w_snow, w_so

Group MODE_DWD_ANA_IN
fr_seaice, freshsnow, h_ice, h_snow, pres, qv, t_ice, t_seasfc, t_snow, t_so, temp, u, v, w_so

Group MODE_DWD_FG_IN
alb_si, c_t_lk, gz0, h_ml_lk, qc, qg, qi, qr, qs, qv_s, rho, rho_snow, t_bot_lk, t_g, t_mnw_lk, t_sk, t_so, t_wml_lk, theta_v, tke, vn, w, w_i, w_snow, w_so_ice, z_ifc

Group MODE_IAU_ANAATM_IN
pres, qc, qi, qr, qs, qv, temp, u, v

Group MODE_IAU_ANA_IN
fr_seaice, freshsnow, h_snow, pres, qc, qi, qr, qs, qv, t_seasfc, t_so, temp, u, v, w_so

Group MODE_IAU_FG_IN
alb_si, c_t_lk, freshsnow, gz0, h_ice, h_ml_lk, h_snow, qc, qg, qi, qr, qs, qv, qv_s, rho, rho_snow, snowfrac_lc, t_bot_lk, t_g, t_ice, t_mnw_lk, t_sk, t_snow, t_so, t_wml_lk, theta_v, tke, vn, w, w_i, w_so, w_so_ice

Group MODE_IAU_OLD_ANA_IN
fr_seaice, freshsnow, h_snow, pres, qv, rho_snow, t_seasfc, t_so, temp, u, v, w_snow, w_so

Group MODE_IAU_OLD_FG_IN
alb_si, c_t_lk, gz0, h_ice, h_ml_lk, qc, qg, qi, qr, qs, qv, qv_s, rho, t_bot_lk, t_g, t_ice, t_mnw_lk, t_snow, t_so, t_wml_lk, theta_v, tke, vn, w, w_i, w_so, w_so_ice

Group MODE_INIANA
alb_si, c_t_lk, fr_land, fr_seaice, freshsnow, gz0, h_ice, h_ml_lk, h_snow, pres, qc, qi, qr, qs, qv, qv_s, rho_snow, smi, t_bot_lk, t_g, t_ice, t_mnw_lk, t_snow, t_so, t_wml_lk, temp, tke, u, v, w, w_i, w_snow, w_so_ice, z_ifc

Group NH_PROG_VARS
exner, rho, theta_v, vn

Group PBL_VARS
alhfl_s, aqhfl_s, ashfl_s, gust10, lhfl_bs, lhfl_s, qhfl_s, qv_2m, shfl_s, t_2m, t_2m_land, tch, tcm, td_2m, td_2m_land, tkr, tkvh, tkvm, tvh, tvm, u_10m, v_10m

Group PHYS_TENDENCIES
ddt_qc_conv, ddt_qc_gscp, ddt_qc_turb, ddt_qg_gscp, ddt_qi_conv, ddt_qi_gscp, ddt_qi_turb, ddt_qr_conv, ddt_qr_gscp, ddt_qs_conv, ddt_qs_gscp, ddt_qv_conv, ddt_qv_gscp, ddt_qv_turb, ddt_temp_drag, ddt_temp_gscp, ddt_temp_pconv, ddt_temp_radlw, ddt_temp_radsw, ddt_temp_turb, ddt_tke, ddt_tke_hsh, ddt_tke_pconv, ddt_u_gwd, ddt_u_pconv, ddt_u_sso, ddt_u_turb, ddt_v_gwd, ddt_v_pconv, ddt_v_sso, ddt_v_turb

Group PRECIP_VARS
graupel_gsp, prec_con, prec_gsp, rain_con, rain_gsp, snow_con, snow_gsp, tot_prec

Group PROG_TIMEMEAN
psl_m, wap_m

Group RAD_VARS
albdif, albnirdif, albvisdif, asob_s, asob_t, asod_t, asodifd_s, asodifu_s, asodird_s, asou_t, aswflx_par_sfc, athb_s, athb_t, athd_s, athu_s, sob_s, sob_s_t_*, sob_t, sod_t, sodifd_s, sou_s, sou_t, swflx_par_sfc, thb_s, thb_s_t_*, thb_t, thu_s

Group SNOW_VARS
rho_snow, t_snow

C. Exercises

On the following pages a number of exercises is provided. These exercises revisit the topics of the individual chapters and range from easy tests to the setup of complex forecast simulations.

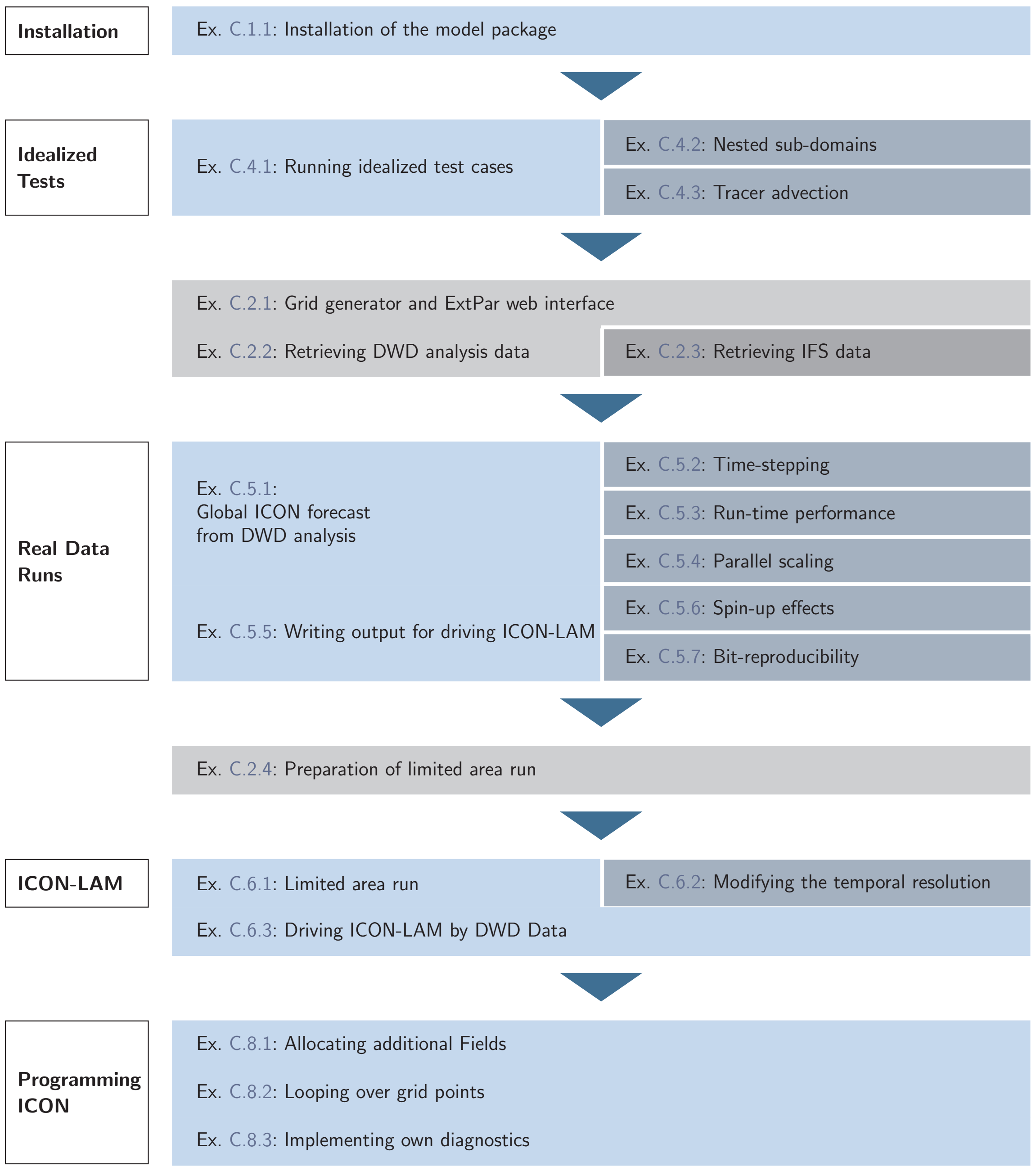
Installation
Ex. C.1.1: Installation of the model package
Idealized Tests
Ex. C.4.1: Running idealized test cases
Ex. C.4.2: Nested sub-domains
Ex. C.4.3: Tracer advection
Ex. C.2.1: Grid generator and ExtPar web interface
Ex. C.2.2: Retrieving DWD analysis data
Ex. C.2.3: Retrieving IFS data
Real Data Runs
Ex. C.5.1: Global ICON forecast from DWD analysis
Ex. C.5.5: Writing output for driving ICON-LAM
Ex. C.5.2: Time-stepping
Ex. C.5.3: Run-time performance
Ex. C.5.4: Parallel scaling
Ex. C.5.6: Spin-up effects
Ex. C.5.7: Bit-reproducibility
Ex. C.2.4: Preparation of limited area run
ICON-LAM
Ex. C.6.1: Limited area run
Ex. C.6.2: Modifying the temporal resolution
Ex. C.6.3: Driving ICON-LAM by DWD Data
Programming ICON
Ex. C.8.1: Allocating additional Fields
Ex. C.8.2: Looping over grid points
Ex. C.8.3: Implementing own diagnostics

List of Exercises

C.1. Installation of the ICON Model Package

For practical work during these exercises, you need information about the use of the computer systems and from where you can access the necessary files and data. In the following, we assume that the test jobs will run on DWD's NEC SX-Aurora supercomputer. For more information on this platform please take a look at Appendix A.

In this exercise we will extract and build the ICON model and its pre-processing tools:

EX 1.1

Log into the NEC SX-Aurora login node `rcl.dwd.de` and **install the ICON model** in the `$WORK` directory of your NEC SX-Aurora user account. For that you have to do the following:

- The necessary files for the ICON tutorial can be found in the subdirectory[1]

  `/hpc/uwork/trng040/packages`

  Copy the tar-files

`icon_tutorial.tar.gz`	. . . training exercise data
`icon-2.6.2.2.tar.gz`	. . . ICON source code
`icontools-2.4.12.tar.gz`	. . . DWD ICON Tools

  into your `$WORK` directory.

- Change into your `$WORK` directory and extract the compressed tar files to yield the directory structure depicted in the Figures 1.1 and 1.2 containing the ICON sources and test data.

- Follow the instructions in Section 1.2.2 to configure and compile the ICON model on the NEC SX-Aurora platform.

  Note:
  You can also compile the routines in parallel by using the GNU-make with the command `gmake -j` *np*

Install also the **DWD ICON Tools**:

- Change into the subdirectory `dwd_icon_tools` and build the DWD ICON Tools according to Section 1.3.2.

C.2. Necessary Input Data

In the following exercises, you will deal with the necessary preparatory steps for performing global real case ICON runs.

[1]Alternatively, external users may download the files from `https://data.dwd.de`, Account: `icon`.

Preparation of Global Runs

In this exercise we will generate the necessary grids and external parameter files using the ICON web service (see Section 2.1.6):

EX 2.1

Grid generator and ExtPar web interface:

- Open the DWD grid generator and ExtPar web interface

  `https://webservice.dwd.de/cgi-bin/spp1167/webservice.cgi`

  in your web browser.

- Select a sequence of three grids: Domain #0 – reduced radiation grid, domain #1 – global grid, domain #2 – refined region over Europe. Make sure that you set the "parent grid ID" appropriately.

- For the reduced radiation grid, select a "synthetic grid" with R3B05 resolution. Select global refinement for the domain #1.

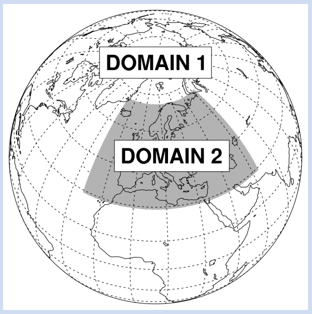

- Specify the R3B07 grid, domain #2, as a regular-shaped refinement region over Europe, see the illustration on the right or Fig. C.1:
  Center lon/lat: 19.5 / 50.0 deg, half width lon/lat: 44.5 / 21.5 deg.

- Submit the web form – but do not forget to provide your e-mail address! Wait for the job to finish, this may take some time. Afterwards, pick the generated data according to the download information that you have received via e-mail.

- Copy and rename the grid files s. t. the file names match the nomenclature `iconR<nroot>B<jlev>_DOM<idom>.nc`, see Section 5.1.2.
  Rename the ExtPar data to `extpar_DOM<idom>.nc`.

- Take a look at the grid data and the external parameters using the `ncdump` utility, see Section 9.1.1 for details. Find out whether the external parameter fields are defined at the grid vertices, edge midpoints or cells.

In this exercise we will retrieve and pre-process DWD analysis data for global forecast runs:

EX 2.2

Retrieving initialized DWD analysis data:

- Request native analysis data from DWD's meteorological data management system SKY for the date 2017-06-01T00:00:00 at a horizontal grid spacing of 13 km using the PAMORE tool, see Section 2.2.1:

  ```
  pamore -d date -hstart 0 -hstop 0 -lt a -model iglo \
            -iglo_startdata_0
  ```

- Take a look at the data with the `grib_ls` command-line tool.
- Export the environment variable `ECCODES_DEFINITION_PATH` with the setting

  ```
   ECCODES_DEFINITION_PATH=/hpc/rhome/software/eccodes/definitions/
               ··· release/$ECCODES_VERSION/definitions
  ```

  and run `grib_ls` once more. Are there any differences w.r.t. the displayed short names? See Section 1.1.2 for an explanation.

Remapping of initial data:

- Create a copy of the run script

  ```
  dwd_icon_tools/icontools/xce_remap_inidata
  ```

  which performs the task of remapping the variables of an uninitialized analysis product (Table 10.2).
- Adapt the set of variables which is to be remapped for initialized analysis products, according to Table 10.3, i. e. replace the fields `VN`, `THETA_V`, `DEN` by the fields `T`, `U`, `V`, `P`.
- Submit the script to the batch system. Afterwards repeat the remapping procedure for the 13 km nest (R3B07) over Europe.
- Copy and rename the remapped analysis files s. t. the file names match the nomenclature `dwdANA_R<nroot>B<jlev>_DOM<idom>.grb`, see Section 5.1.2.

In this exercise we will prepare the initial data for ICON to start from an IFS analysis:

EX 2.3

Retrieving IFS data:

- *Download – This step has to be executed on the ECMWF site:*
  Start the `mars4icon` script and download an IFS analysis file for the date 2017-01-12T00:00:00, see Section 2.2.2.

- Interpolate the data horizontally from the lat/lon grid onto the triangular ICON grid using `iconremap`. The run script

  ```
  dwd_icon_tools/example/runscripts/xce_ifs2icon.run
  ```

  will do this job.
  Fill in the name of the IFS file by setting `in_grid_filename` and `in_filename`.
  Further help on `iconremap` can be found in Section 2.2.3.

- Submit the `iconremap` job to the NEC SX-Aurora.

- List the fields contained in the output file using `cdo` and/or `ncdump`. Compare this to Table 2.2. Besides, find out which field(s) are not defined on cell circumcenters.

Preparation of Limited Area Runs

Note:

The following exercise requires a number of data files which are produced as model output in the real data exercise, Ex. C.5.5.

In this exercise we will pre-process the initial and boundary data for ICON limited area runs:

EX 2.4

Local grid file and its external parameters:

- In the directory `case_lam/input` you find an archive file which is the result of the web-based grid generator described in Section 2.1.6.

  Uncompress this file and visualize its content with the NCL file `case_lam/plot_grid.ncl`.
  See Figure C.3 for a reference (without highlighted boundary).

- Investigate the grid file with the `ncdump` utility (see Section 9.1.1): How many triangle cells are contained in the local grid? – *Answer:* ______ cells

Remapping of initial data:

The directory "`lam_forcing`" generated by the real case run contains a file with the prefix `init`, which will serve as initial conditions for the limited area run. Remap the data onto the local grid.

The subdirectory `case_lam` contains a script `create_ic_dwd2icon` which will do the remapping.

- Insert the path to the ICON Tools binaries, and
- adapt the path to the input data file (directory "`lam_forcing`" generated by real case run).

Inspect the local (`TARGET`) grid file and the grid which was used in Ex. C.5.5 for creating the initial data (`SOURCE`).

- Identify the grid spacing of both grids in ICON's RxBy nomenclature. (You could make use of `ncdump`.)

`SOURCE grid`	remap data	`TARGET grid`
	$\longrightarrow$	

- If the source grid has a horizontal grid spacing of ≈ 13 km, what is the grid spacing of your local (`TARGET`) grid in km, given the $RxBy$ expressions identified above (see Eq. 2.1)?
  – *Answer:* `TARGET` grid res. ______ km

Submit the script to the batch system.

- Check the result: The remapping script should have created a file with prefix `init` in `case_lam/output`.

Remapping of boundary data:

- The subdirectory `case_lam` contains a copy of the DWD ICON Tools script `create_lbc_dwd2icon`, see Section 2.3. Open this script and
  - insert the path to the ICON Tools binaries,
  - adapt the path to input data files (directory "`lam_forcing`" generated by real case run).
- Submit the script to the batch system.
- Check the result: Visualize the boundary data with the NCL script `case_lam/plot_boundary_data.ncl`.
- Investigate the files: How many cells are contained in the boundary grid?
  - *Answer:* ______ cells
- When looking at the set of boundary data variables, do you have any idea for further improvement in terms of storage space?
  - *Answer:* ______

C.4. Running Idealized Test Cases

In this exercise you will learn how to set up idealized runs in ICON with and without nested domains.

With the exception of the compilation process, there will be no need to log into the NEC SX-Aurora interactively. Job submission to the NEC SX-Aurora can be also performed on the Linux cluster `rcl.dwd.de`.

Running the Jablonowski-Williamson Test Case

In this exercise we will set up the Jablonowski-Williamson baroclinic wave test in ICON:

EX 4.1

Preparations:

Retrieve the necessary grid file from the ICON download server (see Section 2.1.4):

- Open the download page for the pre-defined ICON grids `http://icon-downloads.mpimet.mpg.de` in your web browser.
- Pick the R2B05 grid no. `14` from the list and right-click on the hyperlink for the grid file, then choose "copy link location".

- Open a terminal window, login into the Linux cluster `rcl.dwd.de`, and change into the subdirectory `test_cases/case_idealized/input`. Download the grid file into this subdirectory by typing

```
wget link_location -e http-proxy=ofsquid.dwd.de:8080
```

Run the Jablonowski-Williamson (JW) test case without nested domains:

- Change into the run script directory `test_cases/case_idealized`. The run script is named `run_ICON_R02B05_JW`.
- Fill in the name of the ICON model binary (including the path) and several missing namelist parameters. I.e. set `ltestcase`, `ldynamics`, `iforcing`, `nh_test_name` and `itopo`. See Section 1.1.1 for the location of your ICON model binary as well as Section 4.1 and Table 4.1 for additional help on the namelist parameters.
- Submit the job to the NEC SX-Aurora, using the `PBS` command `qsub`.
- Check the job status via `qstat` and `qcat` (see Section A).

Inspecting the output:

- Go to the output directory of `case_idealized`. You will find three NetCDF output files with (a) model level output on the native (triangular) grid, (b) pressure level output on the native grid, (c) model level output interpolated onto a regular lat-lon grid.
- Have a closer look to the different output files and their internal structure to find out which one is which. We suggest to use the tools `cdo` and `ncdump` as described in Section 9.1.
  What output interval (in h) has been used for model level output on the triangular grid? – *Answer:* h
- Visualize the output with one of the tools described in Section 9. An NCL script named `JW_plot.ncl` is available in `test_cases/case_idealized`.
- Compare the output of the NCL script with the reference `JABW_DOM01.ps` given in the subdirectory `reference`.
- Modify the NCL script by setting `lfocus_sh=True` and re-run. This will basically re-generate the first set of plots, but with a focus on the southern hemisphere and different contours.
- Is the flow on the southern hemisphere still purely zonal after 9 days? Describe what you see. Do you have an explanation for the observed behavior?

  – *Answer:*

Nested Sub-Domains

Here we will repeat the previous exercise (Jablonowski-Williamson baroclinic wave test) with one or more nested sub-domains:

EX 4.2

- Go to the run script directory.
  The run script for a nested grid experiment is termed `run_ICON_R02B05N6_JW`.
- Fill in the name of your ICON model binary and missing namelist parameters. I.e. extend
  - `dynamics_grid_filename`,
  - `num_lev` (`run_nml`)

  see Section 4.1.2 for additional help. The same output fields as for the global domain will be generated for the regional domain(s).

  The grid files of the nested domains have already been prepared for you. They are stored in the subdirectory `test_cases/case_idealized/input`. The geographic location of these nests is depicted in Figure 4.3.
  Feel free to add one or both nests to your global domain.
- Submit the job to the NEC SX-Aurora.
- After the job has finished, visualize the output on the global domain as well as on nest(s) using one of the tools described in Section 9. When using NCL (`JW_plot.ncl`), you will have to adapt `workdir` and `domain_nr`.
- Compare the results on the global domain with those of the previous exercise. Does the global domain output differ? If so, do you have an explanation for this?
  - *Answer:*

Additional question: parent-child relationships

The figure to the right depicts an alternative configuration consisting of three grid files, in which two grids are nested into each other. Obviously the parent-child relation of the grids differs from the previous configuration (Figure 4.3). Nevertheless, the correct settings for `dynamics_grid_filename` are identical to those used in the previous nested run.

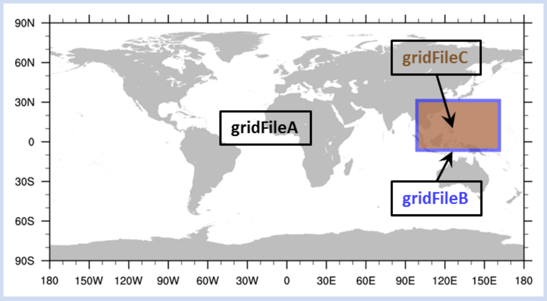

So, how does ICON know about the actual parent-child relationship of the grids in use? See Section 3.9 for an explanation and write down the parameters from which the parent-child relationship is inferred.

– *Answer:*

Optional Exercise: Tracer Advection

The JW test case provides a set of four pre-defined idealized tracer fields (see Figure 4.2). Here, you will learn how to enable and control the transport of passive tracers in idealized tests. See Section 3.6.5 for details on the configuration of the tracer transport for standard NWP runs.

EX 4.3

- Enable tracer advection:
  - Go to the directory `test_cases/case_idealized` and open the run script `run_ICON_R02B05N6_JW`.
  - Enable the transport module by setting the main switch `ltransport` to `.TRUE.`.
  - Enable (uncomment) the namelist `transport_nml`, which specifies details of the applied transport scheme.
  - Select one or more tracers from the set of pre-defined tracer distributions (see Figure 4.2). A specific tracer can be selected by adding the respective tracer number (1,2,3, or 4) to the Namelist variable `tracer_inidist_list` (namelist `nh_testcase_nml`, see Section 4.2.1).
- Extend the output namelist
  - Add the selected tracers to the list of output fields in the namelists `output_nml` (namelist parameters `ml_varlist` and `pl_varlist`).

    For idealized test cases, tracer names can be specified via the namelist variable `tracer_names` (namelist `transport_nml`, comma-separated list of string parameters). The nth entry in `tracer_names` corresponds to the nth entry in `tracer_inidist_list`.

    If nothing is specified, tracers are named `q`x, where x is a number indicating the position of the tracer within the ICON-internal 4D tracer container.
- Submit the job to the NEC SX-Aurora.
- Visualization: Enable `lplot_transport` in your NCL script. You can also have a quick look using `ncview`.
- Have a look at tracer number 4. Initially it is constant (= 1) everywhere. Ideally, an initially constant tracer should stay constant for all times, no matter how complicated the flow.
  Does ICON preserve a constant tracer in a run *without* nest?

  – *Answer:*

  Does ICON preserve a constant tracer in a run *with* nest?

  – *Answer:*
- Avoid non-physical negative values for tracer number 1.

– Every transport scheme that is more than first order accurate generates spurious over- and undershoots in the advected quantity. E.g. have a look at tracer number 1. You will notice that spurious negative values emerge after some time. In NWP runs, such negative values can lead to numerical instabilities and must be avoided.

– Switch on appropriate filter/limiter such that the transport scheme for tracer 1 becomes at least positive definite (i.e. $q(t) \geq 0 \; \forall \, t$). See Section 3.6.5 for additional help. Repeat the run to confirm that your settings are valid. Document your settings:

  – *Answer:* `itype_hlimit` =

  – *Answer:* `itype_vlimit` =

C.5. Running Real Data Test Cases

In this exercise you will learn how to start ICON from DWD analysis data and how to perform a multi-day forecast with 26 km grid spacing globally and 13 km over Europe. Another practical aim of this exercise is to create raw data for driving a limited area ICON run. Further use of this data will be made in Ex. C.6.1.

The configuration and compilation of the ICON code as well as the job submission has to be done on the NEC SX-Aurora login node `rcl.dwd.de`.

Input Data

The exercises in this section require a number of grid files, external parameters and input data. This data is already available in the directory `case_realdata/input`. Their creation process is explained in Ex. C.2.1 and C.2.2 (see p. 238).

On default, ICON expects the input data to be located in the experiment directory (termed `$EXPDIR` in the run scripts). The run script creates symbolic links in the experiment directory, which point to the input files.

Note:

The file names originating from the database requests (see Section 2.2.1) differ from the file names above. The input files have to be renamed in this case in order to match the default filename structure expected by the model.

Starting a Global ICON Forecast from DWD Analysis

In this exercise you will learn how to run ICON in real data mode:

EX 5.1

Open the ICON run script `case_realdata/run_ICON_R03B06_dwdini` and prepare the script for running a global **72 hour forecast** on an R3B06 grid with 26 km horizontal grid spacing without nest. The start date is

2017-01-12T00:00:00 , i.e. January 12, 2017.

Basic settings

- Fill in the missing namelist parameters `ini_datetime_string`, `end_datetime_string`, `ltestcase`, `ldynamics`, `ltransport`, `iforcing`, and `itopo` for real data runs (see Section 5.1.1).
- For better runtime performance, switch on *asynchronous* output by setting the number of dedicated I/O processors (`num_io_procs`) to a value larger than 0 (e.g. 2). See Section 7.4.1 for more details on the asynchronous output module.

Specifying the input data

- The grid file(s) to be used are already specified in the run script. Please identify and write down the respective namelist variables:
  - *Answer: dynamics grid(s)* ____
  - *Answer: radiation grid* ____
- Note that – funnily enough – the initial conditions (i.e. here initialized analysis file) is provided via the namelist parameter `dwdfg_filename`, see Section 5.1.4.

  Due to the appropriate choice of the file names in the experiment directory, ICON is able to locate the analysis file automatically without specifying the namelist variable `dwdfg_filename`. However, it is given in the run script for reference, using the keyword nomenclature mentioned in Section 5.1.2.

  Have a look at these settings and try to understand how these keywords work.

  Which of the following filenames would be accepted by the ICON model?

`dwdANA_R3B06.grb`	☐
`dwdANA_R2B6_DOM01.grb`	☐
`dwdANA_R9B02_DOM02.grb`	☐
`dwdana_R2B06_DOM01.grb`	☐

- Specify the name of the external parameter file (`extpar_filename`). Instead of specifying the full name, try to make use of the keyword *`idom`*.

C. Exercises

Settings for the Initialized Analysis Data

- Choose the appropriate initialization mode `init_mode` for starting the model from initialized DWD analysis data (see Section 5.1.4).
- Activate surface tiles: Please activate 3 dominant land tiles per grid cell by setting `ntiles` (`lnd_nml`) appropriately. Since the initial data contain aggregated (cell averaged) surface fields, a tile coldstart must be performed i.e. each tile must be initialized with the same cell averaged value. The corresponding namelist switch is termed `ltile_coldstart` (see Section 3.8.11).

Running the model and inspecting the output

- Submit the job to the NEC SX-Aurora.
- After the job has finished, inspect the model output:
  - Take a look at the output files in `case_realdata/output`. You should find two files named `NWP_...`. Use `cdo sinfov` to identify the

    time interval between two outputs – *Answer:* ______ h

    total time interval for which output is written – *Answer:* ______ h

    type of atm. vertical output grid (ML, PL, HL) – *Answer:* ______
  - one file contains output on the native ICON grid, the other one output on a regular lat/lon grid. Use `cdo sinfov` to identify which file is which.

    – *Answer: native* ______

    – *Answer: lat/lon* ______
  - Visualize the 2 m temperature, integrated water vapor, gusts at 10 m, and total precipitation using the `ncview` utility. If you like, you can look into other fields as well.

Time-stepping

This exercise focuses on aspects of the ICON time-stepping scheme, explained in Section 3.7.1:

EX 5.2

- Compute the *dynamics* time step $\Delta\tau$ from the specification of the physics time step Δt (`dtime`) and the number of dynamics substeps `ndyn_substeps`.

  – *Answer:* $\Delta\tau =$ ______ s
- Take a look at Equation (3.40) and calculate an estimate for the maximum dynamics time step which is allowed for the horizontal grid spacing at hand.

  – *Answer:* $\Delta\tau_{max} =$ ______ s

  Now compare this to the time step used: Did we make a reasonable choice?

Parallelization and Run-Time Performance

In this exercise you will learn how to specify the details of the parallel execution. We will use the ICON timer module for basic performance measuring.

EX 5.3

Performance assessment using the timer output:

- Open your run script from the previous Exercise C.5.1 and enable the ICON routines for performance logging (timers). To do so, follow the instructions in Section 7.4.4.
- Repeat the model run.
- At the end of the model run, a log file is created. It can be found in your base directory `case_realdata`. Scroll to the end of this file. You should find wall clock timer output comparable to that listed in Section 7.4.4. Try to identify

the total run-time	– *Answer:*	s
the time needed by the radiation module	– *Answer:*	s

This exercise focuses on the mechanisms for parallel execution of the ICON model. These settings become important for performance scalability when increasing the model resolution and core counts:

EX 5.4

Changing the number of MPI tasks: In case your computational resources are sufficient, one possibility to speed up your model run is to increase the number of MPI tasks.

- Create a copy of your run script `run_ICON_R03B06_dwdini` named `run_ICON_R03B06_dwdini_fast`. In order to avoid overwriting your old results, replace the output directory name (`EXPDIR`) by `exp02_dwdini_fast`.
- Double the total number of MPI tasks compared to your previous job and re-submit. In more detail, on the NEC SX-Aurora do the following:
  - Your old script (`run_ICON_R03B06_dwdini`) ran the executable on 30 vector engines using 8 MPI tasks/engine and 1 OpenMP threads/MPI task.
  - Your new script (`run_ICON_R03B06_dwdini_fast`) should run the executable in hybrid mode on 60 vector engines using 8 MPI tasks/node and 1 OpenMP threads/MPI task.

  You need to adjust only the `PBS` settings. See Section 7.4.4 for additional help.
- Compute the speedup that you gained from doubling the number of MPI tasks.
  - Compare the timer output of the dynamical core, `nh_solve`, and the transport module, `transport`, with the timer output of your previous run.

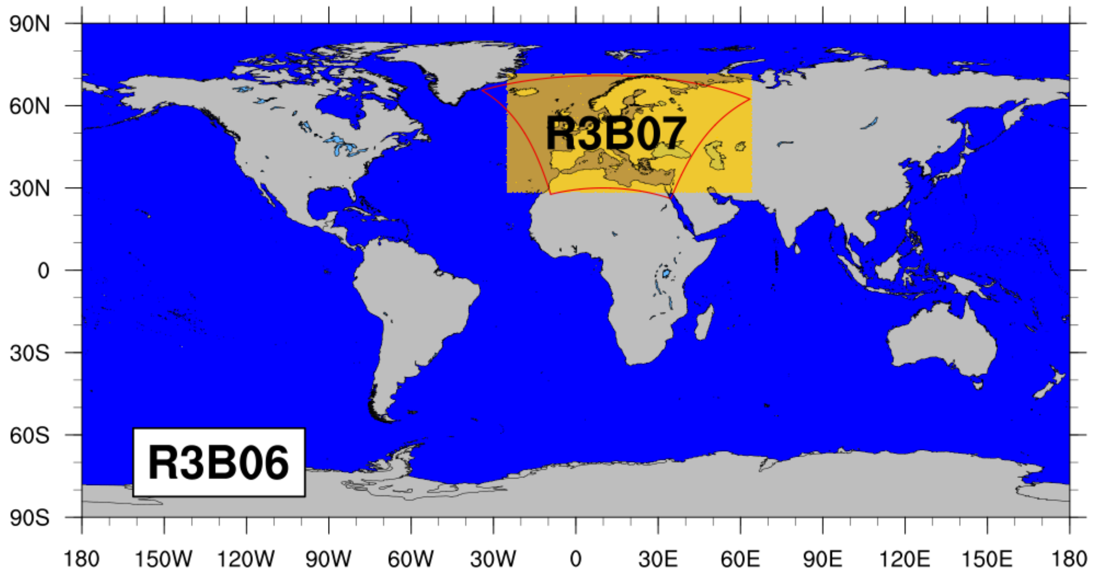

Figure C.1.: Computational grid with a two-way nested region over Europe (yellow shading). The outline of the COSMO-EU domain (formerly used operationally by DWD) is shown in red for comparison.

`nh_solve` **30 engines**	`nh_solve` **60 engines**	`transport` **25 engines**	`transport` **50 engines**
s	s	s	s

What do you think is a more sensible measure of the effective cost: `total min` or `total max`?

– *Answer:*

– Which speedup did you achieve and what would you expect from "theory"?

– *Answer:* Speedup achieved $= \frac{T_{25\text{nodes}}}{T_{50\text{nodes}}} =$

– *Answer:* Speedup expected =

Writing Output for Driving a Limited Area Simulation

In this exercise you will learn about some of the output capabilities of ICON. We will set up a new output namelist and generate a data set which enables us to drive a limited area run of ICON as described in Chapter 6.

EX 5.5

In order to achieve a somewhat higher spatial resolution at acceptable costs, we will switch on a two-way nested region over Europe with a horizontal grid spacing of 13 km (see Figure C.1):

- Create a copy of your run script `run_ICON_R03B06_dwdini` named `run_ICON_R03B06N7_dwdini`. Alternatively, you may adopt the settings of the reference version `reference/case_realdata/run_ICON_R03B06_dwdini`.
- In order to avoid overwriting your old results, replace the output directory name (`EXPDIR`) by `exp02_dwdini_lamforcing`.
- Activate the nest by extending the list of horizontal grids to be used (`dynamics_grid_filename`, see Section 4.1).
- In order to save some computational resources, the nested domain should have a reduced model top height and comprise only the lowermost 60 vertical levels of the global domain (instead of 90 levels). Please extend `num_lev` (`run_nml`) accordingly.

Adding a new output namelist:

- The run script contains two commented-out output namelists. One is meant for writing forcing (boundary) data, the other for writing initial data for driving a limited area run. Activate the namelists and fill in the missing parameters. See Section 7.1 for additional details regarding output namelists. Forcing data should be written
  - in GRIB2 format
  - for the EU-nest only
  - 2-hourly from the start until 48 hours forecast time
  - with one output step per file
  - on the native (triangular) grid
  - into the subdirectory "`lam_forcing`" of your output directory `exp02_dwdini_lamforcing`, using the filename prefix "`forcing`". If the subdirectory does not exist, please create.
  - containing model level output for `U`, `V`, `W`, `PRES`, `TEMP`, `QV`, `QC`, `QI`, `QR`, `QS`, `HHL`.
  - Take a look at the available ICON variable groups listed in Appendix B. Is there an output group that can be used instead of the list of variables? If yes, which group?
    - *Answer:*

C. Exercises

  - Is there also an ICON variable group that writes all variables needed to initialize an ICON-LAM simulation? If yes, which group?
    - *Answer:*

- Submit the job to the NEC SX-Aurora.

Check the correctness of your output files:

- You should find **25 forcing data files** in your output directory "`lam_forcing`". Apply the command `cdo sinfov` *data-file.grb* > *data-file.sinfov* to the last file. Compare with the reference output in Table C.1 to see whether your output namelist is correct.

Table C.1.: Reference output for Ex. C.5.5. Structure and content of file `forcing_ML_20170114T000000Z.grb`

```
    File format : GRIB2
     -1 : Institut Source   Ttype    Levels Num    Points Num Dtype : Parameter name
      1 : DWD      unknown  instant      60   1    172740   1  P16  : U
      2 : DWD      unknown  instant      60   1    172740   1  P16  : V
      3 : DWD      unknown  instant      61   2    172740   1  P16  : W
      4 : DWD      unknown  instant      60   1    172740   1  P16  : P
      5 : DWD      unknown  instant      60   1    172740   1  P16  : T
      6 : DWD      unknown  instant      60   1    172740   1  P16  : QV
      7 : DWD      unknown  instant      60   1    172740   1  P16  : QC
      8 : DWD      unknown  instant      60   1    172740   1  P16  : QI
      9 : DWD      unknown  instant      60   1    172740   1  P16  : QR
     10 : DWD      unknown  instant      60   1    172740   1  P16  : QS
     11 : DWD      unknown  instant      61   3    172740   1  P16  : HHL
    Grid coordinates :
      1 : unstructured             : points=172740
                              grid : number=99  position=1
                              uuid : 890df70c-a566-3b91-438f-f527deb82760
    Vertical coordinates :
      1 : generalized_height       : levels=60
                            height : 1.5 to 60.5 by 1
                            bounds : 1-2 to 60-61 by 1
                             zaxis : number = 4
                              uuid : a0919ba7-df84-ce2b-c4c2-3c215c033520
      2 : generalized_height       : levels=61
                            height : 1 to 61 by 1
                             zaxis : number = 4
                              uuid : a0919ba7-df84-ce2b-c4c2-3c215c033520
      3 : generalized_height       : levels=61
                            height : 0.5 to 30.5 by 0.5
                            bounds : 1-0 to 61-0 by 0.5
                             zaxis : number = 4
                              uuid : a0919ba7-df84-ce2b-c4c2-3c215c033520
    Time coordinate :  1 step
      RefTime =  2017-01-12 00:00:00  Units = minutes  Calendar = proleptic_gregorian
   YYYY-MM-DD hh:mm:ss  YYYY-MM-DD hh:mm:ss  YYYY-MM-DD hh:mm:ss  YYYY-MM-DD hh:mm:ss
   2017-01-14 00:00:00
```

Optional: A Deeper Look into Spin-Up Effects

Depending on the data set used to initialize the model, spin up effects may become visible during the first few hours of a forecast. This is especially true if third party (i.e. non-native) analysis data sets are used. Here we will have a look into the spin up behavior of ICON when starting from native vs. non-native analysis. As an example for a popular non-native analysis, we will choose data from the IFS.

EX 5.6

- Run the NCL script `case_realdata/water_budget.ncl`, to get a deeper insight into the model's spin up properties and water budget when ICON is started from DWD analysis. The script generates time series of vertically integrated water vapor `tqv` and condensate `tqx` from the model level output in `case_realdata/output/exp02_dwdini`.

  Compare the results to Figure C.2 which shows the corresponding results when ICON is started from IFS analysis. Note that Figure C.2 has been produced for a longer time range.

Which analysis data set leads to an increased spin up/down in this particular case?	native analysis (DWD)	☐
	non-native analysis (IFS)	☐

  The additional NCL plots will give you some insight into the global atmospheric water budget

  $$\frac{\mathrm{d}Q_t}{\mathrm{d}t} = P - E + R\,,$$

  where Q_t is the vertically integrated atmospheric water content and $\mathrm{d}Q_t/\mathrm{d}t$ is the rate of change over time. P is the amount of total precipitation, E is the total evaporation, and R is a residuum. Is the budget closed (i.e. is $R = 0$ in your model run)?

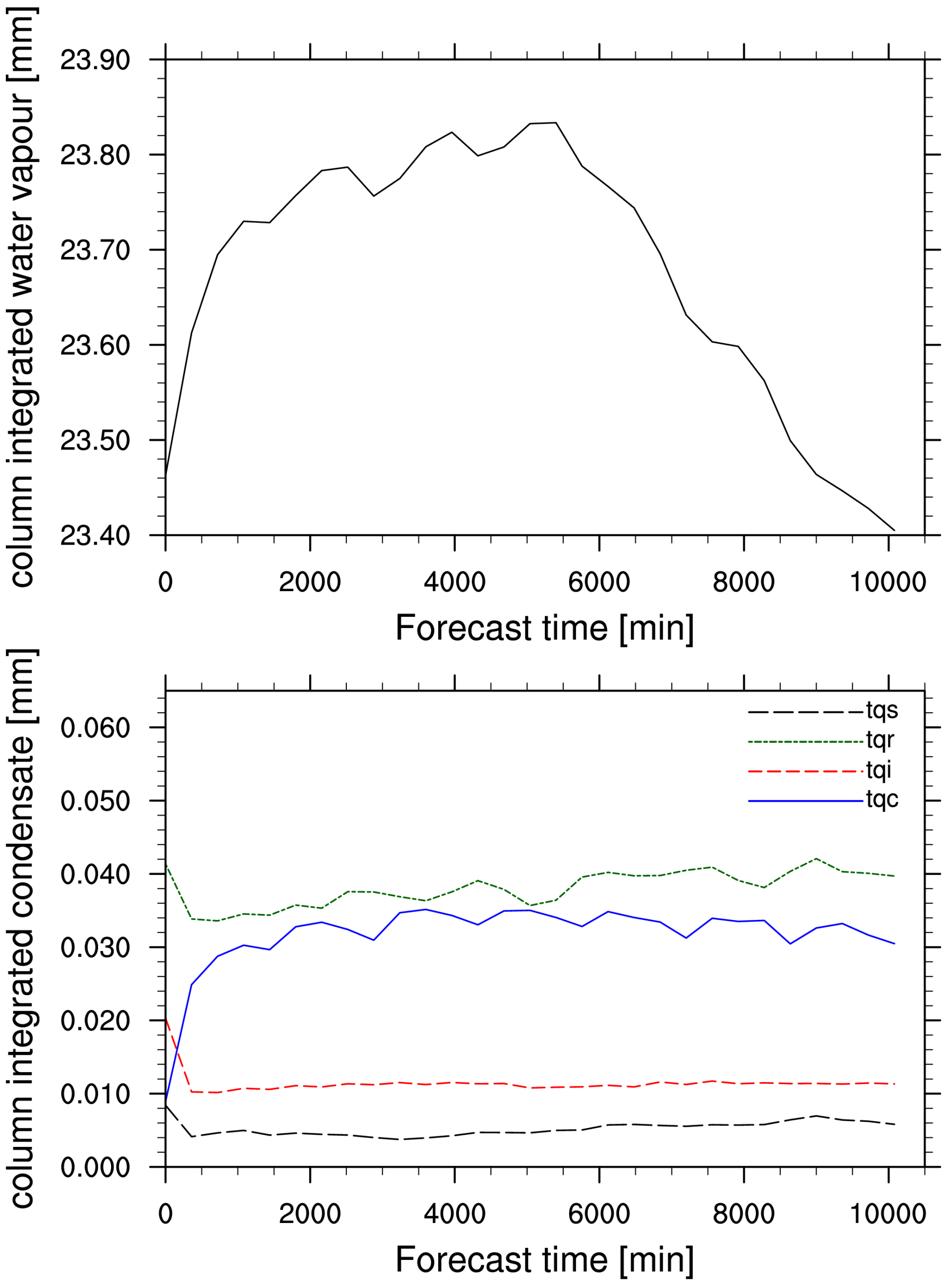

Figure C.2.: Time series of area averaged column integrated specific moisture $\langle tqv \rangle$ (top) and condensate classes $\langle tqx \rangle$ (bottom) for a 7-day forecast **started from IFS analysis** fields. Start date was 2017-01-12T00:00:00. A spin up in $\langle tqv \rangle$ and initial adjustments in $\langle tqx \rangle$ is clearly visible.

Optional: Checking for Bit-Reproducibility

In this exercise we test the ICON model for bit-reproducibility, i. e. the feature that running the same binary multiple times results in bitwise identical results.

EX 5.7

- Compare the model level output of `run_ICON_R03B06_dwdini` with the output that was produced by your modified script `run_ICON_R03B06_dwdini_fast`. You can use `cdo infov` *data-file.nc* for getting information about the contents of your output file. You should dump this information into text files,

  ```
  cdo infov data-file.nc > data-file.infov
  ```

  so that you can compare them later on. Due to the limited number of digits printed by CDO, this is no check for bit-reproducibility in a strict mathematical sense, however experience showed that `cdo infov` is very reliable in revealing reproducibility issues.

- Now compare the model level output produced by your modified script `run_ICON_R03B06N7_dwdini` with the output produced by `run_ICON_R03B06_dwdini`. Is the result different from the previous comparison? Do you have an explanation for this?
  - *Answer:*

  Hint: For a convenient comparison of ASCII files you may use the `tkdiff` utility.

C.6. Running ICON-LAM

The exercises in this section require a number of grid files, external parameters and input data. In particular, initial data and driving boundary data are required. Both were produced in the real data exercise, Ex. C.5.5. The pre-processing of this data is explained in Ex. C.2.4 (see p. 241).

Running ICON in Limited Area Mode

In this exercise we will run ICON in limited area mode. The model will be driven by initial and boundary data which have been produced in Ex. C.2.4.

EX 6.1

Open the run script `case_lam/run_ICON_R3B08_lam` and prepare it for running a **48 hour forecast** on a **limited area grid over Germany** (see Figure C.3). As for the global run, the start date is

2017-01-12T00:00:00 , i.e. January 12, 2017.

The run script is geared up insofar as all soft-links which specify the model binary, grids, initial and boundary data are already set. Your main task will be to set up the ICON namelists for a limited area run.

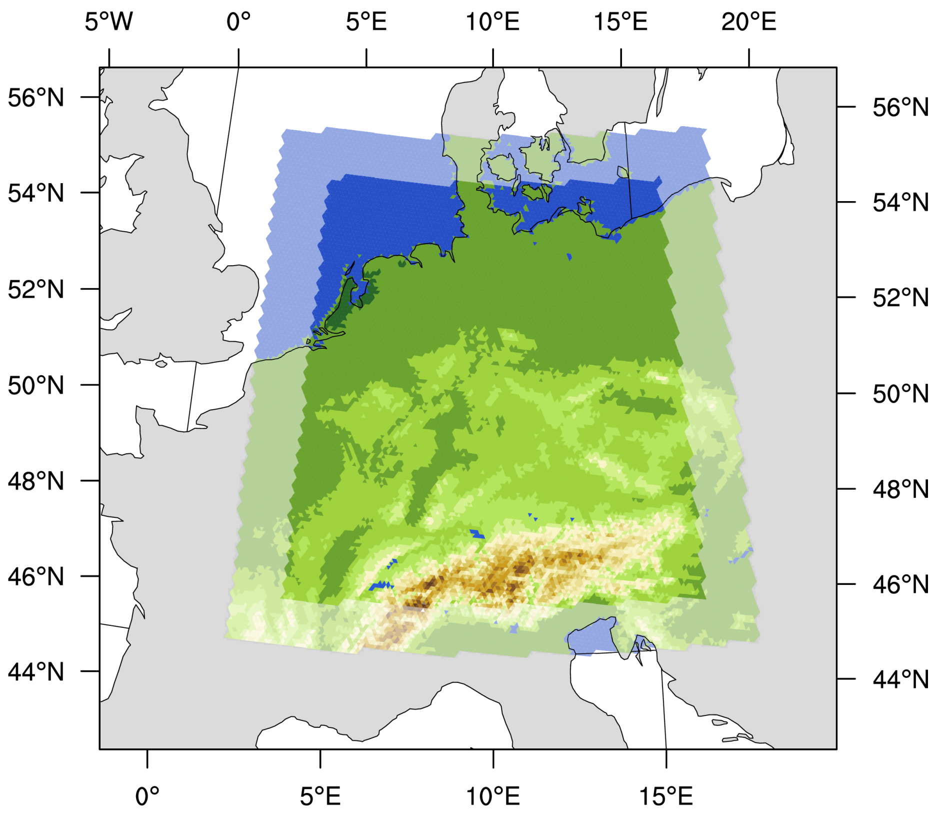

Figure C.3.: Illustration of the local grid used in Exercises C.6.1–C.8.3. The horizontal grid spacing is ≈ 6.5 km (which corresponds to R3B08 in ICON nomenclature). The boundary region is highlighted, where nudging towards the driving data is performed. The driving data for this test case has been created in Ex. C.2.4.

Basic settings:

- Set the correct start and end date: `ini_datetime_string`, `end_datetime_string`
- Switch on the limited area mode by setting `l_limited_area` and `init_mode` (see Section 6.3).

Initial data:

- Specify the initial data file via `dwdfg_filename`. Since we do not make use of additional analysis information from a second data file, remember to set `lread_ana` accordingly (see Section 6.3).
- Specify a dictionary file for the initial data via `ana_varnames_map_file` (see Section 5.1.1).
  Hint: Take a closer look at `case_lam/run_ICON_R3B08_lam`, where a link to the correct dictionary is already set.

The dictionary has the purpose to translate the variable names in the GRIB2 or NetCDF input file into the ICON internal variable names. According to the dictionary used for this exercise, what are the internal variable names and the GRIB2/NetCDF variable names for

- **Pressure:**
  GRIB2/NetCDF: ☐ *ICON internal:* ☐
- **Temperature:**
  GRIB2/NetCDF: ☐ *ICON internal:* ☐
- **Half level height:**
  GRIB2/NetCDF: ☐ *ICON internal:* ☐

Boundary data:

- Specify the lateral boundary grid and data via `latbc_boundary_grid`, `latbc_path` and `latbc_filename`. For the latter you will have to make use of the keywords `<y>`, `<m>` `<d>` and `<h>` (see Section 6.4.1).
- What is the time interval between two consecutive boundary data files? The command `cdo sinfov` may be helpful.
  – *Answer:* ☐ s

  Set the namelist parameter `dtime_latbc` accordingly.
- Inspect the number of vertical levels in a boundary data file. Is it different from the number of vertical levels that is used by the model itself?
  – *Answer:* ☐

Running the model and inspecting the output

- Extend the lat-lon output namelist by the 2 m temperature, surface pressure, mean sea level pressure, and 10 m gusts. See Appendix B for variable names and description.
- Submit the job to the NEC SX-Aurora.
- After the job has finished, inspect the model output. You should find multiple files in the output directory `case_lam/output/exp03_R3B08_dwdlam` which contain hourly output on model levels remapped to a regular lat-lon grid.
  - Take a look at the output fields by using `ncview`. How would you characterize the overall weather situation for that time period?

    southfoehn over the alpine region ☐
    strong frontal system passing over Germany ☐
    weak frontal system passing over Germany ☐
    anticyclonic situation with very calm winds ☐

Temporal Resolution of the Boundary Data

By playing around with the temporal resolution of the boundary data you will get some idea how this might affect your simulation results.

EX 6.2

Create a copy of your run script `run_ICON_R3B08_lam` and name it `run_ICON_R3B08_lam_lowres`. Replace the output directory name (`EXPDIR`) by `exp03_R3B08_dwdlam_lowres` in order to avoid overwriting your results.

- Halve the time resolution of your forcing (boundary) data, see Section 6.3 for the namelist parameter. Write down your chosen value:
  - *Answer:* ____ s
- Submit the job to the NEC SX-Aurora.
- Compare the results with your previous run. Does the time frequency with which the boundary data are updated have a significant impact on the results? You can visualize cross sections with the NCL script `case_lam/plot_cross_section.ncl` and/or make use of `ncview`.

Driving ICON-LAM by DWD Data

This exercise is similar to the previous exercise C.6.1 inasmuch as we will run ICON in limited area mode again. However, rather than using initial and boundary data that we have generated in one of the previous exercises, we will initialize and drive ICON-LAM by official DWD analysis and forecast data. This setting might be closer to what you will encounter when you run ICON-LAM at your home institution.

The data products for this particular exercise will be provided. Note, however, that PAMORE data requests in general require registration via `klima.vertrieb@dwd.de`.

EX 6.3

In the subdirectory[2]

```
/hpc/uwork/trng040/packages/pamore_data
```

you will find the raw data for an ICON limited area run consisting of an initialized analysis and two-hourly forecasts. This data set has been downloaded from the DWD database with the help of the PAMORE tool, see Section 2.2.1 for details.

- For the sake of simplicity, link the above directory into `case_lam/input_dwd`.
- Take a look at the data with the `grib_ls` and/or `cdo` command-line tool. Find out about the analysis date and the time range of the data set.
- *Imagine that your boss at home asks you to retrieve this data set from the DWD database . . .*

Write down the PAMORE commands which you would have to insert into the PAMORE web form. See Section 2.2.1 and 2.3 for help.

– *Analysis:*

– *Forecasts:*

- Export the environment variable `ECCODES_DEFINITION_PATH` with the setting

```
ECCODES_DEFINITION_PATH=/hpc/sw/eccodes/definitions/
    ··· release/$ECCODES_VERSION/definitions
```

  and run `grib_ls` once more. Are there any differences w.r.t. the displayed short names? See Section 1.1.2 for an explanation.

Remapping of initial data:

In order to use the DWD initialized analysis for your LAM run, it must be remapped to your limited area grid.

- Determine the source grid on which the raw data are defined. Write down the grid identifier *numberOfGridUsed*.

  – *Answer:* `numberOfGridUsed`=

- Retrieve the matching grid file from the ICON download server (see Section 2.1.4):
  - Open the download page for the pre-defined ICON grids `http://icon-downloads.mpimet.mpg.de` in your web browser.
  - Pick the matching grid number from the list and right-click on the hyperlink for the grid file, then choose "copy link location".
  - Open a terminal window, login into the Linux cluster `rcl.dwd.de`, and change into the subdirectory `case_lam/input_dwd`. Download the grid file into this subdirectory by typing `wget` *`link_location`* `-e http-proxy=ofsquid.dwd.de:8080`.
  - Write down the resolution in ICON's RxBy nomenclature.

    – *Answer:* `RxBy`=

- Create a copy of the remapping script `create_ic_dwd2icon` located in the subdirectory `case_lam`.
- Open the script and adapt
  - the path to the input data file that has been retrieved from the DWD database (directory `case_lam/input_dwd/pamore_data`).
  - the file name of the input data file.
  - the file name of the input grid.

  - the output directory such as not to overwrite your previous initial data. You might store your output in a new sub-directory `output_dwd` located inside the base directory "`case_lam`".

- Submit the script to the batch system.

Remapping of the lateral boundary conditions:

In contrast to the previous ICON-LAM exercises we will interpolate the forcing data onto the full limited area grid instead of the lateral boundary strip only.

Can you think of simulations where such a setting is required?

– *Answer:*

Create a copy of the remapping script for boundary data `create_lbc_dwd2icon`:

- Open this script and adapt the path to your input data files (directory "`case_lam/input_dwd/pamore_data`"), the file names of the input files, the file name of the input grid and the output directory ("`case_lam/output_dwd`").
- Adapt the script such that the `AUXGRID` auxiliary grid (boundary strip) is no longer used but the full limited area grid (`LOCALGRID`).

Submit the script to the batch system.

Small consistency check: How many grid cells do you expect in the output files?

– *Answer:* cells

Running the model

Create a copy of the run script `case_lam/run_ICON_R3B08_lam` and prepare it for running a **36 hour forecast** on the same limited area grid over Germany as used in Ex. C.6.1 (see Figure C.3). In order to avoid overwriting your old results, replace the name of the output directory.

Initial and boundary data:
As we will use a new set of initial and boundary data, several changes are necessary:

- Change the settings for the analysis input files (initial data).
- Specify the lateral boundary data via `latbc_path` and `latbc_filename`. For the latter you will have to make use of the keyword `<ddhhmmss>` (see Section 6.4.1).
- Check whether the time interval between consecutive boundary data files is set correctly (`dtime_latbc`).

Submit the job to the NEC SX-Aurora.

Did your run finish successfully?

[2]Alternatively, external users may download the files from `https://data.dwd.de`, Account: `icon`.

C.8. Programming ICON

Allocating Additional Fields

In this exercise we learn how to allocate new ICON variables. As a by-product we will visualize ICON's domain decomposition.

EX 8.1

This requires to modify the ICON code, where details are given in Section 8.3.

Remember to create a full copy of your `src` directory. Subsequent exercises will be based upon the unmodified sources!

Step-by-step checklist

In the subdirectory `src/atm_dyn_iconam`:

a) Open the module `mo_nonhydro_types`.

Insert a new 2D variable pointer `process_id` of type `REAL(wp)` to the derived type `TYPE(t_nh_diag)`.

Got it? ☐ Did it! ☐

b) Open the module `mo_nonhydro_state`.

At the end of the subroutine `new_nh_state_diag_list`: initialize meta-data variables for NetCDF and also for GRIB2 with

discipline = *parameterCategory* = *parameterNumber* `= 255`

and place the `add_var` call for the new field.

Got it? ☐ Did it! ☐

c) Now, after the `add_var` call, the new field has been allocated. Fill the data array with a constant value:

`··· process_id(:,:) = get_my_mpi_work_id()`

This auxiliary function from `mo_mpi` returns the MPI rank of the processor (see Section 8.2.4).

Got it? ☐ Did it! ☐

d) Open the namelist of the previous test case C.6.1 and insert the new field in the lat-lon output specification.

Compile and run the model.
Visualize the results (`ncview`).

Please answer the following questions:

- Why is the output field not a constant value?

  – *Answer:*

- Take a closer look at the data: Can you guess why the output field does not only contain integer values?

  – *Answer:*

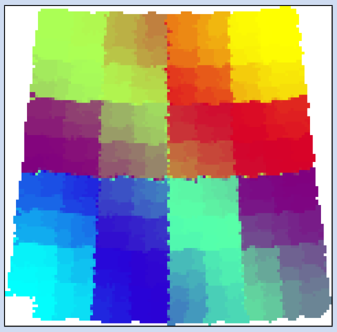

Looping Over Grid Points

In this exercise we will implement the technical setup for the calculation of new diagnostic fields:

EX 8.2

In this exercise we will implement the technical setup for the calculation of the following new diagnostic fields (2D variables):

`RHI_MAX:`	Relative humidity over ice (hourly maximum in the column, [%])
`QI_MAX:`	Maximum cloud ice content (hourly max. in the column, $\left[\frac{\text{kg}}{\text{kg}}\right]$)

Again, this requires to modify the ICON code.

Got it? Did it!

- Repeat the steps a) – b) of Exercise C.8.1 and allocate two new 2D variables `RHI_MAX`, `QI_MAX`.
- Open the module `mo_nh_stepping` (subdirectory `src/atm_dyn_iconam`).

  Got it? Did it!

  Create an (empty) subroutine `calculate_diagnostics` and place a call to this subroutine immediately before the call to the output routine.
- Fill your subroutine with a 2D loop over all prognostic grid points, see p. 183 for help.
  Use this loop to initialize the fields to a constant value.

  ```
  p_nh_state(jg)%diag%RHI_MAX(jc,jb) = 2.0_wp
  p_nh_state(jg)%diag%QI_MAX(jc,jb)  = 2.0_wp
  ```

  All other values should be set to `1.0_wp`.

  How many triangle rows do you expect to have the value `1` in the output?

  – *Answer:* ______ rows.
- Open the namelist of the previous test case C.6.1 and insert the new fields in the lat-lon output specification.
- Compile and run the model. Visualize the results (`ncview`).
- *Final question:* Instead of the value `2.0_wp` we'd now like to initialize `RHI_MAX` with the lower-most level of the (diagnostic) temperature field.
  How could we achieve this?

  – *Answer:* ______

Implementing New Diagnostics

In this exercise we will calculate the new 2D diagnostic fields `RHI_MAX`, `QI_MAX`:

EX 8.3

- Modify the subroutine `calculate_diagnostics`:
  Instead of initializing the fields to a constant value as in Ex. C.8.2, add a loop over the vertical model levels for every prognostic grid point.
- Then fill your subroutine with the calculation of the two new quantities.
  Three hints:
  - The module `mo_util_phys` (subdirectory `src/atm_phy_nwp`) may offer some help with respect to `RHI_MAX`.
  - Exner pressure field: values for domain "`jg`" are accessed via `p_nh_state%prog(nnow(jg))%exner(:,:,:)`.
  - 3D tracer field `QI` (same for `QV`): values for domain "`jg`" are accessed via `p_nh_state%prog(nnow_rcf(jg))%tracer_ptr(iqi)%p_3d(:,:,:)`.
    The constants `iqv`, `iqi` can be found in `mo_run_config`.
- Revisit the `add_var` calls of the quantities `RHI_MAX`, `QI_MAX`: specify an hourly reset, see p. 185 for an explanation.
- Open the namelist of the previous test case C.6.1 and insert the new fields in the output specification.

Compile and run the model. Visualize the results (`ncview`).

Bibliography

Asensio, H., and M. Messmer, 2014: *External Parameters for Numerical Weather Prediction and Climate Application: EXTPAR v2.0.2 User and Implementation Guide*. Consortium for Small-scale Modeling (COSMO), URL http://www.cosmo-model.org/content/model/modules/Extpar_201408_user_and_implementation_manual.pdf.

Avissar, R., and R. Pielke, 1989: A parameterization of heterogeneous land surfaces for atmospheric numerical models and its impact on regional meteorology. *Mon. Weather Rev.*, **117**, 2113–2136.

Baines, P., and T. Palmer, 1990: Rationale for a new physically based parameterization of sub-grid scale orographic effects. Tech. Rep. 169, European Centre for Medium-Range Weather Forecasts, 11 pp. URL http://www.ecmwf.int.

Baldauf, M., A. Seifert, J. Förstner, D. Majewski, M. Raschendorfer, and T. Reinhardt, 2011: Operational Convective-Scale Numerical Weather Prediction with the COSMO Model: Description and Sensitivities. *Mon. Weather Rev.*, **139 (12)**, 3887–3905, doi:10.1175/MWR-D-10-05013.1.

Barker, H. W., G. L. Stephens, P. T. Partain, and Coauthors, 2003: Assessing 1D atmospheric solar radiative transfer models: Interpretation and handling of unresolved clouds. *J. Clim.*, **16 (16)**, 2676–2699, doi:10.1175/1520-0442(2003)016⟨2676:ADASRT⟩2.0.CO;2.

Bechtold, P., 2017: Atmospheric moist convection. *Meteorological Training Course Lecture Series*, ECMWF, 1–78, URL https://www.ecmwf.int/sites/default/files/elibrary/2017/16953-atmospheric-moist-convection.pdf.

Bechtold, P., M. Köhler, T. Jung, F. Doblas-Reyes, M. Leutbecher, M. J. Rodwell, F. Vitart, and G. Balsamo, 2008: Advances in simulating atmospheric variability with the ECMWF model: From synoptic to decadal time-scales. *Q. J. R. Meteorol. Soc.*, **134 (634)**, 1337–1351, doi:10.1002/qj.289.

Bechtold, P., N. Semane, P. Lopez, J.-P. Chaboureau, A. Beljaars, and N. Bormann, 2014: Representing equilibrium and nonequilibrium convection in large-scale models. *J. Atmos. Sci.*, **71 (2)**, 734–753, doi:10.1175/JAS-D-13-0163.1.

Blackadar, A. K., 1962: The vertical distribution of wind and turbulent exchange in a neutral atmosphere. *J. Geophys. Res.*, **67**, 3095–3102.

Bloom, S. C., L. L. Takacs, A. M. D. Silva, and D. Ledvina, 1996: Data assimilation using incremental analysis updates. *Mon. Weather Rev.*, **124**, 1256–1270.

Choulga, M., E. Kourzeneva, E. Zakharova, and A. Doganovsky, 2014: Estimation of the mean depth of boreal lakes for use in numerical weather prediction and climate modelling. *Tellus A*, **66**, 21 295, doi:10.3402/tellusa.v66.21295.

Colella, P., and P. R. Woodward, 1984: The piecewise parabolic method (ppm) for gas-dynamical simulations. *J. Comput. Phys.*, **54**, 174–201.

Crueger, T., and Coauthors, 2018: ICON-A, the atmosphere component of the ICON earth system model: II. model evaluation. *J. Adv. Model Earth Sy.*, **10 (7)**, 1638–1662, doi:10.1029/2017MS001233.

Davies, H., 1976: A lateral boundary formulation for multi-level prediction models. *Q. J. R. Meteorol. Soc.*, **102**, 405–418, doi:10.1002/qj.49710243210.

Davies, H., 1983: Limitations of some common lateral boundary schemes used in regional NWP models. *Mon. Weather Rev.*, **111**, 1002–1012, doi:10.1175/1520-0493(1983)111⟨1002:LOSCLB⟩2.0.CO;2.

Dipankar, A., B. Stevens, R. Heinze, C. Moseley, G. Zängl, M. Giorgetta, and S. Brdar, 2015: Large eddy simulation using the general circulation model ICON. *J. Adv. Model Earth Sy.*, **7 (3)**, 963–986, doi:10.1002/2015MS000431.

Doms, G., and M. Baldauf, 2018: *A Description of the Nonhydrostatic Regional COSMO-Model. Part I: Dynamics and Numerics.* Consortium for Small-Scale Modelling, URL http://www.cosmo-model.org/public/documentation.htm.

Doms, G., and Coauthors, 2011: *A Description of the Nonhydrostatic Regional COSMO Model. Part II: Physical Parameterization.* Consortium for Small-Scale Modelling, URL http://www.cosmo-model.org.

Easter, R. C., 1993: Two modified versions of Bott's positive-definite numerical advection scheme. *Mon. Weather Rev.*, **121**, 297–304.

ECMWF, 2017: *PART IV: PHYSICAL PROCESSES*, chap. Convection, 75–95. IFS Documentation, ECMWF.

ECMWF, 2018a: *PART IV: PHYSICAL PROCESSES*, chap. Subgrid-scale orographic drag, 59–67. IFS Documentation, ECMWF.

ECMWF, 2018b: *PART IV: PHYSICAL PROCESSES*, chap. Non-ogographic gravity wave drag, 69–74. IFS Documentation, ECMWF.

Ern, M., P. Preusse, and C. D. Warner, 2006: Some experimental constraints for spectral parameters used in the warner and mcintyre gravity wave parameterization scheme. *Atmos. Chem. Phys.*, **6 (12)**, 4361–4381, doi:10.5194/acp-6-4361-2006.

Gal-Chen, T., and R. Somerville, 1975: On the use of a coordinate transformation for the solution of the Navier-Stokes equations. *J. Comput. Phys.*, **17**, 209–228.

Gallus, W. A., and M. Ranĉić, 1996: A non-hydrostatic version of the NMC's regional Eta model. *Q. J. R. Meteorol. Soc.*, **122**, 495–513.

Gassmann, A., 2013: A global hexagonal C-grid non-hydrostatic dynamical core (ICON-IAP) designed for energetic consistency. *Q. J. R. Meteorol. Soc.*, **139 (670)**, 152–175, doi:10.1002/qj.1960.

Gassmann, A., and H.-J. Herzog, 2008: Towards a consistent numerical compressible non-hydrostatic model using generalized Hamiltonian tools. *Q. J. R. Meteorol. Soc.*, **134 (635)**, 1597–1613.

Giorgetta, M., and Coauthors, 2018: ICON-A, the Atmosphere Component of the ICON Earth System Model: I. Model Description. *J. Adv. Model Earth Sy.*, **10 (7)**, 1613–1637, doi:10.1029/2017MS001242.

GLOBE-Task-Team, 1999: The Global Land One-kilometer Base Elevation (GLOBE) Digital Elevation Model, version 1.0. Tech. rep., National Oceanic and Atmospheric Administration. URL http://www.ngdc.noaa.gov/mgg/topo/globe.html.

Guerra, J. E., and P. A. Ullrich, 2016: A high-order staggered finite-element vertical discretization for non-hydrostatic atmospheric models. *Geosci. Model Dev.*, **9 (5)**, 2007–2029, doi:10.5194/gmd-9-2007-2016, URL https://gmd.copernicus.org/articles/9/2007/2016/.

Harris, L. M., and P. H. Lauritzen, 2010: A flux-form version of the conservative semi-lagrangian multi-tracer transport scheme (CSLAM) on the cubed sphere grid. *J. Comput. Phys.*, **230**, 1215–1237.

Heinze, R., and Coauthors, 2017: Large-eddy simulations over Germany using ICON: a comprehensive evaluation. *Q. J. R. Meteorol. Soc.*, **143 (702)**, 69–100.

Heise, E., B. Ritter, and R. Schrodin, 2006: Operational implementation of the multilayer soil model. *COSMO Technical Reports No. 9*, Consortium for Small-Scale Modelling, 19pp, URL http://www.cosmo-model.org.

Hesselberg, A., 1925: Die Gesetze der ausgeglichenen atmosphärischen Bewegungen. *Beitr. Phys. Atmos.*, **12**, 141–160.

Heymsfield, A. J., and L. J. Donner, 1990: A scheme for parameterizing ice-cloud water content in general circulation models. *J. Atmos. Sci.*, **47 (15)**, 1865–1877.

Hogan, R. J., and A. Bozzo, 2018: A flexible and efficient radiation scheme for the ecmwf model. *J. Adv. Model Earth Sy.*, **10 (8)**, 1990–2008.

Hogan, R. J., and A. J. Illingworth, 2000: Deriving cloud overlap statistics from radar. *Q. J. R. Meteorol. Soc.*, **126 (569)**, 2903–2909.

Hunt, B. R., E. Kostelich, and I. Szunyogh, 2007: Efficient data assimilation for spatiotemporal chaos: A Local Ensemble Transform Kalman Filter. *Physica D*, **230**, 112–126.

Jablonowski, C., P. Lauritzen, R. Nair, and M. Taylor, 2008: *Idealized test cases for the dynamical cores of Atmospheric General Circulation Models: A proposal for the NCAR ASP 2008 summer colloquium.* National Center for Atmospheric Research (NCAR).

Jablonowski, C., and D. L. Williamson, 2006: A baroclinic instability test case for atmospheric model dynamical cores. *Q. J. R. Meteorol. Soc.*, **132**, 2943–2975.

Klemp, J., 2011: A terrain-following coordinate with smoothed coordinate surfaces. *Mon. Weather Rev.*, **139**, 2163–2169.

Klemp, J., J. Dudhia, and A. Hassiotis, 2008: An upper gravity-wave absorbing layer for NWP applications. *Mon. Weather Rev.*, **136 (10)**, 3987–4004.

Köhler, M., M. Ahlgrimm, and A. Beljaars, 2011: Unified treatment of dry convective and stratocumulus-topped boundary layers in the ECMWF model. *Q. J. R. Meteorol. Soc.*, **137 (654)**, 43–57.

Kolmogorov, A. N., 1968: Local structure of turbulence in an incompressible viscous fluid at very high reynolds numbers. *Sov. Phys. Usp.*, **10 (6)**, 734.

Korn, P., 2017: Formulation of an unstructured grid model for global ocean dynamics. *J. Comput. Phys.*, **339 (C)**, 525–552, doi:10.1016/j.jcp.2017.03.009.

Korn, P., and S. Danilov, 2017: Elementary dispersion analysis of some mimetic discretizations on triangular C-grids. *J. Comput. Phys.*, **330**, 156 – 172, doi:https://doi.org/10.1016/j.jcp.2016.10.059.

Kourzeneva, E., 2010: External data for lake parameterization in Numerical Weather Prediction and climate modeling. *Boreal Env. Res.*, **15**, 165–177.

Kourzeneva, E., H. Asensio, E. Martin, and S. Faroux, 2012: Global gridded dataset of lake coverage and lake depth for use in numerical weather prediction and climate modelling. *Tellus A*, **64**, 15 640, doi:10.3402/tellusa.v64i0.15640.

Lauritzen, P. H., C. Erath, and R. Mittal, 2011a: On simplifying 'incremental remap'-based transport schemes. *J. Comput. Phys.*, **230**, 7957–7963.

Lauritzen, P. H., C. Jablonowski, M. A. Taylor, and R. D. Nair, 2011b: *Numerical Techniques for Global Atmospheric Models*. 1st ed., Springer, 556 pp.

Lauritzen, P. H., R. D. Nair, and P. A. Ullrich, 2010: A conservative semi-Lagrangian multi-tracer transport scheme (CSLAM) on the cubed-sphere grid. *J. Comput. Phys.*, **229**, 1401–1424.

Leuenberger, D., M. Koller, and C. Schär, 2010: A generalization of the SLEVE vertical coordinate. *Mon. Weather Rev.*, **138**, 3683–3689.

Lilly, D. K., 1962: On the numerical simulation of buoyant convection. *Tellus*, **14 (2)**, 148–172, doi:10.1111/j.2153-3490.1962.tb00128.x.

Lin, S.-J., and R. B. Rood, 1996: Multidimensional flux-form semi-lagrangian transport schemes. *Mon. Weather Rev.*, **124 (9)**, 2046–2070, doi:10.1175/1520-0493(1996)124⟨2046:MFFSLT⟩2.0.CO;2.

Lipscomb, W. H., and T. D. Ringler, 2005: An incremental remapping transport scheme on a spherical geodesic grid. *Mon. Weather Rev.*, **133**, 2335–2350.

Lott, F., and M. J. Miller, 1997: A new subgrid-scale orographic drag parametrization: Its formulation and testing. *Q. J. R. Meteorol. Soc.*, **123 (537)**, 101–127, doi:10.1002/qj.49712353704.

Matsuno, T., 1966: Numerical integrations of the primitive equations by a simulated backward difference method. *J. Meteorolog. Soc. Jpn.*, **44 (1)**, 76–84, doi:10.2151/jmsj1965.44.1_76.

McLandress, C., and J. F. Scinocca, 2005: The GCM response to current parameterizations of nonorographic gravity wave drag. *J. Atmos. Sci.*, **62 (7)**, 2394–2413, doi:10.1175/JAS3483.1.

Mellor, G. L., and T. Yamada, 1982: Development of a turbulence closure model for geophysical fluid problems. *Rev. Geophys.*, **20 (4)**, 851–875, doi:10.1029/RG020i004p00851.

Mironov, D., E. Heise, E. Kourzeneva, B. Ritter, N. Schneider, and A. Terzhevik, 2010: Implementation of the lake parameterisation scheme FLake into the numerical weather prediction model COSMO. *Boreal Env. Res.*, **15**, 218–230.

Mironov, D., B. Ritter, J.-P. Schulz, M. Buchhold, M. Lange, and E. Machulskaya, 2012: Parameterisation of sea and lake ice in numerical weather prediction models of the German weather service. *Tellus A*, **64 (0)**, doi:10.3402/tellusa.v64i0.17330.

Mironov, D. V., 2008: Parameterization of lakes in numerical weather prediction. Description of a lake model. COSMO Technical Report, Consortium for Small-Scale Modelling, 41 pp. URL http://www.cosmo-model.org.

Miura, H., 2007: An upwind-biased conservative advection scheme for spherical hexagonal-pentagonal grids. *Mon. Weather Rev.*, **135**, 4038–4044.

Mlawer, E. J., S. J. Taubman, P. D. Brown, M. J. Iacono, and S. A. Clough, 1997: Radiative transfer for inhomogeneous atmospheres: RRTM, a validated correlated-k model for the longwave. *J. Geophys. Res.: Atmos.*, **102 (D14)**, 16 663–16 682, doi:10.1029/97JD00237.

Narcovich, F. J., and J. D. Ward, 1994: Generalized Hermite interpolation via matrix-valued conditionally positive definite functions. *Math. Comp.*, **63**, 661–687, doi:10.1090/S0025-5718-1994-1254147-6.

Neggers, R. A. J., M. Köhler, and A. C. M. Beljaars, 2009: A dual mass flux framework for boundary layer convection. Part I: Transport. *J. Atmos. Sci.*, **66 (6)**, 1465–1487, doi:10.1175/2008JAS2635.1.

Orr, A., P. Bechtold, J. Scinocca, M. Ern, and M. Janiskova, 2010: Improved middle atmosphere climate and forecasts in the ECMWF model through a nonorographic gravity wave drag parameterization. *J. Clim.*, **23 (22)**, 5905–5926, doi:10.1175/2010JCLI3490.1.

Pincus, R., H. W. Barker, and J.-J. Morcrette, 2003: A fast, flexible, approximate technique for computing radiative transfer in inhomogeneous cloud fields. *J. Geophys. Res.: Atmos.*, **108 (D13)**.

Pincus, R., and B. Stevens, 2013: Paths to accuracy for radiation parameterizations in atmospheric models. *J. Adv. Model Earth Sy.*, **5 (2)**, 225–233, doi:10.1002/jame.20027.

Polavarapu, S., S. Ren, A. M. Clayton, D. Sankey, and Y. Rochon, 2004: On the relationship between incremental analysis updating and incremental digital filtering. *Mon. Weather Rev.*, **132**, 2495–2502.

Press, W. H., S. A. Teukolsky, W. T. Vetterling, and B. P. Flannery, 2007: *Numerical Recipes*. 3rd ed., Cambridge University Press, 1235 pp.

Prill, F., 2020: *DWD ICON Tools Documentation*. Deutscher Wetterdienst (DWD), `dwd_icon_tools/doc/icontools_doc.pdf`.

Randall, D. A., 2017: A survey of time-differencing schemes for the oscillation and decay equations. *An Introduction to Numerical Modelling of the Atmosphere*, Colorado State University, 63–104, URL http://kiwi.atmos.colostate.edu/group/dave/at604pdf/AT604_LaTeX_Book.pdf.

Raschendorfer, M., 2001: The new turbulence parameterization of LM. *COSMO News Letter No. 1*, Consortium for Small-Scale Modelling, 89–97, URL http://www.cosmo-model.org.

Rast, S., 2017: Using and programming ICON – a first introduction. Max Planck Institute for Meteorology, URL https://code.mpimet.mpg.de/attachments/download/15898/icon_lecture_2016.pdf, course at Hamburg University 2017.

Reinert, D., 2020: The Tracer Transport Module Part I: A Mass Consistent Finite Volume Approach with Fractional Steps. Reports on icon, Deutscher Wetterdienst, 19 pp. doi:10.5676/DWD_pub/nwv/icon_005, URL https://www.dwd.de/DE/leistungen/reports_on_icon/reports_on_icon.html.

Reinert, D., F. Prill, H. Frank, M. Denhardt, and G. Zängl, 2020: *Database Reference Manual for ICON and ICON-EPS*. Deutscher Wetterdienst (DWD), URL https://www.dwd.de/EN/ourservices/reports_on_icon/reports_on_icon.html.

Rieger, D., M. Köhler, R. J. Hogan, S. A. K. Schäfer, A. Seifert, A. de Lozar, and G. Zängl, 2019: ecRad in ICON - Details on the Implementation and First Results. **(4)**, doi:10.5676/DWD_pub/nwv/icon_004.

Rieger, D., and Coauthors, 2015: ICON–ART 1.0 – a new online-coupled model system from the global to regional scale. *Geosci. Model Dev.*, **8 (6)**, 1659–1676, doi:10.5194/gmd-8-1659-2015.

Rotta, J., 1951a: Statistische Theorie nichthomogener Turbulenz. *J. Z. Physik*, **129 (6)**, 547–572, doi:10.1007/BF01330059.

Rotta, J., 1951b: Statistische Theorie nichthomogener Turbulenz. *J. Z. Physik*, **131 (1)**, 51–77, doi:10.1007/BF01329645.

Ruppert, T., 2007: Diplomarbeit: Vector field reconstruction by radial basis functions. M.S. thesis, Department of Mathematics, Technical University Darmstadt.

Sadourny, R., A. Arakawa, and Y. Mintz, 1968: Integration of the nondivergent barotropic vorticity equation with an icosahedral-hexagonal grid for the sphere. *Mon. Weather Rev.*, **96 (6)**, 351–356, doi:10.1175/1520-0493(1968)096⟨0351:IOTNBV⟩2.0.CO;2.

Satoh, M., 2002: Conservative scheme for the compressible nonhydrostatic models with the horizontally explicit and vertically implicit time integration scheme. *Mon. Weather Rev.*, **130**, 1227–1245.

Schär, C., D. Leuenberger, O. Fuhrer, D. Lüthi, and C. Girard, 2002: A new terrain-following vertical coordinate formulation for atmospheric prediction models. *Mon. Weather Rev.*, **130**, 2459–2480.

Schrodin, R., and E. Heise, 2001: The Multi-Layer Version of the DWD Soil Model TERRA_LM. Tech. Rep. 2, Consortium for Small-Scale Modelling, 1–16 pp. URL http://www.cosmo-model.org.

Schröter, J., and Coauthors, 2018: ICON-ART 2.1: a flexible tracer framework and its application for composition studies in numerical weather forecasting and climate simulations. *Geosci. Model Dev.*, **11 (10)**, 4043–4068, doi:10.5194/gmd-11-4043-2018.

Schulz, J.-P., 2006: The new Lokal-Model LME of the German Weather Service. *COSMO News Letter No. 6*, Consortium for Small-Scale Modelling, 210–212, URL http://www.cosmo-model.org.

Schulz, J.-P., 2008: Introducing sub-grid scale orographic effects in the cosmo model. *COSMO News Letter No. 9*, Consortium for Small-Scale Modelling, 29–36, URL http://www.cosmo-model.org.

Schulz, J.-P., G. Vogel, C. Becker, S. Kothe, U. Rummel, and B. Ahrens, 2016: Evaluation of the ground heat flux simulated by a multi-layer land surface scheme using high-quality observations at grass land and bare soil. *Meteorol. Z.*, **25 (5)**, 607–620, doi:10.1127/metz/2016/0537.

Scinocca, J. F., 2003: An accurate spectral nonorographic gravity wave drag parameterization for general circulation models. *J. Atmos. Sci.*, **60 (4)**, 667–682, doi:10.1175/1520-0469(2003)060⟨0667:AASNGW⟩2.0.CO;2.

Seifert, A., 2008: A revised cloud microphysical parameterization for COSMO-LME. *COSMO News Letter No. 7, Proceedings from the 8th COSMO General Meeting in Bucharest, 2006*, Consortium for Small-Scale Modelling, 25–28, URL http://www.cosmo-model.org.

Seifert, A., and K. D. Beheng, 2006: A two-moment cloud microphysics parameterization for mixed-phase clouds. Part 1: Model description. *Meteorol. Atmos. Phys.*, **92 (1)**, 45–66, doi:10.1007/s00703-005-0112-4.

Siebesma, A. P., and J. W. M. Cuijpers, 1995: Evaluation of parametric assumptions for shallow cumulus convection. *J. Atmos. Sci.*, **52**, 650–666.

Simmons, A., and D. Burridge, 1981: An energy and angular-momentum conserving finite-difference scheme and hybrid vertical coordinates. *Mon. Weather Rev.*, **109**, 758–766.

Skamarock, W., J. B. Klemp, M. G. Duda, L. D. Fowler, S. Park, and T. D. Ringler, 2012: A Multiscale Nonhydrostatic Atmospheric Model Using Centroidal Voronoi Tesselations and C-Grid Staggering. *Mon. Weather Rev.*, **140**, 3090–3105, doi:10.1175/MWR-D-11-00215.1.

Skamarock, W. C., and J. B. Klemp, 2008: A time-split nonhydrostatic atmospheric model for weather research and forecasting applications. *J. Comput. Phys.*, **227**, 3465–3485.

Skamarock, W. C., and M. Menchaca, 2010: Conservative transport schemes for spherical geodesic grids: High-order reconstructions for forward-in-time schemes. *Mon. Weather Rev.*, **138**, 4497–4508.

Smagorinsky, J., 1963: General Circulation Experiments with the Primitive Equations. *Mon. Weather Rev.*, **91**, 99, doi:10.1175/1520-0493(1963)091⟨0099:GCEWTP⟩2.3.CO;2.

Smiatek, G., J. Helmert, and E.-M. Gerstner, 2016: Impact of land use and soil data specifications on COSMO-CLM simulations in the CORDEX-MED area. *Meteorol. Z.*, **25 (2)**, 215–230, doi:10.1127/metz/2015/0594.

Smiatek, G., B. Rockel, and U. Schättler, 2008: Time invariant data preprocessor for the climate version of the COSMO model (COSMO-CLM). *Meteorol. Z.*, **17 (4)**, 395–405, doi:10.1127/0941-2948/2008/0302.

Snyder, J., 1987: *Map Projections – a Working Manual.* No. 1395, U. S. Geological Survey professional paper, U. S. Government Printing Office.

Sommeria, G., and J. W. Deardorff, 1977: Subgrid-Scale Condensation in Models of Non-precipitating Clouds. *J. Atmos. Sci.*, **34 (2)**, 344–355, doi:doi:10.1175/1520-0469(1977)034⟨0344:SSCIMO⟩2.0.CO;2.

Straka, J. M., R. B. Wilhelmson, and K. K. Droegemeier, 1993: Numerical solutions of a non-linear density current: A benchmark solution and comparisons. *Int. J. Numer. Methods Fluids*, **17**, 1–22.

Strang, G., 1968: On the construction and comparison of difference schemes. *SIAM J. Numer. Anal.*, **5 (3)**, 506–517, doi:10.1137/0705041.

Tibaldi, S., 1986: Envelope orography and maintenance of quasi-stationary waves in the ECMWF model. *Adv. Geophys.*, **29**, 339–374.

Tiedtke, M., 1989: A comprehensive mass flux scheme for cumulus parameterization in large-scale models. *Mon. Weather Rev.*, **117 (8)**, 1779–1800, doi:10.1175/1520-0493(1989)117⟨1779:ACMFSF⟩2.0.CO;2.

Tomita, H., M. Satoh, and K. Goto, 2002: An optimization of the icosahedral grid modified by spring dynamics. *J. Comput. Phys.*, **183 (1)**, 307–331, doi:10.1006/jcph.2002.7193.

Wacker, U., and F. Herbert, 2003: Continuity equations as expressions for local balances of masses in cloudy air. *Tellus A*, **55**, 247–254.

Wallace, J., S. Tibaldi, and A. Simmons, 1983: Reduction of systematic forecast errors in the ECMWF model through the introduction of an envelope orography. *Q. J. R. Meteorol. Soc.*, **109**, 683–717.

Wan, H., and Coauthors, 2013: The ICON-1.2 hydrostatic atmospheric dynamical core on triangular grids – Part 1: Formulation and performance of the baseline version. *Geosci. Model Dev.*, **6 (3)**, 735–763, doi:10.5194/gmd-6-735-2013.

Warner, C. D., and M. E. McIntyre, 1996: On the propagation and dissipation of gravity wave spectra through a realistic middle atmosphere. *J. Atmos. Sci.*, **53 (22)**, 3213–3235, doi:10.1175/1520-0469(1996)053⟨3213:OTPADO⟩2.0.CO;2.

Yeh, K.-S., 2007: The streamline subgrid integration method: I. quasi-monotonic second order transport schemes. *J. Comput. Phys.*, **225**, 1632–1652.

Zalesak, S. T., 1979: Fully multidimensional flux-corrected transport algorithms for fluid. *J. Comput. Phys.*, **31**, 335–362.

Zängl, G., 2012: Extending the Numerical Stability Limit of Terrain-Following Coordinate Models over Steep Slopes. *Mon. Weather Rev.*, **140**, 3722–3733, doi:10.1175/MWR-D-12-00049.1.

Zängl, G., D. Reinert, P. Ripodas, and M. Baldauf, 2015: The ICON (ICOsahedral Non-hydrostatic) modelling framework of DWD and MPI-M: Description of the non-hydrostatic dynamical core. *Q. J. R. Meteorol. Soc.*, **141**, 563–579.

Zarzycki, C., M. N. Levy, C. Jablonowski, J. R. Overfelt, M. A. Taylor, and P. Ullrich, 2014: Aquaplanet experiments using CAM's variable resolution dynamical core. *J. Clim.*, **27**, 5481–5503, doi:10.1175/JCLI-D-14-00004.1.

Zdunkowski, W., and A. Bott, 2003: *Dynamics of the atmosphere: A course in theoretical meteorology.* 1st ed., Cambridge University Press, 719 pp.

Zerroukat, M., N. Wood, and A. Staniforth, 2002: SLICE: A Semi–Lagrangian Inherently Conserving and Efficient scheme for transport problems. *Q. J. R. Meteorol. Soc.*, **128**, 2801–2820, doi:10.1256/qj.02.69.

Zerroukat, M., N. Wood, and A. Staniforth, 2005: A monotonic and positive-definite filter for Semi-Lagrangian Inherently Conserving and Efficient (SLICE) scheme. *Q. J. R. Meteorol. Soc.*, **131**, 2923–2936.

Zerroukat, M., N. Wood, and A. Staniforth, 2006: The Parabolic Spline (PSM) Method for conservative transport problems. *Int. J. Numer. Meth. Fluids*, **51**, 1297–1318.

Index of Namelist Parameters

The following index contains only namelist parameters covered by this tutorial. Please take a look at the document

`icon/doc/Namelist_overview.pdf`

for a complete list of available namelist parameters for the ICON model.